

# Genetic Analysis of Arbuscular Mycorrhiza Development in *Lotus japonicus*

**Martin Groth**

Dissertation der Fakultät für Biologie  
der Ludwig-Maximilians-Universität München



---

München, 6. Oktober 2010



**Genetic Analysis of Arbuscular Mycorrhiza  
Development in *Lotus japonicus***

Dissertation  
zur Erlangung des Doktorgrades der Naturwissenschaften  
an der Fakultät für Biologie  
der Ludwig-Maximilians-Universität München

Vorgelegt von  
Martin Groth  
aus München

München, 06.10.2010

**Erstgutachter: Prof. Dr. Martin Parniske**

**Zweitgutachter: Prof. Dr. Thomas Lahaye**

**Tag der mündlichen Prüfung: 6. Dezember 2010**



## **Ehrenwörtliche Versicherung**

Ich versichere hiermit ehrenwörtlich, dass die vorgelegte Dissertation von mir selbständig und ohne unerlaubte Hilfe angefertigt ist.

München, den

Martin Groth

## **Erklärung**

Hiermit erkläre ich, dass die Dissertation nicht ganz oder in wesentlichen Teilen einer anderen Prüfungskommission vorgelegt worden ist.

Ich habe mich nicht anderweitig einer Doktorprüfung unterzogen und ich habe zu keinem früheren Zeitpunkt versucht, eine Dissertation einzureichen oder mich der Doktorprüfung zu unterziehen.

München, den

Martin Groth

## Veröffentlichungen in Fachzeitschriften

Teile bzw. Beiträge der vorliegenden Arbeit wurden in folgenden Artikel veröffentlicht:

**Groth, M., Takeda, N., Perry, J., Uchida, H., Draxl, S., Brachmann, A., Sato, S., Tabata, S., Kawaguchi, M., Wang, T.L., and Parniske, M.** (2010). *NENA*, a *Lotus japonicus* Homolog of *Sec13*, Is Required for Rhizodermal Infection by Arbuscular Mycorrhiza Fungi and Rhizobia but Dispensable for Cortical Endosymbiotic Development. *Plant Cell* **22**, 2509-2526.

**Maekawa-Yoshikawa, M., Muller, J., Takeda, N., Maekawa, T., Sato, S., Tabata, S., Perry, J., Wang, T.L., Groth, M., Brachmann, A., and Parniske, M.** (2009). The temperature-sensitive *brush* mutant of the legume *Lotus japonicus* reveals a link between root development and nodule infection by rhizobia. *Plant Physiol.* **149**, 1785-1796.

**Perry, J., Brachmann, A., Welham, T., Binder, A., Charpentier, M., Groth, M., Haage, K., Markmann, K., Wang, T.L., and Parniske, M.** (2009). TILLING in *Lotus japonicus* identified large allelic series for symbiosis genes and revealed a bias in functionally defective ethyl methanesulfonate alleles toward glycine replacements. *Plant Physiol.* **151**, 1281-1291.

**Takeda, N., Kistner, C., Kosuta, S., Winzer, T., Pitzschke, A., Groth, M., Sato, S., Kaneko, T., Tabata, S., and Parniske, M.** (2007). Proteases in plant root symbiosis. *Phytochem.* **68**, 111-121.

Folgende Manuskripte sind in Vorbereitung:

**Groth, M. and Parniske, M.** Nucleoporins as gatekeepers in root-microbe symbioses.

Addendum auf Anfrage des Chefredakteurs von *Plant Signaling&Behavior*.

**Groth, M., Haage, K., Kosuta, S., Szczyglowski, K. and Parniske, M.** Two loci regulating arbuscule formation identified by microscopical screening of a *Lotus japonicus* EMS mutant population.

Das Manuskript beschreibt den genetischen Screen nach *L. japonicus* Mutanten mit gestörter Entwicklung der Arbuskulären Mykorrhiza, sowie die Etablierung eines Kapillarsequenzierer-basierten Genotypisierungssystems zur Kartierung der entsprechenden Loci. Zentrale Bestandteile sind des Weiteren die detaillierte phänotypische Beschreibung der *red* Mutante, die eine eingeschränkte Arbuskelentwicklung aufweist, und die Kartierung der zugrunde liegenden Mutationen. Entsprechende Kapitel sind auf den Seiten 22-48 und 90-92 der vorliegenden Dissertation enthalten.

**Groth, M. and Parniske, M.** Preliminary title: A glycine to glutamic acid substitution in the RCK domain of *POLLUX* leads to residual root symbiosis with arbuscular mycorrhiza fungi and rhizobia in the absence of calcium spiking.

Das Manuskript beschreibt die Identifizierung der *patchy* Mutante und der kausalen Mutation, welche mit dem *pollux-7* Allel übereinstimmt. Die entsprechenden Resultate, einschließlich einer Analyse des Calcium Spiking, sind auf den Seiten 61-70 der vorliegenden Dissertation enthalten.

Für Moritz Janko



## **ACKNOWLEDGEMENTS**

I would like to thank Prof. Martin Parniske for giving me the opportunity to conduct my doctoral work as part of his team. I am grateful for the received supervision and support, which largely contributed to my scientific formation.

I am thankful to Prof. Thomas Lahaye for reviewing my PhD thesis.

Specials thanks go to every lab member for sharing chemicals, constructs, protocols and all the good times. For the experienced helpfulness and geniality I would like to thank by name Merixell Antolin-Llovera, Ute Bergmann, Andreas Binder, Gabi Büttner, Myriam Charpentier, Matthias Ellerbeck, Kristina Haage, Simone Hardel, Takaki Maekawa, Makoto Maekawa Yoshikawa, Katharina Markmann, Sylvia Singh, Naoya Takeda and Katalin Tóth. My thanks go also to Anna Krementowski for her work in the glasshouse as student helper.

I would like to thank Andreas Brachmann for fruitful discussions and his kind cooperativeness.

I would like to express my gratitude to my parents, Breda and Siegwart, for their care and support. I am thankful to my sister, Kati, and her inspiring cheerfulness. For their support I would furthermore like to thank Bernd and Barbara.

I am deeply grateful for the invaluable joy and backing due to my partner, Julia, and our son, Moritz.



## TABLE OF CONTENTS

SUMMARY .....	13
INTRODUCTION .....	15
Social and Environmental Context .....	15
Most Plants Form Mycorrhizae .....	15
Arbuscular Mycorrhiza Is an Endosymbiosis between Plants and <i>Glomeromycota</i> Fungi.....	16
Roots Secrete Strigolactone to Promote Contact with AM Fungi .....	17
Entry Checkpoint: Reprogramming Root Cells for Fungal Accommodation.....	18
Controlling the Market: Plant Genes Involved in Arbuscule Development.....	20
Most Plants Cannot Engage in Root Nodule Symbiosis.....	23
‘One Ping Only’ – Sending the Right Signal to The Rhizodermis.....	23
Pre-symbiotic AM Fungal Signaling .....	25
Intracellular Accommodation of Rhizobia and AM Fungi Is Controlled by the Common SYM Network .....	26
Aim of this Study.....	28
RESULTS.....	29
A Capillary Sequencer-Based Setup for Microsatellite Genotyping of <i>Lotus</i> .....	29
Genetic Dissection of AM Development by Screening for AM Mutants in <i>Lotus</i> ..	35
Genetics of the Dimorphic Arbuscular Mycorrhiza Phenotype Encountered in the Arbuscule Formation Mutant Line SL0181-N .....	39
Mutants of the AMPOP Impaired in Known Common SYM Genes .....	56
<i>NENA</i> , a <i>Lotus japonicus</i> Homolog of <i>Sec13</i> Is Required for Rhizodermal Infection by Arbuscular Mycorrhiza Fungi and Rhizobia but Dispensable for Cortical Endosymbiotic Development.....	67
DISCUSSION .....	87
Symbiotic Infection of Rhizodermal Cells Is Blocked in <i>nen</i> a.....	87
Symbiotic Development of Cortical Cells Does Not Require <i>NENA</i> .....	88
<i>nen</i> a Reveals an Intercellular Rhizobial Entry Mode in <i>Lotus japonicus</i> .....	89
<i>NENA</i> Is a Scaffold Nucleoporin Required for Calcium Spiking .....	91
<i>patchy</i> Is Leaky for Rhizodermal Infection by Rhizobia .....	93
<i>patchy</i> Affects Intraradical AM Hyphal Spreading .....	94
The Mutation in <i>patchy</i> Might Affect Gating of POLLUX .....	96
<i>red</i> Is Located on the Short Arm of Chromosome VI .....	97
A Comprehensive Model for the Genetics Underlying the <i>red</i> Phenotype.....	97
<i>RED</i> Might be Involved in <i>PT4</i> Regulation.....	98

METHODS.....	101
Plant Growth and AM Assay .....	101
AM Mutant Screen.....	101
Generation of Mapping Populations .....	101
Recombination Screen .....	102
Power Mapping .....	102
TILLING .....	103
Infection Thread and Nodulation Assays .....	103
Calcium Spiking Analysis.....	104
Transgenic Complementation and Sub-cellular Localization .....	104
DNA Gel Blotting .....	105
Expression Analysis.....	105
Promoter GUS Analysis .....	106
Yeast Two-Hybrid Analysis.....	106
Microscopy.....	107
Phylogenetic Analysis.....	107
Homology Modeling .....	108
Accession Numbers .....	108
REFERENCES .....	109
SUPPLEMENT.....	125
Supplemental Figures.....	125
Supplemental Tables .....	140
List of Figures .....	166
List of Tables .....	168
Abbreviations, Measures and Species.....	169
Curriculum Vitae .....	170



## SUMMARY

Legumes can cover their nitrogen demand from air by harboring nitrogen-fixing bacteria (rhizobia) in specialized organs, the root nodules. With the use of forward genetics and model legumes, including *Lotus japonicus*, the general molecular network governing rhizobial infection and nodule organogenesis has been unraveled. Network components involved in the activation of the central regulatory calcium and calmodulin-dependent kinase (CCaMK) also control the intracellular accommodation of arbuscular mycorrhiza (AM) fungi during their passage to the root cortex and thus constitute the so-called common SYM pathway. Yet, no genes specifically required for AM – one of the most widespread symbiosis on earth – have been known at the beginning of this work.

Integral to the present study, a microscopy screen for *Lotus japonicus* mutants defective in AM was performed and mutants affected at different stages of AM development were isolated from more than 5600 individuals inspected. In order to identify the causative mutations by map-based cloning, a genotyping setup was established. By this, mutations in already known symbiotic genes were rapidly discerned. A mutant defective in hyphal root colonization (*patchy*) carried a mutation in the common SYM gene *POLLUX*, encoding an ion channel. Calcium spiking, normally induced by rhizobial Nod factor (NF), was not observed in *patchy*, although its nodulation phenotype indicated residual activity of the mutant protein.

By detailed co-segregation analysis of a mutant with a dimorphic arbuscule phenotype, the position of the *red* locus was determined at the short arm of chromosome VI. Furthermore, induction of the mycorrhizal phosphate transporter *PT4* was abolished in the *red* mutant line.

In *nena*, fungal infection is aborted in the rhizodermis. *NENA* encodes a WD40 repeat protein related to the nucleoporins Sec13 and Seh1. Localization of NENA to the nuclear rim and yeast two-hybrid experiments indicated a role for NENA in a conserved subcomplex of the nuclear pore scaffold. Although *nena* mutants were able to form pink nodules in symbiosis with *Mesorhizobium loti*, root hair infection was not observed. Moreover, NF induction of the symbiotic genes *NIN*, *SbtM4* and *SbtS*, as well as calcium spiking were impaired. Detailed phenotypic analyses of *nena* mutants revealed a rhizobial infection mode that overcame the lack of rhizodermal responsiveness and carried the hallmarks of crack entry, including a requirement for ethylene. CCaMK-dependent processes were only abolished in the rhizodermis but not in the cortex of *nena* mutants. These data support the concept of tissue-specific components for the activation of CCaMK.



# INTRODUCTION

## Social and Environmental Context

The invention of the Haber-Bosch process for the synthesis of ammonia laid the foundation for the 'green revolution' in industrial agriculture during mid 20<sup>th</sup> century. Accompanied by new elite cultivars, pesticides and modern irrigation, the use of synthetic fertilizers increased average global yield of cereals from 1.2 t/ha in 1961 to 3.1 t/ha in 2007 (FAOSTAT, 2010). During the same period, the consumption of N fertilizers has increased from roughly 10 Mt/y to almost 80 Mt/y and more than half of the N in the global cycle currently is of anthropogenic origin (Smil, 1999; Galloway et al., 2008). Similarly, P from inorganic fertilizers is increasingly entering the global cycle of matter, reaching approx. 15 Mt/y recently (Smil, 2003). P<sub>i</sub> fertilizers are mainly produced from mined rock, a nonrenewable resource with economically relevant global reserves for min. 80 y in 2003 (FAO, 2004). P rock from sedimentary deposits often contains elevated concentrations of heavy metals, especially Cd, which enters the food chain with P<sub>i</sub> fertilizer application and the removal of which increases energy costs of the production process, reaching min. rates required for the synthesis of ammonia (32–33 MJ/kg N) (Smil, 2003). Further limitations to the applicability of N and P<sub>i</sub> fertilizers arise from the fact that large amounts of the annual nutrient input in agriculture are not taken up by the crops. N is lost due to the leaching of highly soluble nitrate, as well as microbial denitrification and nitrification that leads to the emission of N<sub>2</sub>O/NO greenhouse gases and N<sub>2</sub> to the atmosphere (Barbier and Viogy, 2003). Conversely, P<sub>i</sub> is quickly immobilized by oxides and oxihydrates from clay particles or precipitation with Al and Fe ions released by soil acidification and thus becomes hardly available to roots by diffusion or mass flow, whereas leaching of surplus P<sub>i</sub> is the main cause of freshwater eutrophication (Smil, 2003). Rather than increasing the levels of nutrient supply to arable land, future food security for developing countries will therefore depend on sustainable practices in agriculture that provide high yield and efficient use of the available resources. Understanding the genetics of plant nutrition through microbial symbioses is one contribution that basic research can make in this context.

## Most Plants Form Mycorrhiza

Plants form symbioses with various microorganisms to improve the uptake of essential nutrients. Among the most widespread are mycorrhizal associations between fungi and roots. Symbioses that take place on the surface of the outer root

cell layers are classified as ectomycorrhizal. They constitute the predominant boreal form established between coniferous, as well as deciduous trees and other woody plants and fungi from diverse lineages (Brundrett, 2004). Endomycorrhizal associations are characterized by symbiotic structures inside the cells of the root cortex. This type includes the ecologically specialized ericoid and orchid mycorrhiza and the ubiquitous arbuscular mycorrhiza (AM), formed by at least 80% of all land plant species, including horn- and liverworts, ferns, gymno- and angiosperms (Brundrett, 2009). The model plant *Arabidopsis thaliana* (*Arabidopsis*) does not form AM. Molecular phylogenetics revealed that AM fungi all belong to the monophyletic *Glomeromycota* (Schüßler et al., 2001). Depending on dataset and calibration of the molecular clock, it was 400 to more than 1000 My ago that the *Glomeromycota* had split from the ancestral lineage of the *Basidiomycota* and *Ascomycota* (Simon et al., 1993; Berbee and Taylor, 2001; Heckman et al., 2001). Fossil records of AM symbiotic structures in primitive land plants without proper roots from the early Devonian Rhynie chert (Remy et al., 1994) and fungal hyphae and spores, resembling modern Glomales, from a 455 – 460 My old geological formation (Redecker et al., 2000) fostered speculations that AM enabled land colonization by plants.

### **Arbuscular Mycorrhiza Is an Endosymbiosis between Plants and *Glomeromycota* Fungi**

AM fungal spores, containing hundreds of nuclei (Croll et al., 2008a), can outlast inhospitable periods. During spore germination, fungal carbohydrates are mobilized and asymbiotic hyphal growth is supported for up to two weeks, before cytoplasm is retracted and the fungus enters dormancy again (Bago et al., 2000). Formation of coenocytic mycelia and reproduction through newly formed spores during the natural lifecycle depends on the presence of a feeding host (Figures 1 and 2A). Under artificial monoxenic conditions, the generation of infectious spores with *Paenibacillus validus* was reported (Hildebrandt et al., 2006). Compatible isolates can exchange nuclei by anastomosis between hyphae, leading to intermixture of different genotypes and phenotypic changes in subsequent subcultures (Croll et al., 2008a). Nevertheless, clear evidence for meiotic recombination is lacking. AM fungi exhibit considerable variation within individual species (ranging from 7% to more than 23% in rDNA; Stockinger et al., 2009) and it remains paradoxical how their genomes are maintained at evolutionary timescale (Rosendahl, 2008).

The ubiquity of AM provides evidence for the advantage on the symbiotic partners and their ecosystem of exchanging plant-derived carbohydrates for mineral nutrients provided by the fungus. The large surface area of the ramified AM fungal mycelium facilitates root interception of mineral nutrients beyond the zone depleted of slow diffusible nutrients, such as  $P_i$ , that surrounds the root for a distance of a few mm (Li et al., 1991). Improving plant growth through phosphate provided by the AM fungal partner is amply documented (Smith et al., 2004). Further beneficial effects include increased tolerance of metal toxicity and resistance to drought, as well as pathogens (Newsham et al., 1995; Finlay, 2008; Smith and Read, 2008). Carbohydrates taken up by AM fungi account for 4 – 20 % of the host's photoassimilate and hence form a substantial portion of the global carbon cycle (Bago et al., 2000). Fueling the rhizosphere with carbohydrates, as well as mobilizing nutrients from mineral and organic stores, the impact of AM on the ecosystem becomes increasingly apparent (Hodge and Fitter, 2010). Microcosm and field trials gave proof of the positive correlations between AM fungal diversity, plant biodiversity and productivity (van der Heijden et al., 1998). Host-specificity is generally low in AM fungi, since under laboratory conditions generalist fungal species, such as *Glomus intraradices*, can colonize any AM-forming plant species. A single plant root can be simultaneously colonized by various AM fungal species and different plants can be interconnected by AM mycelia (Giovannetti et al., 2004). Yet, differing plant growth responses and preferential associations with certain AM fungal species or intra-specific genotype variants have been observed (Croll et al., 2008b; Helgason and Fitter, 2009). The occupation of distinct ecological niches by the different AM fungi probably leads to 'ecological' host specificity and succession in AM fungal communities (Maherali and Klironomos, 2007; Santos-Gonzalez et al., 2007).

### **Roots Secrete Strigolactone to Promote Contact with AM Fungi**

Development of the intimate alliance between roots and AM fungi is subject to concerted genetic interplay. The exchange of diffusible signals precludes the symbiotic phase (Figure 1). Recently, the identity of the plant's signal, strigolactone, which induces AM fungal metabolic activity leading to spore germination and hyphal branching in sensation of the host's proximity, has been identified (Akiyama et al., 2005; Besserer et al., 2006). Strigolactones are sesquiterpene compounds that are easily hydrolyzed and therefore able to create a concentration gradient towards the root (Parniske, 2005). The same compound has been identified and termed strigol approx. 50 years ago, being a germination stimulant of the parasitic witchweed

(*Striga sp.*) (Cook et al., 1966). Moreover, strigolactone acts as a plant hormone suppressing shoot branching (Gomez-Roldan et al., 2008; Umehara et al., 2008). Strigolactone content and secretion are increased in plants grown under phosphate deficiency (López-Ráez et al., 2008). It is therefore conceivable that the hormone sensing of the parasitic weeds evolved to perceive root secreted strigolactone of host plants, thus exploiting an ancient signal towards AM fungi (Parniske, 2008).

### **Entry Checkpoint: Reprogramming Root Cells for Fungal Accommodation**

The early symbiotic phase, starting with physical contact of the hypha and the rhizodermis (Figure 1), is marked by pivotal cellular responses for the proceeding of AM development. Several transcriptome analyses showed a transient induction of genes related to pathogen defense during this stage (Liu et al., 2003; Guimil et al., 2005; Hohnjec et al., 2005; Liu et al., 2007). The cell wall of AM fungi, as of pathogenic fungi, is build from chitin, a MAMP that is recognized by a least two kinds of plasma membrane integral receptors that contain extracellular LysM-domains (Kaku et al., 2006; Miya et al., 2007). Chitin-induced downstream signaling through the MAPK cascade triggers defense responses (Petutschnig et al., 2010). Yet, it is unclear, whether MAPK cascades are involved in signaling at different stages of mycorrhizal development and how AM fungi manage to evade MAMP-triggered rejection by the plant (Pozo and Azcon-Aguilar, 2007).

At the site of anticipated infection, the hyphal tip forms a flattened structure, called hyphopodium or appressorium. Although the term appressorium suggests that the fungus uses pressure to penetrate the root, it became clear that the plant genetically controls intracellular hyphal accommodation in the rhizodermis and the subjacent cell layer (Duc et al., 1989; Marsh and Schultze, 2001). The passage of the hyphae through the outer cell layers to the cortex of the root is preceded by the PPA, a tubular rearrangement of the cytoskeleton and the endoplasmic reticulum (ER) that determines the route of intracellular infection through rhizodermal and cortical cells (Genre et al., 2005; Genre et al., 2008). Positioning of the nucleus underneath the hyphopodium heralds PPA establishment. The subsequent nuclear movement towards the subjacent cell guides the formation of the cytoplasmic bridge through the vacuole. *Vapyrin*, an AM-induced gene required for successful intracellular accommodation, encodes a protein with a N-terminal VAP/MSP homology domain and C-terminal ankyrin repeats (Pumplin et al., 2010). Although the requirement of

*Vapyrin* for PPA formation is not shown, there might be a functional link. VAMP-associated proteins (VAPs) are integral ER membrane proteins involved in protein-protein interaction and thereby in cellular processes, including vesicle trafficking and microtubule organization. Ankyrin repeats also mediate protein-protein interaction and represent a common motif, encountered in more than 100 proteins predicted from the *Arabidopsis* genome. Subcellular localization of Vapyrin translationally fused to GFP was seen in cytoplasmic dots similar to endosomes (Pumplin et al., 2010).

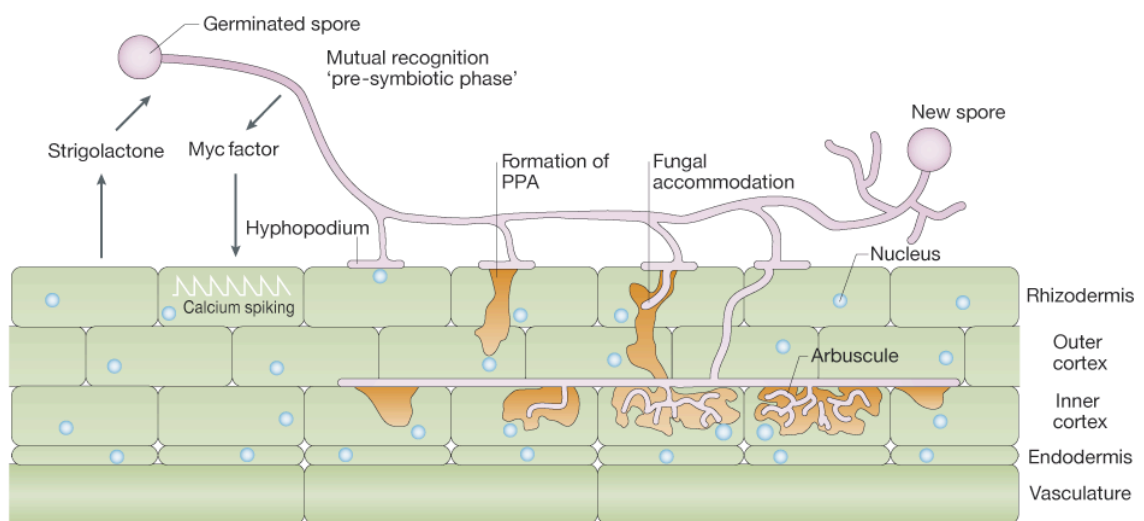


**Figure 1. Development of AM.**

During the pre-symbiotic stage, root exudated strigolactone induces AM fungal spore germination and hyphal branching. In turn, AM fungi secrete the putative Myc factor, which induces rhizodermal  $\text{Ca}^{2+}$  spiking. After contact, a fungal hyphopodium is formed and the plant nucleus migrates to the contact site. Subsequent nuclear movement precedes PPA-formation and intracellular hyphal growth towards the cortex. After the intracellular passage, the hypha spreads in the cortical apoplast. Intracellular arbuscule formation in the inner cortex also involves PPA-like structures. The AM fungal life cycle is completed by the formation of new spores. Figure modified, with permission, from (Parniske, 2008).

The intracellular passage through the outer cortex (Figures 1 and 2B) represents an important control mechanism of hyphal colonization and - in growing roots - cannot be circumvented by intercellular penetration (Demchenko et al., 2004; Genre et al., 2008). Subsequently, AM fungal hyphae enter the apoplastic space, where they spread along the root cortex (Figures 1 and 2C). Branches of apoplastic hyphae enter into cells of the inner root cortex, where the so-called arbuscules are formed. The structure of the arbuscules varies depending on the species combination engaging in symbiosis, the degrees of intracellular ramification ranging from tree-like structures (Arum type; Figure 2B) to hyphal coils (Paris type) (Dickson, 2004). Arbuscule formation involves significant structural reprogramming of cortex cells,

leading to invagination of the plasma membrane and the tonoplast (Cox and Sanders, 1974). Structural changes of the cytoskeleton and the ER, as well as cytoplasmic aggregations partially resemble the PPA arrangements in the outer root cell layers (Genre and Bonfante, 1998; Blancaflor et al., 2001; Genre et al., 2008). Arbuscule development is moreover accompanied by morphological and metabolic changes of plastids and mitochondria (Fester et al., 2001). Activation of plastidic enzymes leads to the synthesis and accumulation of fatty acids and apocarotenoids (Lohse et al., 2005). The latter are carotenoid cleavage products of the methylerythritol phosphate (MEP) pathway and include the metabolites mycorradicin (Klingner et al., 1995), which causes the yellow color of cereal AM, as well as strigolactone (Walter et al., 2007). The parallels between extraradical hyphal branching and arbuscule ramification in the context of apocarotenoid signaling are intriguing. So far, impairment of arbuscule development and reduced induction of AM genes was shown by RNAi-mediated knock down of the *Medicago truncatula* 1-deoxy-d-xylulose 5-phosphate synthase 2 (*DXS2*), encoding a key enzyme of the MEP pathway (Floss et al., 2008). Noteworthy, hyphal colonization levels were not significantly reduced. This contrasts to reduced AM colonization of *ccd8* pea mutants impaired in strigolactone synthesis (Gomez-Roldan et al., 2008), but might be due to activity of the 2<sup>nd</sup> DXS1 isoform.

### **Controlling the Market: Plant Genes Involved in Arbuscule Development**

Two *M. truncatula* genes, *STR* and *STR2*, encoding half-ABC transporters that are required for arbuscule development have recently been reported (Zhang et al., 2010). *STR* represents the first AM-specific gene described, which was identified through forward genetics; *STR2* was subsequently identified by homology searching. Both genes are expressed exclusively in roots and up regulated during AM. *str* mutants and *STR2* RNAi knock down lines were impaired in arbuscule development and hyphal colonization, but not during earlier stages of AM development, e.g. rhizodermal infection. The interaction of *STR* and *STR2* was observed only around the arbuscules. Based on their phylogenetic relation to subfamily members from other plant species and mammals, being involved in the transport of various metabolites, including sterols and other lipids, a transport function for AM-specific apocarotenoids was predicted.

The periarbuscular membrane (PAM), which surrounds the fungal cell wall and the periarbuscular space, is in continuation of the plant plasma membrane and creates



a large surface area for nutrient exchange (Harrison, 2005). The PAM has a distinctive protein content, as evidenced by *in-vivo* localization of the AM-specific phosphate transporter MtPT4 (Pumplin and Harrison, 2009). P<sub>i</sub> transporters that are only expressed during AM belong to one subfamily of the *Pht1* family and have been described from different monocot and dicot species, including *PT11* from rice (Paszkowski et al., 2002), *PT4* from *M. truncatula* (Harrison et al., 2002), tomato and potato, as well as *PT5* from potato (Nagy et al., 2005). Symbiotic P<sub>i</sub> acquisition can contribute for the most part to the plant's P content (Smith et al., 2004). *StPT3* (Rausch et al., 2001), *LjPT3* (Maeda et al., 2006) and *OsPT13* (Paszkowski et al., 2002) are up regulated in AM, but basally expressed under non-AM conditions, whereas several other rhizodermal P<sub>i</sub> transporters were shown to be down regulated during AM. Functional overlap is implied by the multitude of constitutively, AM-induced or AM-suppressed Pht1 transporters present in each species (Nagy et al., 2005; Javot et al., 2007a). Analysis of *StPT3* promoter-GUS expression, *in-situ* localization of *LjPT3* transcripts and immunolocalization of MtPT4 have shown specific expression in arbuscule-containing cells and subcellular targeting to the membrane surrounding the arbuscule branches (Rausch et al., 2001; Harrison et al., 2002; Maeda et al., 2006). Similar expression and localization patterns have previously been observed for P-type H<sup>+</sup>-ATPases from *M. truncatula* and tobacco (Gianinazzi-Pearson et al., 2000; Krajinski et al., 2002). It is likely that these are involved in phosphate transport across the PAM, since *Pht1* family members are P<sub>i</sub>:H<sup>+</sup> symporters that use proton gradients across the plasmamembrane to translocate their substrate (Karandashov and Bucher, 2005). The phenotype of loss-of-function *mtpt4* mutants showed that phosphate transport via the arbuscule is indispensable for full arbuscule development and maintenance of AM (Javot et al., 2007b). Arbuscules are transient structures with a life expectancy of 7 to 10 d until hyphal collapse and degeneration in the cortical cells (Pumplin and Harrison, 2009). Detailed time laps observation of the arbuscule development in *mtpt4* and wild type *M. truncatula* roots revealed that the majority of the arbuscules formed in both genetic backgrounds were of medium size at 3 days after inoculation (DAI) with pre-germinated spores of *G. versiforme*. Three d later the size distribution of arbuscules formed in *mtpt4* mutants was shifted towards smaller values, in contrast to an increase of larger arbuscules in the wild type (Javot et al., 2007b). Since full AM establishment is not supported in *mtpt4*, it is conceivable that the host can discontinue its association with the AM fungus in unprofitable situations. From an

ecological point of view, this would imply a factor of competition among different AM fungi (Javot et al., 2007b; Parniske, 2008).

Defective arbuscule development and reduced hyphal colonization resembling the phenotype of *mtpt4* mutants was recently shown by using *M. truncatula* RNAi lines that exhibited reduced transcript levels of *Sucrose Synthase 1 (SucS1)*. *SucS1* is normally up regulated during fungal and bacterial root symbioses (Baier et al., 2010). Since the RNAi lines showed various pleiotropic defects, it remained unclear, whether the mycorrhizal phenotype was a secondary effect of impaired root metabolic activity and/or carbohydrate source-sink balance, or AM development was incomplete because of the reduced sugar merit for the fungus.

Arbuscules are most likely also the interface for N delivery from AM fungi to plants. It has recently been proposed that the AM fungal contribution to the global N cycle is of considerable amount (Hodge and Fitter, 2010). An amino-acid permease and an ammonium transporter that are probably involved in AM fungal uptake of N from the soil have been identified (Lopez-Pedrosa et al., 2006; Cappellazzo et al., 2008). Lately, non-orthologous ammonium transporters from *Lotus japonicus (Lotus)* and soybean that are transcriptionally activated in arbuscule containing cells have been described (Guether et al., 2009; Kobae et al., 2010). Being part of gene families with several members, they all belong to the AMT2 subfamily of plant ammonium transporters. For *GmAMT4.1*, *in-vivo* localization specifically to the branched region of the PAM has been shown (Kobae et al., 2010).

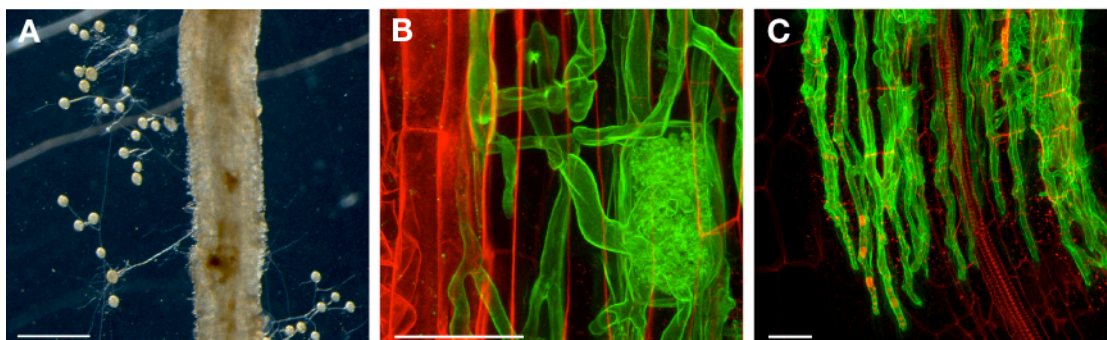


**Figure 2. AM, as Seen by Stereo- and Confocal Microscopy.**

**(A)** Stereomicroscopy image of *Glomus sp.* spores and hyphae connected to carrot root organ culture.

**(B) and (C)** CLSM z-projections of an AM fungal infection site leading to cortical colonization and arbuscule formation (B) and a colonization front formed by apoplastic hyphae in the root cortex (C). Fungal structures (green) were stained with WGA-Alexa Fluor 488 and root cells (red) were counterstained with propidium iodide. Scale bars: (A) 500  $\mu\text{m}$ , (B) and (C) 50  $\mu\text{m}$ .

Moreover, 4 AM-induced subtilisin-like serine proteases (subtilases), which are localized to the apoplastic space surrounding the intraradical hyphae and to the PAS, are involved in AM development. Knock down of *SbtM1* and *SbtM3* in *Lotus* led to reduced hyphal and arbuscular colonization. The substrates of these subtilases are still unknown, but functions comparable to proteases involved in fungal pathogen defense or for weakening of cell-connections were predicted (Takeda et al., 2009).

### **Most Plants Cannot Engage in Root Nodule Symbiosis**

In contrast to the wide spread AM, root nodule symbiosis (RNS) with nitrogen-fixing bacteria occurs only in 4 orders constituting a monophyletic clade within the eudicots, namely the Fabales, Fagales, Cucurbitales and Rosales (FaFaCuRo). RNS therefore must have evolved much later than AM, in a common ancestor of the FaFaCuRo from the late Cretaceous (Soltis et al., 1995; Kistner and Parniske, 2002). One of the two main types of RNS is Actinorrhiza, formed between *Frankia spp.* bacteria and members of the Fagales, Cucurbitales and Rosales. The 2<sup>nd</sup> type is the symbiosis between Legumes and a diverse group of gram-negative bacteria collectively called rhizobia (Markmann and Parniske, 2009). Symbiotic nitrogen fixation is of great agricultural importance: crop legumes include pea, peanut, beans and, last not least, soybean, which in 2007 ranked at 4<sup>th</sup> position after wheat, maize and rice in terms of world area harvested (90 Mha; FAOSTAT, 2009). Moreover, legumes such as clover or vetch are used as green manure in crop rotation (Palm et al., 2010). RNS involves – as the name implies – the development of a symbiosis specific organ, which provides the oxygen-restricted microenvironment for the reduction of atmospheric nitrogen to ammonia by the bacterial nitrogenase (Seefeldt et al., 2009). Nevertheless, AM and RNS share striking similarities in the mechanisms leading to the accommodation of the respective endosymbionts.

### **‘One Ping Only’ – Sending the Right Signal to The Rhizodermis**

Pre-symbiotic crosstalk between rhizobia and legumes leads to rhizobial production of Nod factor (NF) molecules. NFs are amphiphilic molecules generally consisting of 4 or 5  $\beta$ -1,4-linked *N*-acetylglucosamine residues and a *N*-linked fatty acid moiety at the nonreducing end of the chitin backbone. Length and saturation of the fatty acid, as well as further modifications of the terminal glucosamine residues define the host specificity of the rhizobial strain (Denarié et al., 1996). Usually the rhizobial host range is narrow, but broad range strains, e.g. *Rhizobium sp.* NGR234, can infect dozens of

legume genera (Pueppke and Broughton, 1999). On the host side, recognition specificity is provided by the extracellular LysM-domains of transmembrane receptor-like kinases (RLKs) (Radutoiu et al., 2007). In *Lotus*, *LysM-RLKs* belong to a gene family with 17 members (Lohmann et al., 2010), two of which have been identified as NF receptors (*NFR1* and *NFR5*) by forward genetics (Madsen et al., 2003; Radutoiu et al., 2003). Loss-of-function mutants of *NFR1*, as well as *NFR5* and its ortholog from *M. truncatula*, *NFP*, lack any of the physiological and morphological responses to NF observed in the wild type (Amor et al., 2003; Radutoiu et al., 2003).

$\text{Ca}^{2+}$  influx into the root hair cytoplasm is the fastest NF response measured in legumes, followed by  $\text{Cl}^-$  efflux and concomitant membrane depolarization, as well as alkalization of the extracellular space (Ehrhardt et al., 1992; Felle et al., 1998). These transient responses are triggered by nanomolar concentrations of NF within 1 min and persist for several minutes. Moreover, investigation of cytoplasmic  $[\text{Ca}^{2+}]$  by microinjection of a reporter dye into root hairs of alfalfa seedlings revealed persistent and regular oscillations of perinuclear  $\text{Ca}^{2+}$  levels ( $\text{Ca}^{2+}$  spiking) (Ehrhardt et al., 1996). This  $\text{Ca}^{2+}$  signature represents a hallmark of NF signaling and has meanwhile been investigated in 5 different legumes with microscopical, genetic and pharmacological approaches (Oldroyd and Downie, 2008). Although a correlation between  $\text{Ca}^{2+}$  spiking and expression of the early nodulation gene *ENOD11* was established (Miwa et al., 2006a), the function of  $\text{Ca}^{2+}$  spiking in RNS is not resolved so far.  $\text{Ca}^{2+}$  spiking starts about 5 – 10 min after application of picomolar NF concentrations and takes place in up to 90% of the growing root hairs, but also in mature root hairs, atrichoblasts and sub-rhizodermal cells (Miwa et al., 2006a; Sieberer et al., 2009). Applied at nanomolar concentrations, NFs induce a transient increase in cytoplasmic  $[\text{Ca}^{2+}]$  that originates at the root tip ( $\text{Ca}^{2+}$  flux) and precedes  $\text{Ca}^{2+}$  spiking (Shaw and Long, 2003). Chitintetramers, chitinpentamers and NFs with modified decorations were shown to induce repeated  $\text{Ca}^{2+}$  spikes, although these responses were less sensitive and varied between different legume species.  $\text{Ca}^{2+}$  flux however was not observed after application of chitinoligomers and mutated NFs (Walker et al., 2000; Oldroyd et al., 2001b; Shaw and Long, 2003). Further supported by genetic data, it therefore seems that  $\text{Ca}^{2+}$  flux and  $\text{Ca}^{2+}$  spiking are independent responses (Shaw and Long, 2003; Miwa et al., 2006b) downstream of *NFR1* and *NFR5/NFP*-mediated signaling (Amor et al., 2003; Radutoiu et al., 2003).

## Pre-symbiotic AM Fungal Signaling

The eye-catching analogies in AM and RNS suggest that fungal signaling molecules, corresponding to the NF, might be involved in the initiation of AM (Gianinazzi-Pearson and Denarié, 1997). The existence of diffusible AM fungal signals became apparent when *M. truncatula* roots carrying a *GUS* marker fused to the promoter of *ENOD11* stained blue, after the plants were co-cultivated with different AM fungi and physical contact had been prevented by a cellophane membrane (Kosuta et al., 2003). *GUS* expression was not observed upon cultivation with pathogenic fungi, confirming symbiosis specificity of *ENOD11*. Intriguingly, *ENOD11* promoter-*GUS* induction was also observed in the genetic background of symbiosis deficient mutants lacking  $\text{Ca}^{2+}$  spiking (*dmi1* and *dmi2*). Assessed by a similar experimental setup, induction of lateral root formation was observed in wild type plants, but not in *dmi1* and *dmi2* mutants (Olah et al., 2005). Rice mutants of the *DMI1* ortholog, in turn, were not affected in AM-induced lateral root formation (Gutjahr et al., 2009a). Additional evidence for an AM diffusible signal was provided by starch accumulation in *Lotus* roots upon membrane-separated cultivation with an AM fungus (Gutjahr et al., 2009b). The observations raise the impression that different AM fungal factors and signaling pathways are involved in the respective host responses. Recently, *DMI1* and *DMI2*-dependent  $[\text{Ca}^{2+}]$  oscillations were demonstrated in *M. truncatula* root hairs located in the vicinity of branched AM fungal hyphae (Kosuta et al., 2008). The  $\text{Ca}^{2+}$  signatures spatially resembled NF-induced  $\text{Ca}^{2+}$  spiking but differed in their periodicity and duration of individual spikes. In analogy to RNS, LysM-RLKs were suggested as candidates for the recognition of a NF-related hypothetical 'Myc factor' (Parniske, 2008). *nfr1*, *nfr5* and *nfp* mutants are able to form AM, but there are 12 more LysM-RLKs in *Lotus* that are expressed in the root (Lohmann et al., 2010).

Transcriptome analysis of roots at the developmental stage of hyphopodia formation revealed a gene that is transiently up regulated during AM fungal infection and is predicted to encode a membrane steroid-binding protein (*MSBP1*) (Kuhn et al., 2010). Using time-lapse imaging of *M. truncatula* root organ cultures, which were transformed with *GFP-GUS* fused to the promoter of *MSBP1*, it was shown that *MSBP1* is induced in rhizodermal and root cortical cells in the proximity of the AM fungus before hyphal contact. The up regulation of *MSBP1* expression was *DMI2* dependent and RNAi-mediated knock down of *MSBP1* led to impaired arbuscule formation. The results indicate that *MSBP1* is not directly involved in the perception

of the diffusible AM fungal signal, but rather in metabolic changes, which precede AM fungal infection and may be attending PPA formation.

### **Intracellular Accommodation of Rhizobia and AM Fungi Is Controlled by the Common SYM Network**

The discovery that pea and field bean mutants defective in RNS are also impaired in AM provided the first genetic evidence for a shared developmental program (Duc et al., 1989). Genetic dissection of RNS using model legumes, including *Lotus* and *M. truncatula*, revealed host genes that were equally important in AM and therefore termed common SYM genes. Since AM symbiosis is evolutionary older, this led to the idea that the genetic program for intracellular accommodation has been adopted from AM during the evolution of RNS (La Rue and Weeden, 1994; Kistner and Parniske, 2002). Recognition of NFs by NFR1 and NFR5/NFP elicits signal transduction via SYMRK/DMI2/NORK (Endre et al., 2002; Stracke et al., 2002), a receptor kinase with extracellular leucine-rich repeats and the convergence point with AM-induced signal transduction (Figure 3). Unknown downstream events depend on 3 nuclear pore proteins (nucleoporins), NUP133, NUP85 and NENA (Kanamori et al., 2006; Saito et al., 2007; Groth et al., 2010), and presumably lead to membrane potential alterations at the nuclear envelope involving the ion channels CASTOR and POLLUX/DMI1 (Ané et al., 2004; Imaizumi-Anraku et al., 2005; Charpentier et al., 2008) required for Ca<sup>2+</sup> spiking. The Ca<sup>2+</sup> and calmodulin-dependent kinase CCaMK/DMI3 (Lévy et al., 2004; Mitra et al., 2004) in cooperation with the nuclear protein CYCLOPS/IPD3 (Messinese et al., 2007; Yano et al., 2008) may act as decoder of Ca<sup>2+</sup> spiking. The CCaMK-CYCLOPS complex regulates rhizobial infection thread (IT) development, which requires downstream activation of RNS-specific GRAS (NSP1 and 2) (Kaló et al., 2005; Smit et al., 2005; Heckmann et al., 2006; Murakami et al., 2006) and AP2-ERF (ERN1 to 3) transcription factors (Andriankaja et al., 2007; Middleton et al., 2007). These can bind to *cis*-regulatory elements of early nodulins, including *ENOD11* and *NIN*, and thereby regulate target gene expression in response to NF (Andriankaja et al., 2007; Hirsch et al., 2009). *NIN* itself contains domains related to transcription factors, as well as predicted transmembrane domains. Like NSP1 and 2, *NIN* is essential for rhizobial infection (Schauser et al., 1999).

After rhizobia attach to the root hair of a compatible host, redirected growth of the root hair tip is induced by local NF. This leads to root hair curling (RHC) and the

formation of a discrete cavity where a rhizobial microcolony develops. Maybe triggered by the local increase in NF concentration, an IT initiates from the microcolony through local cell wall decomposition and invagination of the plasma membrane, which guides the proliferating rhizobia towards the subepidermal cell layer (Oldroyd and Downie, 2008). Further cortical infection is preceded by the formation of cytoplasmic bridges termed pre-ITs (van Brussel et al., 1992). Nodule organogenesis is tightly coordinated with the progression of infection and endocytosis of rhizobia into nodule cortical cells, where they mature into nitrogen-fixing bacteroids inside organella-like symbiosomes (Van de Velde et al., 2010).

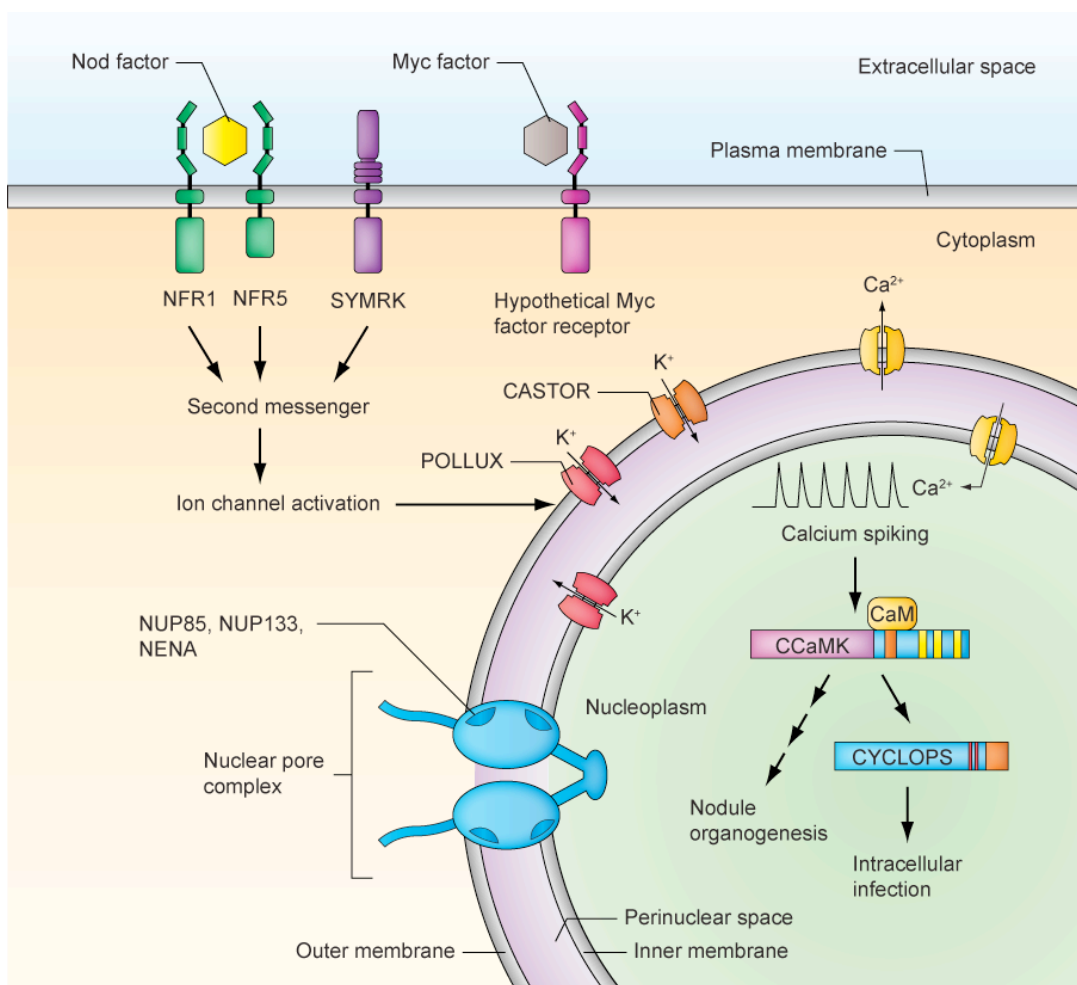


**Figure 3. The Common SYM Signaling Network.**

Intracellular accommodation of rhizobia and AM fungi in the rhizodermis requires at least 8 common SYM genes, as well as specific transmembrane LysM receptor kinases that recognize Nod factors (NFs). Similar recognition of Myc factor (MFs) is believed to occur. Integration of NF and MF signaling by SYMRK probably leads to ion fluxes through CASTOR and POLLUX at the nuclear envelope and nuclear Ca<sup>2+</sup> spiking. Components of the nuclear pore complex are also required for Ca<sup>2+</sup> spiking. CCaMK and CYCLOPS are interacting nuclear downstream components. Modified, with permission, from (Parniske, 2008).

The epistatic nature of genes required for early NF signaling potentially masks tissue-specific processes. Gain-of-function mutations in CCaMK (Gleason et al., 2006; Tirichine et al., 2006a) and the cytokinin receptor LHK1 (Murray et al., 2007; Tirichine et al., 2007) lead to nodulation in the absence of rhizobia, thereby uncoupling infection from nodule formation. NIN and the NSP1 and 2 transcription factors are proposed candidates for coordinating infection with nodule formation, since they are required during NF signaling and for nodulation in autoactive CCaMK mutants (Gleason et al., 2006; Marsh et al., 2007). Natural variation of RNS also provides insights into different prerequisites for infection initiation and nodule development. Aquatic and semi-aquatic legumes from tropical and sub-tropical regions have an intercellular infection mode that does not require intracellular entry through RHC, but utilizes rhizodermal cracks at sites of lateral root emergence (Ndoye et al., 1994). Subsequently, rhizobia proliferate in subepidermal infection pockets that are caused by local apoptosis promoted by reactive oxygen species and ethylene (D'Haese et al., 2003). From there on, infection proceeds inter- and intracellularly and concludes in the release of bacteroids into cortical cells of the nodule. Some legumes, e.g. *Sesbania rostrata*, can switch between intracellular infection during aerated conditions and crack entry during root submergence (Goormachtig et al., 2004).

Disruption of common *SYM* genes typically results in the abortion of fungal infection in the epidermal root layer (Kistner et al., 2005). In addition, dissection of AM development by forward genetic screens in tomato, maize or petunia discerned two additional stages - before fungal infection and during root colonization - that are controlled by the plant (Barker et al., 1998; David-Schwartz et al., 2001; Paszkowski et al., 2006; Reddy et al., 2007). Information about the respective genes is pending.

### **Aim of this Study**

With the genetic resources at hand, i.e. high-resolution linkage maps (Wang et al., 2008), genome sequence covering more than 90 % of the predicted gene content (Sato et al., 2008) and a suitable mutagenized population of the model legume *L. japonicus* (Perry et al., 2009), this study targeted at the identification of genes required for the development of AM. For this purpose, a screen for AM mutants was initiated. Function of the identified genes and interconnection with RNS should be elucidated. The results of this work should be conducive to understanding of the plant's genetics governing the development of intracellular root-microbe symbioses.



## RESULTS

### **A Capillary Sequencer-Based Setup for Microsatellite Genotyping of *Lotus***

#### **Background**

Forward genetics combined with map-based cloning nowadays constitute a straightforward strategy for the identification of new symbiosis genes (Jander et al., 2002). The availability of advanced genetic resources greatly facilitates map-based cloning in *L. japonicus*. Map-based cloning is typically applied in context with mutagenesis induced by chemicals, e.g. the guanine alkylating agent EMS, which produces hundreds of non-tagged point mutations that are randomly distributed across the genome (Greene et al., 2003). In order to identify the mutation responsible for a specific phenotype, co-segregation of the phenotype with defined DNA loci (markers) has to be assessed. Recent technological advances in sequencing made it possible to pinpoint DNA polymorphisms including the causal mutation within a 200 kb interval by deep sequencing with 11x coverage of pooled DNA from 500 mutant siblings of a segregating population (Lister et al., 2009; Schneeberger et al., 2009). Although the potential of this innovative strategy for identification of new gene functions is beyond dispute, deep sequencing is unnecessary and too elaborate for the determination of allelic groups, which usually precedes gene mapping in forward genetic studies.

Map-based cloning requires a genetic map generated by recombination analysis of genetic markers within a mapping ( $F_2$ ) population (Peters et al., 2003). Since recombination frequency is proportional to the distance between two loci (Sturtevant et al., 1919; Ohmido et al., 2010), the degree of linkage between a genetic marker and the mutant phenotype indicates the genetic location of the causal mutation. In practice, map based-cloning proceeds in two phases: During rough mapping, the chromosomal location of the causal mutation is delineated by collecting mutants from a population of 100-200  $F_2$  individuals and subsequent genotyping of the mutants, in order to identify those markers showing a co-segregation of alleles from the mutant (Gifu) background. Thereby, mutants affected in already known symbiosis genes are identified through sequencing of linked candidate genes. By this, tedious determination of complementation groups through crossing becomes obsolete (e.g. considering the amount of crosses required to test for allelism with the common *sym* mutants). During the 2<sup>nd</sup> phase of map-based cloning, the co-segregating target

region is narrowed down to a contiguous sequence interval containing a limited number of candidate genes to be tested by sequencing or transgenic complementation. This is achieved by screening for individuals, which carry recombination events between markers flanking the target region and lying apart in the range of 1 cM. The size of the population to be screened increases dramatically with decreasing recombination intervals anticipated beyond 50 kb, as simulated for *Arabidopsis*, given a recombination frequency of 250 kb/cM (Jander et al., 2002). To this end, genotyping or phenotyping of 3000-4000 F<sub>2</sub> individuals is recommended.

*L. japonicus* ecotype B-129 (Gifu), which has been used for mutagenesis in order to generate TILLING populations (Perry et al., 2009), exhibits approximately 5 % overall nucleotide sequence polymorphism to ecotype MG-20 (Miyakojima) based on AFLP analysis (Hayashi et al., 2001). High-resolution linkage maps were derived from Gifu x MG-20 populations and the segregation of different chromosomal regions has been described in detail (Hayashi et al., 2001; Sandal et al., 2005; Wang et al., 2008). Crosses between wild type MG-20 and Gifu mutants have been successfully used in previous map-based cloning projects, which led to the identification of *SYMRK* and numerous symbiotic genes thereafter (Kawaguchi et al., 2001; Stracke et al., 2002; Sandal et al., 2005). MG-20 is subject of the *Lotus* genome-sequencing project and most parts of the genome covering more than 90 % of the predicted gene content have been sequenced (Sato et al., 2008). As a result, genetic positions, allele sizes and sequence information of 782 genetic markers for the MG-20 x Gifu cross are currently available via the miyakogusa.jp website (<http://www.kazusa.or.jp/lotus/>). Moreover, most markers are located in large sequence assemblies (contigs), which greatly facilitate the forthwith delineation of the physical target region containing the causative mutation and the assignation of candidate genes.

### **Using Capillary Instead of Agarose Gel Electrophoresis**

The use of capillary electrophoresis for microsatellite marker genotyping has been documented (Mansfield et al., 1996). Genotyping by capillary array electrophoresis has been implemented for many species, including soybean (Oliveira et al., 2010), and commercial kits are available, e.g. for horse, cattle and dog (StockMarks, Applied Biosystems). In collaboration with the in house sequencing facility, we have established a high throughput *Lotus* genotyping setup, named 'power mapping', capable of processing 512 PCR samples per hour. Using two standard sets of 24

simple sequence repeat (SSR) markers that are evenly distributed over the 6 linkage groups (LGs) of the *Lotus* genome (Figure 4 and Supplemental Table 4) comprising approx. 480 cM in total (Sandal et al., 2005), determination of a rough mapping position for a novel mutant locus was accomplished within 7 workdays. Prerequisite was the isolation of genomic DNA from at least 16 monogenic recessive F<sub>2</sub> mutants that had been identified from an established mapping population.

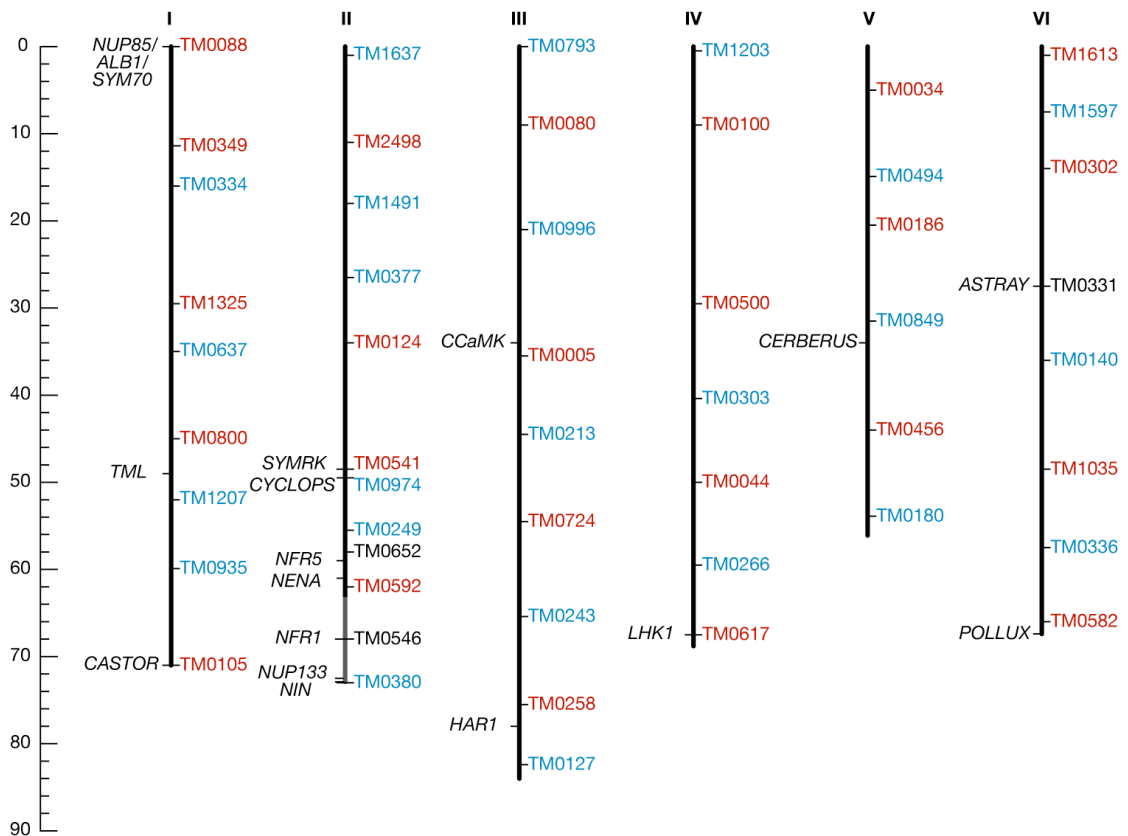


**Figure 4. Genetic Positions of 'Power Mapping' Markers and Symbiosis Genes.**

LGs are indicated by roman numerals. The scale to the left indicates cM. 1<sup>st</sup> and 2<sup>nd</sup> rough mapping set are indicated in red and blue, respectively. References: *ALB1* (Yano et al., 2006), *ASTRAY* (Nishimura et al., 2002a), *CASTOR*&*POLLUX* (Imaizumi-Anraku et al., 2005), *CCaMK* (Tirichine et al., 2006b), *CERBERUS* (Yano et al., 2009), *CYCLOPS* (Yano et al., 2008), *KLAVIER* (Oka-Kira et al., 2005), *LHK1* (Murray et al., 2007; Tirichine et al., 2007), *NENA* (Groth et al., 2010), *NFR1* (Radutoiu et al., 2003), *NFR5* (Madsen et al., 2003), *NIN* (Schäuser et al., 1999), *NUP133* (Kanamori et al., 2006), *NUP85* (Saito et al., 2007), *SYMRK* (Stracke et al., 2002), *SYM70* (Murakami et al., 2002), *TML* (Magori et al., 2009).

Power mapping takes advantage of automated detection and analysis of SSR polymorphisms by the ABI3730 (Applied Biosystems) 48 capillary sequencer in conjunction with the GeneMapper software (version 3.7). With this technique, fluorescent-labeled DNA fragments are electrophoretically injected and size-

separated through polymer-coated capillaries (Barbier and Viovy, 2003). Size-dependent migration of the DNA fragments is recorded by the defined excitation and detection of fluorescence labels (Mansfield et al., 1996).

In order to fluorescently label PCR products for automatic detection, we have adopted a single-PCR approach that uses one universal fluorescence-labeled primer with 17 or 18 nucleotides (A-primer) and two marker-specific primers (AF- and R-primer), of which the AF-primer has an additional 5' tail that is sequence-identical to the universal primer (Schuelke, 2000). Two PCR conditions had been empirically determined to be decisive for the quality of the fluorescent amplification product: Firstly, the amount of A-primer should be 4x the amount of AF-primer, while the amount of A-primer and AF-primer together should equal the amount of R-primer. Secondly, the melting temperatures of the marker specific primer sequences should be at least 3°C higher than the melting temperature of the A-primer. Together, these factors ensured that SSR markers were specifically amplified during the first 28 PCR cycles and labeled during the subsequent 8 cycles of amplification that were performed with 3 °C lower annealing temperature. The advantage of using universal fluorescent primers is primarily cost saving, due to the higher turnover of universal primers compared to marker specific primers (especially those that are merely used for a specific mapping purpose). Fluorescent labels compatible with the in house sequencing utility comprise the Dye Set G5 (6-FAM, PET, NED, VIC and LIZ for the size standard; DS-33 Matrix, Applied Biosystems) and Dye Set F (5-FAM, JOE, NED and ROX for the size standard; DS-32 Matrix, Applied Biosystems). For power mapping, we have designed 4 different universal primers, each of which was labeled with a different dye of the Dye Set G5. Thereby, multiplex amplification of 4 markers is theoretically possible. In practice, PCR amplification of two SSR markers was accomplished for the purpose of recombination screening (Table 1).

**Table 1.** Multiplex PCR for Marker Combination G69/70

Positive <sup>a</sup>	2114
Negative <sup>a</sup>	37
Success Rate <sup>b</sup>	98.3%
False Positives <sup>c</sup>	5.3%

<sup>a</sup>Number of PCRs leading to successful (positive) or unsuccessful (negative) allele calling.

<sup>b</sup>Percentage of positive/total number of PCRs.

<sup>c</sup>Percentage of allele calls/PCRs without template (n=152).

The automated determination of alleles (allele calling) from MG-20 or Gifu by defined fragment sizes and fluorescence labels of individual SSR markers in the GeneMapper software greatly speeds up genotyping analyses. The digitalized readout is transferable to spreadsheet programs for further evaluation of co-segregation. All markers were tested for reliability of allele calling and replaced if necessary (Supplemental Table 4). Three factors turned out to be critical for correct allele calling and, consequently, the expenditure of time for manual readjustment: In the 1<sup>st</sup> place, large differences in fluorescence intensity of Gifu and MG-20 alleles from heterozygous individuals led to allele calling failures. The differences were due to discrimination of the shorter allele in heterozygous samples and behaved roughly proportional to the size difference between the alleles (Figure 5A). In order to reduce allele-specific discrimination, the reaction conditions were optimized by increasing salt concentrations to 1.5 X PCR buffer and reducing the elongation temperature to 70 °C (Henegariu et al., 1997). Secondly, 'plus A' artifacts generated by the *Taq* DNA polymerase-catalyzed addition of a single adenosine to the 3' end of PCR products (Clark, 1988) sometimes led to false allele calling. The addition of 3' adenosine is sequence dependent and can be modified by the complementary strand through the 5' nucleotide sequence of the reverse primer (Brownstein et al., 1996). For unknown reasons, the ratio of plus A fragments varied between samples or reactions at equal cycling conditions. Consequently, plus A artifacts were problematic if they led to double peaks of approximately the same height, which were both detected by the allele calling algorithm (Figure 5B) (Smith et al., 1995). In order to avoid double allele calls, extension of the final elongation step at 72 °C to 30 min was sufficient for the addition of 3' adenosine to the majority of PCR products of most markers. The 3<sup>rd</sup> source of allele calling mistakes was background noise created by unspecific or additional PCR products within the size range of the marker alleles. The level of background noise depended on marker-specific amplification efficiency, which in turn was sensitive to template quality and concentration. Markers with bad amplification efficiency had to be replaced.

Currently, the power mapping setup comprises 170 SSR markers (further information is available at the Genomics Service Unit, Biocenter LMU Munich), which have been established in the course of different mapping projects (Maekawa-Yoshikawa et al., 2009; Perry et al., 2009; Groth et al., 2010).

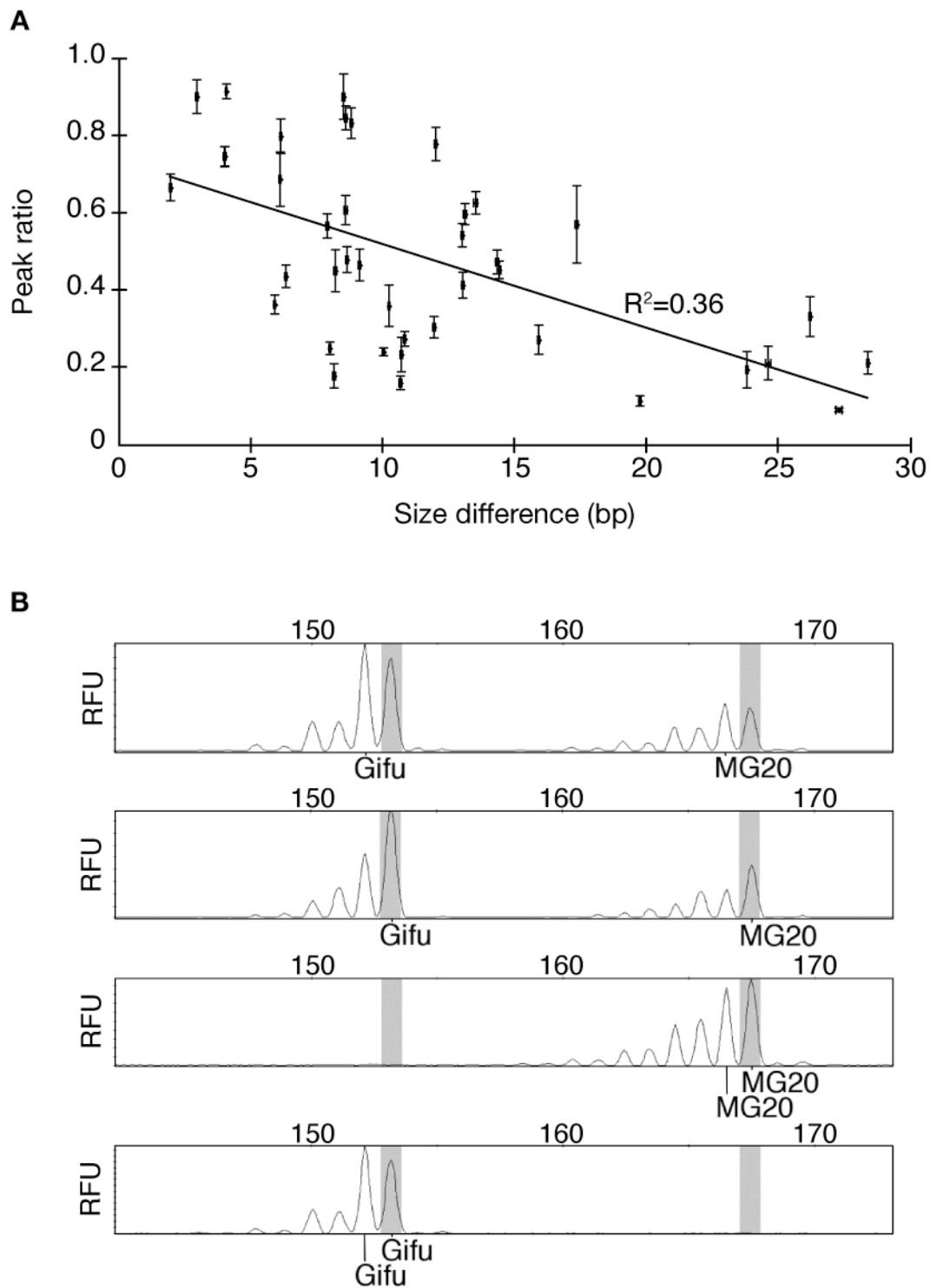


**Figure 5. Pitfalls for Automated Allele Calling.**

**(A)** The ratio of relative fluorescence units (RFU) detected from PCR product corresponding to the shorter allele divided by the RFU level of the longer allele (peak ratio) from heterozygous samples roughly correlates negatively with the size difference between the alleles. Small peak ratios can lead to false allele calling.

**(B)** Electropherograms of two heterozygous and two homozygous samples and the corresponding allele calling results (Gifu and/or MG20). Height variation of the plus-A peak (grey bars) can lead to erroneous double allele calls. Numbers indicate fragment sizes.

## **Genetic Dissection of AM Development by Screening for AM Mutants in *Lotus***

The BULK population used for screening for AM mutants consisted of 2131  $M_3$  families (SL lines) (Figure 6). TILLING data acquired from the GENPOP indicated a 1/10 ratio of homozygous vs. heterozygous EMS-induced mutations in the  $M_2$  generation (Perry et al., 2009). Meiotic recombination consequently would lead to an average distribution of one homozygous vs. 1.4 heterozygous mutations in the  $M_3$  generation, if no homozygous mutants were lost due to deleterious effects (Supplemental Figure 14). Moreover, bulked propagation of  $M_2$  siblings that belonged to the same SL line diminished the probability of losing mutations due to meiotic recombination in the  $M_3$  BULK population. In order to minimize the risk of missing monogenic recessive alleles below 2%, while maintaining a feasible number of individuals to be screened, 8 plants per  $M_3$  family were analyzed during the 1<sup>st</sup> AM screen (Figure 6). For that purpose, individual root samples were inspected under a stereomicroscope for differences in the abundance and shape of AM structures compared to the wild type by the following criteria: (1) hyphae growing outside or on the surface of the root, (2) hyphopodia, (3) infection, (4) hyphae inside the root, (5) arbuscules and (6) vesicles. The AM screen has been performed in succession by Sonja Kosuta, Martin Groth (author) and Kristina Haage. For the sake of completeness, the joint results are summarized herein after and the authors' contributions are specified. Using an AM staining protocol that has been adapted to 96-well format (Marquez and Stougaard, 2005) it was possible to screen up to 192 root samples per day and person. In total, 617  $M_3$  families (approx. 5000 root samples) were analyzed by the author (Supplemental Table 1); the rest of the BULK population was screened in equal parts by Sonja Kosuta and Kristina Haage. During the 1<sup>st</sup> round of the AM screen 229 SL lines containing individuals with aberrant AM structures were identified as putative mutants, of which 76 have been identified by the author (Supplemental Tables 1 and 2). In order to confirm the mutant phenotypes in the next generation, self-progeny of 150 putative mutants were grown, while the remaining  $M_3$  mutants did not produce offspring due to pleiotropic defects and/or premature death. A subset of the putative mutant lines without offspring was AM phenotyped by re-screening remaining  $M_3$  seed. Eight siblings from each of the 140  $M_4$  lines from individual  $M_3$  putative mutants were AM phenotyped by stereomicroscopy during a 2<sup>nd</sup> round of screening. Finally, 14 mutant lines were confirmed and assigned to the AMPOP (Figure 6, Supplemental Figure 13 and Supplemental Table 2),

whereas the remaining putative mutant lines did not show aberrant AM structures or did not reproduce the original phenotype. The high level of non-confirmations (>90% of putative mutant lines) might have been caused by inhomogeneity of the fungal inoculum that led to weak AM colonization of AM wild type SL lines during the 1<sup>st</sup> AM screen (false positives), in addition to non-heredity of the putative mutant phenotype for unknown reasons.

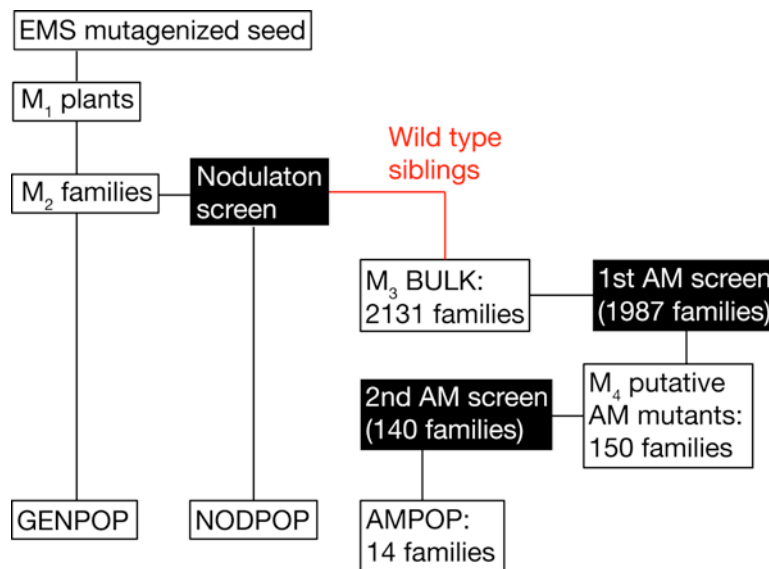
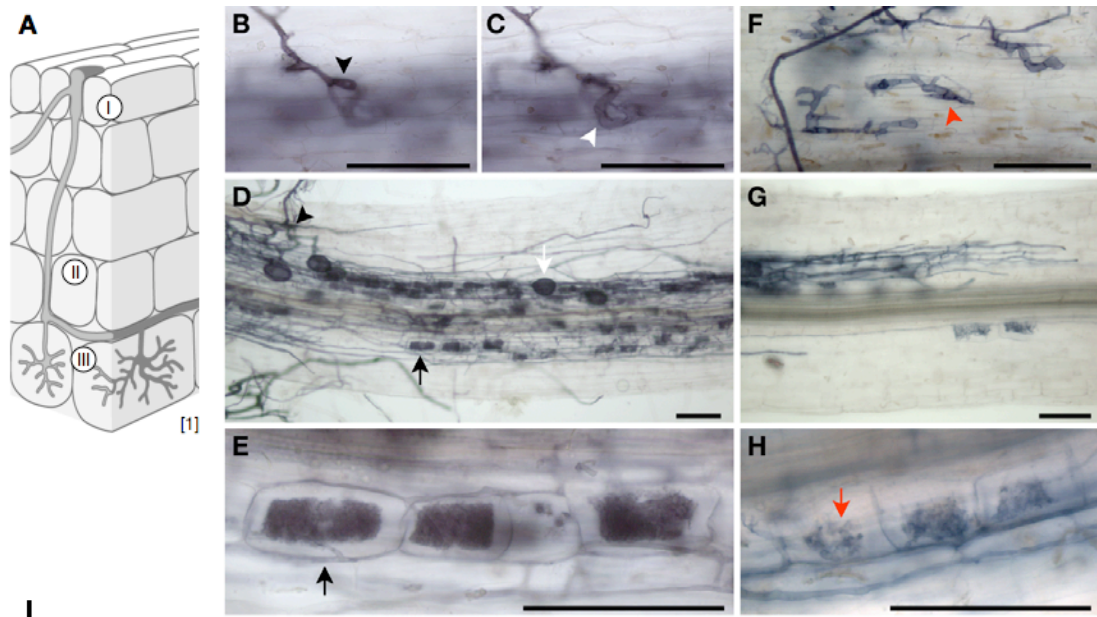


**Figure 6. Relationship of Identified AM Mutants (AMPOP) to the *Lotus* TILLING Populations (GENPOP and NODPOP) (Perry et al., 2009).**

The population used for AM mutant screening (M<sub>3</sub> BULK) consists of 2131 families. Each family originates from bulked M<sub>2</sub> siblings from individual M<sub>2</sub> families that did not show nodulation defects during the nodulation screen (Perry et al., 2003). During the AM screens, 8 siblings per family were analyzed.

Based on the confirmed mutants we could distinguish 3 phenotypic classes (Figure 7): (I) The 1<sup>st</sup> class comprised 4 mutant lines, which had abundant AM fungal hyphae growing on the root surface but almost no hyphae colonizing the root interior. This was due to impaired AM fungal penetration of the outer cell layers leading to balloon-like hyphal swelling and concomitant abortion of infection. (II) 4 lines containing mutants with impaired hyphal colonization were accounted to the 2<sup>nd</sup> class. Mutants from 3 lines showed successful AM fungal infection but strongly reduced colonization of the root cortex, compared to the wild type. Conversely, mutants belonging to SL0989-N were excessively colonized by hyphae and arbuscules. Arbuscule formation was unaffected in the first two mutant classes. (III) The 3<sup>rd</sup> mutant class comprised 6 lines that were impaired in arbuscule formation, while being unapparent regarding AM fungal infection of the rhizodermis.





Developmental stage	Mutant line (designation)	F2 segregation WT:mutant (P[χ])	Co-segregating marker (LG, cM)	Mutant allele [Reference]
I. Intracellular infection	SL1345-N	289:84 (P[3:1]=0.27)	TM0974 (II, 49.3)	<i>cyclops-5</i> [3,6]
	SL1841-N ( <i>nena</i> )	201:75 (P[3:1]=0.40)	SSR17 (II, 60.9)	<i>nena-1</i> [2]
	SL1856-N	46:16 (P[3:1]=0.88)	TM0191 (II, 72.5)	<i>nup133-21</i> [3,4,5]
	SL2042-N	-	-	<i>pollux-20</i> [3]
II. Colonization	SL0989-N	83:31 (P[3:1]=0.59)	-	unknown
	SL1013-N	44:25 (P[3:1]=0.03)	-	unknown
	SL1755-N	-	-	unknown
	SL1816-N ( <i>patchy</i> )	365:121 (P[3:1]=0.96)	TM0885 (VI, 67.4)	<i>pollux-7</i> [7]
III. Arbuscule formation	SL0154-N ( <i>dis</i> )	-	-	unknown
	SL0181-N ( <i>red</i> )	496:262 (P[3:1]<0.01)	TM0553 (VI, 1.7)	unknown
	SL0289-N ( <i>small</i> )	-	-	unknown
	SL1266-N	-	-	unknown
	SL1439-N	111:52 (P[3:1]=0.04)	-	unknown
	SL1864-N	16:16 (P[3:1]<0.01)	-	unknown

**Figure 7. Genetic Dissection of AM Development by the *Lotus* AM Mutant Screen.**

**(A)** Three developmental stages were discerned by the AM mutant phenotypes: (I) Intracellular infection of the outer root layers, (II) colonization of the root cortex and (III) arbuscule formation.

**(B) to (H)** BF light micrographs of ink-stained AM fungal structures in wild type (B to E) and mutant (F to H) root samples. In the WT, a hyphopodium (black arrowhead) was formed on the root surface (B), from where the hypha penetrated (white arrowhead) the outer root layers. From the infection site (black arrowhead) hyphae colonized the root cortex, where arbuscules (black arrows) and vesicles (white arrow) were formed (D). Mature arbuscules with highly branched hyphae originating at the arbuscule trunk (black arrow) filled the cortical cells. Mutants impaired during intracellular infection showed aborted infection events (red arrowhead) accompanied by balloon-like hyphal swelling (F, SL1856-N mutant shown). Defective colonization was manifested by attenuated hyphal spreading in the root cortex (G, SL1816-N mutant shown). No mature arbuscules were observed in mutants with defective arbuscule formation (red arrow, H, SL1439-N mutant shown). Scale bars: 100μm.

**(I)** Segregation analysis of the mapping populations from the respective mutant lines and identified mutant loci are indicated. [1] Modified from (Parniske, 2004), [2] (Groth et al., 2010), [3] (Perry et al., 2009), [4] (Kanamori et al., 2006), [5] (Schäuser et al., 1998), [6] (Yano et al., 2008), [7] (Imaizumi-Anraku et al., 2005). <sup>a</sup> Analyzed by K. Haage.

In order to delineate the genetic positions of the causative mutations of the AMPOP lines, a map-based cloning strategy has been adopted. Causative mutations in previously described symbiotic loci were identified relatively quickly by power mapping and sequencing of candidate genes. The AM mutant phenotypes of SL0989-N, SL1013-N, SL1439-N, SL1755-N and SL1864-N mutants were poorly pronounced or not observed by stereomicroscopy of ink-stained root samples in F<sub>2</sub> mapping populations, impeding co-segregation analyses in these lines (Figure 7).

## Genetics of the Dimorphic Arbuscular Mycorrhiza Phenotype Encountered in the Arbuscule Formation Mutant Line SL0181-N

### Background

Three lines from the *Lotus* TILLING BULK population, SL0154-N, SL0181-N and SL0289-N, with individuals impaired in arbuscule development have been identified by S. Kosuta in the course of the AM mutant screen. Complementation crosses indicated that different loci were affected in all 3 mutant lines (Table 2, Kosuta unpublished). The AM phenotypes displayed were heritable in self-progeny and no pleiotropic defects were observed during further examinations, including a preliminary nodulation test by inoculation with *M. loti*. A detailed analysis of the AM phenotype, involving light microscopy of ink-stained roots, as well as scanning and transmission electron microscopy of root segments and histological sections containing AM structures, was performed (Kosuta unpublished).

**Table 2.** Complementation analysis between three mutants impaired in arbuscule formation<sup>a</sup>

Mutant (SL line)	<i>red</i> (SL0181)	<i>small</i> (SL0289)	<i>dis</i> (SL0154)
<i>red</i> (SL0181)	-	N/A	WT (6/2)
<i>small</i> (SL0289)	WT (7/2)	-	WT (1/1)
<i>dis</i> (SL0154)	WT (7/2)	WT (4/1)	-

<sup>a</sup> Arbuscule phenotype of F<sub>1</sub> plants, WT = wild type, and, in parentheses, the number of F<sub>1</sub> individuals tested / the number of crosses. (Kosuta, unpublished)

Light microscopy revealed clear differences in AM fungal colonization patterns of wild type and SL0181-N mutant roots (Figure 8A). In wild type roots cultivated in chive nurse pots with *G. intraradices*, the inner cortex was densely colonized with hyphae and arbuscules that seemed square, as they filled nearly the entire space within individual cells. In SL0181-N mutants, internal hyphae and vesicles were abundant, but no mature arbuscules were detected. Arbuscule-like structures resembled trees with lopped-off branches (Figure 8A). Similar phenotypes were observed in plants inoculated with the AM fungus *Gigaspora rosea*. Electron micrographs indicated that the arbuscule formation defect resulted from premature collapse of the hyphal structures, resembling arbuscule senescence in wild type roots (Figure 8C to F), rather than stunted arbuscules due to a suppression of further hyphal branching and intracellular colonization. Consequently, hyphae inside cortical

cells of SL0181-N mutants occupied only a limited space and were less ramified, compared to the wild type (Figure 8G to I). Quantification of AM structures 10 d after cultivation with *G. intraradices* showed a general reduction at different stages of AM development, including hyphopodia formation, infection, arbuscule and vesicle formation. Yet, most prominent in comparison to wild type levels was the reduction in arbuscule numbers (Figure 8B). The phenotype of SL0181-N mutants was designated *red*, for *reduced and degenerate arbuscules*.

With regards to the other two lines, SL0154-N and SL0289-N, degeneration of the arbuscules was strongest in *red* mutants. SL0154-N mutants formed arbuscules that consisted of irregular shaped coils instead of the regularly branched hyphae observed in the wild type, and the phenotype was designated *dis*, for *disorganized arbuscules*. The arbuscules formed in SL0289-N mutants retained a tree-like structure but were smaller than wild type arbuscules, due to an attenuated ramification. The phenotype of SL0289-N mutants was designated *small*. Further investigation and identification of the causative mutations in *dis* and *small* was taken charge by Sonja Kosuta, whereas map-based cloning of the hypothetical *red* locus became matter of the present PhD work. Analysis of *red* was furthermore integral part of the laboratory internship of Syndi Vieweg and the diploma thesis of Sebastian Wilhelm, which were performed under the supervision of Martin Parniske and the author. Through detailed segregation analysis of the AM phenotype in different mapping populations we obtained data suggesting that the parental *red* mutant was a dihybrid. Genotyping of the respective F<sub>2</sub> and F<sub>3</sub> individuals indicated that one of the mutations causing defective arbuscule formation is located on the short arm of chromosome VI. The target region furthermore showed a distortion of segregation, which was not observed previously in wild type F<sub>2</sub> populations derived from the intraspecific cross between *L. japonicus* Gifu and MG-20 (Hayashi et al., 2001).

---

**Legend continuation, Figure 8 (G) to (I)** Scanning electron micrographs of *G. intraradices*-infected wild type and *red* mutant roots. In wild type (G), turgid young arbuscule branches were distributed throughout the host cell (arrowheads). In *red* (H and I), intracellular hyphae crossed host cells from several directions (H) and arbuscule branches (arrowheads) were spatially restricted (I).

Scale bars: (A) 100 µm and 10 µm (arbuscule close ups), (C) to (F) 2 µm, (G) to (I) 10 µm.

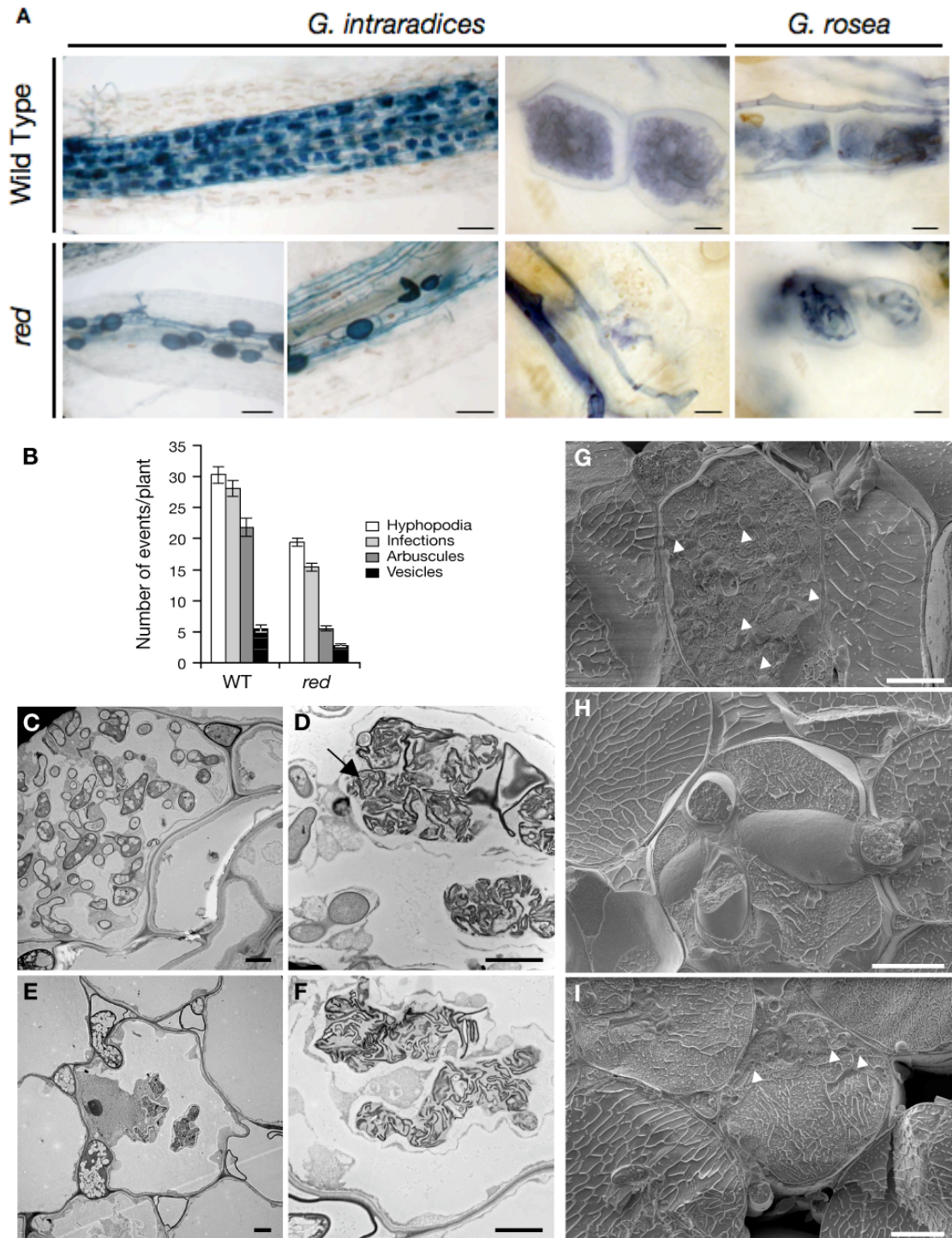


**Figure 8. AM Phenotype of red (Kosuta, unpublished).**

**(A)** BF light micrographs of ink stained AM fungal structures in roots from wild type plants and *red* mutants co-cultivated with *Glomus intraradices* or *Gigaspora rosea* for 5 w.

**(B)** Numbers of AM events observed on wild type and *red* roots at 10 d after cultivation in chive pots with *G. intraradices*. Mean and standard errors (SE) of 6 to 12 replicate plants.

**(C) to (F)** Transmission electron micrographs of *G. intraradices*-infected roots. In the wild type, young arbuscule branches filled the available space in the host cell (C) and granular electron-dense material (arrow) was observed between adjacent branches of collapsed arbuscule (D). In *red*, only spatially restricted arbuscular branches were observed (E), resembling collapsed wild type arbuscule, except that electron dense material was absent in *red* mutant roots (F). (Figure legend continues on left page.)



## Phenotypic Analysis of *red* F<sub>2</sub> Individuals Reveals Two Different Arbuscule Traits

Two mutant M<sub>3</sub> individuals, J849 and J850 (lab internal nomenclature), were originally identified in the line SL0181-N during the AM screen. In order to determine the segregation and genetic position of *red*, J849 was crossed with a wild type individual of *L. japonicus* MG-20, giving rise to the F<sub>1</sub> siblings J5149 and J5150. All self-progeny used for mapping of *red* originated from these two F<sub>1</sub> individuals. AM phenotypes of F<sub>2</sub> individuals were assessed 3 w after cultivation in chive nurse pots with '*G. intraradices*-like' BEG195 (Stockinger et al., 2009). The segregation of the arbuscule phenotype varied considerably between sub-populations originating from different seed bags (Table 3). In order to distinguish the segregation patterns, the results from different sub-populations were grouped according to their F<sub>1</sub> parent. Thereby it became apparent that the ratios of wild type vs. arbuscule mutant individuals were mostly close to or exactly 3/1 (corresponding to a monogenic recessive mutation) in sub-populations originating from J5150. In contrast, 4 out of 6 sub-populations originating from J5149 showed segregation ratios that differed significantly from the Mendelian 3/1 segregation, indicating that the arbuscule phenotype observed is not a monogenic recessive trait.

The contrasting segregation ratios might imply that J5149 contained a 2<sup>nd</sup> mutation, which caused the surplus of mutants in its F<sub>2</sub> progeny, compared to the F<sub>2</sub> progeny of J5150. According to the  $\chi^2$  test, the segregation of wild type vs. arbuscule mutant individuals in 5 out of 6 sub-populations, as well as in the sum of all sub-populations originating from J5149 conforms to a 9/7 distribution (Table 3). This would be expected if J5149 was dihybrid and each of the two unlinked recessive mutant loci would have caused an arbuscule defect. Although differences in the arbuscule defects displayed by F<sub>2</sub> mutants were noticed during screening of the 1<sup>st</sup> 3 sub-populations, individual frequencies of the two distinguishable traits (Figure 9) were not thoroughly recorded, since dihybrid segregation was unexpected and discrimination of the different phenotypes was doubtful. Individuals accounted to the weak class did not contain fully developed wild type-like arbuscules but displayed a reduced level of hyphal ramification in root cortex cells (Figure 9B, D and G), similar to the arbuscule defects observed in M<sub>4</sub> progeny of the SL0181-N mutant J850 (Figure 9A). Mutants with a severe phenotype contained cortical runner hyphae but were apparently void of arbuscular structures, when inspected with the

**Table 3.** Segregation Ratios in Different F2 Sub-Populations of *red*.

F1 Plant	F2 Seed bag	WT	Mutant <sup>a</sup>	Severe <sup>a</sup>	Weak <sup>a</sup>	Total	P(3:1) <sup>b</sup>	P(9:7) <sup>b</sup>	P(9:6:1) <sup>b</sup>
J5149	53594	55	62	-	-	117	3x10 <sup>-12</sup>	0.044	-
J5149	53776	53	29	-	-	82	0.030	0.126	-
J5149	55615	137	84	-	-	221	8x10 <sup>-6</sup>	0.085	-
J5149	56244	20	18	3	15	38	0.001	0.653	0.864
J5149	58524 <sup>c</sup>	13	2	0	2	15	0.297	0.018	0.057
J5149	54687	20	11	1	10	31	0.178	0.354	0.589
<b>J5149</b>	<b>Sum</b>	<b>298</b>	<b>206</b>	<b>4</b>	<b>27</b>	<b>504</b>	<b>2x10<sup>-16</sup></b>	<b>0.193</b>	<b>0.440</b>
<b>J5149</b>	<b>Sub-sum<sup>d</sup></b>	<b>285</b>	<b>204</b>	<b>4</b>	<b>25</b>	<b>489</b>	<b>1x10<sup>-17</sup></b>	<b>0.365</b>	<b>0.957</b>
J5150	53601	111	37	-	-	148	1.000	4x10 <sup>-6</sup>	-
J5150	55591	140	50	-	-	190	0.675	1x10 <sup>-6</sup>	-
J5150	56243 <sup>c</sup>	10	0	0	0	10	0.068	0.005	0.020
J5150	58522 <sup>c</sup>	9	1	0	1	10	0.273	0.031	0.097
J5150	54685	28	7	1	6	35	0.495	0.005	0.018
<b>J5150</b>	<b>Sum</b>	<b>298</b>	<b>95</b>	<b>1</b>	<b>7</b>	<b>393</b>	<b>0.705</b>	<b>5x10<sup>-15</sup></b>	<b>7x10<sup>-5</sup></b>
<b>J5150</b>	<b>Sub-sum<sup>e</sup></b>	<b>279</b>	<b>94</b>	<b>1</b>	<b>6</b>	<b>373</b>	<b>0.929</b>	<b>5x10<sup>-13</sup></b>	<b>0.018</b>

<sup>a</sup> Number of individuals with impaired arbuscule formation, showing the severe phenotype, weak phenotype or either of the mutant phenotypes.

<sup>b</sup> Probability of the  $\chi^2$  test for goodness of fit of the observed segregation ratio to the theoretical ratio indicated in brackets (WT:Mutant or WT:Weak:Severe).

<sup>c</sup> Segregation in these sub-populations might be biased due to > 50% loss of individuals.

<sup>d</sup> Number of individuals from all seed bags except seed bag 58524.

<sup>e</sup> Number of individuals from all seed bags except seed bags 56243 and 58522.

stereomicroscope at < 50x magnification (Figure 9E). At higher magnification, arbuscule trunk-like hyphae were visible (Figure 9H). Both mutant phenotypes were furthermore characterized by the presence of septa in the root internal hyphae (Figure 9G and H). Septation of the coenocytic AM fungal mycelium occurs during retraction of the cytoplasm and is therefore an indication of dead hyphal sectors and non-functional mycorrhizal associations (Gerdemann, 1968; Javot et al., 2007b).

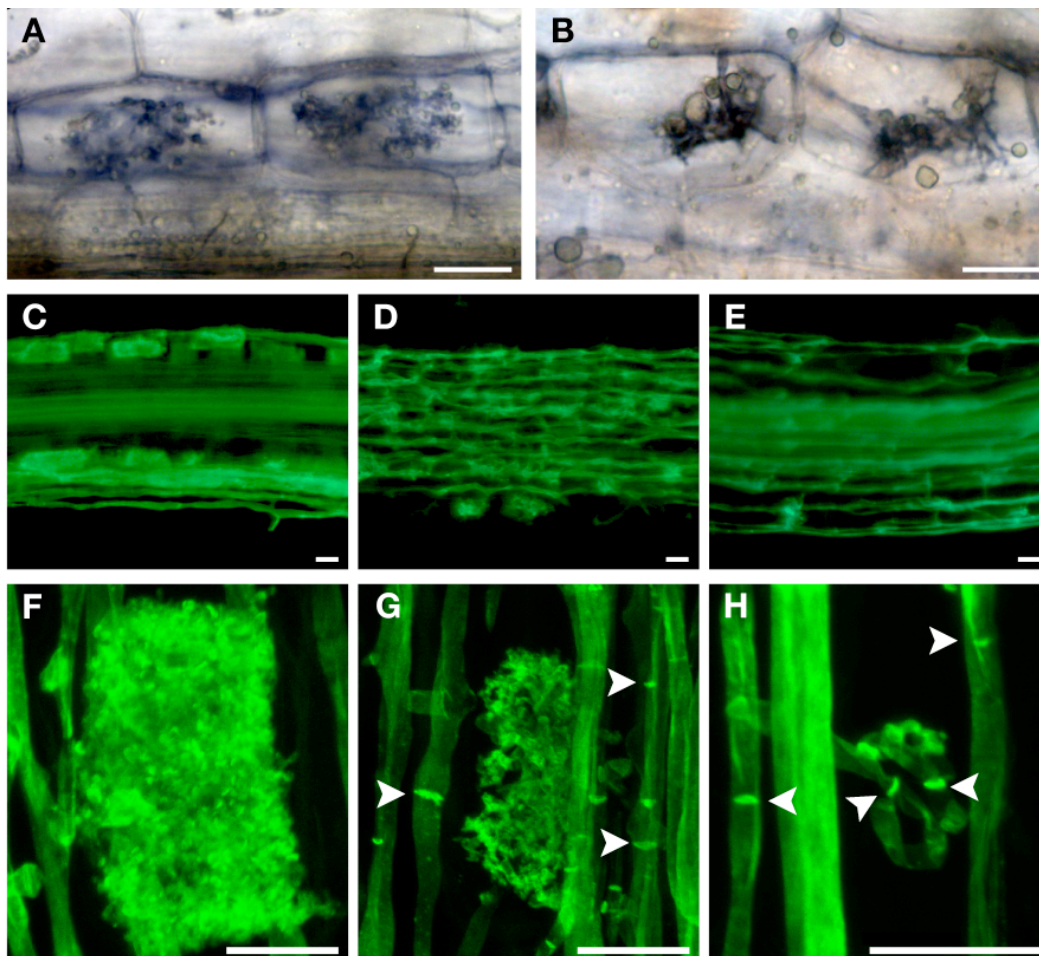


**Figure 9. Weak and Severe Arbuscule Defects in Mapping Populations of SL0181-N.**

**(A) and (B)** The arbuscule phenotype of  $M_4$  mutants originating from J850 (A) resembled the weak arbuscule mutant trait (B) segregating in  $F_2$  and  $F_3$  populations originating from J849, as visualized by ink staining of AM fungal structures and BF microscopy. Scale bars: 20  $\mu$ m.

**(C) to (H)** Wild type (C and F), weak (D and G) and severe (E and H) arbuscule mutant traits segregating in different  $F_2$  and  $F_3$  sub-populations originating from J849. Fungal structures (green) were stained with WGA-Alexa Fluor 488 and visualized by epifluorescence microscopy (C to E) or CLSM (F to H). Arrowheads indicate hyphal septae. Plants were cultivated in the green house for 4 w in chive pots with BEG195. Scale bars: 20  $\mu$ m.



These observations prompted us to assume that the  $M_3$  mutant J849 contained two recessive mutations, one at the *RED* locus and one at an additional locus, *WEAK RED* (*WRD*). Due to the different segregation patterns in the progeny of J5149 and J5150, we further deduced that one of the loci would have been homozygous for the mutant allele, while the other would have been heterozygous in the mutant parent J849 (i.e. *RED red/wrd wrd* or *red red/WRD wrd*). Additional sub-populations originating from each  $F_1$  parent were phenotyped and subsequently genotyped by S. Wilhelm, in order to test the hypotheses that J5149 was dihybrid, *RED red/WRD wrd*, whereas J5150 was monohybrid, *RED RED/WRD wrd* or *RED red/WRD WRD*. 50 seeds from each seed bag were sown per chive nurse pot containing BEG195, and ink-stained roots were phenotyped after 3 weeks. Unfortunately, at that time 70% or more of the seed from 3 seed bags did not produce seedlings for unknown reason (Table 3). The segregation ratios observed in these sub-populations might therefore be biased. Nevertheless, phenotypic segregation in  $F_2$  progeny of J5149 conformed to the dihybrid hypothesis, whereas in the sub-populations originating from J5150 dihybrid segregation, but not monohybrid segregation, was rejected by the  $\chi^2$  test (Table 3). The segregation ratios of J5149 progeny moreover suggested that the severe arbuscule mutant trait corresponds to the double recessive class *red red/wrd wrd*, while equal weak defects correspond to the single recessive classes *RED -/wrd wrd* and *red red/WRD -*. A single mutant with a severe arbuscule phenotype was also recorded in the progeny of J5150. Since the double recessive class should not occur in the progeny of J5150, this observation was contradictory to the monohybrid assumption.

In order to check, whether subsequent genotyping and co-segregation analysis might have been disturbed due to phenotyping mistakes, e.g. wild type individuals scored as mutants, self-progeny from single individuals with conflicting phenotypes and genotypes were reassessed. The results (Table 4) led to 3 conclusions: (I) Simple monohybrid segregation in sub-populations originating from J5150 is not supported, because mutants from the putative double recessive class (severe arbuscule defect) were identified in the  $F_3$  generation. (II) The existence of a 2<sup>nd</sup> locus, *WRD*, in addition to *RED* is underpinned by the confirmation of the mutant arbuscule traits in  $F_3$ , as well as  $F_4$  individuals originating from J5149. (III) In some cases, the phenotypic distribution in  $F_3$  and  $F_4$  progeny of individual plants does not fit to unlinked dihybrid segregation, particularly regarding the large numbers of severe arbuscule mutants. The strong variation between the individual segregation

patterns and the proportions of unclear phenotypes furthermore indicate that an unambiguous determination of the phenotype by stereomicroscopy was not possible. This accounts primarily for the distinction between the wild type and the weak arbuscule mutant trait, as well as between the weak and the strong arbuscule mutant trait.

**Table 4.** Segregation of Arbuscule Traits in *red* F3 and F4 Sub-populations

F1	Parent	F <sup>a</sup>	Genotype <sup>b</sup>	Phenotype <sup>c</sup>	WT	Weak	Severe
J5149	J9317	F2	Gifu/Gifu	Mutant	0	24	1 (+3)
J5149	J9291	F2	Het/Het	Mutant	0	(21)	0
J5149	J9288	F2	MG20/MG20	<u>Mutant</u>	<u>(+2)</u>	8 (+10)	0
J5149	J9293	F2	MG20/MG20	<u>Mutant</u>	<u>9 (+6)</u>	13 (+6)	0
J5149	K8421	F3	Gifu/Gifu	<u>severe</u>	0	<u>4</u>	7
J5149	K8424	F3	Gifu/Gifu	<u>severe</u>	0	<u>3</u>	4
J5149	K8423	F3	Gifu/Gifu	weak	0	12	0
J5150	J9325	F2	- /Het	WT	10 (+7)	2 (+2)	0
J5150	K0154	F2	<u>Gifu/Gifu</u>	<u>WT</u>	0	4	0
J5150	J9559	F2	Gifu/Het	WT	40 (+2)	19 (+8)	14
J5149	K8427	F3	Gifu/Het	WT	7	1	6
J5149	J9304	F2	Het/Het	WT	15	14	2 (+3)
J5150	J9548	F2	Het/Het	WT	3 (+4)	1 (+7)	0
J5150	J9554	F2	Het/Het	WT	2 (+4)	7 (+9)	16
J5150	J9556	F2	Het/Het	WT	5	0	0
J5150	J9561	F2	Het/Het	WT	19 (+3)	9 (+1)	12 (+3)
J5150	J9564	F2	Het/Het	WT	3	19	7

<sup>a</sup> Parental generation.

<sup>b</sup> Parental genotype at markers TM0082/TM1597 (top of LG VI).

<sup>c</sup> Parental phenotype. Conflicting phenotypes between parent and self-progeny and irregular segregation patterns are underlined.

Numbers of unclear phenotypes are given in brackets.

### Co-segregation Analysis Indicates *red* Target Region at the Short Arm of Chromosome VI

In order to identify *red* and/or *wrd* by map-based cloning, co-segregation of the arbuscule formation defects and the mutagenized genetic background, Gifu, in the different F<sub>2</sub> sub-populations described above was assessed by power mapping. Since wild type individuals and arbuscule mutants segregated at approx. 3/1 ratios in sub-populations originating from the F<sub>1</sub> parent J5150, these were genotyped in 1<sup>st</sup> place. The DNA of 43 F<sub>2</sub> mutants was isolated and 47 SSR markers covering the 6

LGs of the *Lotus* genome (Hayashi et al., 2001) were PCR amplified from individual DNA samples. Genotype analysis revealed significant excess of individuals, which were homozygous Gifu at markers located at the north end of LG VI (Figure 10 and Supplemental Figure 1A). Besides, significant deviations from the expected 1/2/1 distribution of homozygous Gifu/heterozygous/homozygous MG-20 genotypes at TM0127 on the south end of LG III and TM0100, TM0283 and TM0046 on LG IV were detected (Figure 10 and Supplemental Figure 1A). Primarily the latter two markers showed a deficit in homozygous Gifu genotypes, which might be due to linkage with a deleterious mutation, whereas heterozygous genotypes were over-represented at the other markers. Inspection of the genotype patterns moreover revealed a repulsion of homozygous Gifu genotypes between LG VI and the region flanked by TM0800 (45.0 cM) and TM0356 (51.4 cM) on LG I. The majority of mutants that were not homozygous Gifu on LG VI had homozygous Gifu genotypes at the marker TM0356. Assuming that the double recessive class *red red/wrd wrd* was detrimental, this would be the only marker that indicated a possible linkage to the 2<sup>nd</sup> locus. The assumption however does not fit to the monohybrid segregation of the arbuscule defect in F<sub>2</sub> plants originating from J5150.

Co-segregation of Gifu alleles at the north end of LG VI was confirmed in F<sub>2</sub> mutants originating from J5149 (Figure 11A and Supplemental Figure 1B). Accordingly, most of the wild type F<sub>2</sub> individuals were genotyped heterozygous or homozygous MG-20 in this region (Figure 11B) and only two wild type individuals were homozygous Gifu for all markers analyzed on LG VI between 0 and 14 cM (Supplemental Figure 2). The wild type attribution of one of these two individuals was falsified by phenotypic analysis of its self-progeny, which entirely showed the weak arbuscule phenotype (Table 4 and Supplemental Figure 2). Self-progeny of the 2<sup>nd</sup> wild type F<sub>2</sub> plant were not checked.

Although 7 SSR markers with a maximum spacing of 7.6 cM covered the co-segregating region corresponding to the short arm of chromosome VI (Pedrosa et al., 2002), the fraction of MG-20 alleles at the tested markers did not go below 0.21 and 0.32 in F<sub>2</sub> mutants originating from J5150 (Figure 10) and J5149 (Figure 11A), respectively. This was due to 32% and 47% F<sub>2</sub> mutants originating from J5150 and J5149, respectively, that were not homozygous Gifu for any of the markers tested between BM1714 and TM1514 (Supplemental Figure 1).

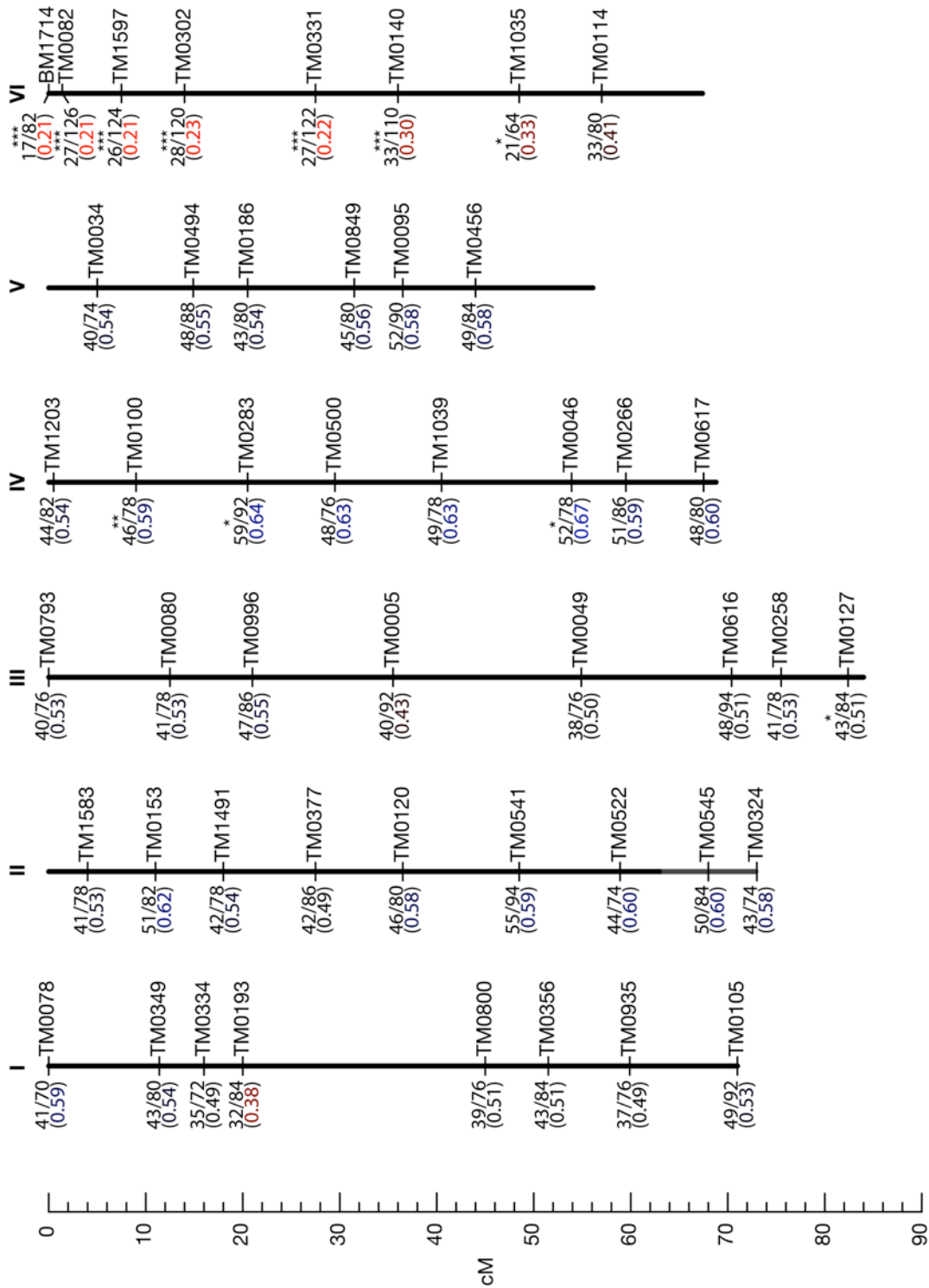


**Figure 10. Co-segregation Analysis of 43 F2 Mutants Originating from J5150.**

Ratios indicate recombinant (MG-20) alleles vs. total alleles at the corresponding markers, which are shown to the right of the bars. Bars represent the *Lotus* LGs I to VI. The scale indicates genetic distances (cM). Asterisks indicate deviations from the expected 1/2/1 distribution of (MG-20 MG-20)/(MG-20 Gifu)/(Gifu Gifu) genotypes at 0.05 (\*), 0.01 (\*\*), 0.001 (\*\*\*) significance levels according to the  $\chi^2$  test. Data corresponds to Suppl. Fig. 3A.

Phenotypic confirmation of self-progeny from 3 F<sub>2</sub> mutants indicated that weak arbuscule defects might have been caused by a 2<sup>nd</sup> mutation outside the identified region of co-segregation (Table 4). Moreover, segregation of wild type and mutant offspring was recorded for one of the F<sub>2</sub> mutants, which were not homozygous Gifu in the co-segregating region, suggesting that some of the F<sub>2</sub> individuals scored as weak mutants might have been wild type plants (Table 4).

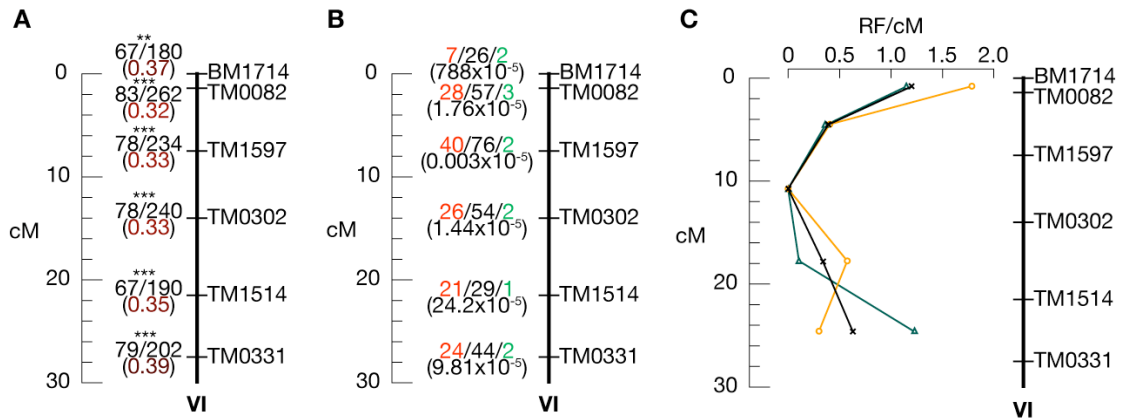


**Figure 11. Allele Distributions in the red Target Region.**

**(A)** Ratios of MG-20 alleles vs. total alleles from mutants originating from J5149 are shown. Asterisks indicate deviations from the expected 1/2/1 distribution of (MG-20 MG-20)/(MG-20 Gifu)/(Gifu Gifu) genotypes at 0.01 (\*\*) and 0.001 (\*\*\*) significance levels of the  $\chi^2$  test. Data corresponds to Suppl. Fig. 3B.

**(B)** Ratios indicate (MG-20 MG-20)/(MG-20 Gifu)/(Gifu Gifu) genotypes of wild type F<sub>2</sub> individuals originating from J5149 and J5150. Probabilities of the  $\chi^2$  test for 1/2/1 distribution are given in parentheses.

**(C)** Frequencies of recombination (RF) between adjacent markers in mutant (green), wild type (yellow) and all (black) F<sub>2</sub> individuals genotyped indicate lack of recombination between TM1597 and TM0302.

The genotypic analysis of F<sub>2</sub> individuals revealed a reduction of recombination in the co-segregating region on chromosome VI (Figure 11C). The region of suppressed recombination was flanked by the markers TM0082 (1.3 cM) and TM1514 (21.6 cM) and affected wild type, as well as mutant plants. Most notably, not a single recombination was observed in 279 F<sub>2</sub> individuals between the markers TM1597 (7.7 cM) and TM0302 (14.0 cM). Since 35 recombinant alleles in 279 F<sub>2</sub> individuals are expected according to the genetic distance derived from the wild type Gifu x MG-20 mapping population (Hayashi et al., 2001), the observed lack of recombination in SL0181-N F<sub>2</sub> populations might be caused by a large deletion or inversion that had occurred in M1 or M2 spontaneously or as an indirect effect of the EMS mutagenesis (Greene et al., 2003). Moreover, the chromosomal mutation might include the

*RED* or *WRD* locus and thus might be causing one of the observed arbuscule defects.

Since the compilation of genotyping data were obtained from phenotypically pre-selected population, we performed an unbiased genotype analysis of 48  $F_2$  individuals originating from J5149 and J5150, respectively, in order to test two hypotheses that were based on the previous data: (A) The contrasting segregation patterns observed in  $F_2$  populations from J5149 and J5150 are due to a recessive lethal allele (*let*) on LG I, which is carried by J5150, but not by J5149. (B) There is a repulsion of homozygous Gifu genotypes between LG VI and the south region of LG I (46.2 – 56.6 cM). The results fully supported hypothesis A, whereas hypothesis B was not supported (Figure 12). Only one out of 45  $F_2$  individuals originating from J5150 was homozygous Gifu at TM1325, in contrast to 16/45 homozygous Gifu individuals in the J5149  $F_2$  population. The allele distribution in the J5150  $F_2$  population indicated that *let* is located in the Gifu background between TM1325 (29.7 cM) and TM0316 (46.2 cM) on LG I. The originally observed repulsion was not confirmed and might have been caused by the depletion of Gifu alleles on LG I in the J5150  $F_2$  population. Noteworthy, a suppression of recombination was confirmed on LG VI.

Due to the complex segregation of arbuscule defects in SL0181-N  $F_2$  populations,  $F_3$  progeny of selected  $F_2$  individuals were genotyped at the short arm of chromosome VI (Supplemental Figure 3). Co-segregation analysis of 336  $F_3$  plants in total confirmed the results obtained from the  $F_2$  generation: None out of 89 wild type  $F_3$  plants from 9  $F_2$  parents that had been heterozygous in the target region were homozygous Gifu for all of the markers tested between TM1613 (1.3 cM) and TM0302 (14.0 cM) and only one out of 40 arbuscule mutants accounted to the severe phenotype was not homozygous Gifu in this region. 60 out of 103 weak arbuscule mutants were not homozygous Gifu in the target region.

In the  $F_2$  generation, we had identified 11 arbuscule mutants and 2 wild type plants with recombination events between the markers BM1714 (0.0 cM) and TM1514 (21.6 cM), thereby confining the target region by the flanking markers TM0082 (1.3 cM) and TM1597 (7.7 cM) (Figure 13). By genotyping the self-progeny of one recombinant wild type  $F_2$  individual, J9559, the southern border of the target region was set by the marker TM0722 (4.1 cM). Since the corresponding weak mutant phenotype might be due to the 2<sup>nd</sup> locus *wrd*, a conservative localization of the

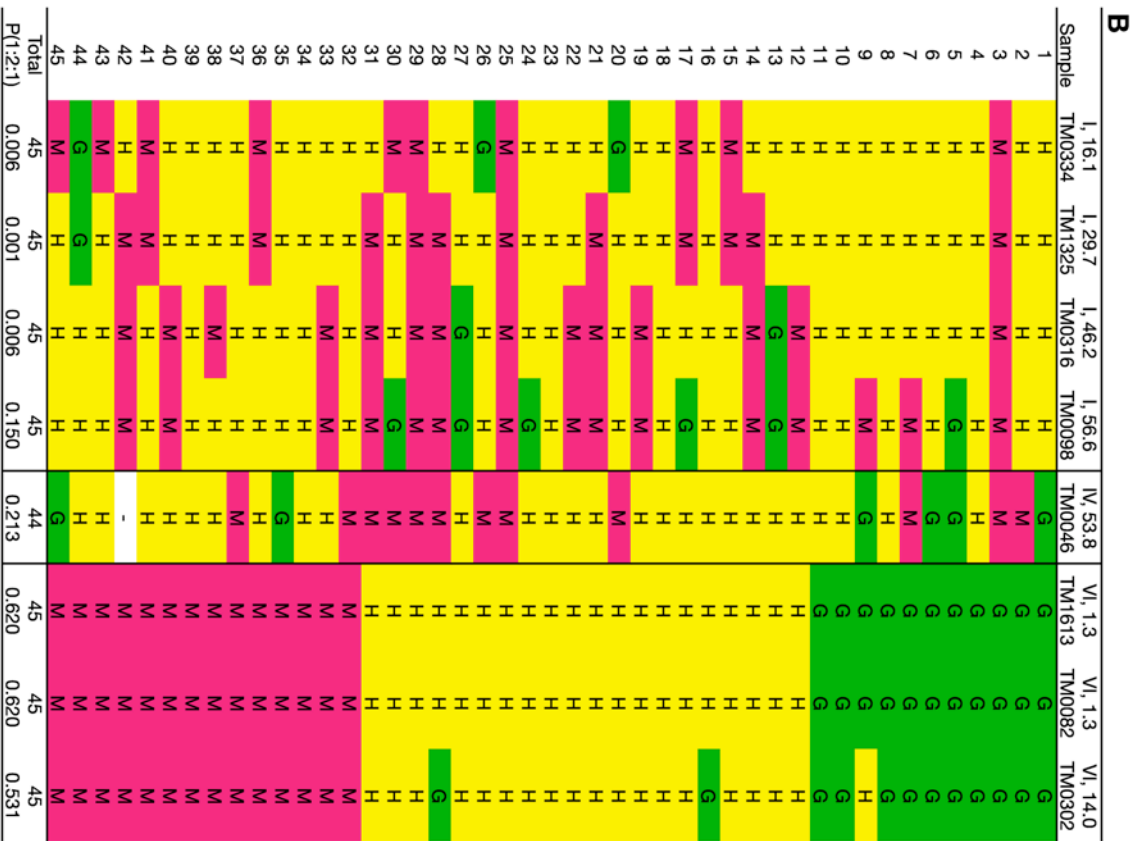
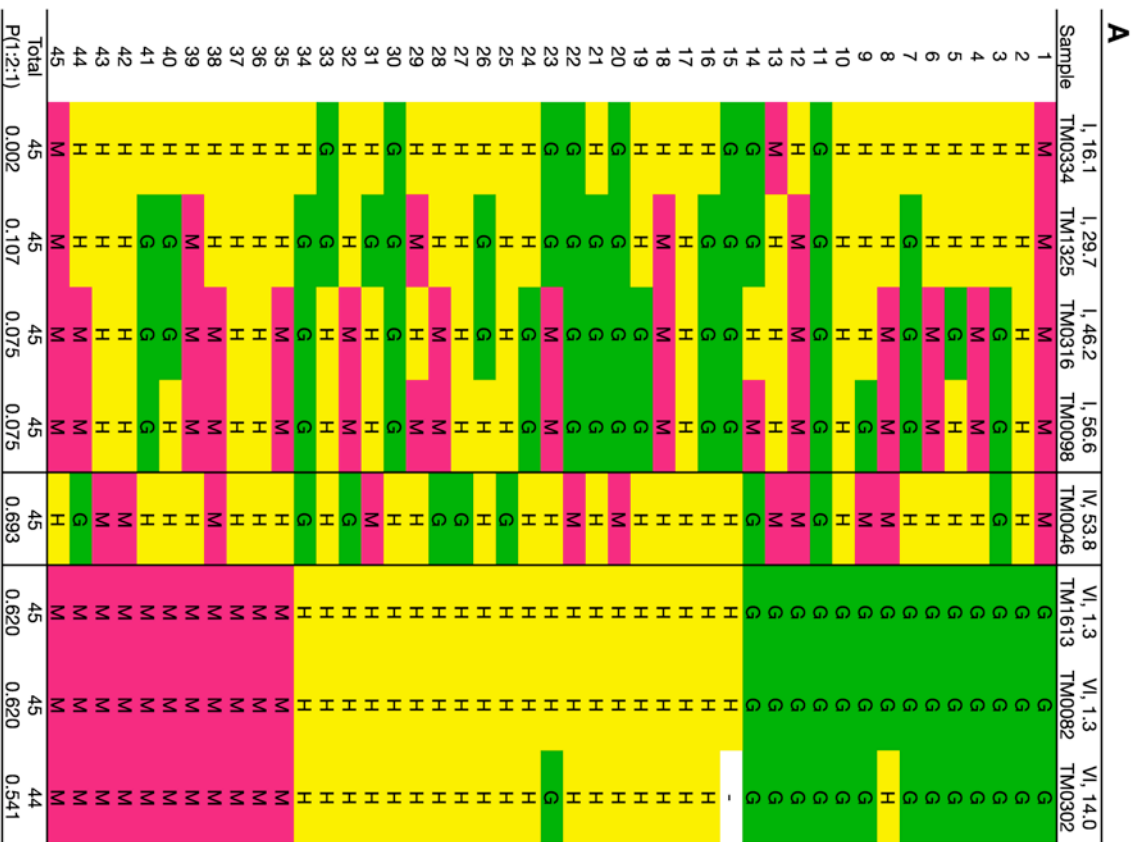


**Figure 12. Genotype Patterns of Whole Sub-populations.** (A) Genotypes of 45  $F_2$  individuals originating from J5149. (B) Genotypes of 45  $F_2$  individuals originating from J5150. G/green: (Gifu Gifu), H/yellow: (Gifu MG-20), M/magenta: (MG-20 MG-20). Markers and their genetic positions (L, cM) are indicated in the heading line.  $\chi^2$  test probabilities for the genotype distributions of the corresponding markers are indicated in the bottom line.

southern flanking marker at TM1514 (21.6 cM) is given by a wild type recombinant individual. An additional wild type F<sub>3</sub> recombinant was identified setting TM0553 (1.7 cM) as the northern marker flanking the target region.

F1 Plant	Parent	Seed Bag	Generation	Plant ID	Phenotype	BM1714, VI, 0.0	TM1613, VI, 1.3	TM0082, VI, 1.3	TM0553, VI, 1.7	TM0472, VI, 1.7	TM0722, VI, 3.3	TM1597, VI, 4.1	TM0302, VI, 7.7	TM1514, VI, 14.0	TM0331, VI, 21.6
J5149	J5149	53594	F2	J8752	mutant	H	-	G	-	-	-	G	G	H	-
J5149	J5149	53594	F2	J8762	WT	H	-	H	-	-	-	H	H	G	G
J5149	J5149	53776	F2	J9298	mutant	-	-	G	-	-	-	H	H	H	M
J5149	J5149	55615	F2	K0156	mutant	H	H	H	-	-	-	G	G	-	G
J5149	J5149	55615	F2	K0158	mutant	G	G	G	-	-	-	H	H	-	H
J5149	J5149	55615	F2	K0160	mutant	H	H	H	-	-	-	G	G	-	-
J5149	J5149	55615	F2	K0164	mutant	H	H	H	-	-	-	G	G	-	-
J5149	J5149	55615	F2	K0183	mutant	G	G	G	-	-	-	H	H	-	H
J5149	J5149	55615	F2 (scr3_pl2_19)	mutant	H	H	G	-	-	-	G	G	-	-	
J5149	J5149	55615	F2 (scr3_pl2_46)	mutant	H	H	G	-	-	-	G	G	-	G	
J5149	J5149	55615	F2 (scr3_pl2_51)	mutant	H	H	H	-	-	-	G	G	-	H	
J5149	J5149	55615	F2 (scr3_pl2_69)	mutant	-	G	H	-	-	-	-	-	-	-	
J5149	J9304	59042	F3	K8427	WT	-	G	-	G	H	H	-	H	-	M
J5150	J5150	53601	F2	J9559	WT	-	-	G	-	-	-	H	-	-	-
J5150	J9559	59073	F3	N/A	weak	-	G	G	-	G	H	H	H	-	-
J5150	J9561	59075	F3	N/A	WT	-	G	-	H	H	H	-	H	-	H
J5150	J9564	59078	F3	N/A	severe	-	H	G	-	-	G	-	G	-	-

**Figure 13. Recombinations Confining the *RED* Target Region.**

Phenotypes and available genotypes of recombinant individuals are shown. Filled (conservative) and open triangles indicate the confining recombinations. Respective markers and genetic positions are indicated in the heading line. G/green: (Gifu Gifu), H/yellow: (Gifu MG-20), M/magenta: (MG-20 MG-20).

### ***PT4* is Not Induced in *red* Mutants During AM**

Arbuscules are believed to be the main site of symbiotic phosphate uptake by the plant (Javot et al., 2007a). AM-induced phosphate transporters, including *StPT3*, *LjPT3* and *MtPT4*, are specifically expressed in arbuscule containing cells and localization to the periarbuscular membrane was demonstrated for *MtPT4* (Harrison et al., 2002; Karandashov et al., 2004; Maeda et al., 2006). Moreover, the arbuscule phenotypes of SL0181-N mutants are reminiscent of the loss-of-function EMS mutant *mtpt4-1* (Javot et al., 2007b). In collaboration with the Kazusa DNA Research Institute we obtained the *Lotus* genomic sequences of 4 *PT4*-related genes along with positional information for 3 of them. LjSGA\_014433.2, encoding a partial protein predicted from the draft sequence of clone LjB14J02, showed 97 % amino acid (AA) sequence identity to *MtPT4* and was subsequently annotated as *PT4* from *L. japonicus*. The expression of *PT4* was analyzed by quantitative RT-PCR and a strong induction in the wild type was assessed at 6 w after cultivation in chive pots



containing BEG195 (Figure 14A). This is in accordance with the AM-specific expression of orthologous *MtPT4* and *OsPT11* (Harrison et al., 2002; Paszkowski et al., 2002). At the same time, transcript levels in roots from *red* M<sub>4</sub> plants originating from J850 were not significantly different from non-mycorrhized control roots (Figure 14A). AM colonization levels were assessed in parallel to the expression analysis (Figure 14B). Hyphal colonization of *red* roots was in the range of wild type colonization levels, whereas arbuscular colonization was strongly attenuated in *red*. The results corroborate the decrease of arbuscular colonization in *red* mutants after 10 d of cultivation (Figure 8), and furthermore suggest that this decrease is larger after longer periods of cultivation with AM fungi. Interestingly, vesicles were more abundant in *red* than in wild type plants.

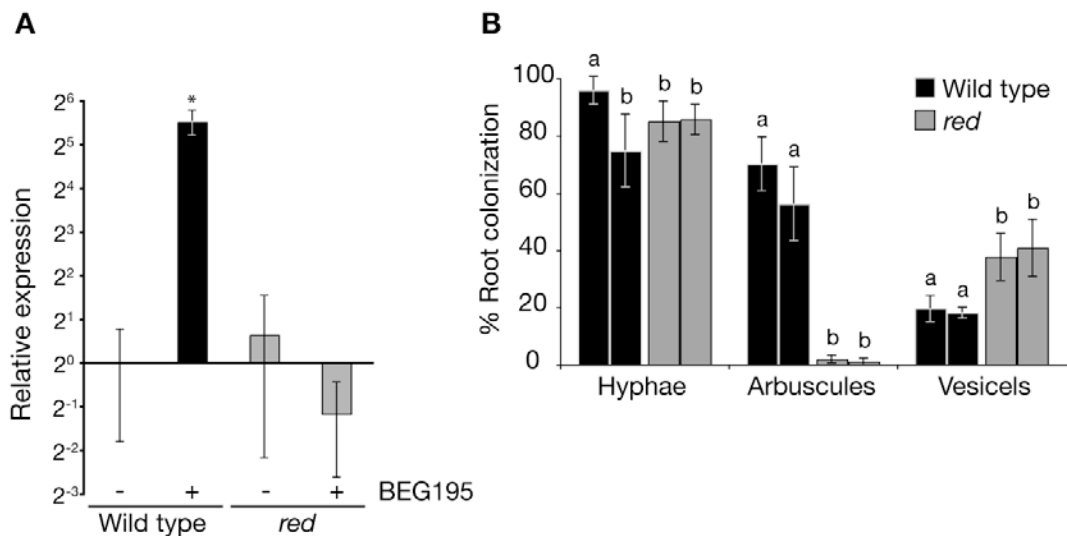


**Figure 14. AM Colonization and Relative Expression of *PT4* in Wild Type and *red* Roots.** (A) Quantitative RT-PCR analysis of *PT4* expression in WT and *red* roots at 6 w after cultivation in chive pots with BEG195 (+) or in substrate only (-). Expression is relative to (-) samples from wild type roots and normalized to *EF-1 $\alpha$*  and *Ub* transcript levels. Mean and standard deviation (SD) were derived from two biological replicates. Asterisk indicates significant ( $p < 0.05$ ) difference in gene expression between (+) and (-) samples. (B) Hyphal, arbuscular and vesicular colonization levels in roots from WT and *red* plants grown together with the plants for expression analysis. Duplicate bars indicate parallel experiments with different chive pots. Mean and SD are derived from 4 plants per genetic background. Different letters above bars indicate significant differences according to *t*-test statistics.

The correlation of suppressed arbuscule formation and *PT4* induction in *red* mutants raises the question, which of the two observations is cause or effect. An arbuscule cell specific expression of *PT4*, as in other AM hosts, would imply that arbuscule formation is epistatic to *PT4* expression. Conversely, a functional impairment of *PT4*

might inhibit full arbuscule development in *red* mutants, correspondingly to *mtpt4-1* (Javot et al., 2007b). Therefore the available part of the predicted *PT4* gene was sequenced from two M<sub>4</sub> individuals originating from J850, in order to check for EMS-induced mutations that might be causing the *red* phenotype (Table 5). The only sequence variation identified represents a silent polymorphism between Gifu and MG-20 close to the 5' end of the CDS. Moreover, a microsatellite with 9 and 13 AT repeats in MG-20 and Gifu, respectively, located in the 1<sup>st</sup> intron and starting at nucleotide position 628 relative to the start of the predicted CDS was identified. The genotypes derived from the generated SSR marker, MS014433, in the F<sub>2</sub> subpopulation 55591 were completely linked to the marker TM0078 (Supplemental Figure 4) and hence *PT4* was mapped to 0 cM on chromosome I of MG-20, corresponding to the chromosomal translocation breakpoint between Gifu and MG-20 (Hayashi et al., 2001). The genetic positions of the remaining 3 predicted genes encoding proteins that are sequence related to *MtPT4* are located at the tip of the short arm of chromosome VI (chr6.CM1613.70 and chr6.CM1613.60) and distally on the long arm of chromosome I (chr1.CM0295.60). Due to their proximity to the co-segregating region of *red* F<sub>2</sub> mutants on chromosome VI and the putative target region on chromosome I, the CDS of all 3 genes was sequenced, but no DNA polymorphisms were identified in the M<sub>4</sub> mutants originating from J850 (Table 5). Annotation from Kazusa and GenBank indicate that gene predictions named as chr6.CM1613.70 and chr6.CM1613.60 are related to *MtPT5*, whereas chr1.CM0295.60 corresponds to *MtPT2*.

**Table 5.** Sequencing of *RED*-candidate genes

Gene ID <sup>a</sup>	LjSGA_014433.2	CM0295.60	CM1613.70	CM1613.60
GenBank Accession	AP010874	AB257216	N/A	N/A
Alias <sup>b</sup>	LjB14J02, BM2121_c18	TM1643.6	BM1714.2	BM1714.7
Annotation	<i>LjPT4</i>	<i>LjPT2</i>	Homolog of <i>MtPT5</i>	Homolog of <i>MtPT5</i>
Chromosome	1	1	6	6
Position (cM)	0	61	0	0
% CDS Sequenced (bp)	88.9 (1581)	100 (1617)	100 (1768)	100 (1608)
Result	C96T (D32D) <sup>c</sup>	No polymorphism	No polymorphism	No polymorphism

<sup>a</sup>According to Kazusa ([www.kazusa.or.jp](http://www.kazusa.or.jp)). <sup>b</sup>Clone names, gene predictions. <sup>c</sup>Intraspecific polymorphism between Gifu and MG-20.

### M<sub>4</sub> Mutants Originating from J850 are Impaired in Infection Thread Formation

Assessment of the nodulation phenotype of M<sub>4</sub> mutants originating from J850 revealed a severe impairment in IT formation (Diploma thesis of S. Wilhelm). Impaired IT formation led to the arrest of nodule formation at the primordial stage. I have confirmed these defects in M<sub>4</sub> mutants originating from J850 at 2 and 3 weeks after inoculation (WAI) with *M. loti* expressing DsRed (Figure 15). Nevertheless, I did not observe a single F<sub>2</sub> plant with impaired IT formation and abolished nodulation in 56 individuals originating from J5150 and 92 individuals originating from J5149. This is in accordance with wild type nodulation of *red* mutants initially assessed by S. Kosuta. It is unknown, which mutant individuals were initially analyzed, but the contrasting nodulation phenotypes of *red* mutants suggest that J849 was able to nodulate. The mutation, which causes the nodulation defect in J850 progeny, was apparently not inherited to the mapping populations. Therefore, the nodulation defect in J850 self-progeny is independent of the arbuscule defects observed in the mapping populations.

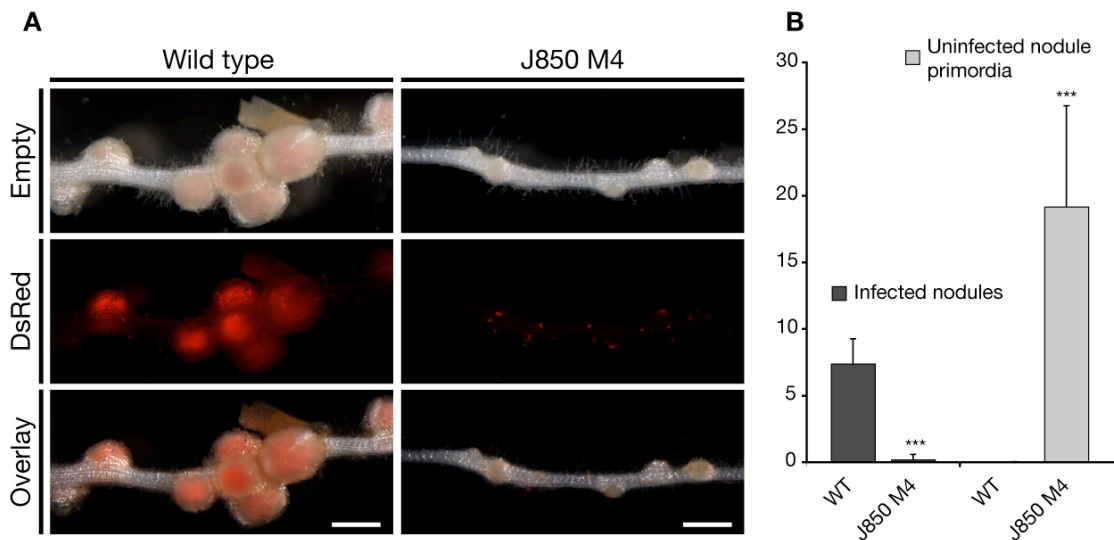


**Figure 15. M<sub>4</sub> Mutants Originating from J850 Are Impaired in Rhizobial Infection.**

**(A)** Stereomicroscopy images of a nodulated root from the WT and a root with uninfected nodule primordia from the J850-originating M<sub>4</sub> genetic background. Fluorescence detected with the DsRed filter indicates rhizobial DsRed expression. Scale bars: 1mm.

**(B)** Mean of infected nodules and uninfected nodule primordia observed on WT (n=8) and M<sub>4</sub> mutants originating from J850 (n=12) at 14 DAI with *M. loti* expressing DsRed. Error bars show SD. Asterisks indicate significant differences (p<0.001, t-test).

## Mutants of the AMPOP Impaired in Known Common *SYM* Genes

### SL1345-N and SL1856-N Symbiotic Mutants Correspond to *cyclops-5* and *nup133-21*

By the use of power mapping, 4 of the confirmed AM mutant lines turned out to harbor the causal mutation in a previously identified common *SYM* locus (Figure 7). Mutants from 3 of these lines, SL1345-N, SL1856-N and SL2042-N, were impaired during rhizodermal infection. Balloon-like hyphal swellings at aborted infection sites (Figure 7 and Supplemental Figure 13) were reminiscent of the AM phenotypes displayed by common *sym* mutants (Kistner et al., 2005). Inoculation of M<sub>4</sub> and/or F<sub>2</sub> individuals from SL1345-N, SL1856-N and SL2042-N with *M. loti* revealed that AM mutants from all 3 lines were also nodulation defective (data not shown). M<sub>3</sub> mutants K1583 from SL1345-N and K1364 from SL1856-N were crossed with wild type MG-20 individuals and F<sub>2</sub> populations were generated from each cross. Segregation of the AM phenotype in the F<sub>2</sub> populations did not deviate from monogenic recessive ratios (Figure 7). Co-segregation analyses indicated *CYCLOPS* as candidate gene affected in SL1345-N and *NUP133* in SL1856-N mutants (Figure 16).

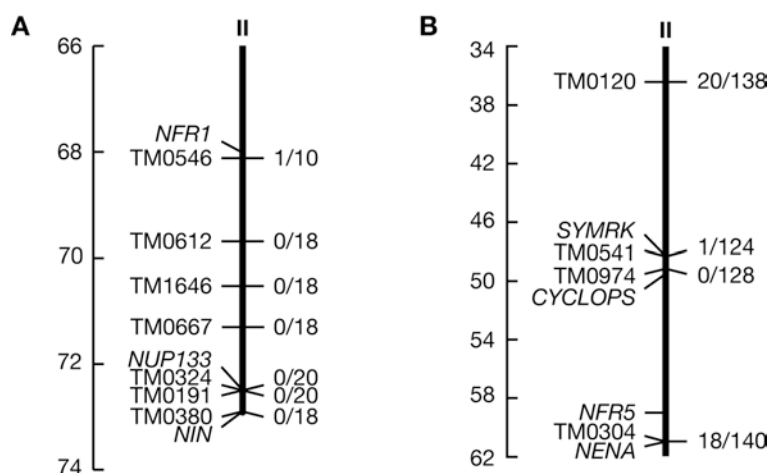


**Figure 16. Co-segregation Analysis of SL1856-N and SL1345-N F<sub>2</sub> Mutants.**

**(A) and (B)** Co-segregating regions in mutants from SL1856-N (A) and SL1345-N (B). Ratios indicate MG-20 alleles vs. total alleles at the corresponding markers, which are shown together with linked *SYM* loci to the left of the bars. Bars represent the *Lotus* LG II. Scales indicate genetic distances (cM). Co-segregation analyses were performed by K. Haage (A) and S. Wilhelm (B).

Sequencing of *CYCLOPS* in SL1345-N mutants revealed a frameshift mutation caused by a deleted G nucleotide at position 1281 of the CDS, identical to the *cyclops-5* allele (Yano et al., 2008; Perry et al., 2009). (Detailed description of the mutant is provided in the report of the lab internship from Oct.-Dec. 2006 by S. Wilhelm.) In SL1856-N mutants a G to A transition was identified by K. Haage at the predicted 5' splice site of intron 5, corresponding to nucleotide position 4496, relative to the A of the start codon, of the genomic *NUP133* sequence. The mutant allele was designated *nup133-21* (Perry et al., 2009).

F<sub>1</sub> plants originating from the cross between SL2042-N M<sub>3</sub> mutants and MG-20 wild type plants failed to produce self-progeny. Known common *SYM* genes were sequenced in SL2042-N mutants in order to check for mutations. In *POLLUX*, a nonsense mutation corresponding to *pollux-20*, caused by a G to A transition at nucleotide position 1953 of the *POLLUX* CDS, was identified (Figure 7).

#### **A Glycine to Glutamic Acid Substitution in the RCK Domain of *POLLUX* Attenuates AM Colonization and Nodulation in *patchy***

In contrast to the AM mutants that were blocked during rhizodermal infection and therefore showed a typical common *sym* phenotype, mutants from SL1816-N were commonly infected by BEG195, but the root cortex was not thoroughly colonized (Figure 17). After 21 d of cultivation in chive pots, hyphal colonization was significantly reduced in comparison with wild type plants, in which approx. 80% of the root system was colonized (Figure 17G). Successful infections were significantly less abundant on *patchy* than on wild type roots, whereas aborted infections were increased in *patchy*. Although some aborted infections were accompanied by balloon-like hyphal structures, successful infections appeared wild type-like (Figure 17C to E). Reduced hyphal colonization might have been a consequence of impaired AM infection of the outer root cell layers. In addition, investigation of ink-stained roots by light microscopy indicated that the growth of cortical runner hyphae might have been suppressed, resulting in sharp hyphal fronts at the transition from colonized to uncolonized root sectors (Figure 17B). Arbuscule formation appeared not to be affected in *patchy* mutants, because arbuscule shape did not differ from the wild type and the frequency of arbuscules within colonized sectors was not significantly different (Figure 17B, C, F and G).

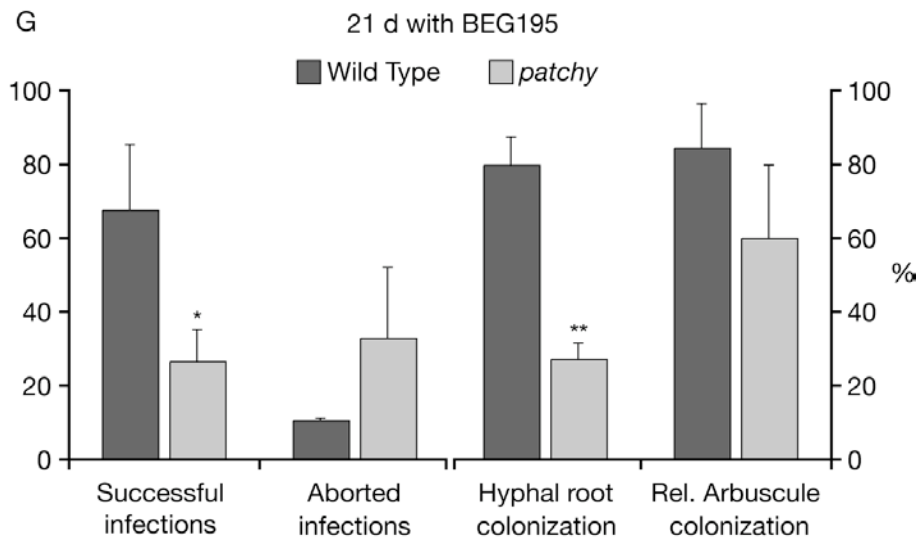
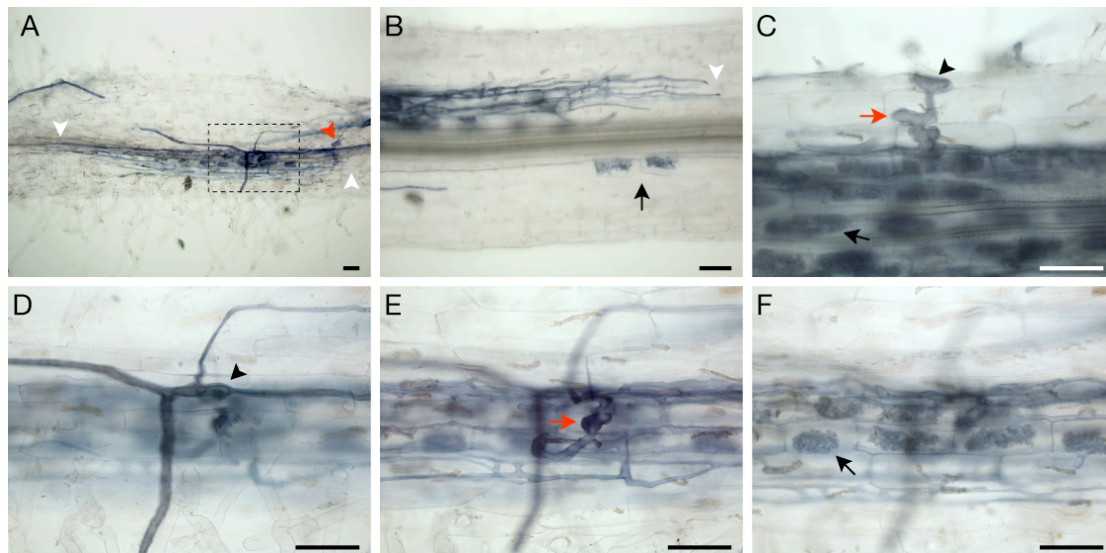


**Figure 17. AM Phenotype of *patchy*.**

(A) to (F) BF light micrographs of ink-stained AM fungal structures from *patchy* root samples at 3 w after greenhouse cultivation in chive pots with BEG195. AM colonized root patches were confined by hyphal fronts (white arrowheads in A and B) and contained fully developed arbuscules (black arrows in B, C and F). Root infections proceeded from hyphopodia (black arrowheads in C and D) into the cortex, accompanied by slight hyphal swellings (red arrows in C and E). Occasionally, balloon-like infection sites were observed (red arrowhead in A). Scale bars: 50  $\mu$ m.

(G) Successful and aborted infection sites per root, as well as mean hyphal colonization and arbuscular colonization within colonized root patches (Rel. Arbuscule colonization) from WT and *nena* plants ( $n \geq 8$ ) after 3 w of greenhouse cultivation. Error bars show standard deviations (SD). Asterisks above bars indicate significant differences ( $*p \leq 0.05$ ,  $**p \leq 0.01$ , *t*-test) between pairwise comparisons.

The  $M_3$  mutant J7244 was crossed with wild type MG-20 and the segregation of the AM phenotype was assessed in the  $F_2$  generation. The ratio of wild type versus mutant  $F_2$  plants accords to a monogenic recessive mutation (Figure 7) and the respective allele was named *patchy*, relating to the mutants' AM colonization

pattern. 24 mutant  $F_2$  individuals were genotyped by power mapping using the 1<sup>st</sup> set of 24 SSR markers (Figure 4) distributed over the *Lotus* genome. A significant surplus of alleles from the mutant Gifu background was observed at makers located on the long arm of chromosome VI and additional 72  $F_2$  mutants were genotyped in the co-segregating region, indicating that the causal mutation is located in the telomeric region south of TM0508 or TM0885 (Figure 18A). Since the frequency of recombinant alleles in the  $F_2$  mutants at TM0508 (6.25%) exceeds the genetic distance to the south tip of LG VI, according to the map published on the Kazusa website (<http://www.kazusa.or.jp/lotus/index.html>), it is likely that at least a subset of these  $F_2$  individuals were falsely assigned as mutants. Nevertheless, the mutant co-segregation analysis was confirmed by the lack of homozygous Gifu genotypes in the target region of 29 analyzed wild type  $F_2$  plants (Figure 18B).

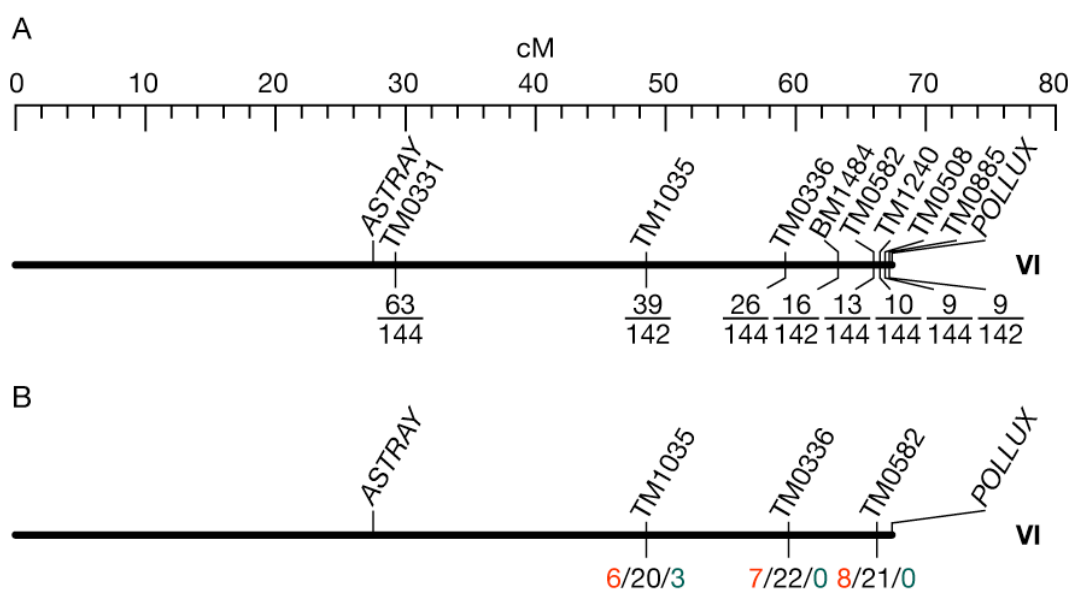


**Figure 18. Co-segregation Analysis of *patchy*.**

**(A)** Ratios indicate MG-20 alleles vs. total alleles in  $F_2$  mutant individuals from SL1816-N at the corresponding markers.

**(B)** Ratios indicate (MG-20 MG-20)/(MG-20 Gifu)/(Gifu Gifu) genotypes of wild type  $F_2$  individuals from SL1816-N at the corresponding markers.

Positions of markers and linked *SYM* loci are shown above the bars. Bars represent the *Lotus* LG VI. The scale indicates genetic distances (cM).

The proximity to *POLLUX* of the co-segregating markers TM0508 and TM0885 prompted sequencing of this candidate gene. In the SL1816-N M<sub>4</sub> mutant (K2011, self-progeny of J7244), a G to A transition was identified at nucleotide position 1592 of the CDS (Figure 19A). This leads to a predicted glycine (Gly) to glutamic acid (Glu) substitution at AA position 530 of the encoded *POLLUX* protein (Figure 19B). The mutation is located in a domain, which is highly conserved between the homologs of different plant species, spanning approx. 250 amino acids C-terminal of the predicted transmembrane region. Searching the NCBI conserved domains database moreover indicated that this domain is related to TrkA, an intracellular NAD<sup>+</sup>-binding component of the prokaryotic K<sup>+</sup> transport complex Trk (Schlosser et al., 1993). TrkA-related domains are also present in various ligand-gated K<sup>+</sup> channels, including prokaryotic KcsA, Ca<sup>2+</sup>-gated MthK from *Methanobacterium thermoautotrophicum* and the eukaryotic high-conductance Ca<sup>2+</sup>-activated channels (BK channels) (Jiang et al., 2001; Jiang et al., 2002; Wu et al., 2010). Structural, electrophysiological and molecular genetic data suggest that the free energy released by Ca<sup>2+</sup> binding to the domains regulating the conductivity of K<sup>+</sup> (RCK domains) induces structural rearrangements of the gating ring composed of multiple pairs of RCK domains and thereby opens the pore formed by the inner transmembrane helices (Jiang et al., 2002; Wu et al., 2010). The Gly530 to Glu mutation in *patchy*, which is identical to the *pollux-7* mutant allele (Imaizumi-Anraku et al., 2005), is located in a predicted  $\alpha$ -helix corresponding to  $\alpha$ F of the human BK channel, where it forms a helix-crossover domain with  $\alpha$ G (Figure 19C) (Wu et al., 2010). This  $\alpha$ F-turn- $\alpha$ G interconnects two tandem RCK domains within one BK monomer and, noteworthy, two hydrophobic residues within  $\alpha$ F that interface with  $\alpha$ G appear conserved in *POLLUX*. It is therefore possible that a similar helix-turn-helix conformation is adopted in the RCK domain of *POLLUX* and the acidic substitution in *patchy/pollux-7* in the 1<sup>st</sup> helix might disrupt proper pairing of the RCK domains, required for assembly of the gating ring.

A cross between *pollux-2* and *patchy* has been made in order to test for complementation. F<sub>1</sub> plants that were grown for 28 d in chive pots containing BEG195 were less colonized than wild type plants and contained balloon-like hyphae indicative of impaired rhizodermal infection (Figure 20). The lack of complementation proved that the identified mutation in *POLLUX* caused the AM defect observed in the *patchy* mutant. This was further confirmed by restoration of



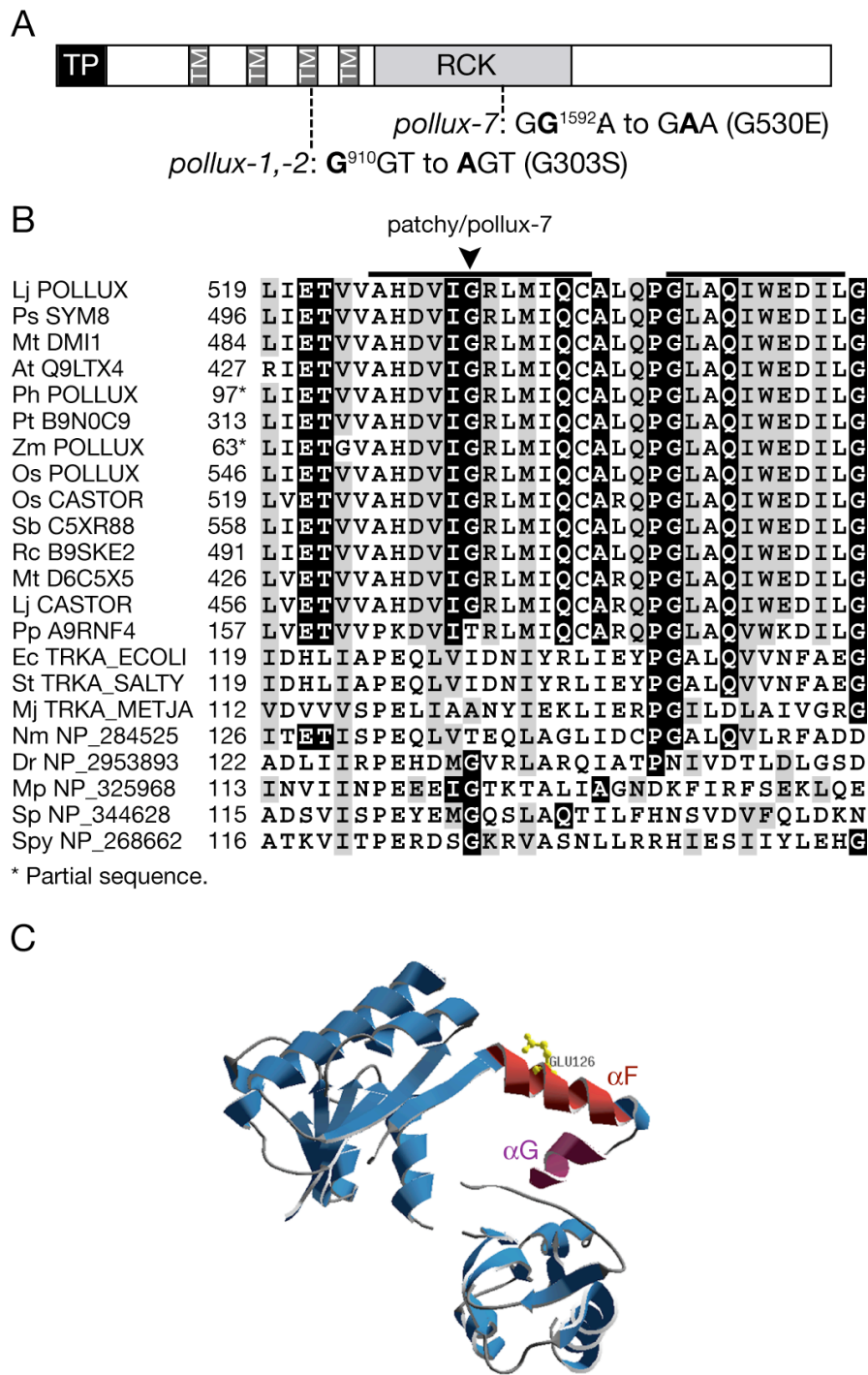


**Figure 19. Predicted G to E Substitution in the RCK Domain of POLLUX in *patchy*.**

**(A)** The protein structure of POLLUX contains a N-terminal transient peptide (TP), 4 trans-membrane domains (TM) and a conserved sequence related to the K conductivity regulating (RCK) domain. Mutations in *pollux-2* and *patchy/pollux-7* are indicated.

**(B)** Multiple sequence alignment of the conserved AAs surrounding the predicted helix-crossover motif in the RCK domain. The arrowhead marks the mutated AA in *patchy/pollux-7*. Bars above the sequence indicate predicted helices. Identical and similar AAs with more than 60% conservation are highlighted by inverted colors or grey background, respectively. Species acronyms, GenBank accession numbers and 1<sup>st</sup> AA positions are shown to the left.

**(C)** 3D homology model of the POLLUX RCK domain. The helices of the predicted  $\alpha$ F-turn- $\alpha$ G motif and the Gly to Glu substitution in *patchy/pollux-7* are highlighted. The model is based on the crystal structure of the human BK channel (Wu et al., 2010).

AM fungal infection and colonization of hairy roots from *patchy* mutants that were transformed with a binary vector containing the wild type *POLLUX* CDS (pK7WG2D,1-POLLUX<sub>CDNA</sub>12xHis, kindly provided by M. Charpentier) (data not shown; see Diploma thesis of S. Wilhelm).

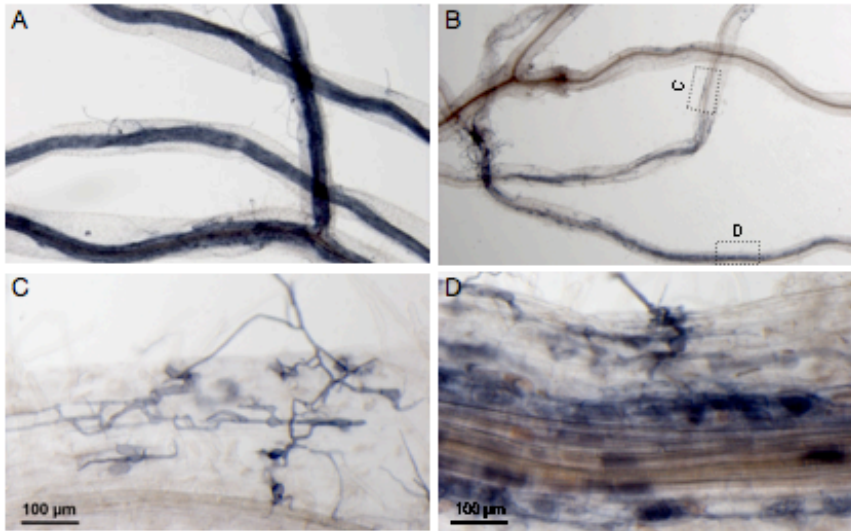


**Figure 20. Crossing *patchy* with *pollux-2* Did Not Restore AM.**

**(A) to (D)** BF light micrographs of ink-stained AM fungal structures in root samples from WT (A) and *patchy x pollux-2* F<sub>1</sub> individuals (B to D). Plants were cultivated for 4 w in chive pots with BEG195 under greenhouse conditions. Segments marked by dashed boxes (B) are shown at higher magnification (C and D).

Since *POLLUX* is required for Ca<sup>2+</sup> spiking (Imaizumi-Anraku et al., 2005), we tested whether NF-induced Ca<sup>2+</sup> spiking is affected in *patchy* mutants. None of the 20 root hairs from 12 different seedlings that were analyzed by microinjection of Ca<sup>2+</sup> reporter dye Oregon Green 488 BAPTA-1 showed Ca<sup>2+</sup> spiking, whereas 12 from 13 wild type seedlings responded positively (Figure 21). The lack of Ca<sup>2+</sup> spiking contrasts with the nodulation capability of *patchy* mutants that was assessed in the course of the AM mutant screen. In order to reassess the nodulation phenotype of *patchy*, the development of RNS was analyzed at different stages by light microscopy and quantitative RT-PCR amplification of the symbiotic marker genes *NIN* and *SbtM4*. Expression of both genes is induced by NF and during nodule development (Schauser et al., 1999; Takeda et al., 2009). Accordingly, expression of *NIN* and *SbtM4* was upregulated in wild type roots at 7 DAI with *M. loti*, relative to pre-inoculation levels (Figure 22). In accordance with previous analyses (Mitra et al., 2004; Kistner et al., 2005), no changes in transcript abundance were found in roots from loss-of-function *pollux-2* mutants. In contrast to *pollux-2*, relative expression of

*NIN* and *SbtM4* was significantly upregulated in roots from *patchy* mutants, albeit *NIN* induction was weaker than in the wild type.

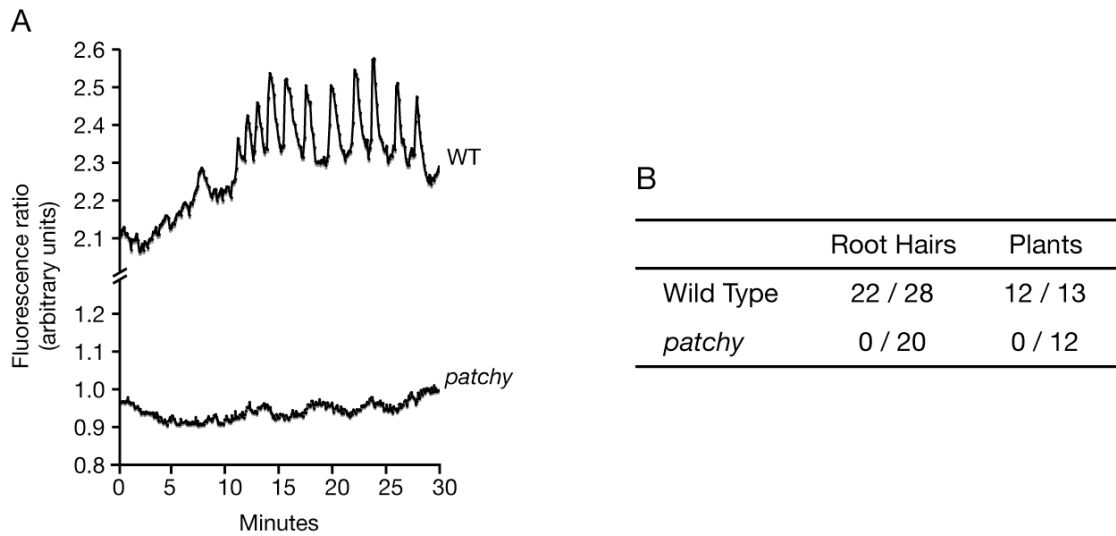


**Figure 21. *patchy* Mutants Are Impaired in NF-induced Ca<sup>2+</sup> Spiking.**

**(A)** Fluorescence ratios between ratiometric Ca<sup>2+</sup> indicator Oregon Green 488 BAPTA-1 and reference dye Texas Red after application of 10<sup>-8</sup> M NF at 0 min to roots of young WT and *patchy* seedlings. Images were taken with an epifluorescence microscope at 5 sec intervals over 30 min.

**(B)** Ratios indicate positive spiking/total analyses of root hair from WT or *patchy* seedling. Representative traces for positive Ca<sup>2+</sup> spiking in the WT and Ca<sup>2+</sup> spiking measurements in *patchy* are shown in (A).

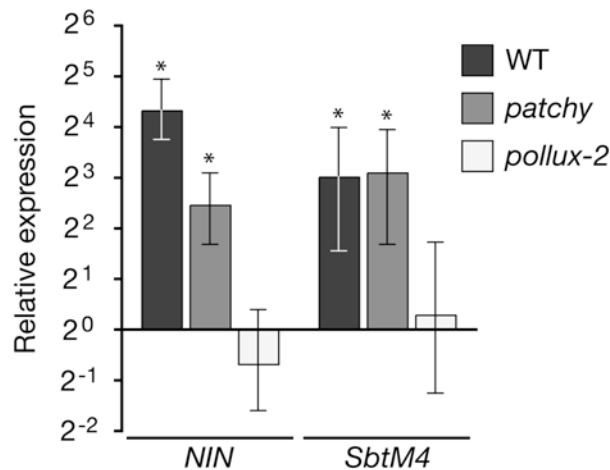
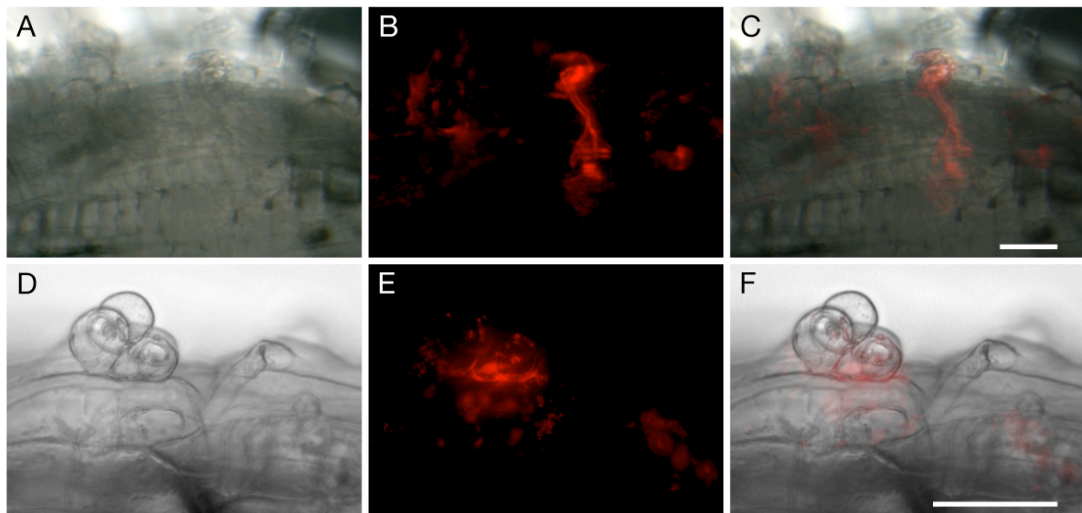


**Figure 22. *NIN* and *SbtM4* Expression Is Induced in *patchy* Roots at 7 DAI with *M. loti*.**

Expression levels were analyzed by quantitative RT-PCR and are relative to expression levels in roots samples before inoculation. Expression was normalized to *EF-1α* and *Ub* transcript levels. Mean and standard deviation (SD) were derived from 3 biological replicates. Asterisks indicate significant ( $p < 0.05$ ) difference in gene expression before and after inoculation.

Symbiotic mutants carrying loss-of-function *pollux/dmi1* alleles show morphological root hair responses to NF, including tip swelling and branching, but are unable to form RHC structures nor ITs (Catoira et al., 2000; Imaizumi-Anraku et al., 2005). Using a *M. loti* strain constitutively expressing the fluorescent protein DsRed (Markmann et al., 2008), we have tested whether *patchy* mutants are invaded via RHC and IT formation. At 10 DAI, ITs were abundant on wild type roots, whereas only single ITs were observed on *patchy* mutants that were grown in closed jars at 24 or 18 °C (Figure 23A to C and G). Still, nodule primordia had frequently formed coinciding with rhizobial foci that appeared to have proliferated at the base of deformed root hairs (Figure 23D to F). At 3 WAI with *M. loti*, mature nodules had developed on *patchy* mutants. The nodules contained bacteroids, as indicated by DAPI staining of 80-µm histological sections, and were indistinguishable from the wild type (Figure 24A to D). The frequency of nodule primordia and mature nodules at 3 WAI was similar in wild type and *patchy* plants, but significantly more mature nodules had developed on wild type plants 12 WAI (Figure 24E). We furthermore tested, whether growth temperature had an effect on the nodulation frequency, as it is the case with *Lotus* nucleoporin mutants (Kanamori et al., 2006; Saito et al., 2007). While there were no differences between *patchy* and wild type plants at 18 °C, wild type plants contained significantly more nodule primordia and mature nodules at 24 °C than *patchy* mutants (Figure 24F). This indicates that nodulation conditions were better at 24 °C than at 18 °C but the maximum number of nodules formed by *patchy* mutants had been reached at 18 °C. Consequently, differences in nodule numbers became apparent only at 24 °C. Our observation suggest that the nodules might be infected via rare IT formation, which then leads to thorough rhizobial colonization of the nodule cortex. Since POLLUX function is required for rhizodermal infection, the *patchy/pollux-7* seems to be a weak allele that has residual signaling activity leading to the activation of symbiotic gene expression.



G

		IT ratio <sup>a</sup>	IT mean (SD) <sup>b</sup>
Wild Type	18°C	6/6	24.17 (4.30)
	24°C	6/6	17.93 (4.46)
<i>patchy</i>	18°C	1/7	0.04 (0.10)
	24°C	1/6	0.04 (0.09)

<sup>a</sup>Root systems with ITs divided by all root systems analyzed.

<sup>b</sup>Number of ITs divided by root length.

**Figure 23. Rhizobial Entrapment at Root Hairs and Rare Infection Thread Formation in *patchy*.**

**(A) to (F)** Light micrographs of *patchy* root sites, where rhizobial entry via an IT (A to C) or rhizobial proliferation at the root surface (D to F) had occurred. At both sites the formation of a nodule primordium was initiated. BF (A and D) and epifluorescence using RFP N3-filter (B and E) images were taken 10 DAI with *M. loti* expressing DsRed. Overlays are shown in (C) and (F). Scale bars: 50 μm.

**(G)** Frequencies and amounts of ITs observed on WT and *patchy*.



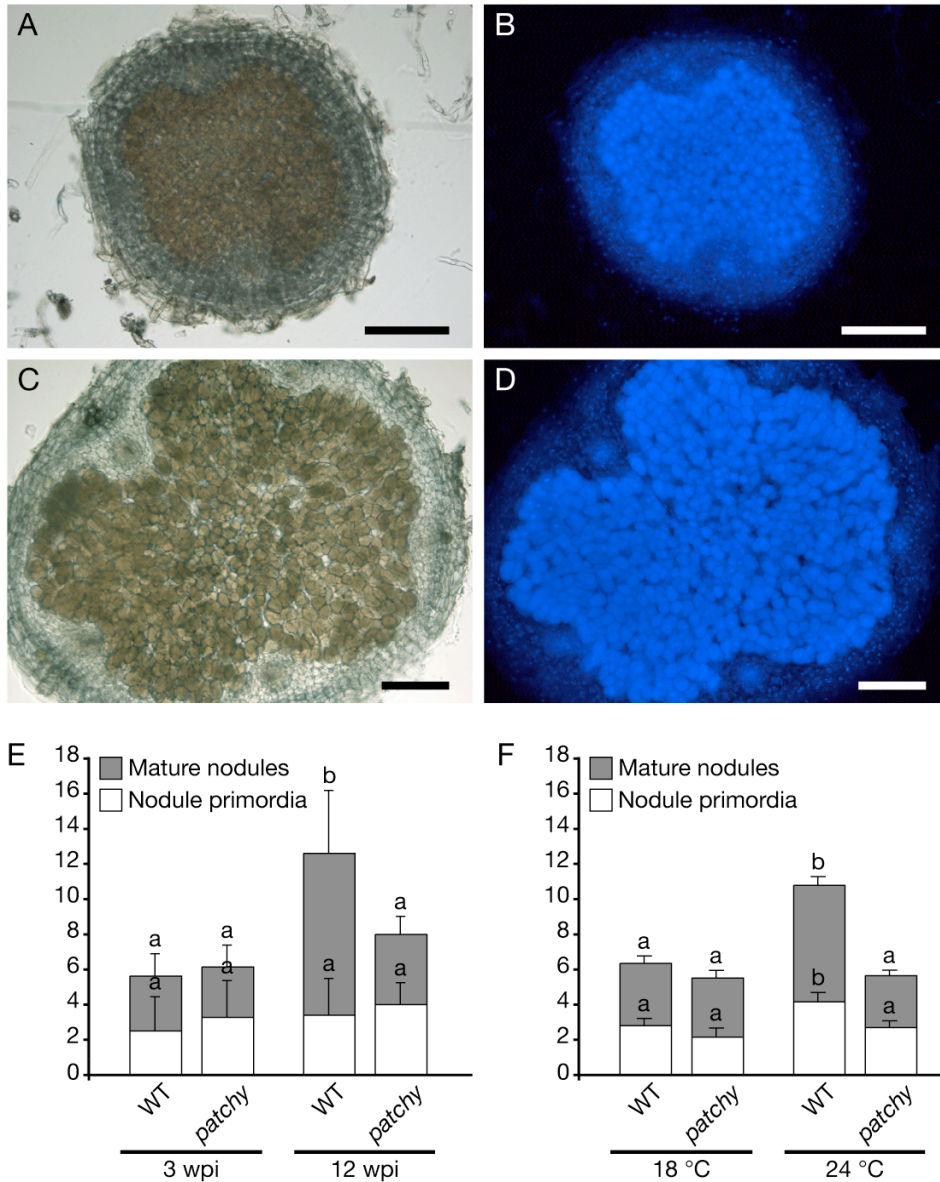


**Figure 24. Mature Nodule Are Formed at Reduced Frequency in *patchy*.**

**(A) to (D)** Light micrographs of 80- $\mu$ m sections from mature WT (A and B) and *patchy* (C and D) nodules. Nodules were harvested 3 WAI with *M. loti*. Rhizobial colonization was visualized by DAPI staining and epifluorescence microscopy using a DAPI A4-filter. Scale bars: 100  $\mu$ m.

**(E) to (F)** Mean ( $n \geq 5$  in E and  $n \geq 14$  in F) mature nodules and nodule primordia formed on WT and *patchy* roots at 3 and 12 WAI with *M. loti* and cultivation in the glasshouse (E) or 3 WAI with *M. loti* and cultivation at 18°C or 24°C constant (F). Error bars indicate SD and different letters above bars indicate significant differences ( $p \geq 0.05$ , *t*-test).

## ***NENA*, a *Lotus japonicus* Homolog of *Sec13* Is Required for Rhizodermal Infection by Arbuscular Mycorrhiza Fungi and Rhizobia but Dispensable for Cortical Endosymbiotic Development**

### **Identification of the AM Mutant *nena***

Among the mutants isolated that exhibited heritable AM defects, we obtained one family (SL1841-N) containing individuals with a severe and early defect during AM development. In the course of this work the causative mutation has been identified (see below) and the corresponding mutant allele was named *nena-1*. When cultivated together with '*G. intraradices*-like' BEG195 (Stockinger et al., 2009) *nena-1* mutants displayed balloon-shaped swollen hyphal structures that had formed at sites of attempted fungal penetration of the root surface (Figure 25B). These structures were not observed on wild type plants (Figure 25A). Confocal laser scanning microscopy (CLSM) revealed that AM fungal infection of *nena-1* mutants was aborted after invasion between rhizodermal cells at the stage of intracellular passage through the outer root layers (Inset in Figure 25B; Supplemental Figure 8B). This stage is essential for the succeeding colonization in the wild type (inset in Figure 25A; Supplemental Figure 8A). Consequently, roots of *nena-1* mutants that were co-cultivated with BEG195 at 24 °C were nearly void of internal hyphae (Figure 25E). Successful infection of *nena-1* was observed at low frequency. In these cases, hyphae traversed the rhizodermal layer despite obvious obstructions (Supplemental Figure 8C) and led to cortical colonization and formation of arbuscules that were indistinguishable from the wild type (Figure 25C and D).

### ***nena* Mutants Have Temperature Dependent Defects in AM and RNS**

The AM phenotype of *nena* mutants was assessed at different growth temperatures. The initial AM phenotypic analyses were performed at 24°C and the observations (Figure 25E) differed strongly to the AM phenotype obtained at 18°C growth temperature (Figure 26A and B). The frequency of successful infections ( $1.36 \pm 0.14$  per cm root tissue) in *nena-2* cultivated at 18°C approached wild type levels ( $2.24 \pm 0.62$ ), although balloon-like hyphal structures were still present. Consequently, average hyphal and arbuscule colonization of *nena-2* did not differ significantly from the wild type.

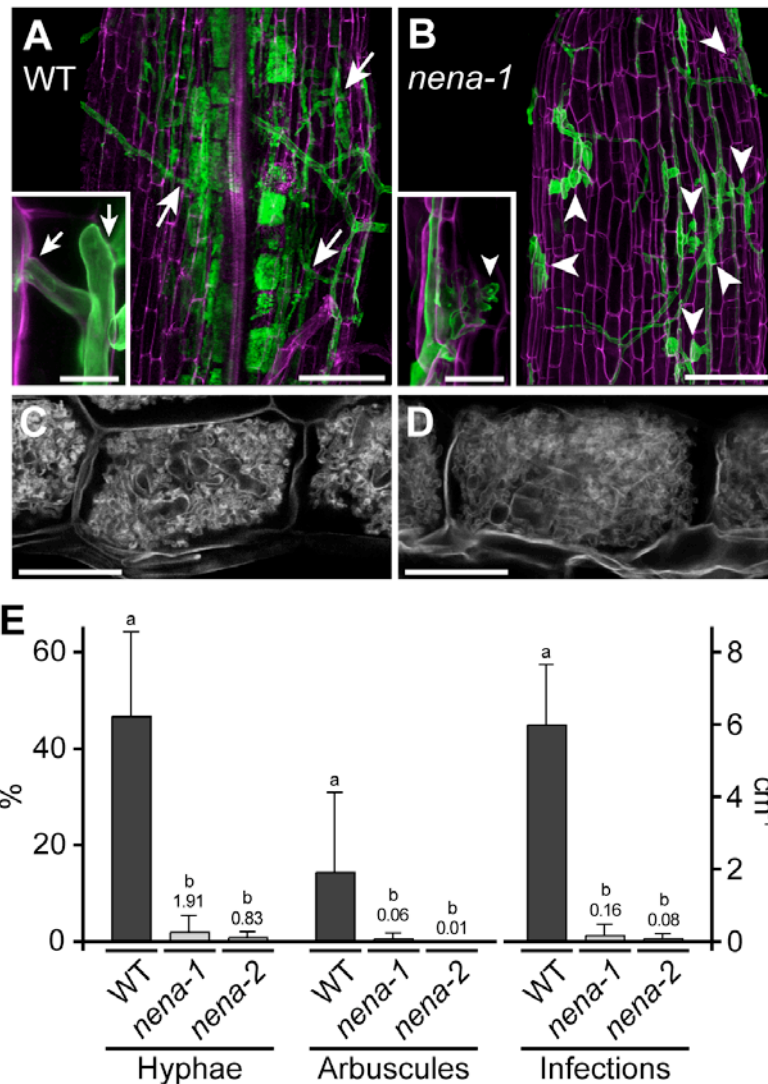


**Figure 25. *nena* Is Impaired in AM Fungal Infection.**

**(A) to (D)** Confocal micrographs of WGA-Alexa Fluor 488 stained AM fungal structures (green in (A) and (B)) associated with WT and *nena* plants. In WT (A) the AM fungus penetrated the outer cell layers (arrows), colonized the root cortex and formed arbuscules. In *nena-1* (B) hyphae grew on the root surface and balloon-shaped hyphal structures (arrowheads) occurred at aborted infection sites. Insets show infection sites at higher magnification. Root cell walls were stained with propidium iodide and are shown in magenta. Arbuscules formed in *nena-2* (D) did not differ from WT (C). AM phenotypes of *nena-1* and *nena-2* did not differ. Images represent observations from  $\geq 8$  plants per line co-cultivated with BEG195 for 3 w. (A) and (B) Z-projections of GFP/RFP overlays; (C) and (D) GFP channel. Scale bars: (A) and (B) 100  $\mu\text{m}$  (C), (D) and insets 20  $\mu\text{m}$ .

**(E)** Mean hyphal colonization (Hyphae, %), arbuscular colonization (Arbuscules, %) per root and successful infection sites per cm per root (Infections) from WT and *nena* plants ( $n \geq 4$ ) after 3 w of cultivation at 24  $^{\circ}\text{C}$ . Small values are shown by numbers above bars. Error bars show standard deviations (SD). Different letters above bars indicate significant differences ( $p \leq 0.05$ , *t*-test) between pairwise comparisons.



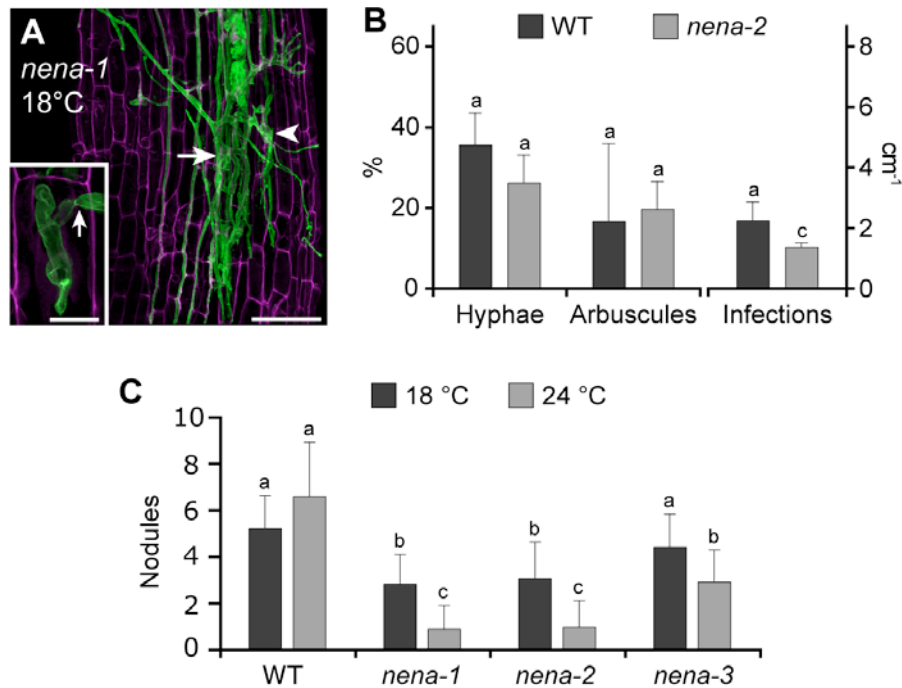


**Figure 26. AM and Nodulation Defects of *nena* Are Temperature Dependent.**

**(A)** Confocal z-projection of AM structures (green) in *nena-1* co-cultivated with BEG195 for 3 w at 18°C. Arrows and arrowheads indicate successful and aborted infection events, respectively. Inset shows an infection site at higher magnification. Scale bars: 100 µm, inset 20 µm.

**(B)** Mean hyphal colonization (Hyphae, %), arbuscular colonization (Arbuscules, %) per root and mean successful infection sites per cm per root (Infections) from WT and *nena-2* plants ( $n \geq 4$ ) after 3 w of cultivation at 18°C. Error bars show SD. Different letters above bars indicate significant differences ( $p \leq 0.05$ , t-test) between pair wise comparisons.

**(C)** Average nodule numbers at 18°C vs. 24°C growth temperature on WT and *nena* individuals ( $n \geq 10$ ). *nena* formed less nodules at 24°C than at 18°C and, except for *nena-3* at 18°C, nodulation was reduced in *nena* compared to WT. Error bars show SD. Different letters above bars indicate significant differences ( $p \leq 0.05$ , t-test) between pair wise comparisons.

Aborted AM fungal infection displayed by *nena* was similar to AM phenotypes of common *sym* mutants (Kistner et al., 2005). Therefore, *nena* mutants were inoculated with *Mesorhizobium loti* strains that are compatible with wild type *L. japonicus*. The nodulation assays at different temperatures revealed that *nena-1*, *nena-2* and *nena-3* formed fewer nodules than wild type plants and that this reduction was also stronger at 24°C compared to 18°C (Figure 26C). Temperature dependent defects in nodulation, AM colonization and arbuscule formation have previously been described for *nup133* and *nup85* *Lotus* mutants (Kanamori et al., 2006; Saito et al., 2007).

### Map-based Cloning of *NENA*

In order to assess the phenotypic segregation and identify the causative mutation by map-based cloning, a mutant  $M_3$  individual from SL1841-N was crossed to the

polymorphic mapping parent *L. japonicus* ecotype MG-20 (Miyakojima) (Kawaguchi et al., 2001) and F<sub>2</sub> mapping populations were generated from self-progeny. From these, 75 out of 276 phenotyped F<sub>2</sub> individuals were scored as AM defective, matching the segregation of a monogenic recessive trait ( $\chi^2$  probability = 0.40).

AM phenotypes of 276 F<sub>2</sub> self-progeny from MG-20 x *nena-1* (SL1841-N, M<sub>3</sub> mutant J8690) were determined (see AM mutant screen), genomic DNA was isolated and scanned for co-segregation with SSR markers. Primer sequences and marker information were retrieved from the miyakogusa.jp website (<http://www.kazusa.or.jp/lotus/>). Within the scored F<sub>2</sub> individuals, the allelic distribution of 30 SSR markers evenly covering the 6 chromosomes of *L. japonicus* displayed co-segregation of Gifu alleles with the mutant phenotype at the south end of LG II, between SSR markers TM0550 and TM0329 (Figure 27, top). After delimiting the location of *NENA* to a 0.4 cM interval on the south end of LG II, co-segregating markers were positioned on a physical contig of transformation-competent artificial chromosomes clones that were completely sequenced in the context of the *Lotus* genome project (Figure 27, bottom). Additional markers were derived from the contig sequence and used for identification of recombination events between markers flanking the target region. 2093 F<sub>2</sub> individuals were genotyped by power mapping using SSR markers TM0304 and TM0018 flanking the *nena* locus. AM phenotypes of 7 recombinant individuals, which carried only one MG-20 allele at one of the two marker positions, were determined in the F<sub>2</sub> generation and the F<sub>3</sub> self-progeny. Further co-segregation analysis was performed with the SSR markers TM0060, TM0635 and SSR17, which was predicted from the CM0060 contig sequence by SSRIT (Temnykh et al., 2001). After reducing the *nena* locus to less than 150 kb by map-based cloning (Figure 27), bioinformatic analysis of the sequence within the target region annotated 32 *NENA* candidate genes. Due to the interaction of yeast proteins Sc Seh1 and Sc Nup85 (Brohawn et al., 2008; Debler et al., 2008) and the previous identification of the symbiosis gene *NUP85* in *Lotus* (Saito et al., 2007), a *SEH1*-like annotated gene was picked out as a candidate. The candidate gene was sequenced and a C-T transition leading to a premature stop codon at AA 87 of the putative 326 AA (35.5 kD) protein was identified in the *nena-1* mutant (Supplemental Figure 6 and Table 6).

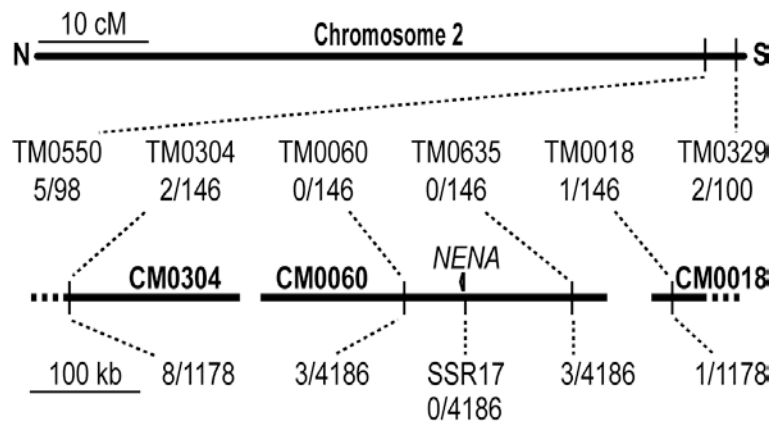


**Figure 27. Map-based Cloning of *NENA*.**

Genetic map of chromosome II (top) and physical map of contigs CM0304 and CM0018 encompassing CM0060 incl. the *NENA* locus (bottom). Positions and names of co-segregating SSR markers and the *NENA* gene are indicated. Ratios are numbers of recombinant/non-recombinant alleles of respective markers in *nen-1* x MG20 F<sub>2</sub> sub-populations. Marker names (except SSR17) and distances accord to the *Lotus* genome project.

The predicted *NENA* gene has an open reading frame (ORF) of 2023 nucleotides that is composed of 7 exons (Figure 28A). The gene structure has been verified by sequencing cDNA clones obtained from the *Lotus* Resource Center (Asamizu et al., 2000). The cDNA sequences carried 5' and 3' untranslated regions of 57 and 429 bp, respectively. The co-segregating marker SSR17 is located directly 5' of the start codon of *NENA*.

BLAST analysis of the *L. japonicus* genome revealed a partial duplication of the *NENA* gene,  $\psi$ *NENA*, which aligns to the first 409 nucleotides of the *NENA* ORF with 94% sequence identity.  $\psi$ *NENA* has an ORF of 488 bp and has not been physically mapped yet. Interrogation of public EST and protein databases gave no indication for the expression of  $\psi$ *NENA*. In addition, RT-PCR analyses on samples from different *Lotus* tissues did not show any corresponding transcripts (data not shown). Therefore,  $\psi$ *NENA* most likely represents a pseudogene.

We confirmed the obtained *in silico* data by genomic DNA gel blot analysis with two probes corresponding to 1.1 kb 5' sequence (I) and 0.5 kb from the centre (II) of *NENA* (Figure 28B). Probe I showed two hybridization bands per genomic digest and the patterns were as predicted by the genomic sequences surrounding *NENA* and  $\psi$ *NENA*. Probe II yielded one band per digest corresponding to the predicted *NENA* fragments.

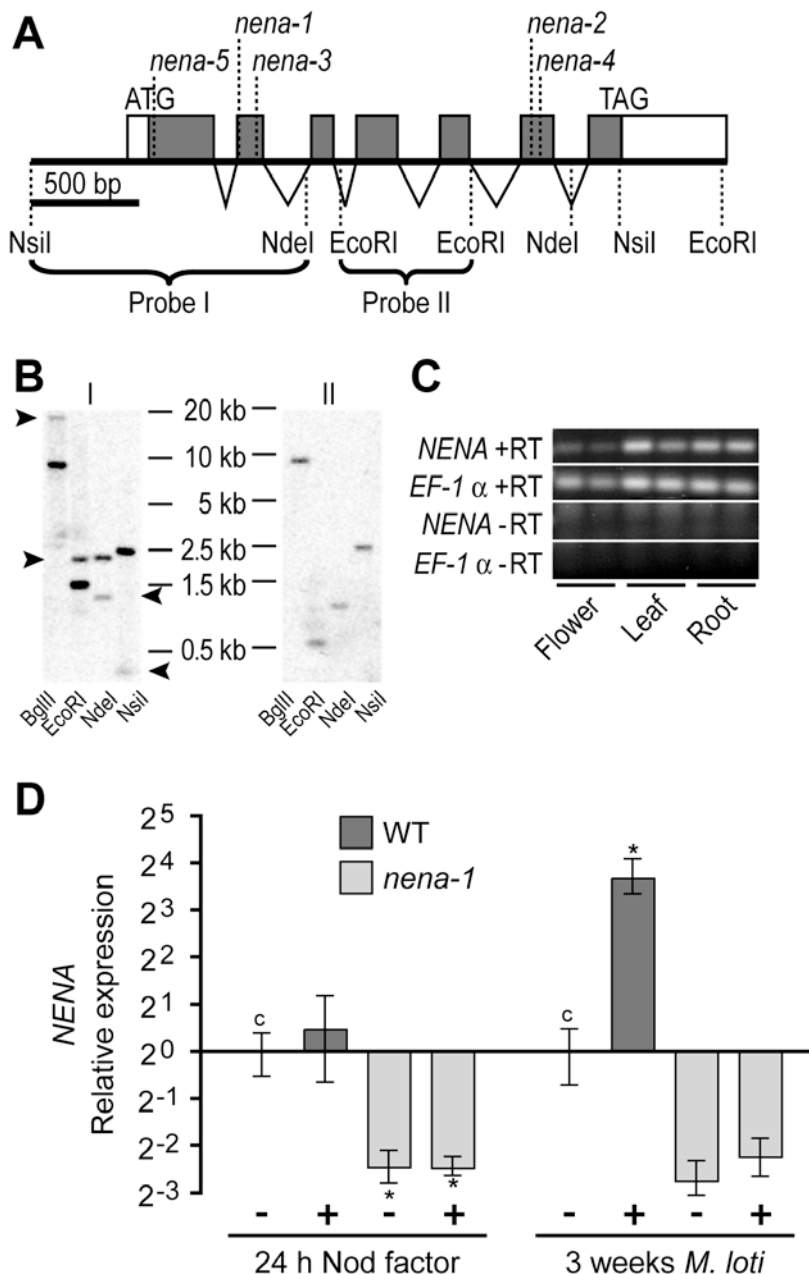


**Figure 28. *NENA* Is a Single Copy Gene That Is Expressed in Various Tissues and Upregulated in Nodulated Roots.**

**(A)** Gene structure of *NENA*. Filled boxes, white boxes and triangles represent coding exons, untranslated regions and introns, respectively. Positions of start and stop codons of the *NENA* ORF, mutations in different *nena* alleles and restriction sites of selected endonucleases are indicated. Braces span the restriction fragments used as probes in DNA gel blot analyses, as referred to in (B).

**(B)** DNA gel blot radiographs of *L. japonicus* genomic DNA digested with BgIII, EcoRI, NdeI or NsiI hybridized with Probe I or Probe II. Arrowheads mark bands that do not correspond to the genomic context of *NENA* but are due to partial gene duplication.

**(C)** Expression of *NENA* in leaves, flowers and roots (2 biological replicates) analyzed by RT-PCR. *NENA* and the reference gene *EF-1α* were amplified with (+RT) or without (-RT) preceding reverse transcription.

**(D)** Quantitative PCR analysis of *NENA* expression in WT and *nena-1* roots 24 h after NF treatment or 3 w after *M. loti* inoculation (+). Expression is relative to mock (-) treated WT controls (c) and normalized to *EF-1α* levels. Mean values and standard errors (SE) were derived from 3 biological replicates. Asterisks indicate significant ( $p < 0.05$ ) differences to c levels.

Using the *Lotus* TILLING resource (Perry et al., 2003) we obtained an allelic series for *NENA* that includes one additional nonsense allele (*nen-2*, W257Stop) and various alleles with missense mutations (*nen-3* to 5; Supplemental Figure 6 and Table 6). *nen-6* was identified by forward genetics using a C<sup>6+</sup> ion beam irradiated MG-20 population (M. Kawaguchi, unpublished). The AM and RNS phenotypes of *nen-2* were the same as of *nen-1* (Figure 25E), confirming the involvement of *NENA* in root symbiosis. The nodulation phenotype of *nen-3* was comparatively weaker but nodulation was still significantly reduced at 24 °C compared to wild type (Figure 26C). No symbiotic defects have been observed in *nen-4* and *nen-5* (Table 6).

**Table 6.** *nen-1* Alleles and Symbiotic Phenotypes

Allele	Line	Mutation	Nodulation	AM <sup>a</sup>
<i>nen-1</i>	SL1839-1, SL1841-N	Q97Stop	-, t.s.	+/-, t.s.
<i>nen-2</i>	SL0181-1	W257Stop	-, t.s.	+/-, t.s.
<i>nen-3</i>	SL1546-1	G117E	+/-, t.s.	n.d.
<i>nen-4</i>	SL0703-1	P270S	+	n.d.
<i>nen-5</i>	SL1747-1	G11S	+	n.d.
<i>nen-6</i>	C1978	Del./Inversion*	-**	-**

<sup>a</sup>, hyphal colonization; -, significantly reduced at 24°C and 18°C; +/-, significantly reduced at 24 °C only; +, wild type-like; t.s., temperature sensitive, significantly lower symbiotic performance at 24 °C vs. 18 °C; \*, *NENA* disruption by chromosomal rearrangements from C<sup>6+</sup> irradiation of MG-20; \*\*, determined at 22 °C only; n.d., not determined.

### ***NENA* Is Expressed in Shoots and Roots and Up-regulated during Nodulation**

Expression of *NENA* was determined by RT-PCR analysis. Transcripts were detected in all analyzed tissues including roots, flowers and leaflets, without major variation in expression levels relative to the reference gene *EF-1 α* (Figure 28C). Expression of *NENA* in wild type roots was unaltered after NF treatment, but increased 3 WAI with *M. loti* relative to mock-treated roots. Strong down regulation relative to wild type levels indicated a post-transcriptional degradation of *nen-1* mRNA possibly due to nonsense-mediated decay (Figure 28D). Therefore, *nen-1* most likely is a null allele.

## The *NENA* Gene Complements *nen-1* Mutants

We have introduced the *NENA* gene including 2 kb of putative promoter region lacking further predicted genes into a binary vector containing an RFP marker for C-terminal translational fusions (*NENA:RFP*). Transgenic (hairy) roots were generated by *Agrobacterium rhizogenes* mediated transformation with the T-DNA construct and complementation of the symbiotic phenotype was assayed. AM was fully restored in the *nen-1* mutant background, confirming that the identified mutation is causative for the *nen-1* phenotype (Figure 29D). Introduction of *NENA:RFP* also restored *nen-1* nodulation deficiency upon *M. loti* inoculation (Figure 29A to C and Table 7). As negative control, transformation with the same binary vector containing only the 2 kb 5' regulatory *NENA* sequence (*NENA<sub>pro</sub>:RFP*) did not complement *nen-1* (Figure 29E to H and Table 7). Nodule colonization was visualized by rhizobial DsRed expression (Figure 29B). The binary vector contains an ER-targeted enhanced green fluorescent protein (ER-GFP) marker (Karimi et al., 2002), which was used to monitor successful transformation (Figure 29A and E). Furthermore, expression of *NENA:RFP* and *NENA<sub>pro</sub>:RFP* was confirmed by CLSM (Figure X B, C and G).

Complementation of *nen-1* mutants was also achieved by *A. rhizogenes* mediated transformation with C-terminal *NENA* fusion to *GFP* controlled by the constitutive *CaMV 35S* promoter (*35S<sub>pro</sub>:NENA:GFP*) and by the predicted *NENA* ortholog from *Arabidopsis* (*At1g64350*) under control of the 5' regulatory *NENA* sequence from *L. japonicus* (Table 7).

**Table 7.** Complementation Analysis of *nen-1* by *A. rhizogenes*-Mediated Transformation

Line	Construct	Nodulation Ratio <sup>a</sup>	Nodules (SD) <sup>b</sup>
<i>nen-1</i>	<i>NENA<sub>pro</sub>:RFP</i>	4/30	0.3 (0.7)
<i>nen-1</i>	<i>NENA:RFP</i>	35/37	7.4 (5.5)
<i>nen-1</i>	<i>NENA<sub>pro</sub>:AtSeh1</i>	34/45	5.3 (5.2)
<i>nen-1</i>	<i>35S<sub>pro</sub>:NENA:GFP</i>	8/9	7.3 (6.9)
WT	<i>NENA<sub>pro</sub>:RFP</i>	5/5	6.6 (3.1)
WT	<i>NENA:RFP</i>	5/5	10.6 (5.4)
WT	<i>NENA<sub>pro</sub>:AtSeh1</i>	12/12	11.6 (7.4)

<sup>a</sup> Ratios indicate numbers of successfully transformed plants that formed nodules vs. all plants of the indicated line that were successfully transformed with the indicated construct

<sup>b</sup> Mean nodule number per successfully transformed plant

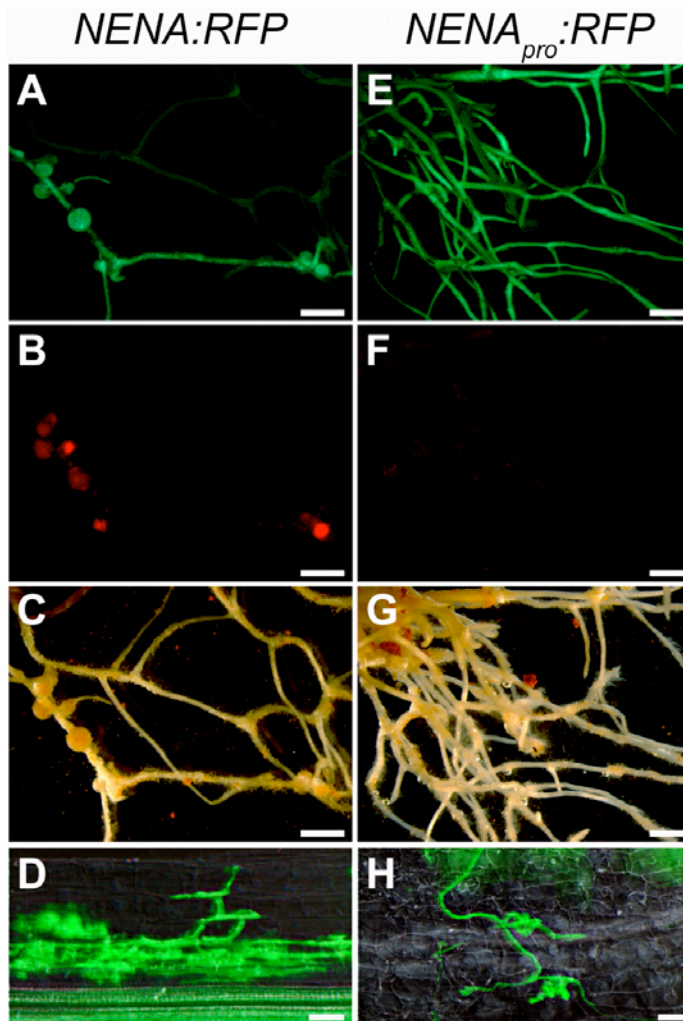


**Figure 29. Transgenic Complementation of *nena-1*.**

**(A) to (D)** *A. rhizogenes*-mediated transformation of *nena-1* mutants with genomic *NENA* including 2 kb of 5' regulatory sequence fused to *RFP* (*NENA:RFP*) led to restoration of RNS (A to C) and AM establishment (D).

**(E) to (H)** *A. rhizogenes*-mediated transformation of *nena-1* with the 2 kb 5' regulatory sequence fused to *RFP* (*NENA<sub>pro</sub>:RFP*) did not restore RNS (E to G) and AM (H). Epifluorescence microscopy images show GFP expression in transgenic roots (A and E) and DsRed expression by *M. loti* in root nodules (B and F) using a GFP and a RFP filter, respectively. Corresponding white light illumination images are shown in (C) and (G). Root segments containing AM fungal structures (green) stained with WGA-Alexa Fluor 488 were visualized by DIC/epifluorescence microscopy using a GFP filter (D and H). Scale bars: (A) to (C) and (E) to (G) 2 mm, (D) and (H) 40  $\mu$ m.

### **NENA Belongs to the Sec13/Seh1 Protein Family**

BLAST analysis of the NENA protein revealed 25% AA identity to Sec13 homolog 1 (Seh1) from yeast or humans. Moreover, there is 25% and 24% identity to the Sec13 protein of humans and yeast, respectively. Sec13 and Seh1 both are nucleoporins belonging to the yeast Nup84/ human Nup107-160 subcomplex (herein after referred to as the Nup84 subcomplex) (Siniosoglou et al., 1996; Belgareh et al., 2001). In addition, Sec13 together with Sec31 forms the framework of COPII vesicle coats (Fath et al., 2007). We have reconstructed the phylogenetic relationships of Seh1, Sec13 and NENA related sequences from yeast, humans and different plant species (Figure 30). The trees obtained comprise two clearly separated clusters: the 1<sup>st</sup> cluster contains proteins that are closely related to Sec13. The 2<sup>nd</sup> cluster contains one member per plant species and includes NENA. Seh1 from yeast and humans form a 3<sup>rd</sup> branch. Based on the calculated phylogenetic distances, members of the 2<sup>nd</sup> cluster, including NENA, are more closely related to Seh1 than to



Sec13. The *L. japonicus* genome contains in addition at least two genes, *SEC13-like 1* and *SEC13-like 2*, which are more closely related to *Sec13* than the *NENA* gene.

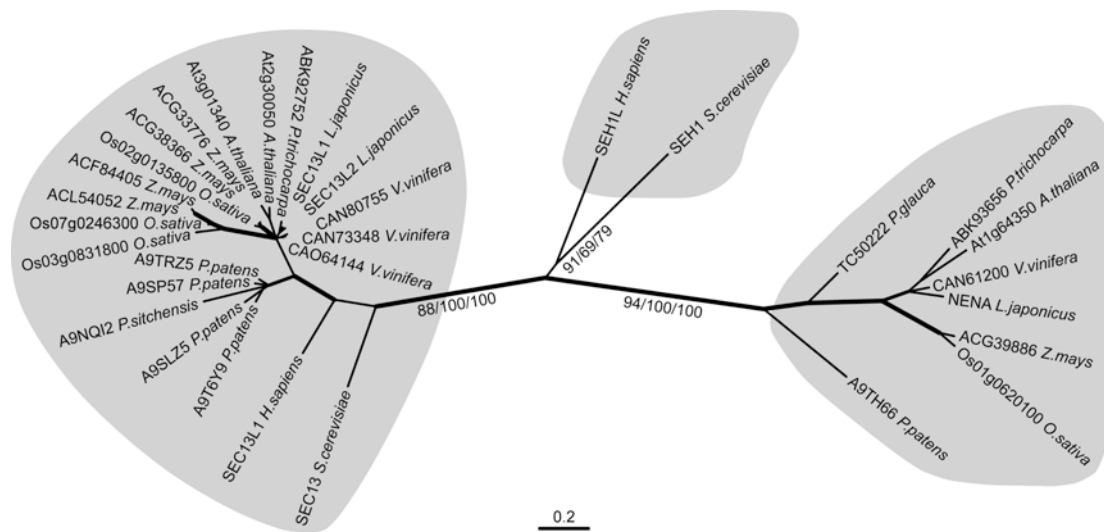


**Figure 30. Phylogenetic Relationships of Sec13/Seh1-like Proteins.**

The phylogenetic tree includes AA sequences from yeast, humans and representative species of bryophytes (*Physcomitrella patens*), gymnosperms (*Picea spp.*), monocots (*Oryza sativa* and *Zea mays*) and dicots (*A. thaliana*, *L. japonicus*, *Populus trichocarpa* and *Vitis vinifera*). Three statistically supported clusters are highlighted: Sec13 related sequences on the left, yeast/human Seh1 in the middle and plant Seh1 related sequences including NENA on the right. Distances correspond to the best fitting Maximum-Likelihood (ML) tree. Branch labels indicate bootstrap values (n=1000) of ML/NJ/maximum-parsimony consensus trees. Thick, medium and thin branches indicate bootstrap values  $\geq 90$ ,  $\geq 80$  and  $< 80$  in at least two consensus trees, respectively. Labels at the branch tips include GenBank accession numbers or gene names (accession numbers in METHODS). Isoforms from splice variants were excluded from the analysis.

### **NENA and NUP85 of *L. japonicus* Interact in Yeast**

Sc Seh1 and Sc Nup85 are *bona fide* constituents of nuclear pores and interact in yeast (Siniosoglou et al., 1996). *In vitro* reconstitution of recombinant Sc Seh1, Sc Nup85 and remaining components of the Nup84 subcomplex, including Sc Nup133, revealed their relative positions in a Y-shaped complex (Figure 31B) (Lutzmann et al., 2002). Therefore, we tested for interaction between NENA, NUP85 and NUP133 by yeast two-hybrid analysis. The results fully support homologous functions in *Lotus*: co-transformation of *NENA* fused to the *Gal4* activating domain (*AD*) and *NUP85* fused to the *Gal4* binding domain (*BD*) allowed yeast growth on selection media, whereas no growth was observed when *AD:NENA* was combined with *BD:NUP133*, *BD:NENA* or the empty *BD* vector (Figure 31A). This was confirmed by switching *AD* and *BD* (Supplemental Figure 31B). Furthermore, SEC13-like 1 and



SEC13-like 2 did not show interaction with NUP85, but interacted with the corresponding partner from yeast, Sc Nup145 (Supplemental Figure 31A).

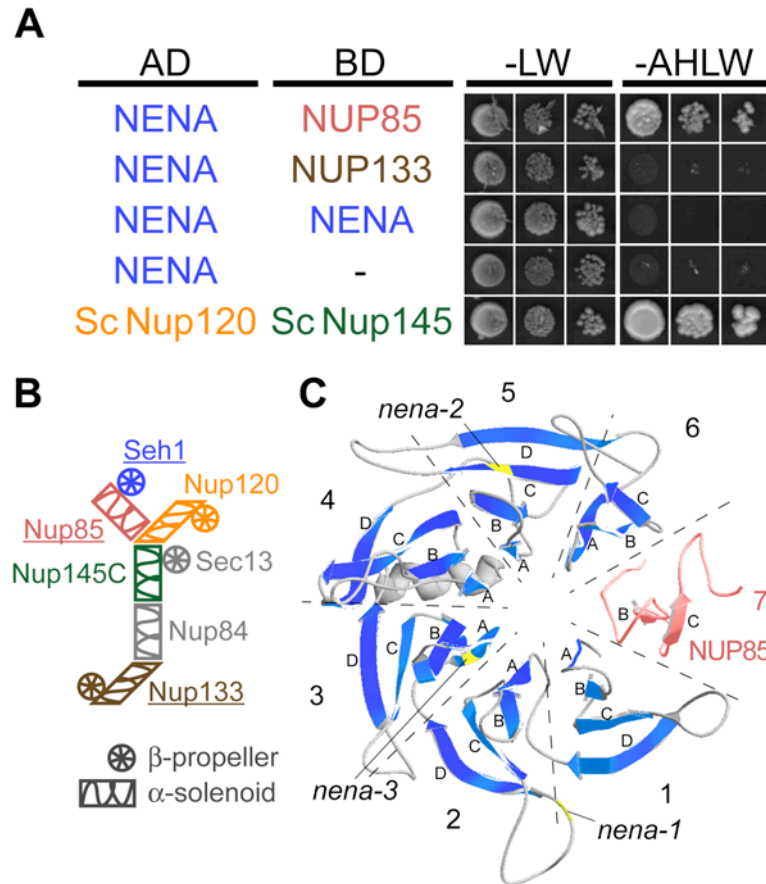


**Figure 31. NENA Interacts with NUP85 from *L. japonicus* and Adopts a  $\beta$ -propeller Structure According to Homology Modeling.**

**(A)** Gal4-based yeast two-hybrid assay for interaction between NENA as prey (AD) and NUP85, NUP133 or NENA as bait (BD). The empty bait vector (-) was used as negative control, AD:Sc NUP120 and BD:Sc NUP145 as positive control. Co-transformed yeast was grown in 3 dilutions on synthetic dropout medium lacking leucine and tryptophan (-LW) or adenine, histidine, leucine and tryptophan (-AHLW).

**(B)** Schematic representation of the yeast Nup84 subcomplex and the arrangement of its components (Lutzmann et al., 2002). Putative homologs known to be required for root symbioses in *L. japonicus* are underlined. Color scheme refers to (A) and (C).

**(C)** Ribbon representation of a conceptual  $\beta$ -propeller formed by NENA (blue  $\beta$  strands, model comprises residues 11-317) and the N-terminus of NUP85 (red, res. 36-94). The model is based on crystal structures of Sc Seh1•Sc Nup85. Individual blades are delimited by dashed lines and numbered. Letters correspond to successive  $\beta$  strands in each blade. Lack of  $\beta$  strands in blades 6 and 7 is due to missing template data and incomplete sequence alignment. Positions of mutations in alleles *nena-1*, -2 and -3 are indicated.

## **NENA Is a WD40 Repeat Protein**

Structural prediction of the NENA protein indicated that the distribution of identified WD40 repeats matches well to the architecture of Sc Seh1 (Supplemental Figure 6) and places NENA into the large family of  $\beta$ -transducin-like/WD40 repeat proteins (Neer et al., 1994). Members of this family exhibit a highly conserved 3-dimensional ' $\beta$ -propeller' structure, typically composed of 7 circularly arranged blades. Each blade is formed by 4 anti-parallel  $\beta$  strands, of which the last and the first 3  $\beta$  strands of two adjacent blades correspond to one WD40 unit (Smith et al., 1999). Based on crystal structures of the Sc Seh1•Sc Nup85 pair (Brohawn et al., 2008; Debler et al., 2008) and the alignment of Sc Seh1 and NENA (Supplemental Figure 6) we created a 3D model of the NENA protein (Figure 31C). The arrangement of predicted secondary structures is largely consistent with the 6 bladed  $\beta$ -propeller fold of Seh1, except for a helix between strands 3D and 4A and the C-terminal loop, which are not supported due to alignment gaps and the lack of template data in disordered regions. The Seh1•Nup85  $\beta$ -propeller is completed and stabilized by the domain invasion motif (DIM) of Sc Nup85 (Brohawn et al., 2008; Debler et al., 2008). Therefore we created a homology model of NUP85 comprising residues 36 to 94 and fitted it to the DIM of yeast Nup85. Although complete modeling of the seventh blade including the strands required for the Velcro closures (Smith et al., 1999) between Sc Seh1 and Sc Nup85 was not possible due to sequence divergence at the beginning of the aligned sequences,  $\beta$  strands 7B and C matched well to the template structure.

## **NENA and NUP85 Are Located at the Nuclear Rim**

In order to determine the sub-cellular localization of the NENA protein in *Lotus* roots, the *NENA:RFP* fusion construct, which complemented the symbiotic defects of *nen-1* (Figure 29A to D and Table 7), was introduced into *nen-1* mutants by *A. rhizogenes*-mediated transformation. RFP signal detected by CLSM of transgenic roots was located at the nuclear rim, as shown in optical sections from rhizodermal cells (Figure 32B and C). The identity of the sub-cellular compartment was verified by perinuclear ER-GFP expression of the transformation marker and by comparison with brightfield micrographs (Figure 32E and F). In contrast, hairy roots that were transformed with *NENA<sub>pro</sub>:RFP* showed red fluorescence in the cytoplasm and inside the nucleus (Figure 32G to J), as expected for freely diffusible RFP. Moreover,

$35S_{pro}:NUP85:GFP$  that has been introduced into wild type roots by *A. rhizogenes*-mediated transformation was also localized at the nuclear rim (Figure 32A).

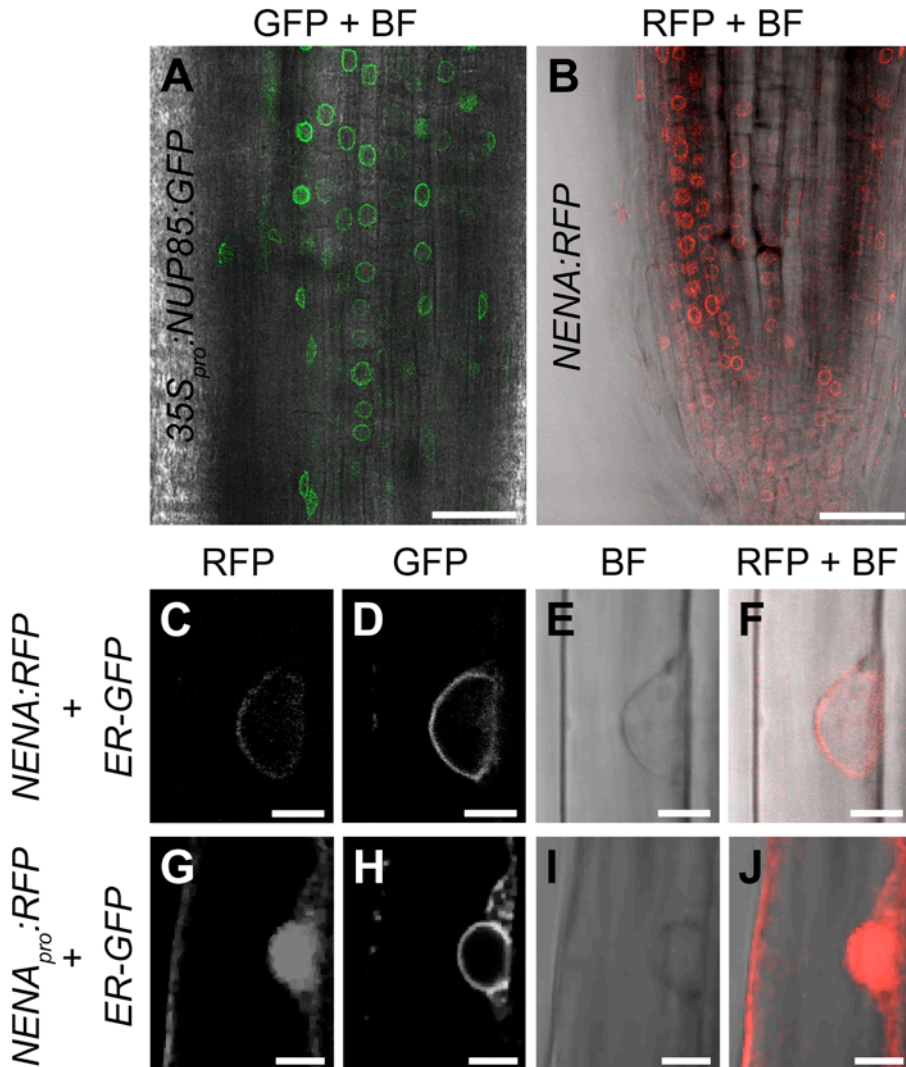


**Figure 32. Perinuclear *in vivo* Localization of NUP85 and NENA Fusion Proteins.**

(A) Overlay of fluorescence and brightfield confocal micrographs showing perinuclear green fluorescence in root tip cells expressing  $35S_{pro}:NUP85:GFP$ .

(B) Overlay of fluorescence and brightfield confocal micrographs showing perinuclear red fluorescence in root tip cells expressing  $NENA:RFP$  and the  $ER-GFP$  marker (not shown).

(C) to (F) Confocal micrographs of a rhizodermal cell expressing  $NENA:RFP$  (C and F) and the  $ER-GFP$  marker (D).

(G) to (J) Confocal micrographs of a rhizodermal cell expressing cytonucleoplasmic  $NENA_{pro}:RFP$  (G and J) and the  $ER-GFP$  marker (H).

Images are from WT (A) and *nen-1* (B to J) *A. rhizogenes*-transformed roots and were acquired in sequential mode at Excitation<sub>λ</sub>=561nm/Detection<sub>λ</sub>=570–630nm (RFP), Excitation<sub>λ</sub>=488nm/Detection<sub>λ</sub>=495–555nm (GFP) or brightfield (BF). Scale bars: (A) and (B) 40 μm, (C) to (J) 5 μm.

## NENA Is Required for Rhizodermal Nod Factor Response

*NUP133* and *NUP85* are both required for NF-induced  $\text{Ca}^{2+}$  spiking (Kanamori et al., 2006; Saito et al., 2007). Therefore, we measured intracellular  $\text{Ca}^{2+}$  concentrations by microinjection of a reporter dye into root hairs of young seedlings. 75 % of wild type root hairs showed  $\text{Ca}^{2+}$  spiking after NF application. In contrast, there was only one positively scored response in 90 analyzed *nena-1* root hairs (Figure 33). This single  $\text{Ca}^{2+}$  spiking response was weaker and observed in a young root hair, where the nucleus was located at the base of the trichoblast. Usually, older root hairs, with more apical nuclei, are used for  $\text{Ca}^{2+}$  spiking measurements by microinjection (Supplemental Figure 33B) (Miwa et al., 2006).

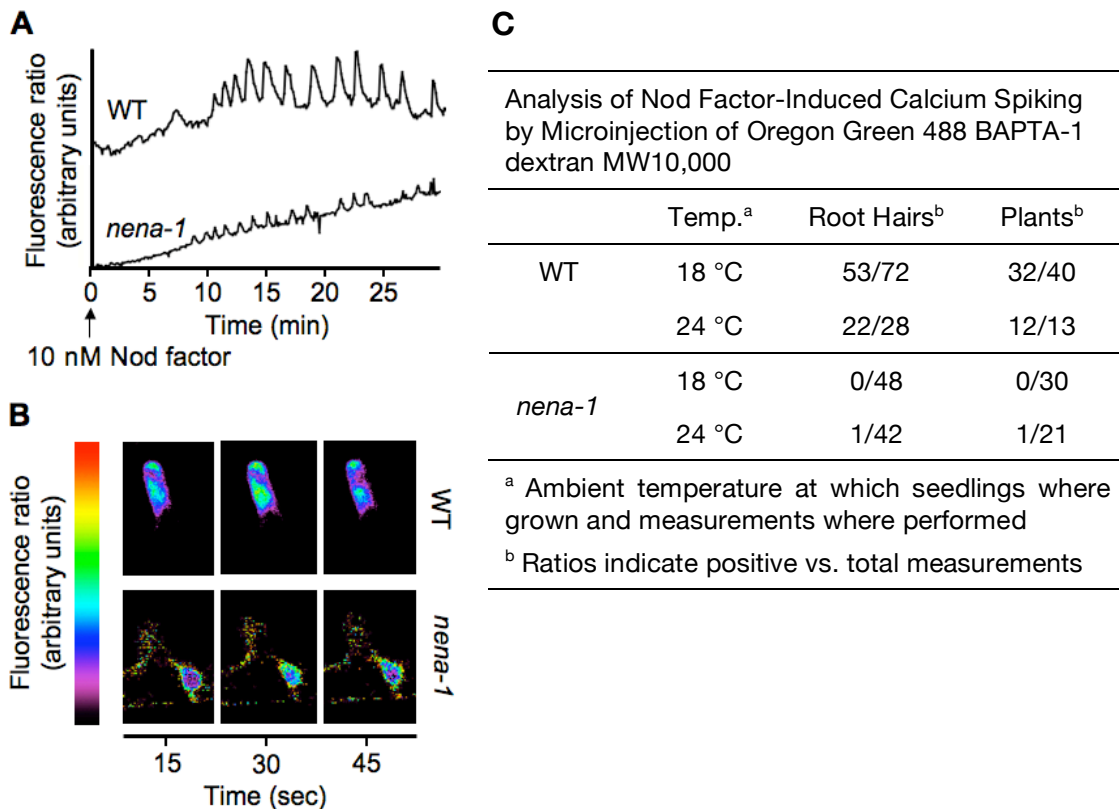


**Figure 1. Calcium Spiking in Root Hairs of Wild Type and *nena-1*.**

**(A)** Fluorescence ratios between ratiometric  $\text{Ca}^{2+}$  indicator Oregon Green 488 BAPTA-1 (OG) and reference dye Texas Red (TR) after NF application to roots are indicated over time. The upper trace is representative of positive spiking in *L. japonicus* Gifu wild type. The lower trace represents an exceptional positive spiking in *nena-1*.

**(B)** Images of one  $\text{Ca}^{2+}$  spike before (15 sec time point), during (30 sec) and after (45 sec) a perinuclear  $\text{Ca}^{2+}$  burst in a WT root hair and a *nena-1* trichoblast. False colors represent fluorescence ratios between OG and TR.

**(C)** Representative traces for positive  $\text{Ca}^{2+}$  spiking are shown in (A).

Since residual nodulation in *nena* might be connected to rare  $\text{Ca}^{2+}$  spiking events, we further investigated the expression of genes that are induced by NF or rhizobia. Among these, *NIN* expression provides temporal and spatial information, because it is rapidly induced in rhizodermal cells, including root hairs, of the susceptible zone (Radutoiu et al., 2003) and later on in cortical cells of developing nodules (Schauser et al., 1999). Using the *GUS* reporter gene fused to the *NIN* promoter region, *NIN* induction was shown to be absent in *nfr1* mutants (Radutoiu et al., 2003). Hence, we used this reporter construct to analyze *NIN* expression patterns in *nena-1*. In contrast to the wild type, none of the transformed root systems showed *GUS* activity in rhizodermal cells of the susceptible zone in response to NF or *M. loti* up to 3 DAI. At 7 and 16 DAI, however, transformed *nena-1* mutants showed strong *GUS* activity in the cortex and single cells of the outer layers of developing nodules (Table 3, Figure 34A and Supplemental Figure 9).

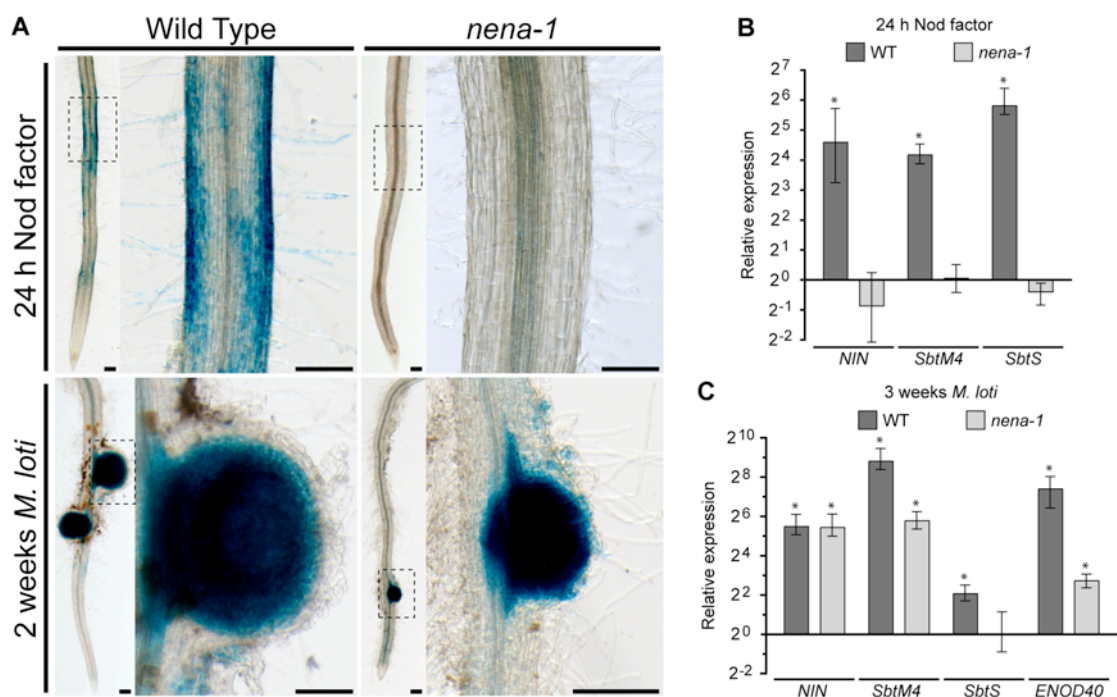


**Figure 34. Rhizodermal Nod Factor Response Is Impaired Whereas Induction of Symbiosis Genes at Nodule Primordia Is Not Affected in *nena*.**

**(A)** Brightfield images of X-Gluc incubated roots transformed with *NIN<sub>pro</sub>:GUS* after NF treatment or inoculation with *M. loti*. No blue rhizodermal staining was observed in *nena-1* roots after NF treatment. Images correspond to Table 3. Boxed regions are shown at higher magnification. Scale bars: 0.2 mm.

**(B)** and **(C)** Quantitative PCR analysis of symbiosis gene expression in WT and *nena-1* roots 24 h after NF treatment (B) or 3 w after *M. loti* inoculation (C). Expression is relative to mock treated samples and normalized to *EF-1 $\alpha$*  levels. Mean and SE were derived from 3 biological replicates. Asterisks indicate significant ( $p < 0.05$ ) differences in gene expression between NF or *M. loti* and mock treatments.

The absence of early NF responsiveness was further corroborated by quantitative RT-PCR analysis of *NIN* and additional early-induced symbiosis genes (Figure 34B). *SbtM4* and *SbtS* encode subtilisin-like serine proteases that are specifically expressed during AM and RNS. Rhizodermis-specific expression of *SbtS* is induced by NF and ceases after approx. two w of nodule development, whereas *SbtM4* remains up regulated in nodules (Kistner et al., 2005; Takeda et al., 2009). While none of these genes was up regulated in *nen-1* roots treated with NF, *NIN*, *SbtM4* and the early nodulin *ENOD40-1*, which is strongly expressed in nodules (Takeda et al., 2005), were significantly induced in nodulated *nen-1* and wild type roots at 3 WAI with *M. loti*. *SbtS* was not induced in *nen-1* but upregulated in the wild type after NF treatment and 3 w after *M. loti* inoculation (Figure 34C).

**Table 8.** *NIN<sub>pro</sub>:GUS* Expression Analysis in Transgenic Roots of Wild Type and *nen-1* Genetic Background

Treatment	Line	Blue staining <sup>a</sup>
24 h Nod factor	WT	8/10
	<i>nen-1</i>	0/12
1 day <i>M. loti</i>	WT	5/6
	<i>nen-1</i>	0/8
3 days <i>M. loti</i>	WT	8/10
	<i>nen-1</i>	0/11
7 days <i>M. loti</i>	WT	8/11
	<i>nen-1</i>	1/12
16 days <i>M. loti</i>	WT	11/11
	<i>nen-1</i>	10/11

<sup>a</sup> Ratios indicate numbers of plants that showed *GUS* expression in rhizodermal or nodule cortical cells divided by the total number of analyzed root systems per indicated treatment.

### Rhizobial Infection of *nen-1* Resembles Crack Entry

The lack of early responses to rhizobia displayed by *nen-1* conflicted with our prior observation of infected nodules on *nen-1* mutants, as visualized by inoculation with DsRed expressing *M. loti*. Therefore, we quantified the ITs that lead to rhizobial invasion of nodules via RHC, in order to check for rare infection events. However, no root hair ITs were observed by fluorescence microscopy of *nen-1* mutants at 7 DAI (n=19) and 12 DAI (n=21) (Figure 8A). In parallel, plants were inoculated with *M. loti* strain R7A expressing the *lacZ* reporter and microscopically analyzed after 7 d of growth at 18 °C. Wild type plants showed normal symbiotic development, including

RHC, rhizobial microcolonies and root hair ITs (Figure 36A). In contrast, *nen-1* mutants exhibited abnormal deformation of root hairs in responsive parts of the root. Occasionally, rhizobial microcolonies were observed at the base of deformed root hairs (Fig. 36B). RHC or root hair ITs were not observed in any of the inspected *nen-1* mutants.

In order to test for delayed nodule formation and rhizobial infection in *nen-1*, plants were analyzed at additional time points after inoculation with *M. loti* expressing DsRed. In the wild type, the number of nodules increased throughout the time course. All nodules were infected and colonized (Figure 36C), except at 51 DAI, where in two cases a small, uninfected nodule was observed (Figure 35B and D). In contrast, initiation of nodulation was delayed in *nen-1*, followed by a moderate increase in nodulation until 21 DAI. More than 90% of these nodules were uninfected. At 51 DAI, the average number of infected nodules increased to 1.11, while uninfected nodules decreased to 1.00, suggesting a proportional infection of initially uninfected nodules between 21 DAI and 51 DAI (Figure 35B). Nodulation in *nen-1* was strongly reduced compared to the wild type and no root hair ITs were observed in *nen-1* throughout the time course. However, we observed small patches of rhizobia on the root surface that coincided with uninfected nodules. Sectioning and CLSM of such empty nodules confirmed that rhizobia were confined to the surface and did not enter the cortex (Figure 36D). By contrast, analysis of *nen-1* nodules that showed rhizobial colonization at 21 DAI revealed intercellular intrusions of rhizobia spanning several cell layers from the apex into the nodule cortex. Hence this route was the most probable entry site for further nodule colonization (Supplemental Figure 10).

The infection structures observed in *nen-1* were reminiscent of crack entry. Some legumes, e.g. *S. rostrata*, can switch between intracellular infection during aerated conditions and crack entry during root submergence (Goormachtig et al., 2004). Therefore, we tested whether the water regime had an effect on RNS in wild type Gifu and *nen-1* plants. Indeed, the proportion of infected nodules per *nen-1* plant was significantly increased under waterlogging conditions compared to aerated conditions (Figure 35C and D). Since ethylene accumulation in the water saturated root environment is the chief cause for intercellular infection, we further tested if inhibition of endogenous ethylene production by AVG treatment can suppress infection during waterlogged conditions. The proportion of infected nodules was



significantly reduced by the addition of 5  $\mu\text{M}$  AVG prior to rhizobial inoculation (Figure 35C and D). The data confirm that nodule infection under waterlogging conditions depended on ethylene and thus provides strong evidence for intercellular infection of *nena-1* nodules. Infection rates did not significantly change in wild type plants, although the average nodulation rate was reduced under waterlogging conditions with or without AVG (Figure 35C and D).

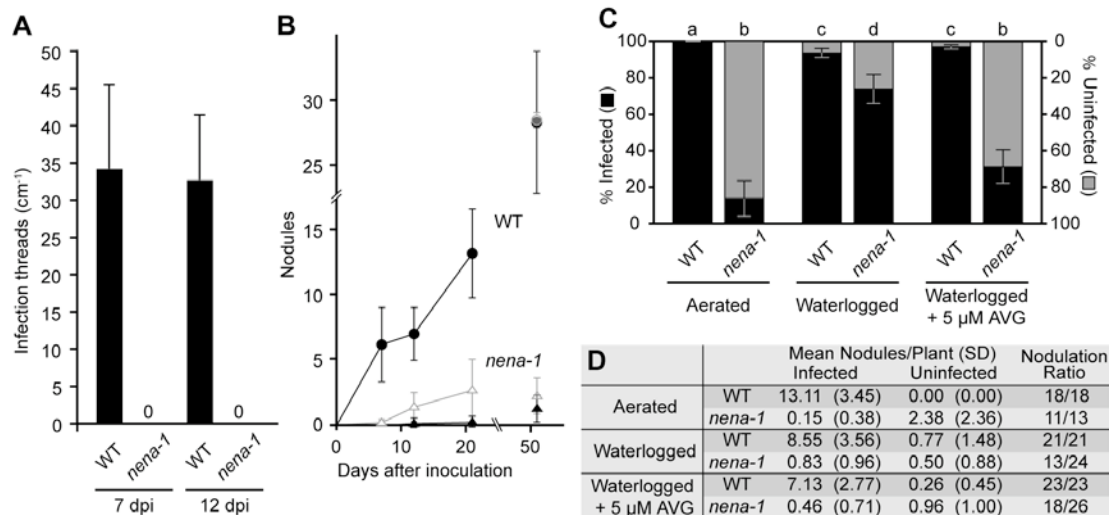


**Figure 35. Rhizobial Infection of *nena-1* Does Not Occur via Root Hairs and Is Promoted by Ethylene.**

**(A)** Quantification of root hair ITs 7 and 12 DAI with *M. loti* expressing DsRed and growth under aerated conditions; no ITs were observed in *nena-1*. Mean and SD were calculated from  $\geq 19$  (*nena-1*) and  $\geq 14$  (WT) root systems per time point.

**(B)** Nodulation time course during aerated growth conditions after inoculation with *M. loti* expressing DsRed. Mean and SD were calculated from 13 to 21 *nena-1* (triangles) and 12 to 18 WT (squares) root systems per time point. Open/gray and closed/black symbols represent total and infected nodules, respectively. If all nodules were infected, only infected nodules are indicated. If all nodules were uninfected, only total nodules are indicated.

**(C)** and **(D)** Quantification of nodules from WT and *nena-1* plants cultivated under different conditions 21 DAI with *M. loti* expressing DsRed. **(C)** Bars indicate mean percentages of uninfected (gray) and infected (black) nodules per nodulated individual. Error bars indicate SE. Different letters above bars indicate significant differences ( $p \leq 0.05$ , *t*-test) between pairwise comparisons. **(D)** Mean per plant, SD and number of nodulated plants vs. total number of plants per line and treatment (nodulation ratio) are indicated.

Further evidence for an intercellular infection mode was obtained by brightfield microscopy of 4  $\mu\text{m}$  sections from young *nena-1* nodules that contained subepidermal infection foci (Figure 36F). In addition, ITs were observed in the root cortex (Figure 36G). No subepidermal infection foci were observed in any of the sections from young wild type nodules (Figure 36E). Despite the apparent defects during the early infection process, sections of mature nodules did not indicate any structural



alterations in cortical infection and nodule development in *nena-1* compared to the wild type (Figure 36H to K).

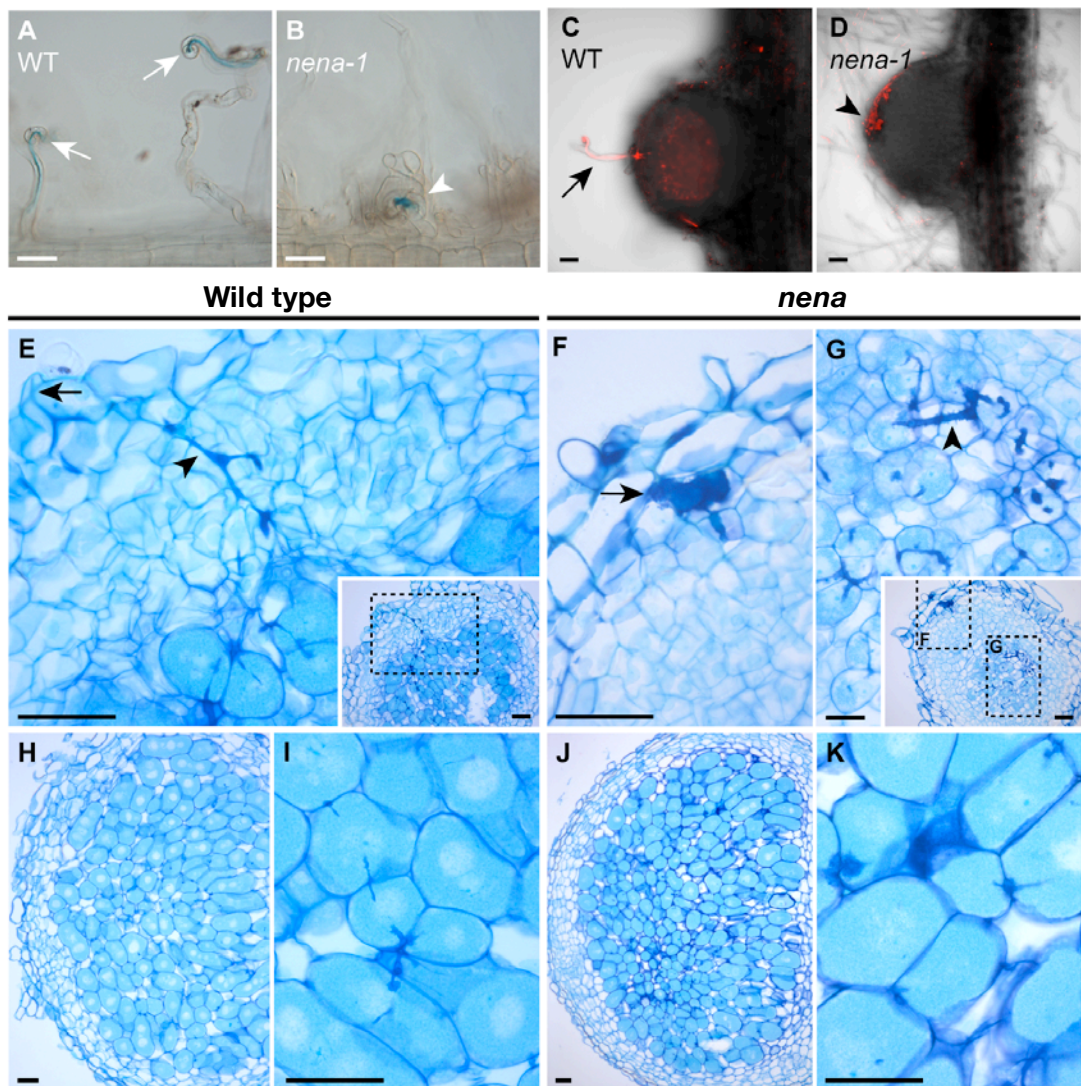


**Figure 36. Rhizobial Microcolonies at the Root Surface of *nena-1* Lead to Nodule Formation and Intercellular Entry.**

(A) and (B) BF DIC images from roots hairs 7 DAI with lacZ-expressing *M. loti* and 18 °C growth temperature. WT plants show root hair curling (arrows) and ITs, whereas *nena-1* mutants display abnormal root hair deformation and occasional colony formation by rhizobia (arrowhead). Images represent observations from  $\geq 8$  plants per line.

(C) and (D) Confocal z-projections of 80-μm longitudinal sections of a young infected WT (C) and an uninfected *nena-1* (D) nodule. (C) DsRed expressing rhizobia (red) have colonized the nodule via an intracellular root hair IT (arrow). (D) An uninfected nodule developed coinciding with accumulation of rhizobia at the root surface (arrowhead). Images represent samples from 16 DAI/aerated (C) and 21 DAI/waterlogged + 5 μM AVG (D) treatments.

(E) to (K) Thin sections of nodule tissue stained with toluidine blue. (E) Young WT nodule with intracellular IT (arrowhead) spanning from the infection site (arrow) into the cortex. (F) and (G) Young *nena-1* nodule with a subepidermal infection pocket (arrow) and cortical ITs (arrowhead). Insets in (E) and (G) show respective sections at lower magnification; dashed boxes indicate magnified areas. Longitudinal sections of mature nodules from WT (H) or *nena-1* (J) and corresponding magnifications (I) and (K) showing colonized host cells. Plants were grown under waterlogging conditions and sampled 3 WAI with *M. loti* R7A.

Scale bars: 50 μm, except (G) 20 μm.



## DISCUSSION

### Symbiotic Infection of Rhizodermal Cells Is Blocked in *nen1*

We found that the *nen1* mutation impairs symbiotic responses of the rhizodermis. AM development at non-permissive temperature was mostly blocked in the outer root cell layers. The balloon-like hyphal structures at the infection sites resembled the phenotypes of other *Lotus* common *sym* mutants lacking  $\text{Ca}^{2+}$  spiking (Kistner et al., 2005). Ultrastructural analyses of AM infection sites of *castor-2* (*sym4-2*) mutants indicate that abortion of infection is accompanied by the death of cells containing balloon-like hyphal swellings (Bonfante et al., 2000). Corresponding to the loss of PPA formation in *M. truncatula dmi2* and *dmi3* roots (Genre et al., 2005), PPA formation might also be deficient or absent in *nen1*.

Likewise, the establishment of RNS in *nen1* was blocked at the rhizodermis. Despite scrutinizing more than 98 root systems and using two different and sensitive methods that both detected ITs in the wild type, we could not detect a single infection thread in root hairs of *nen1* mutants grown at 24 °C, indicating that NENA is required at this stage of the symbiosis. Expression analysis of marker genes corroborated the specific lack of symbiotic responses in the rhizodermis. It has previously been shown that the expression of *SbtS* in response to *M. loti* is confined to the rhizodermis (Takeda et al., 2009). While we observed a consistent induction of *SbtS* in wild type roots, *SbtS* was not up regulated in *nen1* after 24 h NF treatment or 3 w after rhizobial inoculation. Moreover, the rhizodermal *NIN<sub>pro</sub>::GUS* induction observed in the wild type was absent in *nen1*. The lack of rhizodermal responsiveness in the *nen1* mutant was further manifested in defective NF-induced  $\text{Ca}^{2+}$  spiking. Residual  $\text{Ca}^{2+}$  spiking was detected in a single *nen1* root hair, however, this low frequency occurrence of spiking cells does not support detectable infection thread formation or symbiotic gene activation in the rhizodermis. In accordance to these data, *nup133* and *nup85* mutants were previously shown to be impaired in NF-induced rhizodermal responses, including  $\text{Ca}^{2+}$  spiking, RHC and IT formation at non-permissive temperatures (Kanamori et al., 2006; Saito et al., 2007). Residual nodulation was observed in various *nup133* mutants and in *nup85-2*, raising the possibility that these mutants are infected via a mechanism similar to the one described here for *nen1* mutants.

## Symbiotic Development of Cortical Cells Does Not Require *NENA*

In striking contrast to the non-responsiveness of the rhizodermal cell layer, nodules developed regularly on *nena* roots, albeit at reduced frequency. The appearance of the infected cortical region in *nena-1* nodules was indistinguishable by light microscopy from wild type nodules indicating that rhizobial accommodation in the cortex was largely unaffected. Consistent with an intact symbiotic response of *nena-1* cortical cells was the observed *NIN<sub>pro</sub>:GUS* expression in nodule primordia and the induction of *ENOD40-1* and *SbtM4*, which are also expressed in the nodule cortex (Takeda et al., 2005; Takeda et al., 2009). The somewhat lower transcript abundance of these genes in *nena-1* compared to wild type roots is likely due to the lower nodule number on *nena* roots.

It is unclear at present why the cortical programs for nodule organogenesis and infection do not require *NENA*. It is unlikely that nodulation is caused by residual functional capability provided by the mutant allele, because *nena-1* seems to be a null allele. The formation of empty nodules on *nena-1* roots coincided with the presence of superficial rhizobial microcolonies. Spot inoculation of *Lotus* roots with NF is sufficient to induce nodule primordia (Niwa et al., 2001). We therefore think that microcolonies on the surface of *nena* roots, which have not been described in other common *sym* mutants, produce local NF concentrations sufficiently high to trigger the formation of nodule primordia. NF molecules are bound and immobilized by cell wall material and probably do not penetrate into the root cortex (Goedhart et al., 2000). This would imply *NENA*-independent signaling through the rhizodermal cell layer for NF-induced activation of cortical cell division.

The apparent dispensability of *NENA* for cortical CCaMK activation reveals tissue specific differences of common *SYM* signaling. Accumulating evidence suggests that the sole function of common *SYM* genes upstream of  $Ca^{2+}$  spiking is the efficient and context-dependent activation of CCaMK for AM fungal or rhizobial infection and nodule organogenesis. Gain-of-function versions of CCaMK introduced into the genetic background of common *sym* mutants, which lack NF-induced  $Ca^{2+}$  spiking, not only activated nodule organogenesis in the absence of rhizobia, but also restored rhizobial infection via RHC and IT formation, as well as AM fungal infection (Madsen et al., 2010; Hayashi et al., 2010). These mutants also supported rhizobial colonization of the nodule inner tissue by transcellular ITs and release of bacteria from ITs into nodule cortical cells. *NFR1* and *NFR5*, in contrast,

were indispensable for infection via root hair ITs, but not required for NF-dependent IT formation inside nodules induced by autoactive CCaMK, suggesting alternative NF receptors operate in the cortex (Madsen et al., 2010). The present data suggest that not only NF recognition, but also downstream signaling via components of the common SYM network required for Ca<sup>2+</sup> spiking and CCaMK activation differs between rhizodermal and nodule cortical tissue.

In contrast to rhizobial infection of *Lotus*, AM fungi have a propensity to overcome a genetic block for rhizodermal infection (Wegel et al., 1998). This revealed that mutants defective in *SYMRK*, *NENA*, *NUP85*, *NUP133*, *CASTOR* and *POLLUX* all support arbuscule development in the cortex. In the case of *symrk* it has been shown that AM fungal hyphae enter the root via an extracellular route, which is consistent with the mutant's inability to provide intracellular access to rhizodermal and subjacent cell layers (Demchenko et al., 2004). Successful hyphal penetration of the outer root layer in *nena* mutants, leading to arbuscule formation, was clearly different from the wild type and might occur similarly to *symrk* mutants. Only mutants defective in the common SYM genes *CCaMK* and *CYCLOPS*, which are positioned downstream of Ca<sup>2+</sup> spiking, are blocked in arbuscule development (Demchenko et al., 2004; Kistner et al., 2005). These observations together with the intact rhizobial infection of *nena* cortical cells suggests that not only in AM but also during nodule development the common SYM genes upstream of Ca<sup>2+</sup> spiking are more stringently required in the rhizodermal cell layer than in the cortex. This opens the possibility that common SYM-mediated Ca<sup>2+</sup> spiking may be dispensable for cortical responses in RNS and, in turn, implies that an alternative regulation of CCaMK may exist in the cortex.

### ***nena* Reveals an Intercellular Rhizobial Entry Mode in *Lotus japonicus***

By employing an intercellular infection mode, which carries the hallmarks of crack entry, *nena* overcomes the requirement for symbiotic responsiveness of the rhizodermis. Ethylene is a potent inhibitor of rhizodermal Ca<sup>2+</sup> spiking (Oldroyd et al., 2001) and its negative regulatory role in RNS has been confirmed genetically (Penmetsa and Cook, 1997; Penmetsa et al., 2003). Water tolerant legumes evade the inhibitory effect of ethylene and even take advantage of increased ethylene concentrations during root submergence (Goormachtig et al., 2004). The subepidermal infection pockets observed in *nena-1* resemble those seen during typical crack entry (Ndoye et al., 1994). As in *S. rostrata* aerated roots, the root hair is the

primary route for nodule infection during aerated conditions in *Lotus*, but this is blocked in *nen1* and hence leads to the formation of mostly uninfected nodules. During waterlogging, nodule infection is significantly promoted in *nen1-1*. Importantly, as in *S. rostrata*, rhizobial infection of *nen1-1* nodules during waterlogging is suppressed by the ethylene biosynthesis inhibitor AVG, providing compelling evidence that infection occurs via crack entry. Because of the promoting effect of ethylene on *nen1-1* infection, residual  $\text{Ca}^{2+}$  spiking in rhizodermal cells is unlikely to play a role in initiating infection in *nen1-1*. At the permissive temperature, single infection events via root hair ITs were found in *nup133-1* and *nup133-4* mutants (Kanamori et al., 2006). Although it is possible that rare root hair infection also occurs in *nen1* mutants grown at permissive temperatures, the lack of  $\text{Ca}^{2+}$  spiking in seedlings grown and examined at 18 °C indicates that, independent of the temperature, crack entry is the predominant infection route on *nen1* mutants under waterlogging conditions.

Based on surveys of infection strategies in different legume lineages, it has been proposed that root hair infection is a more recent trait than the ancestral intercellular infection involving cortical ITs (Sprent, 2007). Crack entry might have been maintained in legumes that are challenged to engage in RNS under submerged conditions. The observation of crack entry in *nen1* provides genetic support for an ancient nature of this trait in legumes and might be a relic of the common ancestor of *Lotus* spp. and *Sesbania* spp., which both belong to the same subclade within the Robinoids (Wojciechowski et al., 2004). Intercellular infection occurring in *L. uliginosus*, a temperate legume adapted to wetland conditions, further substantiates the conservation of crack entry by other members of this genus (James and Sprent, 1999). Rhizobial infection structures indicating intercellular infection of nodule primordia were also observed in the *Lotus root hairless 1* (*rhl1*) mutant, but further evidence for crack entry as defined by its dependence on ethylene was not provided (Karas et al., 2005). In addition to rare rhizobial entry between rhizodermal cells, intracellular infection of NF-induced cortical root hairs was shown and this was proposed as the main route to sustain RNS in the absence of epidermal root hairs. It is of note that the symbiotic signaling program was most likely not perturbed by *rhl1*. The recent demonstration of rare rhizobial infection of synthetic mutants carrying the gain-of-function CCaMK allele *snf1* together with *nfr1* and/or *nfr5* loss-of-function alleles is in accordance with crack entry of rhizobia overcoming a genetic block of rhizoder-

mal infection (Madsen et al., 2010). This supports the idea that crack entry is evolutionary older and in part genetically independent of rhizobial root hair infection.

### **NENA Is a Scaffold Nucleoporin Required for Calcium Spiking**

Together with NUP133 and NUP85, NENA represents the 3<sup>rd</sup> common SYM protein that shows sequence similarity to a nucleoporin from the Nup84 subcomplex of the nuclear pore. For all 3 proteins, conservation compared to their counterparts in yeast or humans does not exceed 25 % identity. Irrespective of high sequence divergence among homologous nucleoporins from various organisms, nuclear pore components are structurally conserved and certain protein domains therein, e.g. WD40 repeats, are found across kingdoms (Baptiste et al., 2005). Based on our yeast two-hybrid data, *in silico* structural and phylogenetic analyses and *in vivo* protein localization, we conclude that NENA represents the *Lotus* version of nucleoporin Seh1. The present data further suggest that NENA and NUP85 function together as scaffold proteins within the NPC.

The specific involvement of NENA in symbiotic signaling is curious. The Nup84 subcomplex is part of the nuclear pore complex (NPC), a macromolecular assembly of approx. 30 different proteins in multiple copies (Alber et al., 2007). Disruption of the Nup84 subcomplex by deletion of individual components typically leads to severe developmental defects in yeast and mammalian cells due to impaired NPC assembly (Siniossoglou et al., 1996; Harel et al., 2003; Walther et al., 2003). The absence of obvious pleiotropic defects in the different *nena* mutant backgrounds may be due to partial and temperature dependent redundancy with other structurally related nucleoporins. Different degrees of redundancy among the components of the *Lotus* Nup84-like subcomplex might further account for the phenotypic differences between *nup133*, *nup85* and *nena* mutants, e.g. the extent of residual nodulation (Kanamori et al., 2006; Saito et al., 2007).

Yeast nucleoporin mutants also show temperature dependent defects. Seh1 is exceptional, as yeast *seh1* null mutants are not affected in mRNA export and can grow at temperatures above 30 °C (Siniossoglou et al., 1996). Nevertheless, *seh1* and *nup84* are synthetic lethal, as this is the case for any other pair wise combination of knock out alleles of Nup84 subcomplex members (Heath et al., 1995; Goldstein et al., 1996; Siniossoglou et al., 1996). Yeast Nup85•Seh1 and Sec13•Nup145C complexes have similar architectures and interaction of co-ex-

pressed Nup85 and Sec13 has been shown (Hsia et al., 2007; Debler et al., 2008). Therefore, structurally homologous SEC13-like 1 or SEC13-like 2, which might assemble with NUP85 during NPC formation in the *nen1* mutant background, probably could partially complement a loss of NENA function. Moreover, the stability of the SEC13-like 1•NUP85 or SEC13-like 2•NUP85 complex might be temperature dependent, causing temperature sensitive symbiotic phenotypes in *nen1* mutants. We have tested these hypotheses by yeast two-hybrid analysis performed at 18 °C and 24 °C growth temperature. The results, however, did not support interaction of SEC13 homologs and NUP85 (Supplemental Figure 11A).

Detailed microscopic analysis using nuclear-targeted cameleon for Förster resonance energy transfer (FRET)-mediated  $\text{Ca}^{2+}$  measurements indicated that  $\text{Ca}^{2+}$  spiking originates at the nuclear periphery and spreads to the center of the nucleus (Sieberer et al., 2009). By analogy to animal cells, the lumen of the nuclear envelope is a likely  $\text{Ca}^{2+}$  source (Gerasimenko et al., 1995). In this context, we propose two models for the symbiotic function of the NPC (Figure 37). Firstly, scaffold nucleoporins, including NENA, might be involved in the selective nuclear import of proteins required for NF-induced  $\text{Ca}^{2+}$  spiking. The import of protein in general does not seem to be affected, as no difference in GFP:CYCLOPS localization was detected between transgenic roots from the wild type and the *nen1* background (Supplemental Figure 12). In *Arabidopsis*, for example, a screen for suppressors of the constitutively active TIR-NB-LRR type *R* gene, *snc1*, resulted in the identification of 3 mutants that are functionally linked to nucleocytoplasmic transport (*nup96/mos3*, *importin  $\alpha$ /mos6* and *nup88/mos7*) (Zhang and Li, 2005; Palma et al., 2005; Cheng et al., 2009). Interestingly, MOS7 turned out to be specifically required for the nuclear import of SNC1 and other defense-related proteins, while nuclear and cytoplasmic pools of control proteins remained unaffected in the *mos7* mutant (Cheng et al., 2009).

Secondly, the NPC might be involved in symbiotic  $\text{Ca}^{2+}$  signaling by regulating nuclear pools of second messengers. It is currently believed that  $\text{Ca}^{2+}$  spiking involves a synchronized flux of second messengers or effector enzymes from the cytoplasm into the nucleus after NF triggering and throughout the period of  $\text{Ca}^{2+}$  oscillations (Oldroyd and Downie, 2008). A reduced permeability of the nuclear envelope (NE), caused by a structural defect or a general reduction in abundance of



nuclear pores might be detrimental, therefore, for NF-induced  $\text{Ca}^{2+}$  spiking in root hairs, while not affecting vital nucleocytoplasmic transport processes.

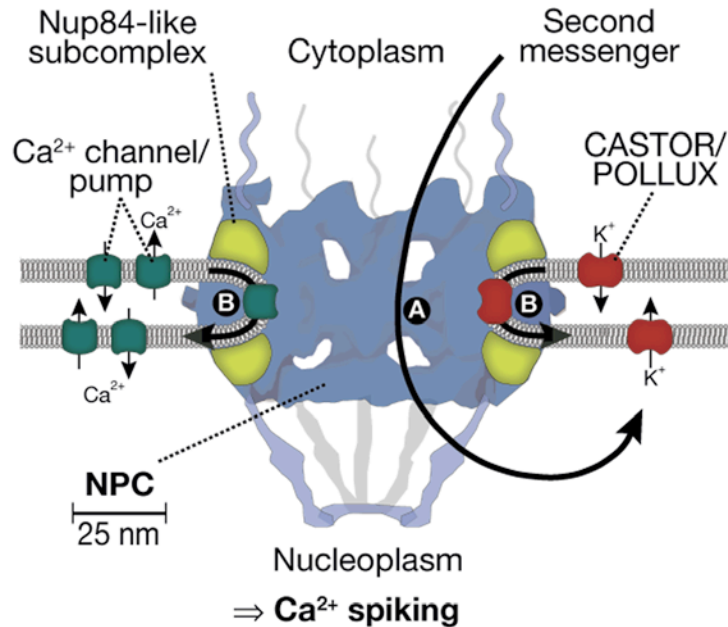


**Figure 37. Two Models for NENA Function in RNS.**

Components of the Nup84-like subcomplex of the NPC, including NENA, NUP85 and NUP133, might be required for (A) targeting integral membrane proteins to the inner face of the NE or for (B) import of 2<sup>nd</sup> messengers. Both processes are essential for eliciting  $\text{Ca}^{2+}$  spiking.

### ***patchy* Is Leaky for Rhizodermal Infection by Rhizobia**

Map-based cloning of *patchy* revealed that a mutation of the *POLLUX* gene is responsible for the AM phenotype. The mutation leads to a predicted Gly to Glu substitution in the RCK domain, identical to the previously identified *pollux-7* allele (Imaizumi-Anraku et al., 2005). Nodule formation was not impaired in *patchy* mutants. In contrast, previously described *castor* and *pollux* mutants, as well as the homologous *dmi1* and *sym8* mutants from *M. truncatula* and pea, respectively, were nodulation deficiency (Schauser et al., 1998; Szczyglowski et al., 1998; Catoira et al., 2000). This difference is of particular importance, since *patchy* mutants were lacking NF-induced  $\text{Ca}^{2+}$  spiking, confirming the requirement of *POLLUX/DMI1* for  $\text{Ca}^{2+}$  spiking (Imaizumi-Anraku et al., 2005; Miwa et al., 2006b). The nodulation rate of *patchy* mutants was decreased compared to the wild type. Nevertheless, the

nodules of *patchy* mutants were morphologically inconspicuous and fully colonized, as demonstrated by light microscopy of histological sections. In this respect, *patchy* resembled the nodulation phenotype of *nen-1*. It is thus possible that the impaired rhizodermal NF responsiveness of *patchy* mutants, as observed by the lack of  $\text{Ca}^{2+}$  spiking, was bypassed by crack entry. The observation of rare ITs yet indicated that nodulation of *patchy* mutants might have been (partially) caused by rhizobial root hair infection. This in turn implies that the *patchy* allele confers residual NF-signaling in the rhizodermis, which was not recorded in our  $\text{Ca}^{2+}$  spiking analysis. Residual function of the *patchy* allele was further indicated by the induction of *NIN* and *SbtM4* at 7 DAI w. *M. loti*, whereas induction was blocked in *pollux-2* loss-of-function mutant. Taken together, the results indicate that *patchy* is a weak allele that confers residual rhizodermal infection by rhizobia and AM fungi. The cortical development of RNS seems unaffected in *patchy* mutants.

### ***patchy* Affects Intraradical AM Hyphal Spreading**

The apparent leakiness of the *patchy* phenotype bears the potential to provide insights into the function of POLLUX and CASTOR that might be concealed in complete loss-of-function mutants. In principle, *patchy* mutants displayed AM defects during rhizodermal infection and subsequent hyphal colonization. Viewed in more detail, parts of the root system completely void of root cortical hyphae were flanked by sectors with fully developed AM, including wild type-like infection sites, abundant cortical hyphae, vesicles and mature arbuscules. The transitions between colonized and uncolonized sectors were marked by hyphal fronts, supporting the notion that apoplastic growth of the cortical hyphae was restricted. The *patchy* phenotype therefore provided an indication that, in addition to rhizodermal infection, hyphal spreading in the root cortex is controlled by the plant. This is in accordance with a previous interpretation of the phenotype displayed by the *taci1* mutant, which was isolated from an AM mutant screen of a transposon mutagenized maize population (Paszkowski et al., 2006). The *patchy* phenotype indeed matches well to the phenotypic description of *taci1*, but it was argued that the wild type-like AM sectors might be due to somatic reversions of the transposon mutation.

Further genetic support for the control of hyphal colonization by the host is given by legume mutants, which are impaired in autoregulation (AUT). The term AUT was coined after the observation that initial nodulation suppresses subsequent nodule formation on younger root tissue (Pierce and Bauer, 1983), a principle that was also

described for mycorrhizal colonization (Vierheilig, 2004). AUT moreover appears to act simultaneously on AM and RNS, as suggested by the inhibitory effect of NF treatment, nodulation or mycorrhization on subsequent nodule formation or AM fungal colonization in alfalfa split root experiments (Cattford et al., 2003). Assessment of AM development in hypernodulating mutants indicated that impaired AUT led to slight, yet significant increases in mycorrhization levels (Morandi et al., 2000; Solaiman et al., 2000; Meixner et al., 2005). Grafting experiments with hypernodulating mutants revealed that AUT of nodulation is regulated by a systemic feedback loop that involves signaling through the shoot (Delves et al., 1986). Map-based cloning of the respective mutant loci in *Lotus*, soybean and *M. truncatula* led to the identification of *HAR1/NARK/SUNN* encoding *CLAVATA1 (CLV1)*-related LRR-RLKs (Krusell et al., 2002; Nishimura et al., 2002b; Searle et al., 2003). Similar to the function of *CLV1* controlling floral meristem differentiation by the recognition of *CLV3*-encoded peptides (Ogawa et al., 2008), *HAR1* might be the receptor of two root derived CLE peptides encoded by *LjCLE-RS1* and *LjCLE-RS2*. These and two other *CLE* genes from *M. truncatula* were shown to be required for *HAR1/SUNN*-dependent negative regulation of nodulation and expressed in a *CASTOR*, *CCaMK* and NF-dependent manner within few hours after rhizobial inoculation (Okamoto et al., 2009; Mortier et al., 2010).

*HAR1/NARK/SUNN*-mediated shoot-to-root signaling leads to changes in hormone balance in the shoot, as well as in the root, including decreased auxin loading of the root (van Noorden et al., 2006). Increased local auxin concentration coincide with meristematic activity of cortical cells during the formation of nodule primordia (Pacios-Bras et al., 2003; Wasson et al., 2006). Deregulated auxin loading was also observed in the ethylene insensitive hyperinfection mutant *sickle (skl)*, suggesting that auxin homeostasis might also be involved in the coordination of nodule organogenesis and infection (Prayitno et al., 2006). Yet, it is unclear whether these hormonal changes are direct effects of AUT signaling, or indirectly caused by the AUT of root symbiosis. Additional hypernodulation mutants indicate the existence of a further local component (*TML*) of the *HAR1* pathway (Magori et al., 2009), as well as other systemic regulatory networks (Nishimura et al., 2002a; Oka-Kira et al., 2005).

The lack of rhizodermal *ENOD11<sub>pro</sub>-GUS* expression in *MtCLE12* and *MtCLE13* over expressing roots gives another hint that AUT might act at an early stage during RNS (Mortier et al., 2010). Ethylene, JA and ABA interfere with NF-signaling upstream of

or directly at the  $\text{Ca}^{2+}$  spiking response (Oldroyd et al., 2001a; Sun et al., 2006; Ding et al., 2008). Moreover, shoot applied methyl-JA has been shown to inhibit rhizobial infection (Nakagawa and Kawaguchi, 2006). Together, the compilation of data provides circumstantial evidence for AUT controlling components of the common SYM network, including POLLUX. Attenuated signaling by a weak *pollux* allele might consequently lead to stronger AUT effects in terms of nodulation rates or mycorrhization levels, as reflected by the *patchy* phenotype.

### **The Mutation in *patchy* Might Affect Gating of POLLUX**

The leaky phenotype of *patchy* implies that the identified missense mutation does not lead to premature degradation or complete destabilization of the complex formed by the mutant's POLLUX protein. A homology model of the POLLUX TrkA-related domain based on the crystal structure of the human BK channel suggests that the Gly 530 to Glu substitution is located in a conserved helix-crossover domain that interlocks the two RCK domains of one subunit. The gating ring of the BK channel is composed of 4 subunits, which interact at the interface between the 1<sup>st</sup> and the 2<sup>nd</sup> RCK domain of two neighboring subunits (Wu et al., 2010). The acidic substitution at the helix-crossover domain might interfere with proper assembly of the gating ring or with the structural changes that are required for proper gating upon ligand binding. Moreover, the mutation might directly interfere with binding of the ligand, which might be a divalent cation. Voltage-dependent gating of the BK channel is activated by  $\text{Ca}^{2+}$  binding to different motifs within the RCK domain (Wu et al., 2010). The activating ligand of POLLUX is yet unknown, but voltage-dependent closing of CASTOR in the presence of  $\text{Mg}^{2+}$  was observed during electrophysiological measurements (Charpentier et al., 2008). In summary, it is tempting to hypothesize that the *patchy* phenotype is caused by desensitized gating function of the mutated POLLUX RCK domain, which might lead to an 'hyper AUT' effect, but further experimental evidence is required to support this speculations.

## ***red* Is Located on the Short Arm of Chromosome VI**

Three mutants with heritable defects during arbuscule formation caused by independent mutations in at least 3 different loci (*dis*, *small* and *red*) were identified from the TILLING BULK population. A map-based cloning approach was adopted in order to investigate the genetic basis of the AM phenotype displayed by the mutant denominated as *red*. Analysis of the data compiled from genotypic and phenotypic assessment of more than 900 individuals from different F<sub>2</sub>, F<sub>3</sub> and F<sub>4</sub> sub-populations indicated that impaired arbuscule formation co-segregates with the mutant genetic background on the short arm of chromosome VI. The target interval is most likely flanked by the SSR markers TM0553 (1.7 cM) and TM0722 (4.1 cM), as indicated by the segregation patterns of recombinant F<sub>3</sub> and F<sub>4</sub> individuals. The target interval is located within a region of reduced recombination, which might be caused by a large deletion mapping south of the target interval between TM1597 (7.7 cM) and TM0302 (14.0 cM). Thus, the large deletion would not comprise the *RED* locus.

## **A Comprehensive Model for the Genetics Underlying the *red* Phenotype**

Mapping of *red* was largely hampered by uncertainties in the phenotype discrimination during screening of the mapping population. Staining of the fungal structures with fluorescent WGA-Alexa Fluor dyes helped to visualize the fine structures of the arbuscules and hyphal septae, indicative of defective AM by epifluorescence microscopy. Further standardization of the AM fungal inoculum and growth conditions might improve the reliability of the phenotyping. By now, there is only one published case of successful map-based cloning of a gene affecting arbuscule development (Zhang et al., 2010), whereas the first published AM-specific gene, *MtPT4*, was identified by reverse genetics (Javot et al., 2007b). Phenotypic plasticity and overlaps in size and structure of wild type and mutant arbuscules, as described for wild type *M. truncatula* and *mtpt4* plants (Javot et al., 2007b), could have been a source of phenotyping mistakes, which might partially account for different segregation patterns observed between different F<sub>2</sub> sub-populations of the *red* mutant.

Moreover, two different arbuscule defects were discerned during the phenotypic analysis of F<sub>2</sub> individuals. Segregation of the arbuscule traits in the F<sub>2</sub> generation suggested a dihybrid pattern, in which the double recessive class confers the severe arbuscule defect, whereas the two single recessive classes have indistinguishable weak arbuscule defects. The monohybrid segregation pattern observed in F<sub>2</sub> progeny of J5150 clashed with the occurrence of weak and severe arbuscule defects in

subsequent generations. An alternative explanation for the different segregation patterns between the offspring from J5150 and J5149 is given by the evidence for a deleterious mutation, which was present in F<sub>2</sub> individuals originating from J5150, but absent in J5149 F<sub>2</sub> plants. This led to the following scenario, in which the original mutant, J849, was homozygous for two unlinked loci, *red* and *wrd*, affecting arbuscule development. In addition, J849 would have carried the recessive lethal allele *let*, which would have been located on chromosome I (between 29.7 cM and 46.2 cM) and linked to *wrd* (Figure 38). This would imply that a recombination event between *let* and *wrd* had occurred in the M2 generation, which led to the combination of the recombinant *LET wrd* with the parental *let wrd* haplotype in J849. Depending on the distance between the two chromosome I loci, the chances of picking up a recombinant individual with this genotype during the AM screen of the M<sub>3</sub> families might have been substantial, because the corresponding phenotype would have displayed a severe arbuscule defect and 50% of the siblings with parental haplotypes would have been *let/let* and therefore extinct. Further recombination between *let* and *wrd* in the F<sub>2</sub> might explain the segregation of weak and severe arbuscule defects in F<sub>3</sub> sub-populations originating from J5150.

### **RED Might Be Involved in PT4 Regulation**

With this a working hypothesis for the final positional cloning of *red* and *wrd* is provided. The lack of *PT4* expression in *red* mutants might give a clue about the functional implications of further candidate genes. In *Medicago* and *Lotus*, *PT4* transcript levels correlate with arbuscule abundance (Floss et al., 2008; Takeda et al., 2009; Baier et al., 2010; Pumpin et al., 2010; Zhang et al., 2010). Interestingly, we did not observe *PT4* induction although *red* mutants do form arbuscule trunks and hyphal branching at a reduced level, similar to the arbuscules formed in *str* mutants. In contrast to *red*, *PT4* was significantly induced in *str* mutants, albeit at reduced levels compared to the wild type (Zhang et al., 2010). Sequencing of 4 different *PT4* homologs in *red* did not reveal a mutation. This might indicate that *RED* and/or *WRD* are involved in transcriptional control or signaling upstream of *PT4* induction.

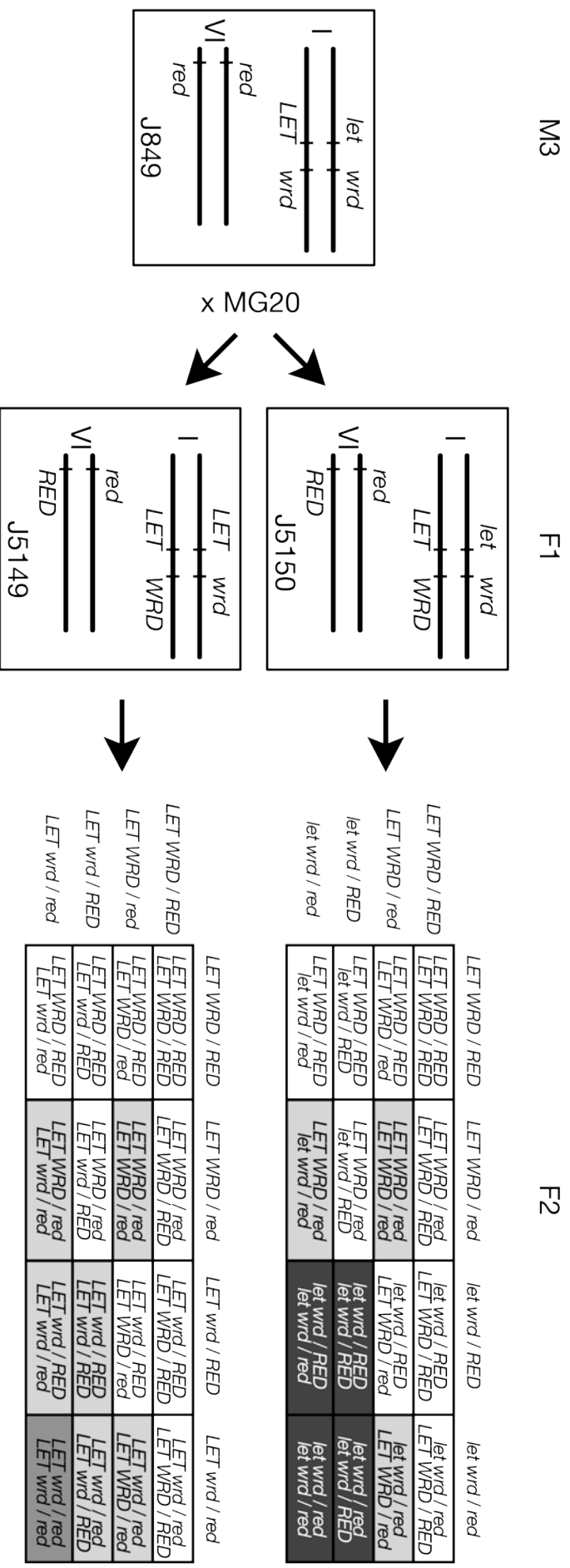


**Figure 38. Segregation Model for red and wrd.**  
 Genotype of the red M<sub>3</sub> mutant used for establishment of the mapping populations is shown on the left: *let* is the recessive lethal locus on chromosome 1 and supposedly linked to *wrd*. Different segregation patterns of the arbuscule trait in F<sub>2</sub> populations originating from J5149 and J5150 might be due to different genotypes at the *LET* locus in the F<sub>1</sub> plants, as illustrated by the F<sub>2</sub> Punnett squares on the right (white background (BG): WT, light grey BG: weak arbuscule mutant trait, dark grey BG: severe arbuscule mutant trait, white letters on black BG: lethal).





## **METHODS**

### **Plant Growth and AM Assay**

Seeds of *L. japonicus* ecotypes Miyakojima MG-20, Gifu B-129 wild type and EMS mutants were scarified and surface sterilized with 1 % NaClO. Imbibed seeds were germinated on 1 % Bacto Agar (Difco) at 18 °C or 24 °C for 5-6 days. Seedlings were cultivated in chive (*Allium schoenoprasum*) nurse pots containing 'G. intraradices-like' BEG195 (Stockinger et al., 2009) as described (Kistner et al., 2005), except that sand/vermiculite (1/1 vol.) was used as substrate. After 3 w of growth in Sunbags (Sigma-Aldrich) at 18 °C or 24 °C constant, 16 h light/ 8 h dark cycles, roots were harvested and cleared with 10 % KOH at 90 °C for 15 min. AM fungal structures were stained with 5 µg/ml WGA-Alexa Fluor 488 conjugate (Molecular Probes) and quantified under the epi-fluorescence microscope using the magnified intersections method (McGonigle et al., 1990). Data were obtained by two independent experiments with at least 4 plants per line and temperature. Roots were counterstained with 1 µg/ml propidium iodide. For detailed AM phenotype analysis, stacked micrographs were acquired by CLSM.

### **AM Mutant Screen**

M<sub>3</sub> individuals of the 'bulked' TILLING population (Perry et al., 2003) were greenhouse cultivated in chive nurse pots for 4 weeks. AM fungal structures were stained with ink and vinegar (Vierheilig et al., 1998), individual root samples were mounted on slides and colonization patterns were scored using a stereomicroscope at 30x – 200x magnification. M<sub>4</sub> self-progeny of scored mutants were re-screened for confirmation. AM mutants were checked for nodulation capacity by examining roots 1 month after inoculation with *M. loti* strain R7A applied at an optical density of 0.01 at 600 nm (OD<sub>600</sub>). Plants were grown in white peat/bark humus soil (Fruhstorfer Typ P, Hawita) under greenhouse conditions.

### **Generation of Mapping Populations**

AM mutants were crossed with wild type MG-20 individuals as described (Jiang and Gresshoff, 1997). In detail, all petals and stamina were removed with fine, ethanol sterilized forceps from young flowers of MG-20 individuals, without disturbing the pistil and bending the pedicel. Crossing success mostly depended on the age of the flower. Closed wing petals and the shape of the style, which had to be straight in the lower two-thirds and bend at the tip, indicated the right age for cross-pollination.

Flowers with open anthers were discarded. Pollen from AM mutants was ‘squeezed out’ of mature flowers and manually transferred onto the stigma. In order to protect the flower, the stalk beneath the flower was wrapped with moistened cotton wad and a 50 ml Falcon tube was put over the flower and fixed with a rod. Mature pods were harvested and seeds were germinated as describe above. Putative F<sub>1</sub> seedlings were transferred to Typ P soil and individually grown at greenhouse conditions. DNA samples of putative F<sub>1</sub> individuals were prepared from young leaves and genotyped, using markers TM0302 and TM0635. Seeds were harvested from confirmed F<sub>1</sub> individuals.

### **Recombination Screen**

Well bottoms of 2.2 ml 96-well plates (ABgene) were perforated (2 mm hole diameter) and plates were filled with Typ P soil/perlite (4/1 vol.). F<sub>2</sub> seedlings were grown in individual wells at greenhouse conditions for 3 weeks. Apical leaves were harvested and transferred to collection microtubes (Qiagen), 300 µl DNA extraction buffer (200 mM TrisCl pH 7.5, 250 mM NaCl, 25 mM EDTA, 0.5% SDS, 2% PVP) was added and samples were homogenized with a TissueLyser (Qiagen). After 30 min of incubation at 65°C, 140 µl KOAc solution (60% 5 M K<sup>+</sup> acetate, 11.5% glacial acetic acid, 28.5% H<sub>2</sub>O) was added and samples were incubated on ice for 15 min before centrifugation at 8000x rcf (g) and 4 °C for 15 min. 320 µl of the supernatant were transferred to 0.8 ml 96-well plates (ABgene) and 0.8 vol. isopropanol was added. Samples were incubated at -20 °C for 2 h and subsequently centrifuged at 8000x rcf and 4 °C for 30 min. DNA was washed with 70 % ethanol, dried and resuspended in 50 µl TE buffer (10 mM TrisCl pH 8.0, 1 mM EDTA). Samples were genotyped by power mapping with multiplex-PCR amplification of markers TM0304 and TM0018 flanking the target region. AM phenotypes of individuals showing recombination between the flanking markers were assessed as described above. Candidate genes within the target region between TM0060 and TM0635 were annotated with GENSCAN (<http://genes.mit.edu/GENSCAN.html>), BLAST and Artemis (Rutherford et al., 2000).

### **Power Mapping**

Template DNA concentrations were adjusted to approx. 50 ng/µl. PCR master mixes contained 1.5x PCR buffer (50 mM KCl, 2.25 mM MgCl<sub>2</sub>), 1 mM dNTP mix, 0.20 µM A-primer, 0.05 µM AF-primer, 0.25 µM R-primer and 0.5 units/µl of Taq polymerase (NEB). For individual PCRs, 1 µl DNA template was mixed with 9 µl of master mix

and incubated in a thermocycler under following conditions: 2min 30sec at 94°C, 4x (30 sec at 94°C, 30 sec at 54°C +0.5°C/cycle, 30 sec at 70°C), 22x (20 sec at 94°C, 20 sec at 56°C, 30 sec at 70°C), 5x (20 sec at 94°C, 20 sec at 55.5°C -0.5°C/cycle, 30 sec at 70°C), 8x (20 sec at 94°C, 20 sec at 53°C, 45 sec at 70°C), 30 min at 72°C. PCR products were diluted according to the empiric primer efficiencies and products that had different fluorescence labels and originated from identical samples were pooled (Supplemental Table 3). 1 µl of pooled PCR products was added to 9.85 µl Hi-Di formamide (Applied Biosystems) and 0.15 µl GeneScan 500 LIZ size standard (Applied Biosystems). Prior to loading of the ABI3730 sequencer, samples were denatured at 95°C for 3 min. Electrophoretic injection parameters were 12 sec and 2.2 kV.

## **TILLING**

1.2 kb 5' and adjacent 1.4 kb 3' fragments of *NENA* genomic sequence, amplified by the respective primer pairs N-166/167 and N-156/157, were used to perform TILLING of *L. japonicus* as described in (Perry et al., 2003).

## **Infection Thread and Nodulation Assays**

Germinated seedlings (see above) were inoculated as described with *M. loti* strains R7A carrying pXLGD4 for *lacZ* expression (Stracke et al., 2002) or MAFF303099 expressing *DsRed* (Markmann et al., 2008), with following modifications: bacterial cultures were diluted to OD<sub>600</sub> 0.005 in 80 ml half-strength B&D medium (Broughton and Dilworth, 1971) and added to 300 ml autoclaved growth substrate.

For waterlogging experiments, seedlings were grown in closed *Weck* jars containing expanded clay granules (Seramis, Mars GmbH). Aminoethoxyvinylglycine (AVG) solution at 5 µM final concentration was added immediately before transfer of the seedlings to *Weck* jars. For aerated growth conditions, seedlings were transferred to polypropylene plant pots containing sand/vermiculite (1/1 vol.) and watered to field capacity at 3 d intervals. All plants were cultivated under 16/8 h light/dark cycle at a constant 24 °C temperature, unless stated otherwise.

ITs and nodules that contained rhizobia were visualized by *DsRed* fluorescence or stained for β-galactosidase activity (Lombardo et al., 2006) and scored by fluorescence and brightfield microscopy.

80 µm tissue sections for CLSM analysis were prepared with a 'Vibratome' microtome (Leica VT1000S) after embedding nodules in 6 % low melting agarose. 80 µm sections from *M. loti* R7A-inoculated roots were stained with 2 µg/ml 4',6-diamidino-2-phenylindole (DAPI) in 1x PBS (pH 7). For brightfield microscopy of nodule colonization, root sections were fixed in 1.5 % glutaraldehyde (Sigma-Aldrich), dehydrated and embedded in Technovit 7100 (Kulzer). 4 µm histological sections were prepared with a microtome (Leica RM2125RT) and stained with 0.1 % toluidine blue in benzoate buffer (pH 4.4).

### Calcium Spiking Analysis

Ca<sup>2+</sup> imaging was performed by microinjection of the fluorescent ratiometric Ca<sup>2+</sup> indicator Oregon Green 488 BAPTA-1 dextran MW10,000 (Invitrogen) and reference dye Texas Red dextran MW10,000 (Invitrogen) as described previously (Charpentier et al., 2008). Measurements were performed at 18 °C or 24 °C ambient temperatures on growing root hairs of *L. japonicus* Gifu B-129 and *nen-1* seedlings that were grown for 2 d in the dark.

### Transgenic Complementation and Sub-cellular Localization

The *NENA* sequence from 1911 bp upstream of the start codon to the last bp before the stop codon was amplified by nested PCR with primer pairs N-172/157 & N-171/168 (Supplemental Table 5) from genomic Gifu wild type DNA and cloned into pENTR/D-TOPO (Invitrogen), giving rise to pENTR-*NENA*. From that construct just the putative promoter region, *NENA*<sub>pro</sub>, was PCR-amplified with primers N-171/173 and cloned into pENTR/D-TOPO. To test complementation of *nen-1* by the *Arabidopsis* ortholog of *NENA*, *At SEH1* genomic CDS was amplified by nested PCR with primers S-176/175 and 5'-phosphorylated primers S-177/178, and ligated with PCR-amplified pENTR-*NENA* fragment lacking the *NENA* CDS using primer pair N-173/179. All 3 entry clones were recombined during Gateway LR reactions (Invitrogen) with a modified destination vector pK7RWG2 (Karimi et al., 2002) containing *ER-GFP* and lacking the 35S promoter (kindly provided by Dr. M. Antolin-Llovera, Biocenter LMU Munich). To confirm sub-cellular localization, *NENA* genomic CDS, amplified with primers N-158/168, was cloned into pENTR/D-TOPO (Invitrogen) and subsequently Gateway-transferred into pK7FWG2 (Karimi et al., 2002). For subcellular localization of NUP85 in hairy roots, the CDS without the stop codon was PCR amplified from the cDNA clone MFB015g09 using primers 85-162/183 and cloned into pENTR/D-TOPO. The resulting entry clone was Gateway-transferred into

pK7FWG2. The fidelity of all entry clones was confirmed by sequencing. A T-DNA construct with GFP fused to the N-terminus of *CYCLOPS* (Yano et al., 2008) was also used for subcellular localization in WT and *nena-1*. T-DNA constructs were transformed into Gifu wild type and *nena-1* via *A. rhizogenes* strain AR1193 as described (Charpentier et al., 2008). Sub-cellular localization of translational fusion proteins in young hairy roots was assessed by CLSM. Nodulation and AM colonization was assayed as described above.

### **DNA Gel Blotting**

Probes I (1148 bp) and II (546 bp) were labeled with [ $\alpha^{32}$ P]dCTP using the NEBlot Kit (New England Biolabs) after excision of the respective restriction fragments of pENTR-*NENA* triple-digested with EcoRI, NdeI and NsiI. 20  $\mu$ g of MG-20 genomic DNA were digested with BglII, EcoRI, NdeI or NsiI, size separated by agarose gel electrophoresis and blotted on Hybond-N+ (GE Healthcare). Nylon membranes were hybridized with Probe I or II in roller bottles at 67 °C overnight, washed with increasing stringency (final wash: 0.1 x SSPE, 0.1 % SDS, 63 °C, 1h) and visualized on a Typhoon scanner (GE Healthcare) after exposure to a phosphor screen.

### **Expression Analysis**

Total RNA was extracted with CTAB buffer and acidic phenol as described (Kistner et al., 2005). RNA samples were TURBO DNase (Ambion) treated, and RNA integrity (RIN  $\geq$  7) was verified with a 2100 Bioanalyzer (Agilent). Absence of genomic DNA was confirmed by PCR. Approx. 200 ng of total RNA were used for 1<sup>st</sup>-strand cDNA synthesis using the SuperScript VILO Kit (Invitrogen) according to the manual. For subsequent PCRs, 2  $\mu$ l of cDNA template were used per 20  $\mu$ l total volume.

For tissue-specific analysis, samples were taken from different organs of two flowering Gifu wild type plants. *NENA* and *EF-1  $\alpha$*  transcript levels were visualized by ethidium bromide staining following agarose gel electrophoresis of PCR products after 28, 31 and 34 cycles with primer pairs N-174/167 or EF1-U23/L19.

Samples for analysis of nodulation gene expression were generated from whole roots of 7-8 pooled seedlings that were grown for 14 d on plates (half-strength B&D medium, 0.75 % GELRITE (Roth), 2 mM MgSO<sub>4</sub>) and treated with 1  $\mu$ M purified NF or transferred from plates to *Weck* jars, inoculated with MAFF303099 and grown for

additional 7 d or 21 d at 24°C and long day light cycle. Mock controls were inoculated with half-strength B&D solution only.

Samples for *PT4* expression analysis were generated from whole roots pooled from 4 plants that were cultivated in chive pots with BEG195 for 6 w at 24°C as described (Kistner et al., 2005). Mock controls were grown in autoclaved sand/vermiculite (1/1) under the same conditions, but without chive plants and BEG195.

Quantitative expression analysis was performed by real-time PCR using Fast SYBR Green Master Mix (Applied Biosystems) and a CFX96 detection system (Bio-Rad). Target transcripts were PCR amplified using primer pairs N-174/167, 40-203/204, NIN-201/202, M4-199/200, SbtS-007/008, PT4-216/217, Ub-218/219 and EF1-U23/L19 and the following cycles: 20 sec at 95 °C, 40x (3 sec at 95 °C, 20 sec at 57 °C, 20 sec at 72 °C, plate read), 10 sec at 95 °C, melt curve 65 °C to 95 °C with 0.5 °C/ 5 sec increments. Amplification efficiencies and  $C_t$  values were calculated with LinRegPCR (Ruijter et al., 2009). Subsequently, relative expression normalized to the reference gene *EF-1  $\alpha$* , standard error and statistical significance based on 3 biological replicates was calculated using REST 2009 software (Pfaffl et al., 2002).

### **Promoter GUS Analysis**

A T-DNA construct with the GUS-reporter gene expressed by the *NIN* promoter (Radutoiu et al., 2003) was transformed into Gifu wild type and *nena-1* via *A. rhizogenes* strain AR1193. Plants with hairy roots were transferred onto plates or into Weck jars and 4-7 d later treated with NF or MAFF303099, respectively (see above). Growth temperature was 24 °C. Treated roots were cut off and incubated in staining solution (0.5 mg ml<sup>-1</sup> X-Gluc, 100 mM sodium phosphate pH 7.0, 5 mM EDTA pH 7.0, 1 mM potassium ferricyanide, 1 mM potassium ferrocyanide, 0.1 % Triton X-100) for 12 h at 37 °C in the dark. A stereomicroscope was used for inspection and documentation.

### **Yeast Two-Hybrid Analysis**

cDNA clones covering the full-length coding regions of *NENA* (MWM052c09), *NUP85* (MFB015g09) and *NUP133* (MFBL049d04) were kindly obtained from the *Lotus* Resource Centre (Asamizu et al., 2000) and PCR-amplified with primer pairs N-158/159, 85-162/163 and 133-160/161. CDS of *SEC13-like 1* and *SEC13-like 2* were amplified by nested PCR from Gifu wild type cDNA using primer pairs 13-1-

195/196&191/194 and 13-2-197/198&192/193. *ScNup120* and *ScNup145* were amplified from genomic DNA of *S. cerevisiae* S288c using primer 120-5'/3' and 145-5'/3', respectively. PCR products were cloned into pENTR/D-TOPO (Invitrogen) and subsequently inserted by LR Clonase II (Invitrogen) into Gateway-compatible bait or prey destination vectors derived from pBD-Gal4 Cam (Stratagene) or pGAG424 (Clontech), as described (Yano et al., 2008). The fidelity of all entry clones was confirmed by sequencing. Y2H analysis was carried out with the yeast strain AH109 (Clontech) following standard procedures (Stratagene Product Manual #235702; Yeast Protocols Handbook PT3024-1, Clontech).

## **Microscopy**

The following microscopes and conditions were used for this work: a fluorescence stereomicroscope (Leica MZ16 FA) with 1x and 2x objectives; inverted microscope (Leica DMI6000 B) with 10x/0.25, 20x/0.5, 40x/0.75 dry objectives, GFP and N3 filter cubes; confocal laser scanning microscope (Leica SP5) with 20x/0.5 dry, 63x/1.2 water immersion objectives, argon and DPSS lasers were used. RFP was excited at  $\lambda = 561$  nm/ detected at  $\lambda = 570 - 630$  nm and GFP was excited at  $\lambda = 488$  nm/ detected at  $\lambda = 495 - 555$  nm. Images were acquired and processed with LAS AF software.

## **Phylogenetic Analysis**

Protein sequences similar to NENA from different plant species with annotated genomes were retrieved by WU-blastp from the Uniprot database. Multiple hits corresponding to one gene, including splice variants, were discarded. Multiple sequence alignment was performed with MAFFT online and edited manually. The final alignment used for phylogenetic analysis is shown in Supplemental Figure 13. Neighbour-joining (NJ) and parsimony analyses were performed online (<http://mobyli.pasteur.fr/cgi-bin/portal.py>) using PHYLIP (version 3.5c, distributed by J. Felsenstein, Department of Genome Sciences, University of Washington, Seattle), and Quartet Puzzling Maximum-Likelihood (QPML) analysis using TREE-PUZZLE (Schmidt et al., 2002). QPML tree was reconstructed from 1000 puzzling steps, exact parameter estimation using Quartet sampling + NJ, amino acid frequency and rate heterogeneity estimations from the data set and the JTT model of substitution. Distances for NJ were obtained from 1000 bootstrap replicates using the JTT model with coefficient of variation = 0.743089312 and fraction of invariant

positions = 0.000117. Consensus NJ and parsimony trees were constructed from 1000-fold bootstrapped analyses.

### **Homology Modeling**

SMART (Schultz et al., 1998) search algorithm was used to define the domain composition of the NENA protein. A 3D-model of NENA was generated using DeepView and SWISS-MODEL (Guex and Peitsch, 1997; Arnold et al., 2006). For this, NENA and the N-terminus of Nup85 were aligned to the PDB templates 3eweC, as shown in Supplemental Figure 6, and 3eweD, respectively. 3D modeling of the TrkA-related domain was based on a structural PSI-BLAST of the POLLUX amino acids 385 to 859 (Supplemental Figure 5), which was generated by the FUGUE program (Shi et al., 2001). The model based on the PDB file 3mt5A, corresponding to the crystal structure of the human BK channel, was selected for illustration and edited with DeepView.

### **Accession Numbers**

Sequence data from this work can be found in the *Arabidopsis* Genome Initiative or GenBank/EMBL/DDBJ databases under the following accession numbers: LjT34D07/TM1188/CM0060 (AP007861), *NENA* (AB506696), *SEC13-like 1* (AB506697), *SEC13-like 2* (AB506698), *LjPT4* (AP010874), *LjPT2* (AB257216), yeast Seh1 (P53011), human Seh1-like (A8K5B1), yeast Sec13 (Q04491), human Sec13-like 1 (P55735), *Arabidopsis* Seh1-like (At1g64350), POLLUX (BAD89022).



## REFERENCES

- Akiyama, K., Matsuzaki, K., and Hayashi, H. (2005). Plant sesquiterpenes induce hyphal branching in arbuscular mycorrhizal fungi. *Nature* 435, 824-827.
- Alber, F., Dokudovskaya, S., Veenhoff, L.M., Zhang, W., Kipper, J., Devos, D., Suprpto, A., Karni-Schmidt, O., Williams, R., Chait, B.T., Sali, A., and Rout, M.P. (2007). The molecular architecture of the nuclear pore complex. *Nature* 450, 695-701.
- Amor, B.B., Shaw, S.L., Oldroyd, G.E., Maillet, F., Penmetsa, R.V., Cook, D., Long, S.R., Dénarié, J., and Gough, C. (2003). The *NFP* locus of *Medicago truncatula* controls an early step of Nod factor signal transduction upstream of a rapid calcium flux and root hair deformation. *Plant J.* 34, 495-506.
- Andriankaja, A., Boisson-Dernier, A., Frances, L., Sauviac, L., Jauneau, A., Barker, D.G., and de Carvalho-Niebel, F. (2007). AP2-ERF transcription factors mediate Nod factor-dependent Mt *ENOD11* activation in root hairs via a novel *cis*-regulatory motif. *Plant Cell* 19, 2866-2885.
- Ané, J.M., Kiss, G.B., Riely, B.K., Penmetsa, R.V., Oldroyd, G.E., Ajax, C., Lévy, J., Debelle, F., Baek, J.M., Kaló, P., Rosenberg, C., Roe, B.A., Long, S.R., Dénarié, J., and Cook, D.R. (2004). *Medicago truncatula* *DMI1* required for bacterial and fungal symbioses in legumes. *Science* 303, 1364-1367.
- Arnold, K., Bordoli, L., Kopp, J., and Schwede, T. (2006). The SWISS-MODEL workspace: a web-based environment for protein structure homology modelling. *Bioinformatics* 22, 195-201.
- Arrighi, J.F., Barre, A., Ben Amor, B., Bersoult, A., Soriano, L.C., Mirabella, R., de Carvalho-Niebel, F., Journet, E.P., Ghéardi, M., Huguet, T., Geurts, R., Dénarié, J., Rouge, P., and Gough, C. (2006). The *Medicago truncatula* lysine motif-receptor-like kinase gene family includes *NFP* and new nodule-expressed genes. *Plant Physiol.* 142, 265-279.
- Asamizu, E., Nakamura, Y., Sato, S., and Tabata, S. (2000). Generation of 7137 non-redundant expressed sequence tags from a legume, *Lotus japonicus*. *DNA Res.* 7, 127-130.
- Bago, B., Pfeffer, P.E., and Shachar-Hill, Y. (2000). Carbon Metabolism and Transport in Arbuscular Mycorrhizas. *Plant Physiol.* 124, 949-958.
- Baier, M.C., Keck, M., Gödde, V., Niehaus, K., Küster, H., and Hohnjec, N. (2010). Knockdown of the Symbiotic Sucrose Synthase MtSucS1 Affects Arbuscule Maturation and Maintenance in Mycorrhizal Roots of *Medicago truncatula*. *Plant Physiol.* 152, 1000-1014.
- Baptiste, E., Charlebois, R.L., MacLeod, D., and Brochier, C. (2005). The two tempos of nuclear pore complex evolution: highly adapting proteins in an ancient frozen structure. *Genome Biol.* 6, R85.
- Barbier, V., and Viovy, J.L. (2003). Advanced polymers for DNA separation. *Curr. Opin. Biotechnol.* 14, 51-57.
- Barker, S.J., Stummer, B., Gao, L., Dispain, I., Connor, P.J.O., and Smith, S.E. (1998). A mutant in *Lycopersicon esculentum* Mill. with highly reduced VA mycorrhizal colonization: isolation and preliminary characterisation. *Plant J.* 15, 791-797.
- Belgareh, N., Rabut, G., Bai, S.W., van Overbeek, M., Beaudouin, J., Daigle, N., Zatssepina, O.V., Pasteau, F., Labas, V., Fromont-Racine, M., Ellenberg, J., and Doye, V. (2001). An evolutionarily conserved NPC subcomplex, which redistributes in part to kinetochores in mammalian cells. *J. Cell Biol.* 154, 1147-1160.
- Berbee, M.L., and Taylor, J.W. (2001). Fungal Molecular Evolution: Gene Trees and Geologic Time. *The Mycota: a comprehensive treatise on fungi as experimental systems for basic and applied research. Volume VII: Systematics and Evolution, Part B*, 229-245.

- Besserer, A., Puech-Pages, V., Kiefer, P., Gomez-Roldan, V., Jauneau, A., Roy, S., Portais, J.C., Roux, C., Bécard, G., and Séjalon-Delmas, N. (2006). Strigolactones stimulate arbuscular mycorrhizal fungi by activating mitochondria. *PLoS Biol.* 4, e226.
- Blancaflor, E.B., Zhao, L., and Harrison, M.J. (2001). Microtubule organization in root cells of *Medicago truncatula* during development of an arbuscular mycorrhizal symbiosis with *Glomus versiforme*. *Protoplasma* 217, 154-165.
- Bonfante, P., Genre, A., Faccio, A., Martini, I., Schauser, L., Stougaard, J., Webb, J., and Parniske, M. (2000). The *Lotus japonicus* *LjSym4* gene is required for the successful symbiotic infection of root epidermal cells. *Mol. Plant Microbe Interact.* 13, 1109-1120.
- Brohawn, S.G., Leksa, N.C., Spear, E.D., Rajashankar, K.R., and Schwartz, T.U. (2008). Structural evidence for common ancestry of the nuclear pore complex and vesicle coats. *Science* 322, 1369-1373.
- Broughton, W.J., and Dilworth, M.J. (1971). Control of leghaemoglobin synthesis in snake beans. *Biochem. J.* 125, 1075-1080.
- Brownstein, M.J., Carpten, J.D., and Smith, J.R. (1996). Modulation of non-templated nucleotide addition by Taq DNA polymerase: primer modifications that facilitate genotyping. *Biotechniques* 20, 1004-1006, 1008-1010.
- Brundrett, M. (2004). Diversity and classification of mycorrhizal associations. *Biological Reviews* 79, 473-495.
- Brundrett, M. (2009). Mycorrhizal associations and other means of nutrition of vascular plants: understanding the global diversity of host plants by resolving conflicting information and developing reliable means of diagnosis. *Plant and Soil* 320, 37-77.
- Cappellazzo, G., Lanfranco, L., Fitz, M., Wipf, D., and Bonfante, P. (2008). Characterization of an amino acid permease from the endomycorrhizal fungus *Glomus mosseae*. *Plant Physiol.* 147, 429-437.
- Catford, J.G., Staehelin, C., Lerat, S., Piché, Y., and Vierheilig, H. (2003). Suppression of arbuscular mycorrhizal colonization and nodulation in split-root systems of alfalfa after pre-inoculation and treatment with Nod factors. *J. Exp. Bot.* 54, 1481-1487.
- Catoira, R., Galera, C., de Billy, F., Penmetsa, R.V., Journet, E.P., Maillet, F., Rosenberg, C., Cook, D., Gough, C., and Dénarié, J. (2000). Four genes of *Medicago truncatula* controlling components of a Nod factor transduction pathway. *Plant Cell* 12, 1647-1666.
- Charpentier, M., Bredemeier, R., Wanner, G., Takeda, N., Schleiff, E., and Parniske, M. (2008). *Lotus japonicus* CASTOR and POLLUX are ion channels essential for perinuclear calcium spiking in legume root endosymbiosis. *Plant Cell* 20, 3467-3479.
- Cheng, Y.T., Germain, H., Wiermer, M., Bi, D., Xu, F., Garcia, A.V., Wirthmueller, L., Despres, C., Parker, J.E., Zhang, Y., and Li, X. (2009). Nuclear pore complex component MOS7/Nup88 is required for innate immunity and nuclear accumulation of defense regulators in *Arabidopsis*. *Plant Cell* 21, 2503-2516.
- Clark, J.M. (1988). Novel non-templated nucleotide addition reactions catalyzed by procaryotic and eucaryotic DNA polymerases. *Nucleic Acids Res.* 16, 9677-9686.
- Cook, C.E., Whichard, L.P., Turner, B., Wall, M.E., and Egley, G.H. (1966). Germination of Witchweed (*Striga lutea* Lour.): Isolation and Properties of a Potent Stimulant. *Science* 154, 1189-1190.
- Cox, G., and Sanders, F. (1974). Ultrastructure of the host-fungus interface in a vesicular-arbuscular mycorrhiza. *New Phytol.* 73, 901.
- Croll, D., Giovannetti, M., Koch, A.M., Sbrana, C., Ehinger, M., Lammers, P.J., and Sanders, I.R. (2008a). Nonself vegetative fusion and genetic exchange in the arbuscular mycorrhizal fungus *Glomus intraradices*. *New Phytol.* 181, 924-937.

- Croll, D., Wille, L., Gamper, H.A., Mathimaran, N., Lammers, P.J., Corradi, N., and Sanders, I.R. (2008b). Genetic diversity and host plant preferences revealed by simple sequence repeat and mitochondrial markers in a population of the arbuscular mycorrhizal fungus *Glomus intraradices*. *New Phytol.* 178, 672.
- David-Schwartz, R., Badani, H., Smadar, W., Levy, A.A., Galili, G., and Kapulnik, Y. (2001). Identification of a novel genetically controlled step in mycorrhizal colonization: plant resistance to infection by fungal spores but not extra-radical hyphae. *Plant J.* 27, 561-569.
- Debler, E.W., Ma, Y., Seo, H.S., Hsia, K.C., Noriega, T.R., Blobel, G., and Hoelz, A. (2008). A fence-like coat for the nuclear pore membrane. *Mol. Cell* 32, 815-826.
- Delves, A.C., Mathews, A., Day, D.A., Carter, A.S., Carroll, B.J., and Gresshoff, P.M. (1986). Regulation of the soybean-Rhizobium nodule symbiosis by shoot and root factors. *Plant Physiol.* 82, 588-590.
- Demchenko, K., Winzer, T., Stougaard, J., Parniske, M., and Pawlowski, K. (2004). Distinct roles of *Lotus japonicus* SYMRK and SYM15 in root colonization and arbuscule formation. *New Phytol.* 163, 381-392.
- Dénarié, J., Debelle, F., and Prome, J.C. (1996). Rhizobium Lipo-Chitooligosaccharide Nodulation Factors: Signaling Molecules Mediating Recognition and Morphogenesis. *Ann. Rev. Biochem.* 65, 503-535.
- D'Haese, W., De Rycke, R., Mathis, R., Goormachtig, S., Pagnotta, S., Verplancke, C., Capoen, W., and Holsters, M. (2003). Reactive oxygen species and ethylene play a positive role in lateral root base nodulation of a semiaquatic legume. *Proc. Natl. Acad. Sci. USA* 100, 11789-11794.
- Dickson, S. (2004). The Arum-Paris continuum of mycorrhizal symbioses. *New Phytol.* 163, 187-200.
- Ding, Y., Kaló, P., Yendrek, C., Sun, J., Liang, Y., Marsh, J.F., Harris, J.M., and Oldroyd, G.E. (2008). Abscisic acid coordinates Nod factor and cytokinin signaling during the regulation of nodulation in *Medicago truncatula*. *Plant Cell* 20, 2681-2695.
- Duc, G., Trouvelot, A., Gianinazzi-Pearson, V., and Gianinazzi, S. (1989). First report of non-mycorrhizal plant mutants (Myc-) obtained in pea (*Pisum sativum* L.) and fababean (*Vicia faba* L.). *Plant Science* 60, 215-222.
- Ehrhardt, D.W., Atkinson, E.M., and Long, S.R. (1992). Depolarization of alfalfa root hair membrane potential by *Rhizobium meliloti* Nod factors. *Science* 256, 998-1000.
- Ehrhardt, D.W., Wais, R., and Long, S.R. (1996). Calcium spiking in plant root hairs responding to Rhizobium nodulation signals. *Cell* 85, 673-681.
- Endre, G., Kereszt, A., Kevei, Z., Mihacea, S., Kaló, P., and Kiss, G.B. (2002). A receptor kinase gene regulating symbiotic nodule development. *Nature* 417, 962-966.
- FAO. (2004). Use of Phosphate Rocks for Sustainable Agriculture. FOOD AND AGRICULTURE ORGANIZATION OF THE UNITED NATIONS ISSN 0532-0488.
- FAOSTAT. (2010). <http://faostat.fao.org/>.
- Fath, S., Mancias, J.D., Bi, X., and Goldberg, J. (2007). Structure and organization of coat proteins in the COPII cage. *Cell* 129, 1325-1336.
- Felle, H.H., Kondorosi, É., Kondorosi, Á., and Schultze, M. (1998). The role of ion fluxes in Nod factor signalling in *Medicago sativa*. *Plant J.* 13, 455-463.
- Fester, T., Strack, D., and Hause, B. (2001). Reorganization of tobacco root plastids during arbuscule development. *Planta* 213, 864-868.
- Finlay, R.D. (2008). Ecological aspects of mycorrhizal symbiosis: with special emphasis on the functional diversity of interactions involving the extraradical mycelium. *J. Exp. Bot.* 59, 1115-1126.

- Floss, D.S., Hause, B., Lange, P.R., Küster, H., Strack, D., and Walter, M.H. (2008). Knock-down of the MEP pathway isogene *1-deoxy-D-xylulose 5-phosphate synthase 2* inhibits formation of arbuscular mycorrhiza-induced apocarotenoids, and abolishes normal expression of mycorrhiza-specific plant marker genes. *Plant J.* 56, 86-100.
- Galloway, J.N., Townsend, A.R., Erismann, J.W., Bekunda, M., Cai, Z., Freney, J.R., Martinelli, L.A., Seitzinger, S.P., and Sutton, M.A. (2008). Transformation of the Nitrogen Cycle: Recent Trends, Questions, and Potential Solutions. *Science* 320, 889-892.
- Genre, A., and Bonfante, P. (1998). Actin versus tubulin configuration in arbuscule-containing cells from mycorrhizal tobacco roots. *New Phytol.* 140, 745-752.
- Genre, A., Chabaud, M., Faccio, A., Barker, D.G., and Bonfante, P. (2008). Prepenetration apparatus assembly precedes and predicts the colonization patterns of arbuscular mycorrhizal fungi within the root cortex of both *Medicago truncatula* and *Daucus carota*. *Plant Cell* 20, 1407-1420.
- Genre, A., Chabaud, M., Timmers, T., Bonfante, P., and Barker, D.G. (2005). Arbuscular mycorrhizal fungi elicit a novel intracellular apparatus in *Medicago truncatula* root epidermal cells before infection. *Plant Cell* 17, 3489-3499.
- Gerasimenko, O.V., Gerasimenko, J.V., Tepikin, A.V., and Petersen, O.H. (1995). ATP-dependent accumulation and inositol trisphosphate- or cyclic ADP-ribose-mediated release of Ca<sup>2+</sup> from the nuclear envelope. *Cell* 80, 439-444.
- Gerdemann, J.W. (1968). Vesicular-Arbuscular Mycorrhiza and Plant Growth. *Ann. Rev. Phytopathol.* 6, 397-418.
- Gianinazzi-Pearson, V., and Dénarié, J. (1997). Red carpet genetic programmes for root endosymbioses. *Trends Plant Sci.* 2, 371-372.
- Gianinazzi-Pearson, V., Arnould, C., Oufattole, M., Arango, M., and Gianinazzi, S. (2000). Differential activation of H<sup>+</sup>-ATPase genes by an arbuscular mycorrhizal fungus in root cells of transgenic tobacco. *Planta* 211, 609-613.
- Giovannetti, M., Sbrana, C., Avio, L., and Strani, P. (2004). Patterns of below-ground plant interconnections established by means of arbuscular mycorrhizal networks. *New Phytol.* 164, 175.
- Gleason, C., Chaudhuri, S., Yang, T., Munoz, A., Poovaiah, B.W., and Oldroyd, G.E. (2006). Nodulation independent of rhizobia induced by a calcium-activated kinase lacking autoinhibition. *Nature* 441, 1149-1152.
- Goedhart, J., Hink, M.A., Visser, A.J., Bisseling, T., and Gadella, T.W., Jr. (2000). In vivo fluorescence correlation microscopy (FCM) reveals accumulation and immobilization of Nod factors in root hair cell walls. *Plant J.* 21, 109-119.
- Goldstein, A.L., Snay, C.A., Heath, C.V., and Cole, C.N. (1996). Pleiotropic nuclear defects associated with a conditional allele of the novel nucleoporin Rat9p/Nup85p. *Mol. Biol. Cell* 7, 917-934.
- Gomez-Roldan, V., Fermas, S., Brewer, P.B., Puech-Pages, V., Dun, E.A., Pillot, J.P., Letisse, F., Matusova, R., Danoun, S., Portais, J.C., Bouwmeester, H., Bécard, G., Beveridge, C.A., Rameau, C., and Rochange, S.F. (2008). Strigolactone inhibition of shoot branching. *Nature* 455, 189-194.
- Goormachtig, S., Capoen, W., James, E.K., and Holsters, M. (2004). Switch from intracellular to intercellular invasion during water stress-tolerant legume nodulation. *Proc. Natl. Acad. Sci. USA* 101, 6303-6308.
- Greene, E.A., Codomo, C.A., Taylor, N.E., Henikoff, J.G., Till, B.J., Reynolds, S.H., Enns, L.C., Burtner, C., Johnson, J.E., Odden, A.R., Comai, L., and Henikoff, S. (2003). Spectrum of chemically induced mutations from a large-scale reverse-genetic screen in *Arabidopsis*. *Genetics* 164, 731-740.
- Groth, M., Takeda, N., Perry, J., Uchida, H., Draxl, S., Brachmann, A., Sato, S., Tabata, S., Kawaguchi, M., Wang, T.L., and Parniske, M. (2010). *NENA*, a *Lotus japonicus*

Homolog of *Sec13*, Is Required for Rhizodermal Infection by Arbuscular Mycorrhiza Fungi and Rhizobia but Dispensable for Cortical Endosymbiotic Development. *Plant Cell* 22, 2509-2526.

- Guether, M., Neuhauser, B., Balestrini, R., Dynowski, M., Ludewig, U., and Bonfante, P. (2009). A mycorrhizal-specific ammonium transporter from *Lotus japonicus* acquires nitrogen released by arbuscular mycorrhizal fungi. *Plant Physiol.* 150, 73-83.
- Guex, N., and Peitsch, M.C. (1997). SWISS-MODEL and the Swiss-PdbViewer: an environment for comparative protein modeling. *Electrophoresis* 18, 2714-2723.
- Guimil, S., Chang, H.S., Zhu, T., Sesma, A., Osbourn, A., Roux, C., Ioannidis, V., Oakeley, E.J., Docquier, M., Descombes, P., Briggs, S.P., and Paszkowski, U. (2005). Comparative transcriptomics of rice reveals an ancient pattern of response to microbial colonization. *Proc. Natl. Acad. Sci. USA* 102, 8066-8070.
- Gutjahr, C., Casieri, L., and Paszkowski, U. (2009a). *Glomus intraradices* induces changes in root system architecture of rice independently of common symbiosis signaling. *New Phytol.* 182, 829-837.
- Gutjahr, C., Novero, M., Guether, M., Montanari, O., Udvardi, M., and Bonfante, P. (2009b). Presymbiotic factors released by the arbuscular mycorrhizal fungus *Gigaspora margarita* induce starch accumulation in *Lotus japonicus* roots. *New Phytol.* 183, 53-61.
- Harel, A., Orjalo, A.V., Vincent, T., Lachish-Zalait, A., Vasu, S., Shah, S., Zimmerman, E., Elbaum, M., and Forbes, D.J. (2003). Removal of a single pore subcomplex results in vertebrate nuclei devoid of nuclear pores. *Mol. Cell* 11, 853-864.
- Harrison, M.J. (2005). Signaling in the arbuscular mycorrhizal symbiosis. *Annu. Rev. Microbiol.* 59, 19-42.
- Harrison, M.J., Dewbre, G.R., and Liu, J. (2002). A phosphate transporter from *Medicago truncatula* involved in the acquisition of phosphate released by arbuscular mycorrhizal fungi. *Plant Cell* 14, 2413-2429.
- Hayashi, M., Miyahara, A., Sato, S., Kato, T., Yoshikawa, M., Taketa, M., Hayashi, M., Pedrosa, A., Onda, R., Imaizumi-Anraku, H., Bachmair, A., Sandal, N., Stougaard, J., Murooka, Y., Tabata, S., Kawasaki, S., Kawaguchi, M., and Harada, K. (2001). Construction of a genetic linkage map of the model legume *Lotus japonicus* using an intraspecific F2 population. *DNA Res.* 8, 301-310.
- Hayashi, T., Banba, M., Shimoda, Y., Kouchi, H., Hayashi, M., and Imaizumi-Anraku, H. (2010). A dominant function of CCaMK in intracellular accommodation of bacterial and fungal endosymbionts. *Plant J.* 63, 141-154.
- Heath, C.V., Copeland, C.S., Amberg, D.C., Del Priore, V., Snyder, M., and Cole, C.N. (1995). Nuclear pore complex clustering and nuclear accumulation of poly(A)<sup>+</sup> RNA associated with mutation of the *Saccharomyces cerevisiae* RAT2/NUP120 gene. *J. Cell Biol.* 131, 1677-1697.
- Heckman, D.S., Geiser, D.M., Eidell, B.R., Stauffer, R.L., Kardos, N.L., and Hedges, S.B. (2001). Molecular Evidence for the Early Colonization of Land by Fungi and Plants. *Science* 293, 1129-1133.
- Heckmann, A.B., Lombardo, F., Miwa, H., Perry, J.A., Bunnewell, S., Parniske, M., Wang, T.L., and Downie, J.A. (2006). *Lotus japonicus* nodulation requires two GRAS domain regulators, one of which is functionally conserved in a non-legume. *Plant Physiol.* 142, 1739-1750.
- Helgason, T., and Fitter, A.H. (2009). Natural selection and the evolutionary ecology of the arbuscular mycorrhizal fungi (Phylum Glomeromycota). *J. Exp. Bot.* 60, 2465-2480.
- Henegariu, O., Heerema, N.A., Dlouhy, S.R., Vance, G.H., and Vogt, P.H. (1997). Multiplex PCR: critical parameters and step-by-step protocol. *Biotechniques* 23, 504-511.

- Hildebrandt, U., Ouziad, F., Marnier, F.J., and Bothe, H. (2006). The bacterium *Paenibacillus validus* stimulates growth of the arbuscular mycorrhizal fungus *Glomus intraradices* up to the formation of fertile spores. *FEMS Microbiol. Lett.* 254, 258-267.
- Hirsch, S., Kim, J., Munoz, A., Heckmann, A.B., Downie, J.A., and Oldroyd, G.E. (2009). GRAS proteins form a DNA binding complex to induce gene expression during nodulation signaling in *Medicago truncatula*. *Plant Cell* 21, 545-557.
- Hodge, A., and Fitter, A.H. (2010). Substantial nitrogen acquisition by arbuscular mycorrhizal fungi from organic material has implications for N cycling. *Proc. Natl. Acad. Sci. USA* 107, 13754-13759.
- Hohnjec, N., Vieweg, M.F., Puhler, A., Becker, A., and Küster, H. (2005). Overlaps in the Transcriptional Profiles of *Medicago truncatula* Roots Inoculated with Two Different *Glomus* Fungi Provide Insights into the Genetic Program Activated during Arbuscular Mycorrhiza. *Plant Physiol.* 137, 1283-1301.
- Hsia, K., Stavropoulos, P., Blobel, G., and Hoelz, A. (2007). Architecture of a coat for the nuclear pore membrane. *Cell* 131,1313-1326.
- Imaizumi-Anraku, H., Takeda, N., Charpentier, M., Perry, J., Miwa, H., Umehara, Y., Kouchi, H., Murakami, Y., Mulder, L., Vickers, K., Pike, J., Downie, J.A., Wang, T., Sato, S., Asamizu, E., Tabata, S., Yoshikawa, M., Murooka, Y., Wu, G.J., Kawaguchi, M., Kawasaki, S., Parniske, M., and Hayashi, M. (2005). Plastid proteins crucial for symbiotic fungal and bacterial entry into plant roots. *Nature* 433, 527-531.
- James, E.K., and Sprent, J.I. (1999). Development of N<sub>2</sub>-fixing nodules on the wetland legume *Lotus uliginosus* exposed to conditions of flooding. *New Phytol.* 142, 219-231.
- Jander, G., Norris, S.R., Rounsley, S.D., Bush, D.F., Levin, I.M., and Last, R.L. (2002). Arabidopsis map-based cloning in the post-genome era. *Plant Physiol.* 129, 440-450.
- Javot, H., Pumplin, N., and Harrison, M.J. (2007a). Phosphate in the arbuscular mycorrhizal symbiosis: transport properties and regulatory roles. *Plant Cell Environ.* 30, 310-322.
- Javot, H., Penmetsa, R.V., Terzaghi, N., Cook, D.R., and Harrison, M.J. (2007b). A *Medicago truncatula* phosphate transporter indispensable for the arbuscular mycorrhizal symbiosis. *Proc. Natl. Acad. Sci. USA* 104, 1720-1725.
- Jiang, Q., and Gresshoff, P.M. (1997). Classical and molecular genetics of the model legume *Lotus japonicus*. *Mol. Plant Microbe Interact.* 10, 59-68.
- Jiang, Y., Lee, A., Chen, J., Cadene, M., Chait, B.T., and MacKinnon, R. (2002). Crystal structure and mechanism of a calcium-gated potassium channel. *Nature* 417, 515.
- Jiang, Y., Pico, A., Cadene, M., Chait, B.T., and MacKinnon, R. (2001). Structure of the RCK domain from the *E. coli* K<sup>+</sup> channel and demonstration of its presence in the human BK channel. *Neuron* 29, 593-601.
- Kaku, H., Nishizawa, Y., Ishii-Minami, N., Akimoto-Tomiyama, C., Dohmae, N., Takio, K., Minami, E., and Shibuya, N. (2006). Plant cells recognize chitin fragments for defense signaling through a plasma membrane receptor. *Proc. Natl. Acad. Sci. USA* 103, 11086-11091.
- Kaló, P., Gleason, C., Edwards, A., Marsh, J., Mitra, R.M., Hirsch, S., Jakab, J., Sims, S., Long, S.R., Rogers, J., Kiss, G.B., Downie, J.A., and Oldroyd, G.E. (2005). Nodulation signaling in legumes requires NSP2, a member of the GRAS family of transcriptional regulators. *Science* 308, 1786-1789.
- Kanamori, N., Madsen, L.H., Radutoiu, S., Frantescu, M., Quistgaard, E.M., Miwa, H., Downie, J.A., James, E.K., Felle, H.H., Haaning, L.L., Jensen, T.H., Sato, S., Nakamura, Y., Tabata, S., Sandal, N., and Stougaard, J. (2006). A nucleoporin is required for induction of Ca<sup>2+</sup> spiking in legume nodule development and essential for rhizobial and fungal symbiosis. *Proc. Natl. Acad. Sci. USA* 103, 359-364.

- Karandashov, V., and Bucher, M. (2005). Symbiotic phosphate transport in arbuscular mycorrhizas. *Trends Plant Sci.* 10, 22-29.
- Karandashov, V., Nagy, R., Wegmuller, S., Amrhein, N., and Bucher, M. (2004). Evolutionary conservation of a phosphate transporter in the arbuscular mycorrhizal symbiosis. *Proc. Natl. Acad. Sci. USA* 101, 6285-6290.
- Karas, B., Murray, J., Gorzelak, M., Smith, A., Sato, S., Tabata, S., and Szczyglowski, K. (2005). Invasion of *Lotus japonicus* root hairless 1 by *Mesorhizobium loti* involves the nodulation factor-dependent induction of root hairs. *Plant Physiol.* 137, 1331-1344.
- Karimi, M., Inze, D., and Depicker, A. (2002). GATEWAY vectors for *Agrobacterium*-mediated plant transformation. *Trends Plant Sci.* 7, 193-195.
- Kawaguchi, M., Motomura, T., Imaizumi-Anraku, H., Akao, S., and Kawasaki, S. (2001). Providing the basis for genomics in *Lotus japonicus*: the accessions Miyakojima and Gifu are appropriate crossing partners for genetic analyses. *Mol. Genet. Genomics* 266, 157-166.
- Kistner, C., and Parniske, M. (2002). Evolution of signal transduction in intracellular symbiosis. *Trends Plant Sci.* 7, 511-518.
- Kistner, C., Winzer, T., Pitzschke, A., Mulder, L., Sato, S., Kaneko, T., Tabata, S., Sandal, N., Stougaard, J., Webb, K.J., Szczyglowski, K., and Parniske, M. (2005). Seven *Lotus japonicus* genes required for transcriptional reprogramming of the root during fungal and bacterial symbiosis. *Plant Cell* 17, 2217-2229.
- Klingner, A., Bothe, H., Wray, V., and Marner, F.-J. (1995). Identification of a yellow pigment formed in maize roots upon mycorrhizal colonization. *Phytochemistry* 38, 53.
- Kobae, Y., Tamura, Y., Takai, S., Banba, M., and Hata, S. (2010). Localized Expression of Arbuscular Mycorrhiza-Inducible Ammonium Transporters in Soybean. *Plant Cell Physiol.* PMID: 20627949.
- Kosuta, S., Chabaud, M., Loughon, G., Gough, C., Dénarié, J., Barker, D.G., and Bécard, G. (2003). A diffusible factor from arbuscular mycorrhizal fungi induces symbiosis-specific *MtENOD11* expression in roots of *Medicago truncatula*. *Plant Physiol.* 131, 952-962.
- Kosuta, S., Hazledine, S., Sun, J., Miwa, H., Morris, R.J., Downie, J.A., and Oldroyd, G.E. (2008). Differential and chaotic calcium signatures in the symbiosis signaling pathway of legumes. *Proc. Natl. Acad. Sci. USA* 105, 9823-9828.
- Krajinski, F., Hause, B., Gianinazzi-Pearson, V., and Franken, P. (2002). *Mtha1*, a Plasma Membrane H<sup>+</sup>-ATPase Gene from *Medicago truncatula*, Shows Arbuscule-Specific Induced Expression in Mycorrhizal Tissue. *Plant Biol.* 4, 754-761.
- Krusell, L., Madsen, L.H., Sato, S., Aubert, G., Genua, A., Szczyglowski, K., Duc, G., Kaneko, T., Tabata, S., de Bruijn, F., Pajuelo, E., Sandal, N., and Stougaard, J. (2002). Shoot control of root development and nodulation is mediated by a receptor-like kinase. *Nature* 420, 422-426.
- Kuhn, H., Küster, H., and Requena, N. (2010). *Membrane steroid-binding protein 1* induced by a diffusible fungal signal is critical for mycorrhization in *Medicago truncatula*. *New Phytol.* 185, 716-733.
- La Rue, T.A., and Weeden, N.F. (1994). The symbiosis genes of the host. In: *Proceedings of the 1st European Nitrogen Fixation Conference* (G.B. Kiss and G. Endre, eds.). Officina Press, Szeged, Hungary. pp 147-151.
- Lévy, J., Bres, C., Geurts, R., Chalhoub, B., Kulikova, O., Duc, G., Journet, E.P., Ané, J.M., Lauber, E., Bisseling, T., Dénarié, J., Rosenberg, C., and Debelle, F. (2004). A putative Ca<sup>2+</sup> and calmodulin-dependent protein kinase required for bacterial and fungal symbioses. *Science* 303, 1361-1364.
- Li, X.-L., George, E., and Marschner, H. (1991). Extension of the phosphorus depletion zone in VA-mycorrhizal white clover in a calcareous soil. *Plant and Soil* 136, 41.

- Lister, R., Gregory, B.D., and Ecker, J.R. (2009). Next is now: new technologies for sequencing of genomes, transcriptomes, and beyond. *Curr. Opin. Plant. Biol.* 12, 107-118.
- Liu, J., Blaylock, L.A., Endre, G., Cho, J., Town, C.D., VandenBosch, K.A., and Harrison, M.J. (2003). Transcript Profiling Coupled with Spatial Expression Analyses Reveals Genes Involved in Distinct Developmental Stages of an Arbuscular Mycorrhizal Symbiosis. *Plant Cell* 15, 2106-2123.
- Liu, J., Maldonado-Mendoza, I., Lopez-Meyer, M., Cheung, F., Town, C.D., and Harrison, M.J. (2007). Arbuscular mycorrhizal symbiosis is accompanied by local and systemic alterations in gene expression and an increase in disease resistance in the shoots. *Plant J.* 50, 529-544.
- Lohmann, G.V., Shimoda, Y., Nielsen, M.W., Jorgensen, F.G., Grossmann, C., Sandal, N., Sorensen, K., Thirup, S., Madsen, L.H., Tabata, S., Sato, S., Stougaard, J., and Radutoiu, S. (2010). Evolution and regulation of the *Lotus japonicus* LysM receptor gene family. *Mol. Plant Microbe Interact.* 23, 510-521.
- Lohse, S., Schliemann, W., Ammer, C., Kopka, J., Strack, D., and Fester, T. (2005). Organization and metabolism of plastids and mitochondria in arbuscular mycorrhizal roots of *Medicago truncatula*. *Plant Physiol.* 139, 329-340.
- Lombardo, F., Heckmann, A.B., Miwa, H., Perry, J.A., Yano, K., Hayashi, M., Parniske, M., Wang, T.L., and Downie, J.A. (2006). Identification of symbiotically defective mutants of *Lotus japonicus* affected in infection thread growth. *Mol. Plant Microbe Interact.* 19, 1444-1450.
- Lopez-Pedrosa, A., Gonzalez-Guerrero, M., Valderas, A., Azcon-Aguilar, C., and Ferrol, N. (2006). *GintAMT1* encodes a functional high-affinity ammonium transporter that is expressed in the extraradical mycelium of *Glomus intraradices*. *Fungal Genet. Biol.* 43, 102-110.
- López-Ráez, J.A., Charnikhova, T., Gómez-Roldán, V., Matusova, R., Kohlen, W., De Vos, R., Verstappen, F., Puech-Pages, V., Bécard, G., Mulder, P., and Bouwmeester, H. (2008). Tomato strigolactones are derived from carotenoids and their biosynthesis is promoted by phosphate starvation. *New Phytol.* 178, 863-874.
- Lutzmann, M., Kunze, R., Buerer, A., Aebi, U., and Hurt, E. (2002). Modular self-assembly of a Y-shaped multiprotein complex from seven nucleoporins. *Embo J.* 21, 387-397.
- Madsen, E.B., Madsen, L.H., Radutoiu, S., Olbryt, M., Rakwalska, M., Szczyglowski, K., Sato, S., Kaneko, T., Tabata, S., Sandal, N., and Stougaard, J. (2003). A receptor kinase gene of the LysM type is involved in legume perception of rhizobial signals. *Nature* 425, 637-640.
- Madsen, L.H., Tirichine, L., Jurkiewicz, A., Sullivan, J.T., Heckmann, A.B., Bek, A.S., Ronson, C.W., James, E.K., and Stougaard, J. (2010). The molecular network governing nodule organogenesis and infection in the model legume *Lotus japonicus*. *Nat. Commun.* 1, 10.
- Maeda, D., Ashida, K., Iguchi, K., Chechetka, S.A., Hijikata, A., Okusako, Y., Deguchi, Y., Izui, K., and Hata, S. (2006). Knockdown of an arbuscular mycorrhiza-inducible phosphate transporter gene of *Lotus japonicus* suppresses mutualistic symbiosis. *Plant Cell Physiol.* 47, 807-817.
- Maekawa-Yoshikawa, M., Muller, J., Takeda, N., Maekawa, T., Sato, S., Tabata, S., Perry, J., Wang, T.L., Groth, M., Brachmann, A., and Parniske, M. (2009). The temperature-sensitive brush mutant of the legume *Lotus japonicus* reveals a link between root development and nodule infection by rhizobia. *Plant Physiol.* 149, 1785-1796.
- Magori, S., Oka-Kira, E., Shibata, S., Umehara, Y., Kouchi, H., Hase, Y., Tanaka, A., Sato, S., Tabata, S., and Kawaguchi, M. (2009). *Too much love*, a root regulator associated with the long-distance control of nodulation in *Lotus japonicus*. *Mol. Plant Microbe Interact.* 22, 259-268.



- Maherali, H., and Klironomos, J.N. (2007). Influence of Phylogeny on Fungal Community Assembly and Ecosystem Functioning. *Science* 316, 1746-1748.
- Mansfield, E.S., Vainer, M., Enad, S., Barker, D.L., Harris, D., Rappaport, E., and Fortina, P. (1996). Sensitivity, reproducibility, and accuracy in short tandem repeat genotyping using capillary array electrophoresis. *Genome Res.* 6, 893-903.
- Markmann, K., and Parniske, M. (2009). Evolution of root endosymbiosis with bacteria: how novel are nodules? *Trends Plant Sci.* 14, 77-86.
- Markmann, K., Giczey, G., and Parniske, M. (2008). Functional adaptation of a plant receptor-kinase paved the way for the evolution of intracellular root symbioses with bacteria. *PLoS Biol.* 6, e68.
- Marquez, A.J., and Stougaard, J. (2005). *Lotus Japonicus* Handbook, p. 384.
- Marsh, J.F., and Schultze, M. (2001). Analysis of arbuscular mycorrhizas using symbiosis-defective plant mutants. *New Phytol.* 150, 525-532.
- Marsh, J.F., Rakocevic, A., Mitra, R.M., Brocard, L., Sun, J., Eschstruth, A., Long, S.R., Schultze, M., Ratet, P., and Oldroyd, G.E. (2007). *Medicago truncatula* NIN is essential for rhizobial-independent nodule organogenesis induced by autoactive calcium/calmodulin-dependent protein kinase. *Plant Physiol.* 144, 324-335.
- McGonigle, T.P., Miller, M.H., Evans, D.G., Fairchild, G.L., and Swan, J.A. (1990). A new method which gives an objective measure of colonization of roots by vesicular-arbuscular mycorrhizal fungi. *New Phytol.* 115, 495-501.
- Meixner, C., Ludwig-Muller, J., Miersch, O., Gresshoff, P., Staehelin, C., and Vierheilig, H. (2005). Lack of mycorrhizal autoregulation and phytohormonal changes in the supernodulating soybean mutant nts1007. *Planta*, 1-7.
- Messinese, E., Mun, J.H., Yeun, L.H., Jayaraman, D., Rouge, P., Barre, A., Loughon, G., Schornack, S., Bono, J.J., Cook, D.R., and Ané, J.M. (2007). A novel nuclear protein interacts with the symbiotic DMI3 calcium- and calmodulin-dependent protein kinase of *Medicago truncatula*. *Mol. Plant Microbe Interact.* 20, 912-921.
- Middleton, P.H., Jakab, J., Penmetsa, R.V., Starker, C.G., Doll, J., Kaló, P., Prabhu, R., Marsh, J.F., Mitra, R.M., Kereszt, A., Dudas, B., VandenBosch, K., Long, S.R., Cook, D.R., Kiss, G.B., and Oldroyd, G.E. (2007). An ERF transcription factor in *Medicago truncatula* that is essential for Nod factor signal transduction. *Plant Cell* 19, 1221-1234.
- Mitra, R.M., Gleason, C.A., Edwards, A., Hadfield, J., Downie, J.A., Oldroyd, G.E., and Long, S.R. (2004). A Ca<sup>2+</sup>/calmodulin-dependent protein kinase required for symbiotic nodule development: Gene identification by transcript-based cloning. *Proc. Natl. Acad. Sci. USA* 101, 4701-4705.
- Mitra, R.M., Shaw, S.L., and Long, S.R. (2004). Six nonnodulating plant mutants defective for Nod factor-induced transcriptional changes associated with the legume-rhizobia symbiosis. *Proc. Natl. Acad. Sci. USA* 101, 10217-10222.
- Miwa, H., Sun, J., Oldroyd, G.E., and Downie, J.A. (2006a). Analysis of calcium spiking using a cameleon calcium sensor reveals that nodulation gene expression is regulated by calcium spike number and the developmental status of the cell. *Plant J.* 48, 883.
- Miwa, H., Sun, J., Oldroyd, G.E., and Downie, J.A. (2006b). Analysis of Nod-factor-induced calcium signaling in root hairs of symbiotically defective mutants of *Lotus japonicus*. *Mol. Plant Microbe Interact.* 19, 914-923.
- Miya, A., Albert, P., Shinya, T., Desaki, Y., Ichimura, K., Shirasu, K., Narusaka, Y., Kawakami, N., Kaku, H., and Shibuya, N. (2007). CERK1, a LysM receptor kinase, is essential for chitin elicitor signaling in Arabidopsis. *Proc. Natl. Acad. Sci. USA* 104, 19613-19618.
- Morandi, D., Sagan, M., Prado-Vivant, E., and Duc, G. (2000). Influence of genes determining supernodulation on root colonization by the mycorrhizal fungus *Glomus mosseae* in *Pisum sativum* and *Medicago truncatula* mutants. *Mycorrhiza* 10, 37-42.

- Mortier, V., Den Herder, G., Whitford, R., Van de Velde, W., Rombauts, S., D'Haeseleer, K., Holsters, M., and Goormachtig, S. (2010). CLE peptides control *Medicago truncatula* nodulation locally and systemically. *Plant Physiol.* 153, 222-237.
- Murakami, Y., Miwa, H., Imaizumi-Anraku, H., Kouchi, H., Downie, J.A., Kawaguchi, M., and Kawasaki, S. (2006). Positional cloning identifies *Lotus japonicus* NSP2, a putative transcription factor of the GRAS family, required for *NIN* and *ENOD40* gene expression in nodule initiation. *DNA Res.* 13, 255-265.
- Murray, J.D., Karas, B.J., Sato, S., Tabata, S., Amyot, L., and Szczyglowski, K. (2007). A cytokinin perception mutant colonized by *Rhizobium* in the absence of nodule organogenesis. *Science* 315, 101-104.
- Nagy, R., Karandashov, V., Chague, V., Kalinkevich, K., Tamasloukht, M., Xu, G., Jakobsen, I., Levy, A.A., Amrhein, N., and Bucher, M. (2005). The characterization of novel mycorrhiza-specific phosphate transporters from *Lycopersicon esculentum* and *Solanum tuberosum* uncovers functional redundancy in symbiotic phosphate transport in solanaceous species. *Plant J.* 42, 236-250.
- Nakagawa, T., and Kawaguchi, M. (2006). Shoot-applied MeJA Suppresses Root Nodulation in *Lotus japonicus*. *Plant Cell Physiol.* 47, 176-180.
- Ndoye, I., de Billy, F., Vasse, J., Dreyfus, B., and Truchet, G. (1994). Root nodulation of *Sesbania rostrata*. *J. Bacteriol.* 176, 1060-1068.
- Neer, E.J., Schmidt, C.J., Nambudripad, R., and Smith, T.F. (1994). The ancient regulatory-protein family of WD-repeat proteins. *Nature* 371, 297-300.
- Newsham, K.K., Fitter, A.H., and Watkinson, A.R. (1995). Arbuscular Mycorrhiza Protect an Annual Grass from Root Pathogenic Fungi in the Field. *J. Ecol.* 83, 991.
- Nishimura, R., Hayashi, M., Wu, G.-J., Kouchi, H., Imaizumi-Anraku, H., Murakami, Y., Kawasaki, S., Akao, S., Ohmori, M., Nagasawa, M., Harada, K., and Kawaguchi, M. (2002b). *HAR1* mediates systemic regulation of symbiotic organ development. *Nature* 420, 426-429.
- Nishimura, R., Ohmori, M., Fujita, H., and Kawaguchi, M. (2002a). From the Cover: A Lotus basic leucine zipper protein with a RING-finger motif negatively regulates the developmental program of nodulation. *Proc. Natl. Acad. Sci. USA* 99, 15206-15210.
- Niwa, S., Kawaguchi, M., Imaizumi-Anraku, H., Chechetka, S.A., Ishizaka, M., Ikuta, A., and Kouchi, H. (2001). Responses of a model legume *Lotus japonicus* to lipochitin oligosaccharide nodulation factors purified from *Mesorhizobium loti* JRL501. *Mol. Plant Microbe Interact.* 14, 848-856.
- Ogawa, M., Shinohara, H., Sakagami, Y., and Matsubayashi, Y. (2008). Arabidopsis CLV3 peptide directly binds CLV1 ectodomain. *Science* 319, 294.
- Ohmido, N., Ishimaru, A., Kato, S., Sato, S., Tabata, S., and Fukui, K. (2010). Integration of cytogenetic and genetic linkage maps of *Lotus japonicus*, a model plant for legumes. *Chromosome Res.* 18, 287-299.
- Oka-Kira, E., Tateno, K., Miura, K., Haga, T., Hayashi, M., Harada, K., Sato, S., Tabata, S., Shikazono, N., Tanaka, A., Watanabe, Y., Fukuhara, I., Nagata, T., and Kawaguchi, M. (2005). *klavier (klv)*, a novel hypernodulation mutant of *Lotus japonicus* affected in vascular tissue organization and floral induction. *Plant J.* 44, 505-515.
- Okamoto, S., Ohnishi, E., Sato, S., Takahashi, H., Nakazono, M., Tabata, S., and Kawaguchi, M. (2009). Nod factor/nitrate-induced *CLE* genes that drive *HAR1*-mediated systemic regulation of nodulation. *Plant Cell Physiol.* 50, 67-77.
- Olah, B., Briere, C., Bécard, G., Dénarié, J., and Gough, C. (2005). Nod factors and a diffusible factor from arbuscular mycorrhizal fungi stimulate lateral root formation in *Medicago truncatula* via the DMI1/DMI2 signalling pathway. *Plant J.* 44, 195-207.
- Oldroyd, G.E., and Downie, J.A. (2008). Coordinating nodule morphogenesis with rhizobial infection in legumes. *Annu. Rev. Plant Biol.* 59, 519-546.

- Oldroyd, G.E., Engstrom, E.M., and Long, S.R. (2001a). Ethylene inhibits the Nod factor signal transduction pathway of *Medicago truncatula*. *Plant Cell* 13, 1835-1849.
- Oldroyd, G.E., Mitra, R.M., Wais, R.J., and Long, S.R. (2001b). Evidence for structurally specific negative feedback in the Nod factor signal transduction pathway. *Plant J.* 28, 191-199.
- Oliveira, M.B., Vieira, E.S., and Schuster, I. (2010). Construction of a molecular database for soybean cultivar identification in Brazil. *Genet. Mol. Res.* 9, 705-720.
- Pacios-Bras, C., Schlaman, H.R.M., Boot, K., Admiraal, P., Mateos Langerak, J., Stougaard, J., and Spaink, H.P. (2003). Auxin distribution in *Lotus japonicus* during root nodule development. *Plant Mol. Biol.* 52, 1169-1180.
- Palm, C.A., Smukler, S.M., Sullivan, C.C., Mutuo, P.K., Nyadzi, G.I., and Walsh, M.G. (2010). Climate Mitigation and Agricultural Productivity in Tropical Landscapes Special Feature: Identifying potential synergies and trade-offs for meeting food security and climate change objectives in sub-Saharan Africa. *Proc. Natl. Acad. Sci. USA*. PMID: 20453198.
- Palma, K., Zhang, Y., and Li, X. (2005). An importin alpha homolog, MOS6, plays an important role in plant innate immunity. *Curr. Biol.* 15, 1129-1135.
- Parniske, M. (2004). Molecular genetics of the arbuscular mycorrhizal symbiosis. *Curr. Opin. Plant Biol.* 7, 414-421.
- Parniske, M. (2005). Plant-fungal associations: cue for the branching connection. *Nature* 435, 750-751.
- Parniske, M. (2008). Arbuscular mycorrhiza: the mother of plant root endosymbioses. *Nature Rev. Microbiol.* 6, 763-775.
- Paszkowski, U., Jakovleva, L., and Boller, T. (2006). Maize mutants affected at distinct stages of the arbuscular mycorrhizal symbiosis. *Plant J.* 47, 165-173.
- Paszkowski, U., Kroken, S., Roux, C., and Briggs, S.P. (2002). Rice phosphate transporters include an evolutionarily divergent gene specifically activated in arbuscular mycorrhizal symbiosis. *Proc. Natl. Acad. Sci. USA* 99, 13324-13329.
- Pedrosa, A., Sandal, N., Stougaard, J., Schweizer, D., and Bachmair, A. (2002). Chromosomal map of the model legume *Lotus japonicus*. *Genetics* 161, 1661-1672.
- Penmetsa, R.V., and Cook, D.R. (1997). A legume ethylene-insensitive mutant hyperinfected by its rhizobial symbiont. *Science* 275, 527-530.
- Penmetsa, R.V., Frugoli, J.A., Smith, L.S., Long, S.R., and Cook, D.R. (2003). Dual genetic pathways controlling nodule number in *Medicago truncatula*. *Plant Physiol.* 131, 998-1008.
- Perry, J., Brachmann, A., Welham, T., Binder, A., Charpentier, M., Groth, M., Haage, K., Markmann, K., Wang, T.L., and Parniske, M. (2009). TILLING in *Lotus japonicus* identified large allelic series for symbiosis genes and revealed a bias in functionally defective ethyl methanesulfonate alleles toward glycine replacements. *Plant Physiol.* 151, 1281-1291.
- Perry, J.A., Wang, T.L., Welham, T.J., Gardner, S., Pike, J.M., Yoshida, S., and Parniske, M. (2003). A TILLING reverse genetics tool and a web-accessible collection of mutants of the legume *Lotus japonicus*. *Plant Physiol.* 131, 866-871.
- Peters, J.L., Cnudde, F., and Gerats, T. (2003). Forward genetics and map-based cloning approaches. *Trends Plant Sci.* 8, 484-491.
- Petutschnig, E.K., Jones, A.M., Serazetdinova, L., Lipka, U., and Lipka, V. (2010). The LysM-RLK CERK1 is a major chitin binding protein in *Arabidopsis thaliana* and subject to chitin-induced phosphorylation. *J. Biol. Chem.* PMID: 20610395

- Pfaffl, M.W., Horgan, G.W., and Dempfle, L. (2002). Relative expression software tool (REST) for group-wise comparison and statistical analysis of relative expression results in real-time PCR. *Nucleic Acids Res.* 30, e36.
- Pierce, M., and Bauer, W.D. (1983). A Rapid Regulatory Response Governing Nodulation in Soybean. *Plant Physiol.* 73, 286-290.
- Pozo, M.J., and Azcon-Aguilar, C. (2007). Unraveling mycorrhiza-induced resistance. *Curr Opin. Plant Biol.* 10, 393-398.
- Prayitno, J., Rolfe, B.G., and Mathesius, U. (2006). The ethylene-insensitive *sickle* mutant of *Medicago truncatula* shows altered auxin transport regulation during nodulation. *Plant Physiol* 142, 168-180.
- Pueppke, S.G., and Broughton, W.J. (1999). *Rhizobium sp.* strain NGR234 and *R. fredii* USDA257 share exceptionally broad, nested host ranges. *Mol. Plant Microbe Interact.* 12, 293-318.
- Pumplin, N., and Harrison, M.J. (2009). Live-cell imaging reveals periarbuscular membrane domains and organelle location in *Medicago truncatula* roots during arbuscular mycorrhizal symbiosis. *Plant Physiol.* 151, 809-819.
- Pumplin, N., Mondo, S.J., Topp, S., Starker, C.G., Gantt, J.S., and Harrison, M.J. (2010). *Medicago truncatula* Vapyrin is a novel protein required for arbuscular mycorrhizal symbiosis. *Plant J.* 61, 482-494.
- Radutoiu, S., Madsen, L.H., Madsen, E.B., Felle, H.H., Umehara, Y., Gronlund, M., Sato, S., Nakamura, Y., Tabata, S., Sandal, N., and Stougaard, J. (2003). Plant recognition of symbiotic bacteria requires two LysM receptor-like kinases. *Nature* 425, 585-592.
- Radutoiu, S., Madsen, L.H., Madsen, E.B., Jurkiewicz, A., Fukai, E., Quistgaard, E.M., Albrektsen, A.S., James, E.K., Thirup, S., and Stougaard, J. (2007). LysM domains mediate lipochitin-oligosaccharide recognition and *Nfr* genes extend the symbiotic host range. *Embo J.* 26, 3923-3935.
- Rausch, C., Daram, P., Brunner, S., Jansa, J., Laloi, M., Leggewie, G., Amrhein, N., and Bucher, M. (2001). A phosphate transporter expressed in arbuscule-containing cells in potato. *Nature* 414, 462-470.
- Reddy, D.M.R.S., Schorderet, M., Feller, U., and Reinhardt, D. (2007). A petunia mutant affected in intracellular accommodation and morphogenesis of arbuscular mycorrhizal fungi. *Plant J.* 51, 739-750.
- Redecker, D., Kodner, R., and Graham, L.E. (2000). Glomalean Fungi from the Ordovician. *Science* 289, 1920-1921.
- Remy, W., Taylor, T.N., Hass, H., and Kerp, H. (1994). Four hundred-million-year-old vesicular arbuscular mycorrhizae. *Proc. Natl. Acad. Sci. USA* 91, 11841-11843.
- Rosendahl, S. (2008). Communities, populations and individuals of arbuscular mycorrhizal fungi. *New Phytol.* 178, 253-266.
- Ruijter, J.M., Ramakers, C., Hoogaars, W.M., Karlen, Y., Bakker, O., van den Hoff, M.J., and Moorman, A.F. (2009). Amplification efficiency: linking baseline and bias in the analysis of quantitative PCR data. *Nucleic Acids Res.* 37, e45.
- Rutherford, K., Parkhill, J., Crook, J., Horsnell, T., Rice, P., Rajandream, M.A., and Barrell, B. (2000). Artemis: sequence visualization and annotation. *Bioinformatics* 16, 944-945.
- Saito, K., Yoshikawa, M., Yano, K., Miwa, H., Uchida, H., Asamizu, E., Sato, S., Tabata, S., Imaizumi-Anraku, H., Umehara, Y., Kouchi, H., Murooka, Y., Szczyglowski, K., Downie, J.A., Parniske, M., Hayashi, M., and Kawaguchi, M. (2007). *NUCLEOPORIN85* is required for calcium spiking, fungal and bacterial symbioses, and seed production in *Lotus japonicus*. *Plant Cell* 19, 610-624.

- Sandal, N., Petersen, T.R., and Murray, J. (2005). Genetics of Symbiosis in *Lotus japonicus*: Recombinant Inbred Lines, Comparative Genetic Maps and Map Position of 35 Symbiotic Loci. *Mol. Plant Microbe Interact.* 19, 80-91.
- Santos-Gonzalez, J.C., Finlay, R.D., and Tehler, A. (2007). Seasonal Dynamics of Arbuscular Mycorrhizal Fungal Communities in Roots in a Seminatural Grassland. *Appl. Environ. Microbiol.* 73, 5613-5623.
- Sato, S., Nakamura, Y., Kaneko, T., Asamizu, E., Kato, T., Nakao, M., Sasamoto, S., Watanabe, A., Ono, A., Kawashima, K., Fujishiro, T., Katoh, M., Kohara, M., Kishida, Y., Minami, C., Nakayama, S., Nakazaki, N., Shimizu, Y., Shinpo, S., Takahashi, C., Wada, T., Yamada, M., Ohmido, N., Hayashi, M., Fukui, K., Baba, T., Nakamichi, T., Mori, H., and Tabata, S. (2008). Genome structure of the legume, *Lotus japonicus*. *DNA Res.* 15, 227-239.
- Schauser, L., Handberg, K., Sandal, N., Stiller, J., Thykjaer, T., Pajuelo, E., Nielsen, A., and Stougaard, J. (1998). Symbiotic mutants deficient in nodule establishment identified after T-DNA transformation of *Lotus japonicus*. *Mol Gen Genet* 259, 414-423.
- Schauser, L., Roussis, A., Stiller, J., and Stougaard, J. (1999). A plant regulator controlling development of symbiotic root nodules. *Nature* 402, 191-195.
- Schlosser, A., Hamann, A., Bossemeyer, D., Schneider, E., and Bakker, E.P. (1993). NAD<sup>+</sup> binding to the Escherichia coli K(+)-uptake protein TrkA and sequence similarity between TrkA and domains of a family of dehydrogenases suggest a role for NAD<sup>+</sup> in bacterial transport. *Mol. Microbiol.* 9, 533-543.
- Schmidt, H.A., Strimmer, K., Vingron, M., and von Haeseler, A. (2002). TREE-PUZZLE: maximum likelihood phylogenetic analysis using quartets and parallel computing. *Bioinformatics* 18, 502-504.
- Schneeberger, K., Ossowski, S., Lanz, C., Juul, T., Petersen, A.H., Nielsen, K.L., Jorgensen, J.E., Weigel, D., and Andersen, S.U. (2009). SHOREmap: simultaneous mapping and mutation identification by deep sequencing. *Nat. Methods* 6, 550-551.
- Schuelke, M. (2000). An economic method for the fluorescent labeling of PCR fragments. *Nat. Biotechnol.* 18, 233-234.
- Schultz, J., Milpetz, F., Bork, P., and Ponting, C.P. (1998). SMART, a simple modular architecture research tool: identification of signaling domains. *Proc. Natl. Acad. Sci. USA* 95, 5857-5864.
- Schüßler, A., Schwarzott, D., and Walker, C. (2001). A new fungal phylum, the Glomeromycota: phylogeny and evolution. *Mycological Research* 105, 1413-1421.
- Searle, I.R., Men, A.E., Laniya, T.S., Buzas, D.M., Iturbe-Ormaetxe, I., Carroll, B.J., and Gresshoff, P.M. (2003). Long-distance signaling in nodulation directed by a CLAVATA1-like receptor kinase. *Science* 299, 109-112.
- Seefeldt, L.C., Hoffman, B.M., and Dean, D.R. (2009). Mechanism of Mo-dependent nitrogenase. *Annu. Rev. Biochem.* 78, 701-722.
- Shaw, S.L., and Long, S.R. (2003). Nod factor elicits two separable calcium responses in *Medicago truncatula* root hair cells. *Plant Physiol.* 131, 976-984.
- Shi, J., Blundell, T.L., and Mizuguchi, K. (2001). FUGUE: sequence-structure homology recognition using environment-specific substitution tables and structure-dependent gap penalties. *J. Mol. Biol.* 310, 243-257.
- Sieberer, B.J., Chabaud, M., Timmers, A.C., Monin, A., Fournier, J., and Barker, D.G. (2009). A nuclear-targetedameleon demonstrates intranuclear Ca<sup>2+</sup> spiking in *Medicago truncatula* root hairs in response to rhizobial nodulation factors. *Plant Physiol.* 151, 1197-1206.
- Simon, L., Bousquet, J., Levesque, R.C., and Lalonde, M. (1993). Origin and diversification of endomycorrhizal fungi and coincidence with vascular land plants. *Nature* 363, 67.

- Siniossoglou, S., Wimmer, C., Rieger, M., Doye, V., Tekotte, H., Weise, C., Emig, S., Segref, A., and Hurt, E.C. (1996). A novel complex of nucleoporins, which includes Sec13p and a Sec13p homolog, is essential for normal nuclear pores. *Cell* 84, 265-275.
- Smil, V. (1999). Nitrogen in crop production: An account of global flows. *Global Biogeochem. Cycles* 13, 647.
- Smil, V. (2003). PHOSPHORUS IN THE ENVIRONMENT: Natural Flows and Human Interferences. *Ann. Rev. Energy Environ.* 25, 53.
- Smit, P., Raedts, J., Portyanko, V., Debelle, F., Gough, C., Bisseling, T., and Geurts, R. (2005). NSP1 of the GRAS protein family is essential for rhizobial Nod factor-induced transcription. *Science* 308, 1789-1791.
- Smith, J.R., Carpten, J.D., Brownstein, M.J., Ghosh, S., Magnuson, V.L., Gilbert, D.A., Trent, J.M., and Collins, F.S. (1995). Approach to genotyping errors caused by nontemplated nucleotide addition by Taq DNA polymerase. *Genome Res.* 5, 312-317.
- Smith, S.E., and Read, D. (2008). Mineral nutrition, toxic element accumulation and water relations of arbuscular mycorrhizal plants. In *Mycorrhizal Symbiosis* (Third Edition) (London: Academic Press), pp. 145.
- Smith, S.E., Smith, F.A., and Jakobsen, I. (2004). Functional diversity in arbuscular mycorrhizal (AM) symbioses: the contribution of the mycorrhizal P uptake pathway is not correlated with mycorrhizal responses in growth or total P uptake. *New Phytol.* 162, 511-524.
- Smith, T.F., Gaitatzes, C., Saxena, K., and Neer, E.J. (1999). The WD repeat: a common architecture for diverse functions. *Trends Biochem. Sci.* 24, 181-185.
- Solaiman, Z.M., Senoo, K., Kawaguchi, M., Imaizumi-Anraku, H., Akao, S., Tanaka, A., and Obata, H. (2000). Characterization of Mycorrhizas Formed by *Glomus* sp. on Roots of Hypernodulating Mutants of *Lotus japonicus*. *J. Plant Res.* 113, 443-448.
- Soltis, D.E., Soltis, P.S., Morgan, D.R., Swensen, S.M., Mullin, B.C., Dowd, J.M., and Martin, P.G. (1995). Chloroplast gene sequence data suggest a single origin of the predisposition for symbiotic nitrogen fixation in angiosperms. *Proc. Natl. Acad. Sci. USA* 92, 2647-2651.
- Sprent, J.I. (2007). Evolving ideas of legume evolution and diversity: a taxonomic perspective on the occurrence of nodulation. *New Phytol.* 174, 11-25.
- Stockinger, H., Walker, C., and Schüßler, A. (2009). '*Glomus intraradices* DAOM197198', a model fungus in arbuscular mycorrhiza research, is not *Glomus intraradices*. *New Phytol.* 183, 1176-1187.
- Stracke, S., Kistner, C., Yoshida, S., Mulder, L., Sato, S., Kaneko, T., Tabata, S., Sandal, N., Stougaard, J., Szczyglowski, K., and Parniske, M. (2002). A plant receptor-like kinase required for both bacterial and fungal symbiosis. *Nature* 417, 959-962.
- Sturtevant, A.H., Bridges, C.B., and Morgan, T.H. (1919). The Spatial Relations of Genes. *Proc. Natl. Acad. Sci. USA* 5, 168-173.
- Sun, J., Cardoza, V., Mitchell, D.M., Bright, L., Oldroyd, G., and Harris, J.M. (2006). Crosstalk between jasmonic acid, ethylene and Nod factor signaling allows integration of diverse inputs for regulation of nodulation. *Plant J.* 46, 961-970.
- Szczyglowski, K., Shaw, R.S., Wopereis, J., Copeland, S., Hamburger, D., Kasiborski, B., Dazzo, F.B., and de Bruijn, F.J. (1998). Nodule Organogenesis and Symbiotic Mutants of the Model Legume *Lotus japonicus*. *Mol. Plant Microbe Interact.* 11, 684-697.
- Takeda, N., Okamoto, S., Hayashi, M., and Murooka, Y. (2005). Expression of *LjENOD40* genes in response to symbiotic and non-symbiotic signals: *LjENOD40-1* and *LjENOD40-2* are differentially regulated in *Lotus japonicus*. *Plant Cell Physiol.* 46, 1291-1298.

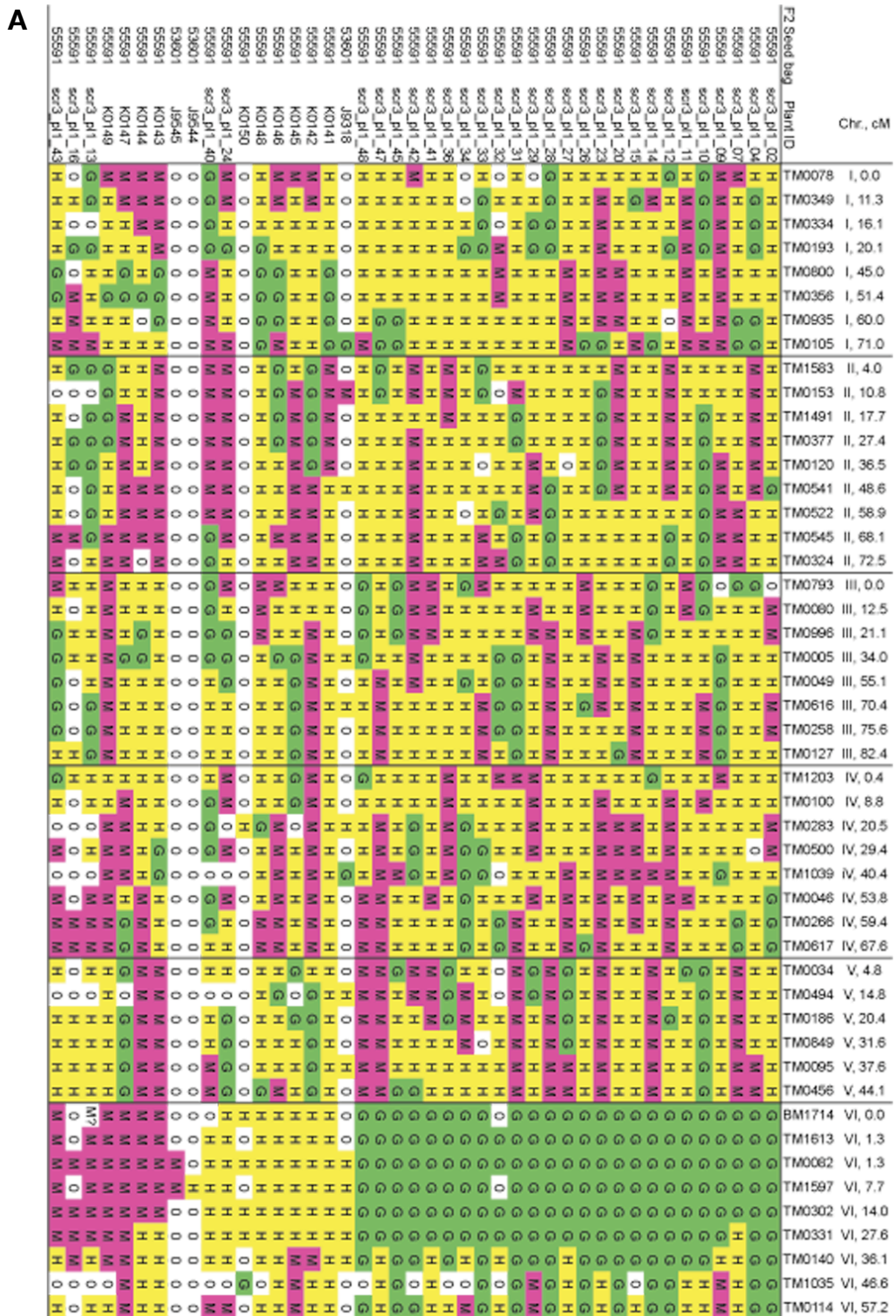
- Takeda, N., Sato, S., Asamizu, E., Tabata, S., and Parniske, M. (2009). Apoplastic plant subtilases support arbuscular mycorrhiza development in *Lotus japonicus*. *Plant J.* 58, 766-777.
- Temnykh, S., DeClerck, G., Lukashova, A., Lipovich, L., Cartinhour, S., and McCouch, S. (2001). Computational and experimental analysis of microsatellites in rice (*Oryza sativa* L.): frequency, length variation, transposon associations, and genetic marker potential. *Genome Res.* 11, 1441-1452.
- Tirichine, L., Imaizumi-Anraku, H., Yoshida, S., Murakami, Y., Madsen, L.H., Miwa, H., Nakagawa, T., Sandal, N., Albrektsen, A.S., Kawaguchi, M., Downie, A., Sato, S., Tabata, S., Kouchi, H., Parniske, M., Kawasaki, S., and Stougaard, J. (2006a). Deregulation of a Ca<sup>2+</sup>/calmodulin-dependent kinase leads to spontaneous nodule development. *Nature* 441, 1153-1156.
- Tirichine, L., James, E.K., Sandal, N., and Stougaard, J. (2006b). Spontaneous root-nodule formation in the model legume *Lotus japonicus*: a novel class of mutants nodulates in the absence of rhizobia. *Mol. Plant Microbe Interact.* 19, 373-382.
- Tirichine, L., Sandal, N., Madsen, L.H., Radutoiu, S., Albrektsen, A.S., Sato, S., Asamizu, E., Tabata, S., and Stougaard, J. (2007). A gain-of-function mutation in a cytokinin receptor triggers spontaneous root nodule organogenesis. *Science* 315, 104-107.
- Umehara, M., Hanada, A., Yoshida, S., Akiyama, K., Arite, T., Takeda-Kamiya, N., Magome, H., Kamiya, Y., Shirasu, K., Yoneyama, K., Kyojuka, J., and Yamaguchi, S. (2008). Inhibition of shoot branching by new terpenoid plant hormones. *Nature* 455, 195-200.
- van Brussel, A.A., Bakhuizen, R., van Spronsen, P.C., Spaink, H.P., Tak, T., Lugtenberg, B.J., and Kijne, J.W. (1992). Induction of pre-infection thread structures in the leguminous host plant by mitogenic lipo-oligosaccharides of *Rhizobium*. *Science* 257, 70-72.
- Van de Velde, W., Zehirov, G., Szatmari, A., Debreczeny, M., Ishihara, H., Kevei, Z., Farkas, A., Mikulass, K., Nagy, A., Tiricz, H., Satiat-Jeunemaitre, B., Alunni, B., Bourge, M., Kucho, K., Abe, M., Kereszt, A., Maroti, G., Uchiumi, T., Kondorosi, E., and Mergaert, P. (2010). Plant peptides govern terminal differentiation of bacteria in symbiosis. *Science* 327, 1122-1126.
- van der Heijden, M.G.A., Klironomos, J.N., Ursic, M., Moutoglou, P., Streitwolf-Engel, R., Boller, T., Wiemken, A., and Sanders, I.R. (1998). Mycorrhizal fungal diversity determines plant biodiversity, ecosystem variability and productivity. *Nature* 396, 69.
- van Noorden, G.E., Ross, J.J., Reid, J.B., Rolfe, B.G., and Mathesius, U. (2006). Defective Long-Distance Auxin Transport Regulation in the *Medicago truncatula* super numeric nodules Mutant. *Plant Physiol.* 140, 1494-1506.
- Vierheilig, H. (2004). Further root colonization by arbuscular mycorrhizal fungi in already mycorrhizal plants is suppressed after a critical level of root colonization. *J. Plant Physiol.* 161, 339-341.
- Vierheilig, H., Coughlan, A.P., Wyss, U., and Piché, Y. (1998). Ink and vinegar, a simple staining technique for arbuscular-mycorrhizal fungi. *Appl. Environ. Microbiol.* 64, 5004-5007.
- Walker, S.A., Viprey, V., and Downie, J.A. (2000). Dissection of nodulation signaling using pea mutants defective for calcium spiking induced by nod factors and chitin oligomers. *Proc. Natl. Acad. Sci. USA* 97, 13413-13418.
- Walter, M.H., Flofl, D.S., Hans, J., Fester, T., and Strack, D. (2007). Apocarotenoid biosynthesis in arbuscular mycorrhizal roots: Contributions from methylerythritol phosphate pathway isogenes and tools for its manipulation. *Phytochemistry* 68, 130.
- Walther, T.C., Alves, A., Pickersgill, H., Loiodice, I., Hetzer, M., Galy, V., Hülsmann, B.B., Köcher, T., Wilm, M., Allen, T., Mattaj, I.W., and Doye, V. (2003). The conserved Nup107-160 complex is critical for nuclear pore complex assembly. *Cell* 113, 195-206.

- Wang, X., Sato, S., Tabata, S., and Kawasaki, S. (2008). A high-density linkage map of *Lotus japonicus* based on AFLP and SSR markers. *DNA Res.* 15, 323-332.
- Wasson, A.P., Pellerone, F.I., and Mathesius, U. (2006). Silencing the flavonoid pathway in *Medicago truncatula* inhibits root nodule formation and prevents auxin transport regulation by rhizobia. *Plant Cell* 18, 1617-1629.
- Wegel, E., Schauser, L., Sandal, N., Stougaard, J., and Parniske, M. (1998). Mycorrhiza mutants of *Lotus japonicus* define genetically independent steps during symbiotic infection. *Mol. Plant Microbe Interact.* 11, 933-936.
- Wojciechowski, M.F., Lavin, M., and Sanderson, M.J. (2004). A phylogeny of legumes (Leguminosae) based on analysis of the plastid *matK* gene resolves many well-supported subclades within the family. *Am. J. Bot.* 91, 1846-1862.
- Wu, Y., Yang, Y., Ye, S., and Jiang, Y. (2010). Structure of the gating ring from the human large-conductance Ca<sup>2+</sup>-gated K<sup>+</sup> channel. *Nature* 466, 393.
- Yano, K., Shibata, S., Chen, W.L., Sato, S., Kaneko, T., Jurkiewicz, A., Sandal, N., Banba, M., Imaizumi-Anraku, H., Kojima, T., Ohtomo, R., Szczyglowski, K., Stougaard, J., Tabata, S., Hayashi, M., Kouchi, H., and Umehara, Y. (2009). CERBERUS, a novel U-box protein containing WD-40 repeats, is required for formation of the infection thread and nodule development in the legume-Rhizobium symbiosis. *Plant J.* 60, 168-180.
- Yano, K., Tansengco, M.L., Hio, T., Higashi, K., Murooka, Y., Imaizumi-Anraku, H., Kawaguchi, M., and Hayashi, M. (2006). New nodulation mutants responsible for infection thread development in *Lotus japonicus*. *Mol. Plant Microbe Interact.* 19, 801-810.
- Yano, K., Yoshida, S., Muller, J., Singh, S., Banba, M., Vickers, K., Markmann, K., White, C., Schuller, B., Sato, S., Asamizu, E., Tabata, S., Murooka, Y., Perry, J., Wang, T.L., Kawaguchi, M., Imaizumi-Anraku, H., Hayashi, M., and Parniske, M. (2008). CYCLOPS, a mediator of symbiotic intracellular accommodation. *Proc. Natl. Acad. Sci. USA* 105, 20540-20545.
- Zhang, Q., Blaylock, L.A., and Harrison, M.J. (2010). Two *Medicago truncatula* half-ABC transporters are essential for arbuscule development in arbuscular mycorrhizal symbiosis. *Plant Cell* 22, 1483-1497.
- Zhang, Y., and Li, X. (2005). A putative nucleoporin 96 Is required for both basal defense and constitutive resistance responses mediated by suppressor of *npr1-1, constitutive 1*. *Plant Cell* 17, 1306-1316.



# SUPPLEMENT

## Supplemental Figures







F1 Plant	Parent	Seed Bag	Generation	Plant ID	Phenotype	BM1714, VI, 0.0	TM1613, VI, 1.3	TM0082, VI, 1.3	TM0722, VI, 4.1	TM1597, VI, 7.7	TM0302, VI, 14.0	TM0331, VI, 27.6	TM1035, VI, 46.6
J5149	J5149	55615	F2	K0154	WT	G	-	G	-	G	G	H	H
J5149	K0154	61993	F3	N/A	weak	-	G	G	G	-	G	-	-
J5149	K0154	61993	F3	N/A	weak	-	G	G	G	-	G	-	-
J5149	K0154	61993	F3	N/A	weak	-	G	G	G	-	G	-	-
J5149	K0154	61993	F3	N/A	weak	-	G	G	G	-	G	-	-
J5149	J5149	55615	F2	K0155	WT	G	-	G	-	G	G	G	H

**Supplemental Figure 2. Genotype Patterns of SL0181-N F<sub>2</sub> Individuals with Conflicting Genotypes.**

G/green: (Gifu Gifu), H/yellow: (Gifu MG-20), M/magenta: (MG-20 MG-20). Markers and their genetic positions (LG, cM) are indicated in the heading line.

(Next page:)

**Supplemental Figure 3. AM Phenotypes and Genotypes of SL0181-N Self-progeny from Selected F<sub>2</sub> Individuals.**

(A) G/green: (Gifu Gifu), H/yellow: (Gifu MG-20), M/magenta: (MG-20 MG-20). Markers and their genetic positions (LG, cM) are indicated in the heading line.

(B) Phenotypic segregation, corresponding to data in (A).





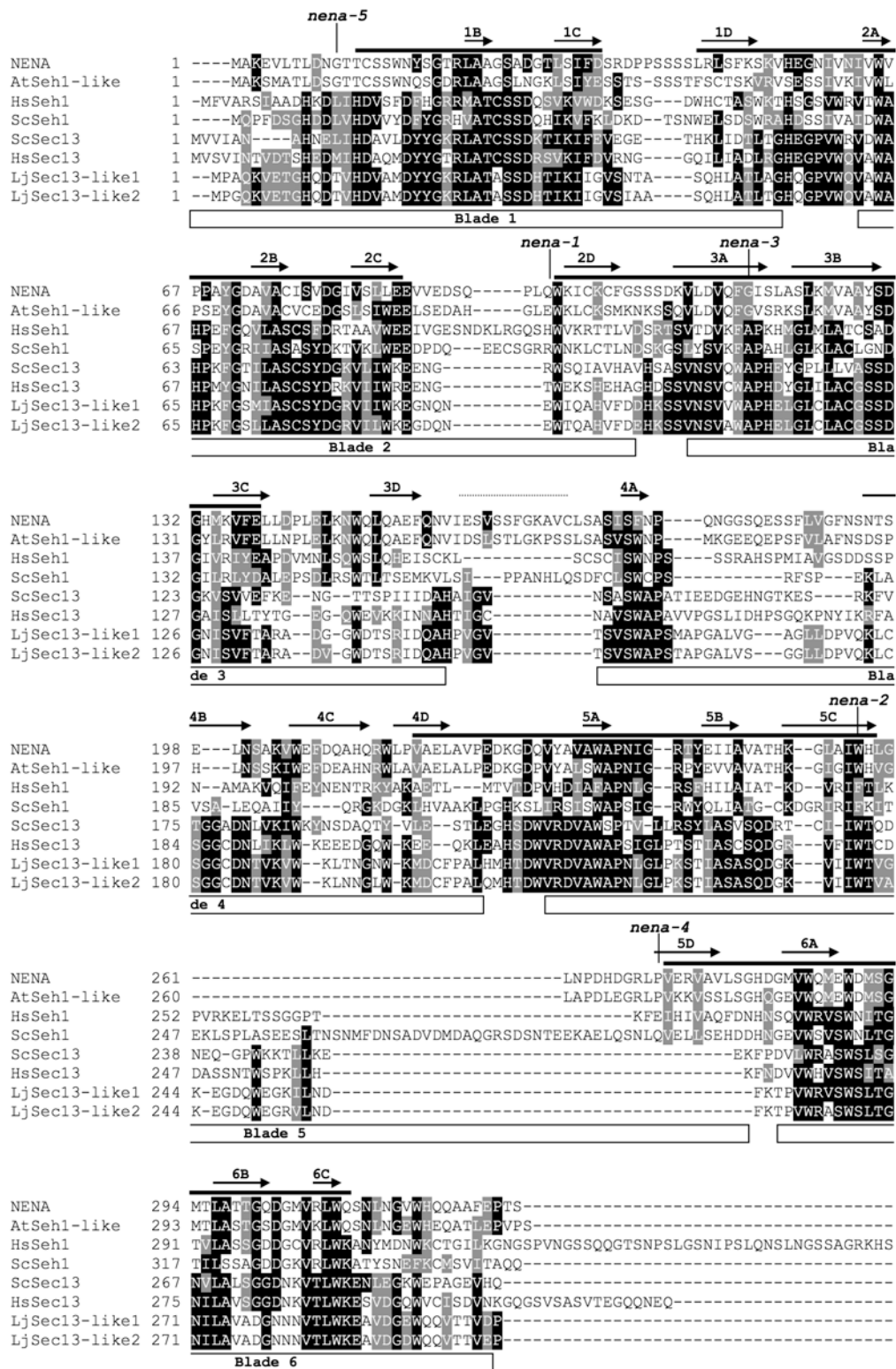
Sample	TM0545, I, 4.8	TM0078, I, 0.0	MS014433	TM0522, II, 61.4	TM0541, II, 51.0
21	M	M	-	M	M
23	H	H	-	H	G
1	-	G	G	G	G
10	G	G	G	G	G
12	G	G	G	H	M
13	G	G	G	G	G
25	G	-	G	-	-
28	G	G	G	G	G
40	G	G	G	M	M
2	H	H	H	H	G
4	H	H	H	H	M
5	M	-	H	-	-
8	H	H	H	H	H
11	H	H	H	H	H
14	H	H	H	H	H
15	H	H	H	H	H
20	H	H	H	H	M
26	H	H	H	H	H
27	H	H	H	H	H
29	H	-	H	M	M
31	G	H	H	H	H
32	H	-	H	G	H

Sample	TM0545, I, 4.8	TM0078, I, 0.0	MS014433	TM0522, II, 61.4	TM0541, II, 51.0
33	M	H	H	H	H
34	H	-	H	-	H
36	H	H	H	H	H
41	H	H	H	H	H
43	M	H	H	H	H
44	H	H	H	H	H
45	H	H	H	H	H
47	H	H	H	H	H
48	H	H	H	H	H
3	-	M	M	M	M
7	M	M	M	M	H
9	M	M	M	M	M
16	M	-	M	-	-
17	M	M	M	M	M
19	M	M	M	M	M
22	M	M	M	M	M
24	M	M	M	M	M
37	M	M	M	H	H
39	M	M	M	M	M
42	M	M	M	M	M
46	M	M	M	H	H

**Supplemental Figure 4. *PT4* Maps to the Translocation Region at the North Tip of LG I.** Genotype pattern of the SSR marker MS014433 linked to *PT4* matches to the pattern of TM0078 in a SL0181-N F<sub>2</sub> sub-population. G/green: (Gifu Gifu), H/yellow: (Gifu MG-20), M/magenta: (MG-20 MG-20). Markers and their genetic positions (LG, cM) are indicated in the heading line.





**Supplemental Figure 6. Alignment of Seh1 and Sec13 Related Protein Sequences from *L. japonicus*, *A. thaliana*, *H. sapiens* and *S. cerevisiae*.**

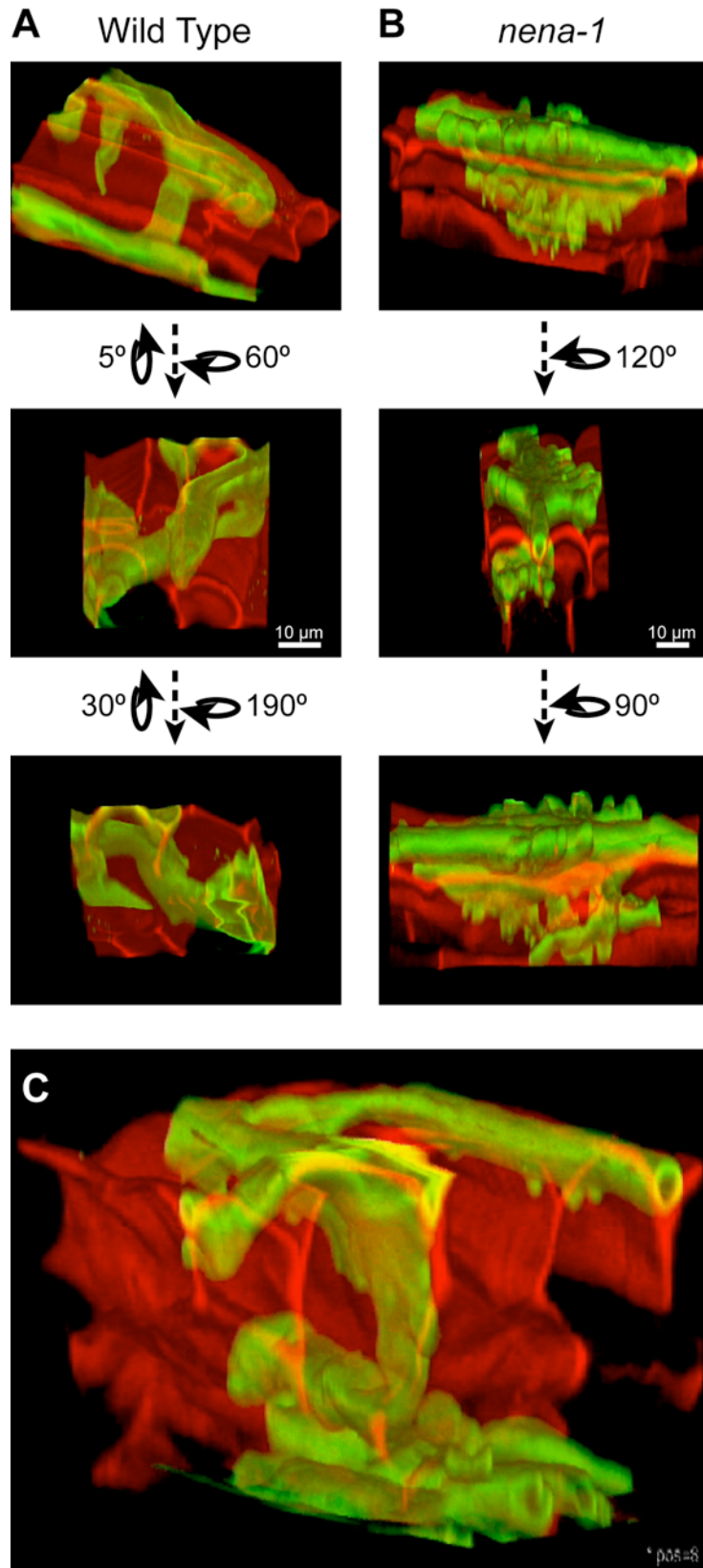
Residues that are identical or similar to the consensus sequence ( $\geq 50\%$  similarities) are inverted or highlighted in gray background, respectively. The secondary structure corresponding to the 3D model of NENA (Figure 5C) is indicated as arrows ( $\beta$  strands, labels refer to blade number and strand order) or dotted line (helix) above the alignment. WD40 repeats that were predicted from the NENA sequence are marked as black lines above the alignment. Boxes under the alignment represent  $\beta$ -propeller blades of yeast Seh1 (Brohawn et al., 2008). Mutated residues of respective alleles are indicated above the alignment. Protein accessions are given in Supplemental Figure 7.



NENA Lj 1 DNQTTCCSSNNK...  
 A5BBL2 Vv 1 DNQTTCCSSNNK...  
 A9PB3 Pt 1 DNQTTCCSSNNK...  
 TCS022 Pg 1 DNQTTCCSSNNK...  
 Q93V8 At 1 DNQTTCCSSNNK...  
 B6T803 Zm 1 DPOTACGWNHC...  
 B6T3J3 Zm 1 DPOTACGWNHC...  
 Q52BP5 Os 1 DGAACGWNHC...  
 A9TH66 Pp 1 DPQVTRNNSS...  
 A8581 Ha 1 DPQVTRNNSS...  
 P53011 Sc 1 DPQVTRNNSS...  
 Q04491 Sc 1 NEIHDVAYDYGK...  
 P55735 Ha 1 DPQVTRNNSS...  
 A98P57 Pp 1 QDVEDVAYDYGK...  
 A9TR25 Pp 1 QDVEDVAYDYGK...  
 A9GL25 Pp 1 QDVEDVAYDYGK...  
 A9T679 Pp 1 QDVEDVAYDYGK...  
 A98P57 Pp 1 QDVEDVAYDYGK...  
 A7QLK1 Vv 1 QDVEDVAYDYGK...  
 A5A800 Vv 1 QDVEDVAYDYGK...  
 A58415 Vv 1 QDVEDVAYDYGK...  
 A98P57 Pp 1 QDVEDVAYDYGK...  
 LjSEC13-like1 1 QDVEDVAYDYGK...  
 LjSEC13-like2 1 QDVEDVAYDYGK...  
 Q64740 At 1 QDVEDVAYDYGK...  
 Q98R11 At 1 QDVEDVAYDYGK...  
 A9P012 Pa 1 QDVEDVAYDYGK...  
 A9N012 Pa 1 QDVEDVAYDYGK...  
 B6T93 Zm 1 QDVEDVAYDYGK...  
 B6TM3 Zm 1 QDVEDVAYDYGK...  
 Q65079 Os 1 QDVEDVAYDYGK...  
 Q81142 Os 1 QDVEDVAYDYGK...  
 Q62LM6 Os 1 QDVEDVAYDYGK...  
 B4PQ12 Zm 1 QDVEDVAYDYGK...  
 B6A1K3 Zm 1 QDVEDVAYDYGK...

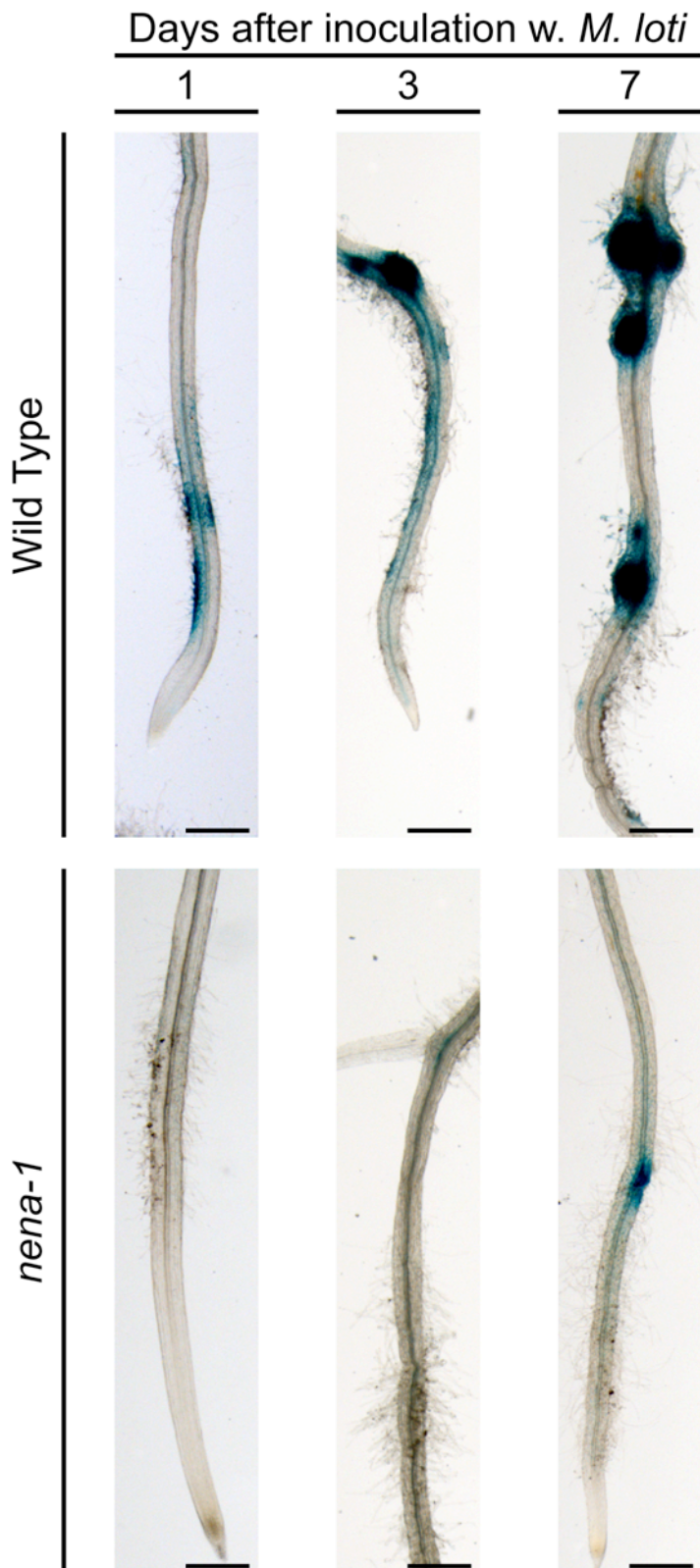
NENA Lj 131 NPD...  
 A5BBL2 Vv 131 NPD...  
 A9PB3 Pt 131 NPD...  
 TCS022 Pg 131 NPD...  
 Q93V8 At 131 NPD...  
 B6T803 Zm 131 NPD...  
 B6T3J3 Zm 131 NPD...  
 Q52BP5 Os 131 NPD...  
 A9TH66 Pp 131 NPD...  
 A8581 Ha 131 NPD...  
 P53011 Sc 131 NPD...  
 Q04491 Sc 131 NPD...  
 P55735 Ha 131 NPD...  
 A98P57 Pp 131 NPD...  
 A9TR25 Pp 131 NPD...  
 A9GL25 Pp 131 NPD...  
 A9T679 Pp 131 NPD...  
 A98P57 Pp 131 NPD...  
 A7QLK1 Vv 131 NPD...  
 A5A800 Vv 131 NPD...  
 A58415 Vv 131 NPD...  
 A98P57 Pp 131 NPD...  
 LjSEC13-like1 131 NPD...  
 LjSEC13-like2 131 NPD...  
 Q64740 At 131 NPD...  
 Q98R11 At 131 NPD...  
 A9P012 Pa 131 NPD...  
 A9N012 Pa 131 NPD...  
 B6T93 Zm 131 NPD...  
 B6TM3 Zm 131 NPD...  
 Q65079 Os 131 NPD...  
 Q81142 Os 131 NPD...  
 Q62LM6 Os 131 NPD...  
 B4PQ12 Zm 131 NPD...  
 B6A1K3 Zm 131 NPD...

**Supplemental Figure 7. Multi-Species Alignment of Seh1 and Sec13 Related Proteins.**  
 Residues that are identical or similar to the consensus sequence ( $\geq 30\%$  similarities) are inverted or highlighted in gray background, respectively. Blocks containing gaps or poorly conserved sequences have been masked. The presented alignment was used to generate the phylogenetic tree in Figure 4. GenBank/UniProt accessions and species acronyms are indicated left to the sequences.



**(A) to (C)** Fungal (green) and plant cell wall (red) structures were stained with WGA-Alexa Fluor 488 and propidium iodide, respectively. Structures were imaged by CLSM and are illustrated from different relative angles, as indicated. In WT (A), a tubular hypha branches perpendicular from a surface 'runner' hypha and trans-versally penetrates a rhizo-dermal cell before diverging inside the root. In *nena-1* (B), a 'runner' hypha penetrates the root surface between rhizo-dermal cells and forms excessive swellings; infection is aborted at the subepidermal layer. (C) Successful penetration of the rhizodermis in *nena-1* is accompanied by hyphal deformations.

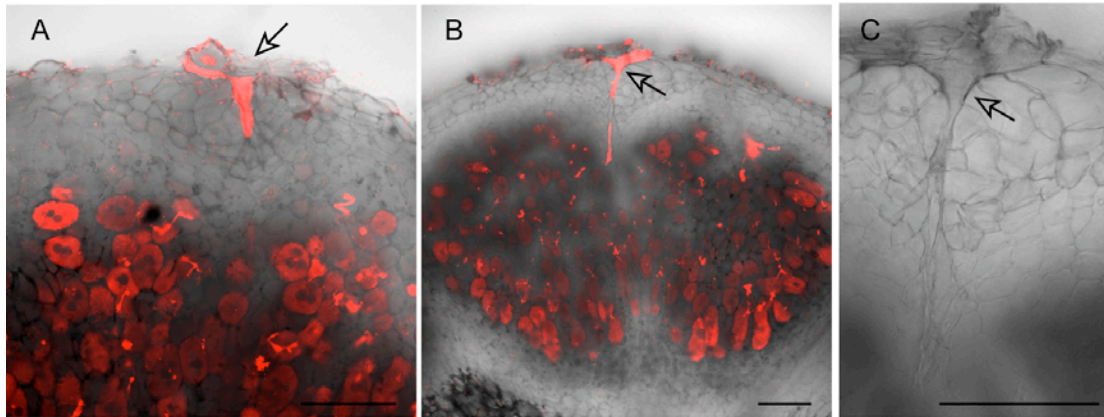
**Supplemental Figure 1. 3D Projection of Typical AM Infection Sites in Wild Type and *nena-1*.**



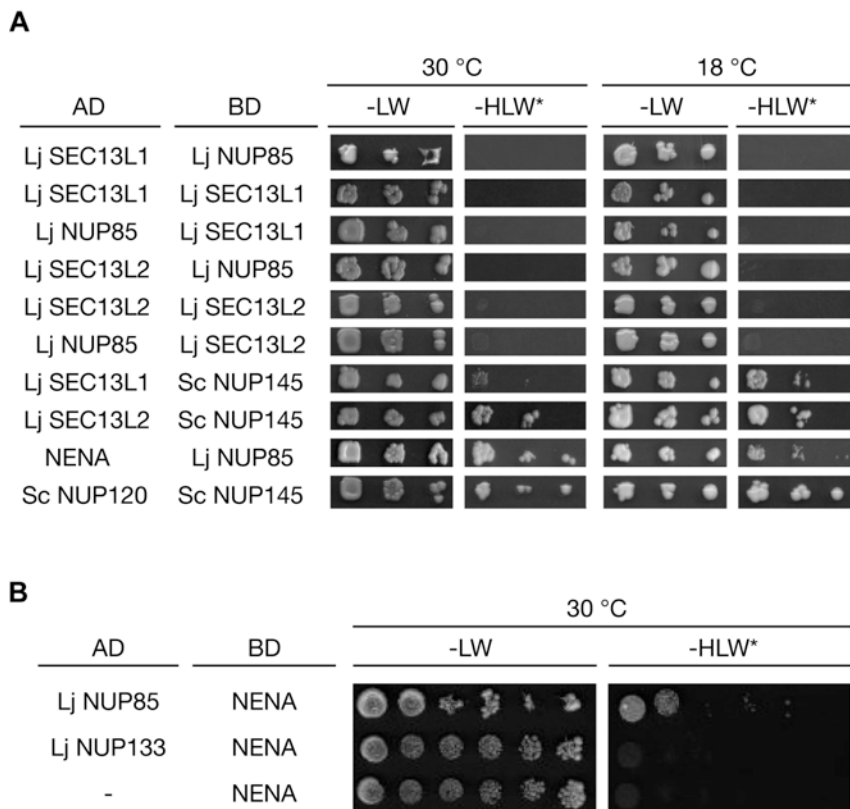
**Supplemental Figure 2. The *NIN* Promoter Is Not Induced During Early Rhizodermal Response to *M. loti* but Active During Nodule Formation in *nena-1*.**

Brightfield images of X-Gluc incubated roots transformed with GUS-reporter fused to the promoter of *NIN*. No blue rhizodermal staining was observed in *nena-1* roots at 1 and 3 DAI. Images represent observations given in Table 8. Scale bars: 0.5 mm.



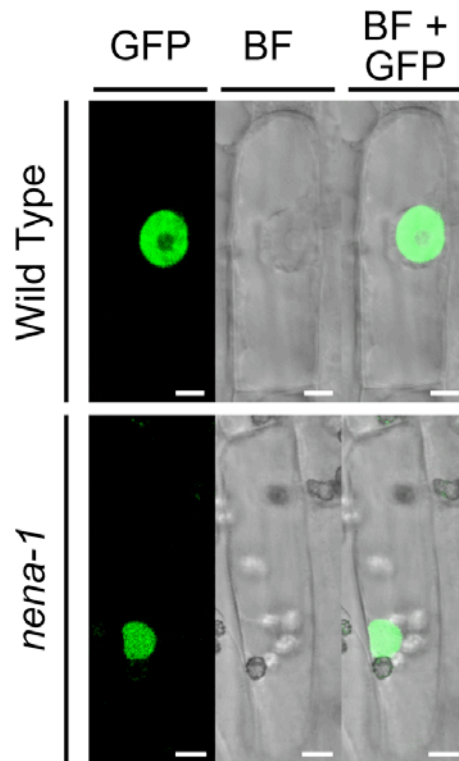


**Supplemental Figure 10. Intercellular Infection of Outer Nodule Cell Layers in *nena-1*.**  
**(A) to (C)** Confocal z-projections of 80-µm longitudinal tissue sections showing intercellular infection (arrows) and cortical cell colonization by DsRed expressing *M. loti* (red). (C) Shows the infection site in (B) at higher magnification in brightfield (BF) channel only. (A) and (B) are overlays of RFP and BF channels. Images represent samples from 21 DAI/waterlogged+5 µM AVG treatments. Scale bars: 100 µm.



**Supplemental Figure 11. In Contrast to NENA, SEC13-like 1 and SEC13-like 2 Do Not Interact with NUP85 in the Gal4-Based Yeast Two-Hybrid Assay.**

**(A) and (B)** Prey (AD) and bait (BD) constructs were co-transformed and yeast was grown in 3 (A) or 5 (B) dilutions on synthetic dropout medium lacking leucine and tryptophan (-LW) or histidine, leucine and tryptophan (-HLW) supplemented with 15 mM 3-amino-1,2,4-triazole (\*). (A) In order to test for temperature dependent interaction, the assay has been carried out at 30 °C and 18 °C. (B) NENA and NUP85 interact in both prey and bait combinations (see Figure 5A). (-) Bait vector containing the Gateway reading frame cassette including *ccdB* and *CmR*.



**Supplemental Figure 12. GFP-Cyclops Localizes to the Nucleus in *nena-1*.**

Confocal micrographs of *A. rhizogenes* transformed root cells in GFP, BF and overlaid channels. No difference in localization of the GFP signal was detected between transgenic roots in WT and *nena-1* backgrounds. Scale bars: 5  $\mu$ m.

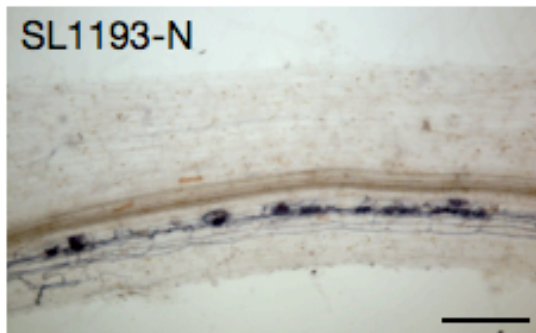
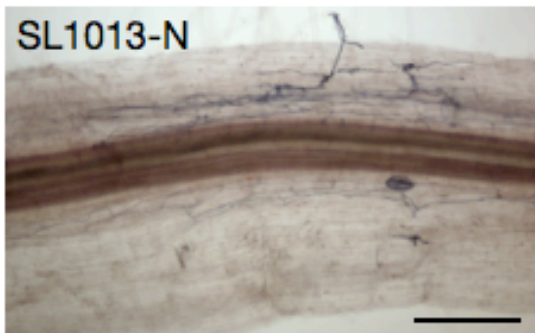
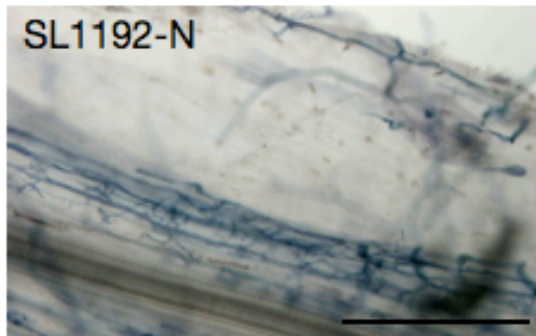
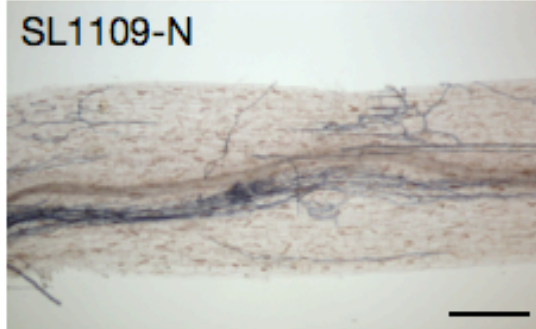
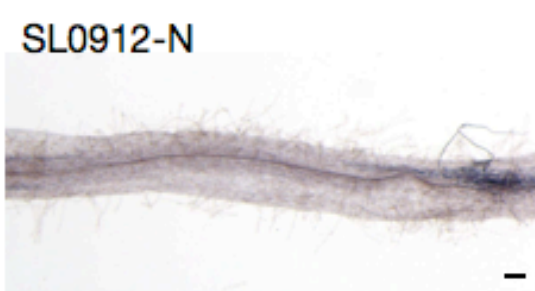
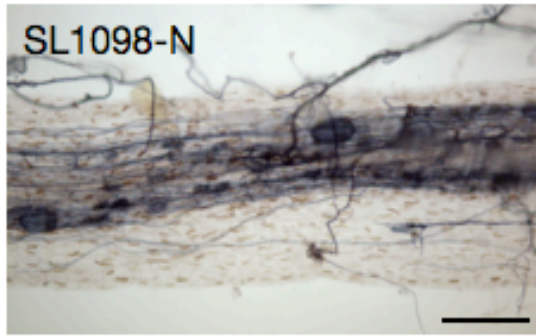
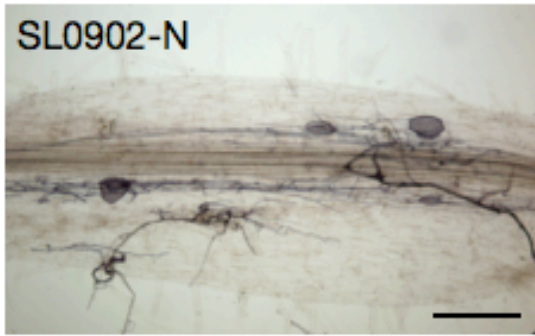
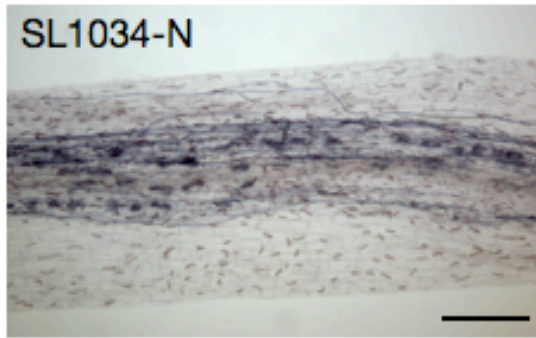
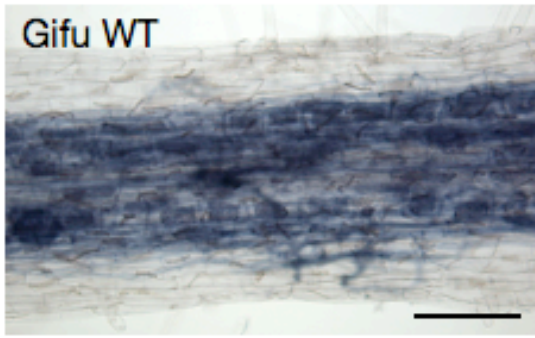
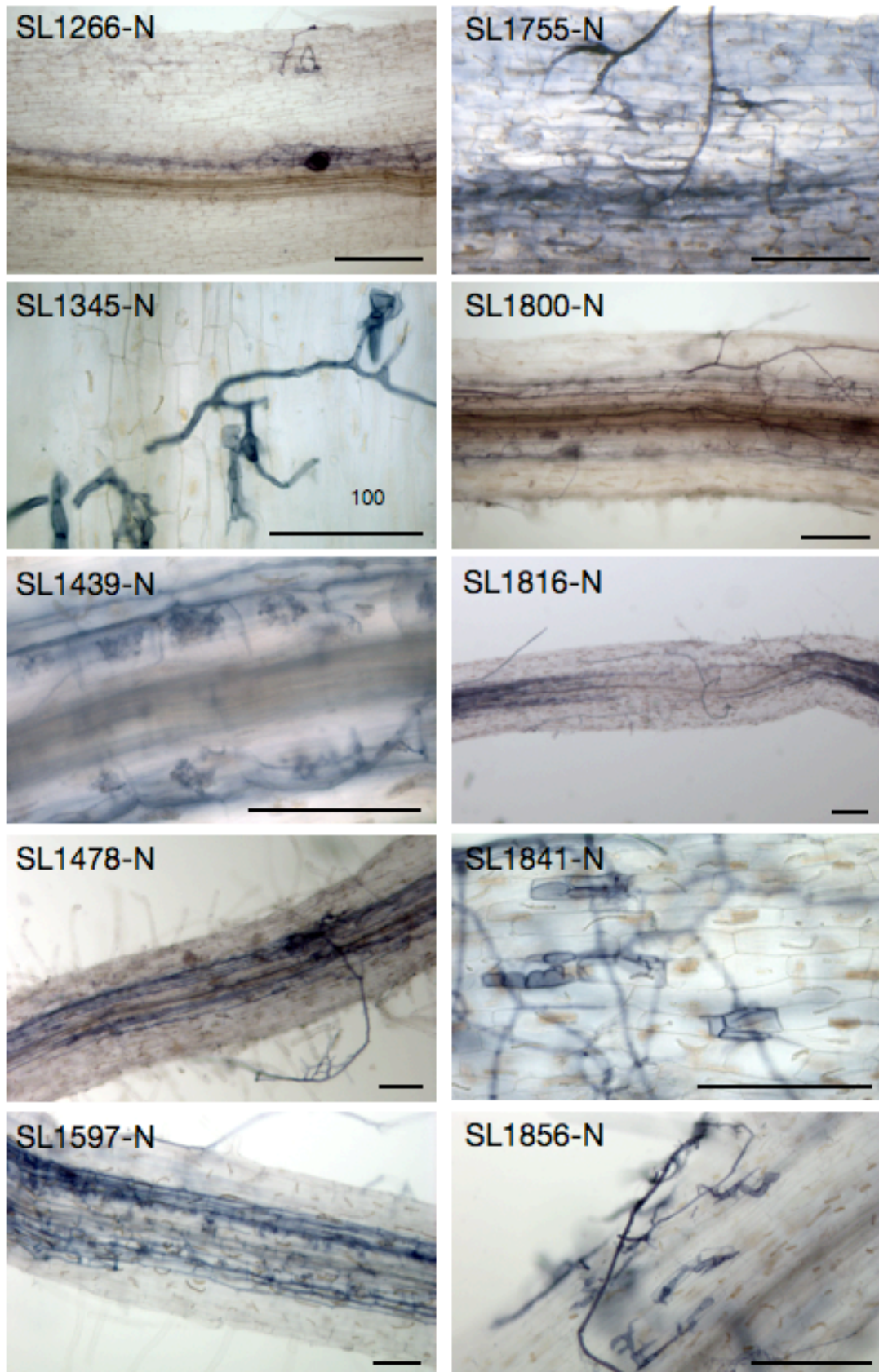


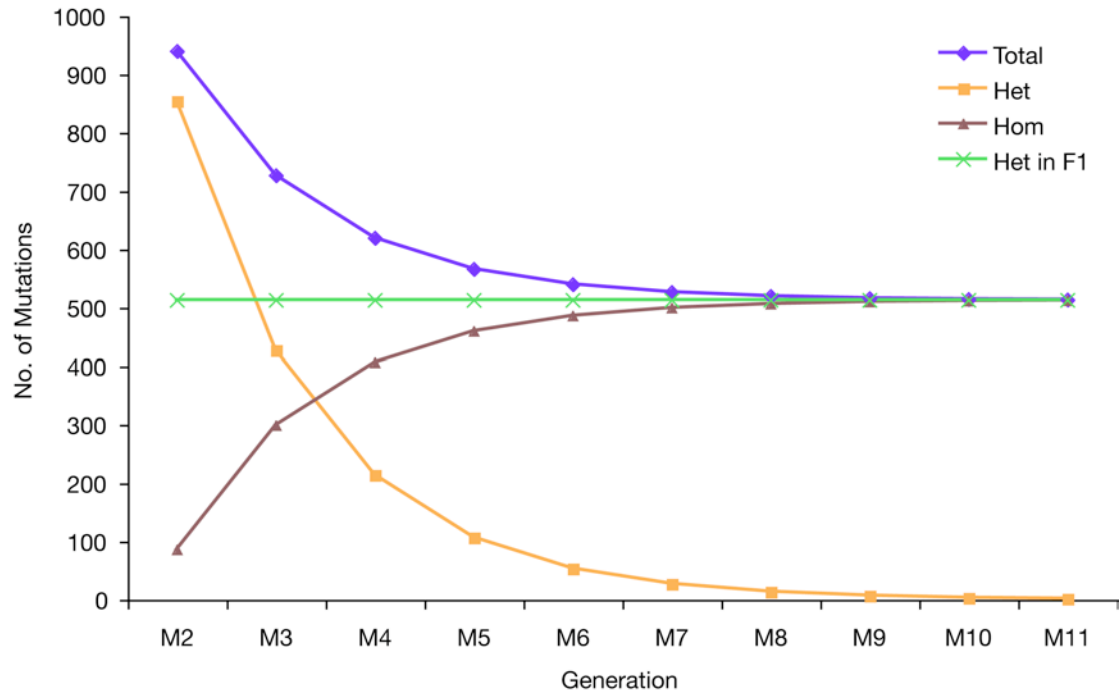
(Figure continues on next page.)



(Figure continuation)



**Supplemental Figure 13. Stereomicroscopy Images of Putative and/or Confirmed Mutants.** Ink-stained AM Fungal Structures. Line numbers are indicated. Scale bars: 400  $\mu$ m.



**Supplemental Figure 14. Theoretical Inheritance of Mutation Load in the General TILLING Population of *Lotus*.**

A 1/10 distribution of homozygous (Hom) vs. heterozygous (Het) loci among the 940 EMS-induced mutation per  $M_2$  plant on average have been calculated (Perry et al., 2009). Based on this, the mutational load and distribution in subsequent selfing or  $F_1$  generations was calculated according to Mendelian segregation, as follows:  $Hom(M_{x+1}) = Hom(M_x) + Het(M_x)/4$ ,  $Het(M_{x+1}) = Het(M_x)/2$ ,  $Total(M_{x+1}) = Hom(M_{x+1}) + Het(M_{x+1})$ ,  $Het(F_1) = Hom(M_P) + Het(M_P)/2$ .



## Supplemental Tables

**Supplemental Table 1.** Results of the AM Screen Performed by the Author.

BULK Line - Seed Bag	Phenotype <sup>1</sup>	M3 Phenotype Strength <sup>2</sup>	M3 Rescreen <sup>2</sup>	M4 Phenotype Strength <sup>2</sup>	Nodulation <sup>3</sup>	Mapping Status <sup>4</sup>	Crosses <sup>5</sup>	Screen Status <sup>6</sup>	M3+M3re+M4 Strength	M3&M3re&M4& Screen Status	Comments
SL1816- 34965	01	4	4	4	1	5	2	2	12	4442	<i>patchy/pollux-7</i>
SL1841- 34988	01	4	4	4	1	5	2	2	12	4442	<i>nen-1</i>
SL1345- 34643	02	3	4	4	1	5	2	2	11	3442	<i>cyclops-6</i>
SL0902- 34343	12	4	4	2	1	0	0	2	10	4422	inconsistent phenotype
SL1266R - 61063	12	4	3	3	0	2	2	2	10	4332	dwarf, nod-?
SL1439- 34708	2	4	3	3	1	3	2	2	10	4332	unclear phenotype in F2
SL1478- 61064	2	4	3	3	1	0	0	2	10	4332	dwarf
SL1098- 34508	012	2	4	3	1	0	0	2	9	2432	inconsistent phenotype
SL0912R -35632	02	3	2	3	0	3	2	2	8	3232	unclear phenotype in F2
SL1013- 34436	1	4	0	4	1	3	2	2	8	4042	rough mapping inconclusive
SL1856- 34999	01	4	4	0	0	5	2	2	8	4402	<i>nup133-7</i>
SL0989- 34413	3	4	0	3	1	3	2	2	7	4032	dwarf, s/w nod, rough mapping inconclusive
SL1034- 34453	12	4	0	3	1	0	0	2	7	4032	segregating M4
SL1109- 34518	12	4	3	0	1	0	0	1	7	4301	blue cloudy material in roots (hyphal degradation?)
SL1193- 34586	12	4	3	0	1	0	0	0	7	4300	tiny nodules line in NODPOP, dominant?
SL1281- 34612	012	3	4	0	1	2	2	1	7	3401	root phenotype
SL1597- 34805	2	4	3	0	1	0	0	1	7	4301	
SL1800- 34949	12	4	3	0	1	0	0	1	7	4301	
SL1864- 35005	2	3	4	0	1	3	2	1	7	3401	rough mapping inconclusive

<sup>1</sup> 0=aborted infection, 1=weak colonization, 2=impaired arbuscule formation, 3=hyper-colonization

<sup>2</sup> 0=n/a, 1=WT, 2=weak, 3=medium, 4=strong

<sup>3</sup> 0=Nod-, 1=Nod+, 10= small white, 2=n/d

<sup>4</sup> 0=not crossed, 2=F2 seed, 3=rough mapping, 5=mapped

<sup>5</sup> 0=not crossed, 1=backcross, 2=MG20

<sup>6</sup> 0=repeat M3, 1=M3 done/ M4 pending, 2=ready

SL0929-34363	12	3	0	3	1	0	0	1	6	3031	weak phenotype
SL1100-34510	12	3	3	0	1	0	0	1	6	3301	small roots
SL1123-34530	0	4	2	0	1	0	0	1	6	4201	
SL1192-34585	01	3	3	0	0	0	0	1	6	3301	nod- in NODPOP?
SL1282-34613	12	4	2	0	1	0	0	1	6	4201	s/w nodules line
SL1284-34615	2	4	2	0	1	0	0	1	6	4201	
SL1337-34638	12	2	4	0	1	0	0	0	6	2400	M3 dead
SL1354-34648	2	3	3	0	1	0	0	1	6	3301	
SL1546-34776	2	4	2	0	1	0	0	1	6	4201	
SL1570-34786	2	4	2	0	1	0	0	1	6	4201	
SL1598-34806	2	4	2	0	10	0	0	1	6	4201	
SL1827-34976	12	4	2	0	2	0	0	0	6	4200	M3 dead
SL1844-34991	12	4	2	0	0	0	0	1	6	4201	
SL1862-35003	12	3	3	0	0	0	0	1	6	3301	
SL0898-34339	12	3	0	2	1	0	0	2	5	3022	root phenotype, segregating M4
SL0900-34341	1	3	2	0	1	0	0	1	5	3201	
SL0907R-35629	12	3	2	0	1	0	0	1	5	3201	
SL0925R-35635	12	3	2	0	1	0	0	1	5	3201	
SL0981-34408	1	3	2	0	1	0	0	0	5	3200	
SL1150-34551	2	2	3	0	1	0	0	1	5	2301	
SL1314-34628	2	2	3	0	1	0	0	1	5	2301	
SL1359-34651	1	2	3	0	1	0	0	1	5	2301	<i>patchy-like</i>
SL1549-34777	2	4	1	0	1	0	0	1	5	4101	
SL1569-34785	2	4	1	0	10	0	0	1	5	4101	
SL1583-34798	2	4	1	0	0	0	0	1	5	4101	
SL1804-34953	12	2	1	2	2	0	0	2	5	2122	
SL1813-34962	12	2	0	3	1	0	0	2	5	2032	dwarf, infertile
SL1848-34995	12	4	1	0	0	0	0	0	5	4100	
SL1863-35004	12	2	3	0	1	0	0	1	5	2301	
SL1880-35019	012	4	1	0	0	0	0	0	5	4100	1st: screen all mutants died! 2nd screen: 8 WT
SL0922-34356	2	2	2	0	1	0	0	1	4	2201	
SL0927-34361	1	2	0	2	1	0	0	2	4	2022	dwarfs, infertile

SL0931-34365	1	2	0	2	10	0	0	2	4	2022	weak phenotype
SL0932-34366	12	2	0	2	0	0	0	0	4	2020	weak phenotype
SL0933-34367	12	2	0	2	1	0	0	2	4	2022	weak phenotype
SL0942-34375	12	2	0	2	1	0	0	2	4	2022	weak phenotype
SL0951R-35636	12	2	0	2	1	0	0	2	4	2022	weak phenotype
SL0962-34392	1	2	0	2	1	0	0	0	4	2020	segregating M4
SL0964-34394	12	2	0	2	1	0	0	2	4	2022	weak phenotype
SL1014-34437	2	2	0	2	2	0	0	2	4	2022	root phenotype
SL1064-34481	12	2	2	0	1	0	0	1	4	2201	
SL1076-35609	0	4	0	0	1	0	0	0	4	4000	Nod- in NODPOP
SL1092-34502	2	2	2	0	1	0	0	1	4	2201	
SL1134-35616	12	2	2	0	1	0	0	1	4	2201	
SL1136-34541	12	2	2	0	1	0	0	1	4	2201	
SL1145-34547	12	2	2	0	1	0	0	1	4	2201	<i>patchy-like</i>
SL1151-34552	12	4	0	0	0	0	0	0	4	4000	all M3 mutants dead
SL1157-34558	12	2	2	0	1	0	0	1	4	2201	
SL1159-34560	2	2	2	0	1	0	0	1	4	2201	
SL1164-34564	12	2	2	0	1	0	0	1	4	2201	
SL1169-34569	2	2	2	0	1	0	0	0	4	2200	
SL1202-34593	2	2	2	0	1	0	0	0	4	2200	
SL1312-34626	2	2	2	0	1	0	0	1	4	2201	
SL1329-34633	12	2	2	0	1	0	0	1	4	2201	
SL1565-34781	2	4	0	0	1	0	0	1	4	4001	dwarf
SL1802-34951	2	2	2	0	1	0	0	1	4	2201	infertile
SL1810-34959	12	2	2	0	1	0	0	1	4	2201	
SL1888-35026	2	3	1	0	1	0	0	2	4	3102	
SL0934-34368	12	2	0	1	1	0	0	2	3	2012	
SL0936-34370	2	2	0	1	1	0	0	2	3	2012	
SL0938-34372	2	2	1	0	1	0	0	2	3	2102	
SL0943-34376	2	2	1	0	1	0	0	2	3	2102	
SL0961-34391	12	2	0	1	2	0	0	2	3	2012	
SL0978-34405	12	2	0	1	1	0	0	2	3	2012	

SL1017-34440	12	3	0	0	1	0	0	0	3	3000	
SL1029-11028	12	2	0	1	1	0	0	2	3	2012	
SL1072-34486	2	2	0	1	1	0	0	2	3	2012	
SL1084-34497	2	2	0	1	2	0	0	2	3	2012	SYMRK TILLING line
SL1118-34526	1	2	1	0	2	0	0	2	3	2102	
SL1124-34531	1	3	0	0	1	0	0	1	3	3001	few nodules line in NODPOP
SL1130-34536	2	3	0	0	1	0	0	1	3	3001	<i>sus1</i> , many nodules
SL1130-35615	2	3	0	0	2	0	0	1	3	3001	
SL1130-35615	2	3	0	0	1	0	0	1	3	3001	<i>sus1</i>
SL1148-34549	2	2	1	0	2	0	0	2	3	2102	
SL1162-34562	2	2	1	0	1	0	0	2	3	2102	
SL1167-34567	12	2	1	0	2	0	0	2	3	2102	
SL1178-34576	2	2	1	0	2	0	0	2	3	2102	
SL1196-34588	2	3	0	0	1	0	0	1	3	3001	
SL1203-34594	2	2	1	0	2	0	0	2	3	2102	
SL1225-34599	12	3	0	0	1	0	0	1	3	3001	
SL1227-34600	2	3	0	0	1	0	0	1	3	3001	nod- in NODPOP
SL1232-34602	12	2	1	0	2	0	0	2	3	2102	
SL1263-34611	2	2	1	0	2	0	0	2	3	2102	
SL1283-34614	12	3	0	0	1	0	0	1	3	3001	
SL1286-34616	2	3	0	0	1	0	0	1	3	3001	
SL1287-34617	2	3	0	0	1	0	0	1	3	3001	
SL1290R - 11289	1	3	0	0	1	0	0	0	3	3000	all dead
SL1291-34619	12	3	0	0	1	0	0	0	3	3000	
SL1298R - 11297	12	3	0	0	2	0	0	0	3	3000	
SL1300-34620	12	3	0	0	1	0	0	0	3	3000	dwarf
SL1336-34637	12	2	1	0	1	0	0	2	3	2102	
SL1342-34641	0	3	0	0	1	0	0	1	3	3001	nod- in NODPOP?
SL1344-34642	12	3	0	0	0	0	0	1	3	3001	nod- in NODPOP?
SL1349-?	1	3	0	0	1	0	0	0	3	3000	
SL1368-34658	02	3	0	0	0	0	0	0	3	3000	
SL1382-34670	2	3	0	0	1	0	0	1	3	3001	

SL1441-34709	012	3	0	0	1	0	0	0	3	3000	
SL1450-34712	12	3	0	0	2	0	0	0	3	3000	small white nodules in NODPOP
SL1469-34725	12	3	0	0	1	0	0	1	3	3001	small nodules
SL1471-34726	12	3	0	0	1	0	0	1	3	3001	
SL1501-34750	2	3	0	0	1	0	0	1	3	3001	
SL1515-34758	1	3	0	0	1	0	0	1	3	3001	<i>patchy-like</i>
SL1539R-?	2	3	0	0	10	0	0	1	3	3001	
SL1540-34773	2	3	0	0	1	0	0	1	3	3001	
SL1548-35666	2	3	0	0	1	0	0	0	3	3000	small root, M3 dead
SL1588-34799	2	3	0	0	2	0	0	1	3	3001	
SL1803-34952	12	2	1	0	2	0	0	2	3	2102	
SL1822-34971	12	2	1	0	2	0	0	2	3	2102	
SL1823-34972	12	2	1	0	2	0	0	2	3	2102	
SL1824-34973	12	2	1	0	2	0	0	2	3	2102	
SL1826-34975	01	2	1	0	2	0	0	1	3	2101	
SL1828-34977	01	2	1	0	2	0	0	1	3	2101	
SL1832-34981	12	3	0	0	0	2	2	1	3	3001	nod- in NODPOP, unclear AM segregation in F2
SL1842-34989	1	2	1	0	1	0	0	2	3	2102	
SL1846-34993	12	2	1	0	2	0	0	2	3	2102	
SL1847-34994	12	2	1	0	2	0	0	2	3	2102	
SL1851-34997	1	2	1	0	2	0	0	2	3	2102	
SL1866-35007	12	2	1	0	2	0	0	2	3	2102	
SL1883-35022	12	2	1	0	2	0	0	2	3	2102	
SL1886-35024	12	2	1	0	1	0	0	2	3	2102	
SL1887-35025	01	2	1	0	2	0	0	0	3	2100	
SL0924-34358	12	2	0	0	1	0	0	0	2	2000	dwarf, discarded
SL0935-34369	12	2	0	0	1	0	0	0	2	2000	small plant and root
SL0940-34373	12	2	0	0	1	0	0	1	2	2001	
SL0945-34378	2	2	0	0	1	0	0	1	2	2001	small root
SL0946-34379	0	2	0	0	1	0	0	1	2	2001	very short lateral roots
SL0947-34380	1	2	0	0	2	0	0	0	2	2000	
SL0973-34403	01	2	0	0	1	0	0	1	2	2001	

SL0982-34409	2	2	0	0	1	0	0	1	2	2001	
SL0994-34417	2	2	0	0	1	0	0	0	2	2000	
SL0995-34418	2	2	0	0	1	0	0	0	2	2000	
SL0996-34419	0	2	0	0	1	0	0	0	2	2000	
SL1009-34432	12	2	0	0	1	0	0	1	2	2001	
SL1024-34445	12	2	0	0	1	0	0	1	2	2001	
SL1038-34457	1	2	0	0	1	0	0	1	2	2001	
SL1040-?	12	2	0	0	1	0	0	0	2	2000	
SL1041-34459	1	2	0	0	2	0	0	0	2	2000	
SL1042-34460	12	2	0	0	1	0	0	1	2	2001	
SL1052-34469	12	2	0	0	1	0	0	0	2	2000	
SL1055-34472	12	2	0	0	2	0	0	0	2	2000	dwarf, no flowers after 10 months, discarded
SL1077-34490	0	2	0	0	1	0	0	1	2	2001	
SL1078-34491	12	2	0	0	1	0	0	0	2	2000	
SL1093-34503	2	2	0	0	2	0	0	0	2	2000	
SL1094-34504	2	2	0	0	2	0	0	0	2	2000	J7749 dwarf infertile, discarded
SL1095-34505	12	2	0	0	2	0	0	1	2	2001	
SL1097-34507	2	2	0	0	1	0	0	1	2	2001	
SL1113-34522	12	2	0	0	2	0	0	0	2	2000	
SL1115-34524	1	2	0	0	2	0	0	1	2	2001	
SL1117-34525	12	2	0	0	2	0	0	0	2	2000	
SL1125-34532	1	2	0	0	1	0	0	0	2	2000	
SL1129-34535	0	2	0	0	1	0	0	0	2	2000	
SL1132-34537	12	2	0	0	1	0	0	1	2	2001	
SL1134-34539	3	2	0	0	1	0	0	1	2	2001	
SL1134-35616	2	2	0	0	2	0	0	1	2	2001	
SL1152-34553	2	2	0	0	1	0	0	1	2	2001	
SL1155-34556	12	2	0	0	2	0	0	1	2	2001	
SL1168-34568	12	2	0	0	1	0	0	0	2	2000	
SL1176-34574	12	2	0	0	2	0	0	0	2	2000	dwarf
SL1177-34575	1	2	0	0	2	0	0	1	2	2001	<i>sus1</i>
SL1180-34578	12	2	0	0	2	0	0	1	2	2001	dwarf

SL1181-34579	2	2	0	0	2	0	0	1	2	2001	infertile
SL1189-34583	12	2	0	0	2	0	0	1	2	2001	
SL1199-34591	2	2	0	0	1	0	0	0	2	2000	
SL1200-34592	2	2	0	0	1	0	0	0	2	2000	
SL1224-34598	2	2	0	0	1	0	0	0	2	2000	
SL1233-34603	12	2	0	0	2	0	0	1	2	2001	small root
SL1240-34606	12	2	0	0	2	0	0	1	2	2001	
SL1248-34607	12	2	0	0	2	0	0	1	2	2001	
SL1271R - 11270	2	2	0	0	2	0	0	0	2	2000	
SL1275R - 11274	0	2	0	0	2	0	0	0	2	2000	
SL1305-34623	12	2	0	0	1	0	0	1	2	2001	
SL1331-34634	12	2	0	0	1	0	0	1	2	2001	
SL1347-34645	12	2	0	0	2	0	0	0	2	2000	small white nodules in NODPOP
SL1363-34653	0	2	0	0	2	0	0	1	2	2001	
SL1365-34655	1	2	0	0	1	0	0	0	2	2000	small root
SL1366-34656	1	2	0	0	1	0	0	0	2	2000	small root
SL1378-34667	12	2	0	0	1	0	0	1	2	2001	
SL1384-34672	2	2	0	0	1	0	0	1	2	2001	
SL1389-34675	2	2	0	0	2	0	0	1	2	2001	few nodules line in NODPOP
SL1391-34677	2	2	0	0	1	0	0	0	2	2000	
SL1393-?	12	2	0	0	1	0	0	1	2	2001	small root
SL1402-34685	1	2	0	0	1	0	0	0	2	2000	
SL1403-34686	12	2	0	0	2	0	0	0	2	2000	small
SL1411-34692	2	2	0	0	1	0	0	1	2	2001	small root
SL1416-34697	2	2	0	0	1	0	0	1	2	2001	
SL1422-34702	12	2	0	0	1	0	0	1	2	2001	
SL1428R - 11427	12	2	0	0	1	0	0	1	2	2001	small root
SL1434R - 11433	12	2	0	0	1	0	0	1	2	2001	small root
SL1437-34707	12	2	0	0	2	0	0	0	2	2000	
SL1442-35656	12	2	0	0	1	0	0	1	2	2001	
SL1443-34710	01	2	0	0	1	0	0	1	2	2001	
SL1454-34714	2	2	0	0	1	0	0	1	2	2001	

SL1457-34717	12	2	0	0	2	0	0	1	2	2001	dwarf
SL1459-34718	12	2	0	0	1	0	0	1	2	2001	
SL1474-34728	12	2	0	0	0	0	0	0	2	2000	
SL1477-34731	12	2	0	0	2	0	0	0	2	2000	nod- in NODPOP
SL1480-34733	12	2	0	0	1	0	0	0	2	2000	
SL1485-34738	12	2	0	0	1	0	0	0	2	2000	small root
SL1486-34739	2	2	0	0	1	0	0	1	2	2001	
SL1490-34743	2	2	0	0	1	0	0	1	2	2001	small plant
SL1496-34747	1	2	0	0	2	0	0	0	2	2000	<i>sus1</i>
SL1499-34749	2	2	0	0	1	0	0	1	2	2001	
SL1521-34762	12	2	0	0	1	0	0	1	2	2001	dwarf
SL1522-34763	01	2	0	0	1	0	0	0	2	2000	dead M3
SL1531-35663	12	2	0	0	1	0	0	0	2	2000	dead M3
SL1541-34774	12	2	0	0	1	0	0	1	2	2001	small root
SL1543-?	2	2	0	0	2	0	0	1	2	2001	
SL1554-35668	2	2	0	0	2	0	0	0	2	2000	<i>sus2</i>
SL1573-34788	12	2	0	0	2	0	0	1	2	2001	small root
SL1574-34789	2	2	0	0	0	0	0	1	2	2001	
SL1581-34796	2	2	0	0	2	0	0	1	2	2001	root phenotype
SL1595-35672	12	2	0	0	2	0	0	1	2	2001	
SL1812-34961	1	2	0	0	2	0	0	0	2	2000	
SL1814-34963	12	2	0	0	2	0	0	0	2	2000	
SL1817-34966	1	2	0	0	2	0	0	0	2	2000	dead M3
SL1829-34978	2	2	0	0	0	0	0	1	2	2001	
SL0897-34338	0	1	0	0	2	0	0	2		1002	
SL0899-34340	0	0	0	0	2	0	0	0		0000	
SL0901-34342	0	1	0	0	2	0	0	2		1002	
SL0904R-35628	0	1	0	0	2	0	0	2		1002	
SL0906-34344	0	1	0	0	2	0	0	2		1002	
SL0908-34345	0	1	0	0	2	0	0	2		1002	
SL0908R-35630	0	1	0	0	2	0	0	2		1002	
SL0909R-35631	0	1	0	0	2	0	0	2		1002	



SL0910-34346	2	2	0	0	1	0	0	1	2001	
SL0911-34347	3	2	0	0	1	0	0	1	2001	
SL0913-34348	0	1	0	0	2	0	0	2	1002	
SL0913R-35633	0	1	0	0	2	0	0	2	1002	
SL0914R-35634	0	1	0	0	2	0	0	2	1002	
SL0915-34349	0	1	0	0	2	0	0	2	1002	
SL0916-34350	0	1	0	0	2	0	0	2	1002	
SL0917-34351	0	1	0	0	2	0	0	2	1002	small root system
SL0918-34352	0	1	0	0	2	0	0	2	1002	
SL0919-34353	0	1	0	0	2	0	0	2	1002	
SL0920-34354	0	1	0	0	2	0	0	2	1002	
SL0921-34355	0	1	0	0	2	0	0	2	1002	
SL0923-34357	0	1	0	0	2	0	0	2	1002	
SL0926-34360	0	1	0	0	2	0	0	2	1002	
SL0928-34362	0	1	0	0	2	0	0	2	1002	
SL0930-34364	0	1	0	0	2	0	0	2	1002	
SL0937-34371	0	1	0	0	2	0	0	2	1002	
SL0941-34374	0	1	0	0	2	0	0	2	1002	
SL0944-34377	0	1	0	0	2	0	0	2	1002	
SL0948-34381	0	1	0	0	2	0	0	2	1002	
SL0949-34382	0	1	0	0	2	0	0	2	1002	
SL0950-34383	0	1	0	0	2	0	0	2	1002	
SL0953-34384	0	1	0	0	2	0	0	2	1002	
SL0954-34385	0	1	0	0	2	0	0	2	1002	
SL0955-34386	0	1	0	0	2	0	0	2	1002	
SL0956-34387	0	1	0	0	2	0	0	2	1002	
SL0957-34388	0	1	0	0	2	0	0	2	1002	
SL0958-34389	0	1	0	0	2	0	0	2	1002	
SL0959-?	0	1	0	1	1	0	0	2	1012	
SL0960-34390	0	1	0	0	2	0	0	2	1002	
SL0963-34393	0	1	0	0	2	0	0	2	1002	
SL0965-34395	0	1	0	0	2	0	0	2	1002	

SL0966-34396	0	1	0	0	2	0	0	2	1002
SL0967-34397	0	1	0	0	2	0	0	2	1002
SL0968-34398	0	1	0	0	2	0	0	2	1002
SL0969-34399	0	1	0	0	2	0	0	2	1002
SL0970-34400	0	1	0	0	2	0	0	2	1002
SL0971-34401	0	1	0	0	2	0	0	2	1002
SL0972-34402	0	1	0	0	2	0	0	2	1002
SL0976R-35637	0	1	0	0	2	0	0	2	1002
SL0977-34404	0	1	0	0	2	0	0	2	1002
SL0979-34406	0	1	0	0	2	0	0	2	1002
SL0980-34407	0	1	0	0	2	0	0	2	1002
SL0983-34410	0	1	0	0	2	0	0	2	1002
SL0984-34411	0	1	0	0	2	0	0	2	1002
SL0985-?	0	1	0	0	2	0	0	2	1002
SL0986-?	0	1	0	0	2	0	0	2	1002
SL0987-?	0	1	0	0	2	0	0	2	1002
SL0988-34412	0	1	0	0	2	0	0	2	1002
SL0990-34414	0	1	0	0	2	0	0	2	1002
SL0991-34415	0	1	0	0	2	0	0	2	1002
SL0993-34416	0	1	0	0	2	0	0	2	1002
SL0997-34420	0	1	0	0	2	0	0	2	1002
SL0998-34421	0	1	0	0	2	0	0	2	1002
SL0999-34422	0	1	0	0	2	0	0	2	1002
SL1000-34423	0	1	0	0	2	0	0	2	1002
SL1001-34424	0	1	0	0	2	0	0	2	1002
SL1002-34425	0	1	0	0	2	0	0	2	1002
SL1003-34426	0	1	0	0	2	0	0	2	1002
SL1004-34427	0	1	0	0	2	0	0	2	1002
SL1005-34428	0	1	0	0	2	0	0	2	1002
SL1006-34429	0	1	0	0	2	0	0	2	1002
SL1007-34430	0	1	0	0	2	0	0	2	1002
SL1008-34431	0	1	0	0	2	0	0	2	1002

SL1010-34433	0	1	0	0	2	0	0	2	1002
SL1011-34434	0	1	0	0	2	0	0	2	1002
SL1012-34435	0	1	0	0	2	0	0	2	1002
SL1015-34438	0	1	0	0	2	0	0	2	1002
SL1016-34439	0	1	0	0	2	0	0	2	1002
SL1019-34441	0	1	0	0	2	0	0	2	1002
SL1021-34442	0	1	0	0	2	0	0	2	1002
SL1022-34443	0	1	0	0	2	0	0	2	1002
SL1023-34444	0	1	0	0	2	0	0	2	1002
SL1025-34446	0	1	0	0	2	0	0	2	1002
SL1026-34447	0	1	0	0	2	0	0	2	1002
SL1027-34448	0	1	0	0	2	0	0	2	1002
SL1028-34449	0	1	0	0	2	0	0	2	1002
SL1031-34450	0	1	0	0	2	0	0	2	1002
SL1032-34451	0	0	0	0	2	0	0	0	0000
SL1033-34452	0	1	0	0	2	0	0	2	1002
SL1035-34454	0	1	0	0	2	0	0	2	1002
SL1036-34455	0	1	0	0	2	0	0	2	1002
SL1037-34456	0	1	0	0	2	0	0	2	1002
SL1039-34458	0	1	0	0	2	0	0	2	1002
SL1043-34461	0	1	0	0	2	0	0	2	1002
SL1044-34462	0	1	0	0	2	0	0	2	1002
SL1044-34463	0	1	0	0	2	0	0	2	1002
SL1045-34464	0	1	0	0	2	0	0	2	1002
SL1046-34465	0	1	0	0	2	0	0	2	1002
SL1048-34466	0	1	0	0	2	0	0	2	1002
SL1049-35603	0	1	0	0	2	0	0	2	1002
SL1050-34467	0	1	0	0	2	0	0	2	1002
SL1051-34468	0	1	0	0	2	0	0	2	1002
SL1052-35604	0	1	0	0	2	0	0	2	1002
SL1053-34470	0	1	0	0	2	0	0	2	1002
SL1054-34471	0	1	0	0	2	0	0	2	1002

SL1056-34473	0	1	0	0	2	0	0	2	1002
SL1057-34474	0	1	0	0	2	0	0	2	1002
SL1058-34475	0	1	0	0	2	0	0	2	1002
SL1059-34476	0	1	0	0	2	0	0	2	1002
SL1060-34477	0	1	0	0	2	0	0	2	1002
SL1061-34478	0	1	0	0	2	0	0	2	1002
SL1062-34479	0	1	0	0	2	0	0	2	1002
SL1063-34480	0	1	0	0	2	0	0	2	1002
SL1065-34482	0	1	0	0	2	0	0	2	1002
SL1066-35605	0	1	0	0	2	0	0	2	1002
SL1066-35606	0	1	0	0	2	0	0	2	1002
SL1067-34483	0	1	0	0	2	0	0	2	1002
SL1068-35607	0	1	0	0	2	0	0	2	1002
SL1068-35608	0	1	0	0	2	0	0	2	1002
SL1069-34484	0	1	0	0	2	0	0	2	1002
SL1070-34485	0	1	0	0	2	0	0	2	1002
SL1073-34487	0	1	0	0	2	0	0	2	1002
SL1074-34488	0	1	0	0	2	0	0	2	1002
SL1075-34489	0	1	0	0	2	0	0	2	1002
SL1077-35610	0	1	0	0	2	0	0	2	1002
SL1079-34492	0	1	0	0	2	0	0	2	1002
SL1080-34493	0	0	0	0	2	0	0	0	0000
SL1081-34494	0	1	0	0	2	0	0	2	1002
SL1082-34495	0	1	0	0	2	0	0	2	1002
SL1082-35611	0	1	0	0	2	0	0	2	1002
SL1083-34496	0	1	0	0	2	0	0	2	1002
SL1084-35612	0	1	0	0	2	0	0	2	1002
SL1086-34498	0	1	0	0	2	0	0	2	1002
SL1087-34499	0	1	0	0	2	0	0	2	1002
SL1087-35613	0	1	0	0	2	0	0	2	1002
SL1088-35614	0	1	0	0	2	0	0	2	1002
SL1089-34500	0	1	0	0	2	0	0	2	1002

SL1091-34501	0	1	0	0	2	0	0	2	1002	
SL1096-34506	0	1	0	0	2	0	0	2	1002	
SL1099-34509	0	1	0	0	2	0	0	2	1002	
SL1101-34511	0	1	0	0	2	0	0	2	1002	
SL1102-34512	0	1	0	0	2	0	0	2	1002	
SL1104-34513	0	1	0	0	2	0	0	2	1002	
SL1105-34514	0	0	0	0	2	0	0	0	0000	
SL1106-34515	0	1	0	0	2	0	0	2	1002	
SL1107-34516	0	1	0	0	2	0	0	2	1002	
SL1108-34517	12	0	0	0	2	0	0	0	0000	
SL1110-34519	0	0	0	0	2	0	0	0	0000	
SL1111-34520	0	1	0	0	2	0	0	2	1002	
SL1112-34521	0	1	0	0	2	0	0	2	1002	
SL1114-34523	0	1	0	0	2	0	0	2	1002	
SL1120-34527	0	1	0	0	2	0	0	2	1002	
SL1121-34528	0	0	0	0	2	0	0	0	0000	
SL1122-34529	0	1	0	0	2	0	0	2	1002	
SL1126-34533	0	1	0	0	2	0	0	2	1002	
SL1127-34534	0	1	0	0	2	0	0	2	1002	
SL1133-34538	0	1	0	0	2	0	0	2	1002	
SL1135-34540	0	1	0	0	2	0	0	2	1002	
SL1139-34542	0	1	0	0	2	0	0	2	1002	
SL1140-34543	0	0	0	0	2	0	0	0	0000	
SL1142-34544	0	1	0	0	2	0	0	2	1002	strong colonization
SL1143-34545	0	1	0	0	2	0	0	2	1002	
SL1144-34546	0	1	0	0	2	0	0	2	1002	
SL1147-34548	0	1	0	0	2	0	0	2	1002	
SL1149-34550	0	1	0	0	2	0	0	2	1002	
SL1153-34554	0	0	0	0	1	0	0	0	0000	
SL1154-34555	0	1	0	0	2	0	0	2	1002	
SL1156-34557	0	1	0	0	2	0	0	2	1002	
SL1158-34559	0	1	0	0	2	0	0	2	1002	

SL1161-34561	0	1	0	0	2	0	0	2	1002
SL1163-34563	0	1	0	0	2	0	0	2	1002
SL1165-34565	0	1	0	0	2	0	0	2	1002
SL1166-34566	0	1	0	0	2	0	0	2	1002
SL1170-34570	0	1	0	0	2	0	0	2	1002
SL1172-34571	0	1	0	0	2	0	0	2	1002
SL1174-34572	0	1	0	0	2	0	0	2	1002
SL1175-34573	0	1	0	0	2	0	0	2	1002
SL1175-35617	0	1	0	0	2	0	0	2	1002
SL1179-34577	0	1	0	0	2	0	0	2	1002
SL1182-34580	0	1	0	0	2	0	0	2	1002
SL1183-35618	0	1	0	0	2	0	0	2	1002
SL1184-35619	0	1	0	0	2	0	0	2	1002
SL1185-34581	0	1	0	0	2	0	0	2	1002
SL1185-35620	0	0	0	0	2	0	0	0	0000
SL1186-34582	0	1	0	0	2	0	0	2	1002
SL1190-34584	0	1	0	0	2	0	0	2	1002
SL1194-35621	0	1	0	0	2	0	0	2	1002
SL1195-34587	0	1	0	0	2	0	0	2	1002
SL1197-34589	0	1	0	0	2	0	0	2	1002
SL1198-34590	0	1	0	0	2	0	0	2	1002
SL1207-34595	0	1	0	0	2	0	0	2	1002
SL1217-34596	0	1	0	0	2	0	0	2	1002
SL1218-34597	0	1	0	0	2	0	0	2	1002
SL1228-34601	0	1	0	0	2	0	0	2	1002
SL1237-34604	0	1	0	0	2	0	0	2	1002
SL1239-34605	0	1	0	0	2	0	0	2	1002
SL1254-34608	0	1	0	0	2	0	0	2	1002
SL1256-34609	0	1	0	0	2	0	0	2	1002
SL1258-34610	0	0	0	0	2	0	0	0	0000
SL1276R-11275	0	1	0	0	2	0	0	2	1002
SL1288-34618	0	1	0	0	2	0	0	2	1002

SL1301-34621	0	1	0	0	2	0	0	2	1002
SL1303-34622	0	1	0	0	2	0	0	2	1002
SL1307-34624	0	1	0	0	2	0	0	2	1002
SL1311-34625	0	0	0	0	2	0	0	0	0000
SL1313-34627	0	1	0	0	2	0	0	2	1002
SL1317-34629	0	1	0	0	2	0	0	2	1002
SL1318-34630	0	1	0	0	2	0	0	2	1002
SL1318-34631	0	1	0	0	2	0	0	2	1002
SL1324-34632	0	1	0	0	2	0	0	2	1002
SL1332-34635	0	1	0	0	2	0	0	2	1002
SL1334-34636	0	1	0	0	2	0	0	2	1002
SL1339-34639	0	1	0	0	2	0	0	2	1002
SL1341-34640	0	1	0	0	2	0	0	2	1002
SL1346-34644	0	1	0	0	2	0	0	2	1002
SL1348-34646	0	0	0	0	2	0	0	0	0000
SL1353-34647	0	1	0	0	2	0	0	2	1002
SL1356-34649	0	1	0	0	2	0	0	2	1002
SL1358-34650	0	0	0	0	2	0	0	0	0000
SL1362-34652	0	1	0	0	2	0	0	2	1002
SL1364-34654	0	1	0	0	2	0	0	2	1002
SL1367-34657	0	1	0	0	2	0	0	2	1002
SL1369-34659	0	1	0	0	2	0	0	2	1002
SL1370-34660	0	1	0	0	2	0	0	2	1002
SL1371-34661	0	1	0	0	2	0	0	2	1002
SL1372-34662	0	1	0	0	2	0	0	2	1002
SL1374-34663	0	1	0	0	2	0	0	2	1002 nod- in NODPOP
SL1375-34664	0	1	0	0	2	0	0	2	1002
SL1376-34665	0	1	0	0	2	0	0	2	1002
SL1377-34666	0	1	0	0	2	0	0	2	1002
SL1379-34668	0	1	0	0	2	0	0	2	1002
SL1381-34669	0	1	0	0	2	0	0	2	1002
SL1383-34671	0	1	0	0	2	0	0	2	1002

SL1386-34673	0	1	0	0	2	0	0	2	1002	
SL1387-34674	0	1	0	0	2	0	0	2	1002	
SL1390-34676	0	1	0	0	2	0	0	2	1002	
SL1392-34678	0	1	0	0	2	0	0	2	1002	
SL1395-34679	0	1	0	0	2	0	0	2	1002	
SL1396-34680	0	1	0	0	2	0	0	2	1002	
SL1397-34681	0	1	0	0	2	0	0	2	1002	
SL1399-34682	0	1	0	0	2	0	0	2	1002	
SL1400-34683	0	1	0	0	2	0	0	2	1002	
SL1401-34684	0	1	0	0	2	0	0	2	1002	
SL1404-34687	0	1	0	0	2	0	0	2	1002	
SL1405-34688	0	1	0	0	2	0	0	2	1002	
SL1407-34689	0	1	0	0	2	0	0	2	1002	
SL1408-34690	0	1	0	0	2	0	0	2	1002	
SL1409-34691	0	1	0	0	2	0	0	2	1002	
SL1412-34693	0	1	0	0	2	0	0	2	1002	
SL1413-34694	0	1	0	0	2	0	0	2	1002	
SL1414-34695	0	1	0	0	2	0	0	2	1002	
SL1415-34696	0	1	0	0	2	0	0	2	1002	nod-line
SL1418-34698	0	1	0	0	2	0	0	2	1002	
SL1419-34699	0	1	0	0	2	0	0	2	1002	
SL1420-34700	0	1	0	0	2	0	0	2	1002	
SL1421-34701	0	1	0	0	2	0	0	2	1002	
SL1423-34703	0	1	0	0	2	0	0	2	1002	
SL1425-34704	0	1	0	0	2	0	0	2	1002	
SL1431-34705	0	1	0	0	2	0	0	2	1002	
SL1436-34706	0	1	0	0	2	0	0	2	1002	
SL1447-34711	0	1	0	0	2	0	0	2	1002	
SL1449-35657	0	0	0	0	2	0	0	0	0000	
SL1453-34713	0	1	0	0	2	0	0	2	1002	
SL1455-34715	0	1	0	0	2	0	0	2	1002	
SL1456-34716	0	1	0	0	2	0	0	2	1002	



SL1461-34719	0	1	0	0	2	0	0	2	1002	nod-line
SL1462-34720	0	1	0	0	2	0	0	2	1002	
SL1464-34721	0	1	0	0	2	0	0	2	1002	
SL1465-34722	0	1	0	0	2	0	0	2	1002	
SL1466-34723	0	1	0	0	2	0	0	2	1002	
SL1467-34724	0	1	0	0	2	0	0	2	1002	sus2
SL1470-?	0	1	0	0	2	0	0	2	1002	
SL1472-34727	0	1	0	0	2	0	0	2	1002	
SL1475-34729	0	1	0	0	2	0	0	2	1002	
SL1476-34730	0	1	0	0	2	0	0	2	1002	
SL1479-34732	0	1	0	0	2	0	0	2	1002	
SL1481-34734	0	1	0	0	2	0	0	2	1002	
SL1482-34735	0	1	0	0	2	0	0	2	1002	
SL1483-34736	0	1	0	0	2	0	0	2	1002	
SL1484-34737	0	1	0	0	2	0	0	2	1002	
SL1487-34740	0	1	0	0	2	0	0	2	1002	
SL1488-34741	0	1	0	0	2	0	0	2	1002	
SL1489-34742	0	1	0	0	2	0	0	2	1002	
SL1491-34744	0	1	0	0	2	0	0	2	1002	
SL1492-34745	0	1	0	0	2	0	0	2	1002	
SL1493-34746	0	1	0	0	2	0	0	2	1002	
SL1498-34748	0	1	0	0	1	0	0	2	1002	
SL1503-35659	0	0	0	0	2	0	0	0	0000	
SL1504-35660	0	0	0	0	2	0	0	0	0000	
SL1505-34751	0	1	0	0	2	0	0	2	1002	
SL1506-34752	0	0	0	0	2	0	0	0	0000	
SL1508-34753	0	1	0	0	2	0	0	2	1002	
SL1509-34754	0	1	0	0	2	0	0	2	1002	
SL1510-34755	0	1	0	0	2	0	0	2	1002	
SL1511-34756	0	1	0	0	2	0	0	2	1002	
SL1512-35661	0	1	0	0	2	0	0	2	1002	
SL1514-34757	0	1	0	0	2	0	0	2	1002	

SL1516-34759	0	1	0	0	2	0	0	2	1002	
SL1517-34760	0	1	0	0	2	0	0	2	1002	
SL1518-34761	0	1	0	0	2	0	0	2	1002	
SL1523-34764	0	0	0	0	2	0	0	0	0000	
SL1524-34765	0	1	0	0	2	0	0	2	1002	
SL1525-34766	0	0	0	0	2	0	0	0	0000	
SL1526-35662	0	1	0	0	2	0	0	2	1002	
SL1528-34767	0	1	0	0	2	0	0	2	1002	
SL1532-34768	0	0	0	0	2	0	0	0	0000	
SL1533-34769	0	1	0	0	2	0	0	2	1002	
SL1535-34770	0	0	0	0	2	0	0	0	0000	
SL1536-34771	0	1	0	0	2	0	0	2	1002	
SL1538-34772	0	1	0	0	2	0	0	2	1002	
SL1542-34775	0	0	0	0	2	0	0	0	0000	
SL1550-35667	0	0	0	0	2	0	0	0	0000	
SL1555-35669	0	0	0	0	2	0	0	0	0000	
SL1558-34778	0	1	0	0	2	0	0	2	1002	
SL1559-34779	0	1	0	0	2	0	0	2	1002	
SL1562-34780	0	1	0	0	2	0	0	2	1002	
SL1566-34782	0	1	0	0	2	0	0	2	1002	
SL1567-34783	0	1	0	0	2	0	0	2	1002	<i>sus1</i>
SL1568-34784	0	0	0	0	2	0	0	0	0000	
SL1571-34787	0	1	0	0	2	0	0	2	1002	
SL1575-34790	0	0	0	0	2	0	0	0	0000	nod- in NODPOP
SL1576-34791	0	1	0	0	2	0	0	2	1002	
SL1577-34792	0	1	0	0	2	0	0	2	1002	
SL1578-34793	0	1	0	0	2	0	0	2	1002	
SL1579-34794	0	1	0	0	2	0	0	2	1002	
SL1580-34795	0	1	0	0	2	0	0	2	1002	
SL1582-34797	0	0	0	0	2	0	0	0	0000	
SL1584-35670	0	1	0	0	2	0	0	2	1002	nod- in NODPOP
SL1590-34800	0	1	0	0	2	0	0	2	1002	

SL1591R	0	0	0	0	2	0	0	0	0000
- 11590									
SL1592-	0	1	0	0	2	0	0	2	1002
34801									
SL1593-	0	0	0	0	2	0	0	0	0000
34802									
SL1594-	0	1	0	0	2	0	0	2	1002
34803									
SL1596-	0	0	0	0	2	0	0	0	0000
34804									
SL1599-	0	1	0	0	2	0	0	2	1002
34807									
SL1600-	0	1	0	0	2	0	0	2	1002
34808									
SL1601-	0	1	0	0	2	0	0	2	1002
34809									
SL1602-	0	1	0	0	2	0	0	2	1002
34810									
SL1603-	0	1	0	0	2	0	0	2	1002
34811									
SL1801-	0	1	0	0	2	0	0	1	1001
34950									
SL1805-	0	1	0	0	2	0	0	2	1002
34954									
SL1806-	0	1	0	0	2	0	0	2	1002
34955									
SL1807-	0	0	0	0	2	0	0	0	0000
34956									
SL1808-	0	0	0	0	2	0	0	0	0000
34957									
SL1809-	0	0	0	0	1	0	0	0	0000
34958									
SL1811-	0	0	0	0	2	0	0	0	0000
34960									
SL1815-	0	1	0	0	2	0	0	2	1002
34964									
SL1818-	0	1	0	0	2	0	0	2	1002
34967									
SL1819-	0	0	0	0	2	0	0	0	0000
34968									
SL1820-	0	0	0	0	2	0	0	0	0000
34969									
SL1821-	0	1	0	0	2	0	0	2	1002
34970									
SL1825-	0	1	0	0	2	0	0	2	1002
34974									
SL1830-	0	0	0	0	2	0	0	0	0000
34979									
SL1831-	0	1	0	0	2	0	0	2	1002
34980									
SL1833-	0	1	0	0	2	0	0	2	1002
34982									
SL1834-	0	0	0	0	2	0	0	0	0000
34983									
SL1836-	0	1	0	0	2	0	0	2	1002
34984									
SL1837-	0	1	0	0	2	0	0	2	1002
34985									
SL1839-	0	1	0	0	2	0	0	2	1002
34986									
SL1840-	0	1	0	0	2	0	0	2	1002
34987									
SL1843-	0	1	0	0	2	0	0	2	1002
34990									

SL1845-34992	0	1	0	0	2	0	0	2	1002
SL1850-34996	0	1	0	0	2	0	0	2	1002
SL1855-34998	0	1	0	0	2	0	0	2	1002
SL1857-35000	0	1	0	0	2	0	0	2	1002
SL1860-35001	0	1	0	0	2	0	0	2	1002
SL1861-35002	0	1	0	0	2	0	0	2	1002
SL1865-35006	0	1	0	0	2	0	0	2	1002
SL1867-35008	0	1	0	0	2	0	0	2	1002
SL1868-35009	0	1	0	0	2	0	0	2	1002
SL1869-35010	0	1	0	0	2	0	0	2	1002
SL1870-35011	0	1	0	0	2	0	0	2	1002
SL1871-35012	0	1	0	0	2	0	0	2	1002
SL1872-35013	0	1	0	0	2	0	0	2	1002
SL1873-35014	0	1	0	0	2	0	0	2	1002
SL1875-35015	0	1	0	0	2	0	0	2	1002
SL1876-35016	0	1	0	0	2	0	0	2	1002
SL1877-35017	0	0	0	0	2	0	0	0	0000
SL1879-35018	0	1	0	0	2	0	0	2	1002
SL1881-35020	0	1	0	0	2	0	0	2	1002
SL1882-35021	0	0	0	0	2	0	0	0	0000
SL1884-35023	0	1	0	0	2	0	0	2	1002
SL1889-35027	0	1	0	0	2	0	0	2	1002

---

---

**Supplemental Table 2.** Number of Families Analyzed by the Author During the AM Screen.

---

AM Phenotype	1 <sup>st</sup> M <sub>3</sub> Screen	2 <sup>nd</sup> M <sub>3</sub> Screen	M <sub>4</sub> Screen
Strong/Clear	30 <sup>a</sup>	9 <sup>b</sup>	4 <sup>b</sup>
Intermediate	46 <sup>a</sup>	15	9
Weak/Unclear	161	28	12
Wild Type	339	32	8

---

<sup>a</sup> Putative Mutants

<sup>b</sup> Mutants accounted to the AMPOP (screened in the 2<sup>nd</sup> M<sub>3</sub> screen and/or the M<sub>4</sub> screen)

**Supplemental Table 3. Power Mapping Marker Information.**

Chr. <sup>a</sup>	cM <sup>a</sup>	Name	Clone	SSR	MG-20 <sup>b</sup>	Gifu <sup>b</sup>	AF-primer (5' to 3')	R-primer (5' to 3')	Label <sup>c</sup>	Dilute	Pool <sup>d</sup>	Set <sup>e</sup>
1	0.0	G080	TM0088	AT	178	168	TCGAGGTCGACGGTATCAGCTATAGTTCATAAAATCACCA	ATTACCACCATCTCTCTGGC	NED	1/30	1	1
1	29.7	G037	TM1325	AT	168	160	CGCCATTTGACCATTATCAATCCACGCTTCTCTCC	TGTATTATGACCATAAAACAAAC	VIC	1/60	1	1
1	71.0	G017	TM0105	AT	157	171	CTCGTAGACTGCGTACCATCGCTGTTAATTTCTATCC	ACATTCCTTAACCTTACTTTGAC	FAM	1/60	1	1
3	12.5	G144	TM0080	AT	154	148	GTA AACGACGGCCAGTAAACAAAATACTAACTATAGCAAAG	CGTCCCACAACTCTCTTTAC	PET	1/40	1	1
1	11.3	G046	TM0349	CT	196	178	TCGAGGTCGACGGTATCAACGAGTAGAAGGAGGTC	TTCTCACTTTCACGCCGTTT	NED	1/60	2	1
2	33.8	G123	TM0124	AAAG	156	160	GTA AACGACGGCCAGTTCGAGTTCACGCGATAAACC	ACAACAAACAGTGGATACCC	PET	1/40	2	1
3	54.7	G165	TM0724	CT	117	113	CTCGTAGACTGCGTACCAATCTCTTCAACCTAAACG	TTCCTCTGGTGCAGTAAAG	FAM	1/30	2	1
4	8.8	G019	TM0100	CT+GT	167	151	CGCCATTTGACCATTATCCCAAGCTCAACAATATATCC	TGTA AACTTCATTTCTTTGGTG	VIC	1/30	2	1
2	48.5	G018	TM0541	AAT	158	166	GTA AACGACGGCCAGTAAATGTGTAATTTATTTTCGATG	GTA AATTTGACATCAAAGTTGAA	PET	1/20	3	1
3	34.0	G008	TM0005	GT	176	188	TCGAGGTCGACGGTATCACAACACAAAGACTTTTGG	CACTACTCATTACCGGCAC	NED	1/60	3	1
4	29.4	G003	TM0500	AT	136	146	CTCGTAGACTGCGTACGAGGAAGATGAAGGCGATGG	GAATAAGCTCTAGGGTGG	FAM	1/20	3	1
5	4.8	G023	TM0034	AAT	200	209	CGCCATTTGACCATTATCACTATGCTCTAGATCACAC	GGTTGGTTTGATTGCGTGC	VIC	1/60	3	1
2	62.1	G065	TM0592	AAG	150	153	GTA AACGACGGCCAGTTCGAGCAAATAGACAAACG	TTCGGAAGCTCTCGATACC	PET	1/60	4	1
3	75.6	G010	TM0258	AT	149	157	TCGAGGTCGACGGTATCAATCTATCTTCTCATTCTCTCC	GTTATGAGTGTACTACATCTTG	NED	1/30	4	1
4	67.6	G011	TM0617	CT	152	140	CTCGTAGACTGCGTACCATCAGCAGTGAATCATGAGAG	CCTCATGAGCATTCTCTG	FAM	1/40	4	1
5	20.4	G012	TM0186	AAC	152	143	CGCCATTTGACCATTATGATATGAACCAACTGAC	ACTCATCACTCGAAAACAC	VIC	1/60	4	1
1	45.0	G013a	TM0800	AAT	181	193	CTCGTAGACTGCGTACAGCCATTTTATTTGAAATATGC	GGTTTTAAAAATTAAGAAATCTCAC	FAM	1/40	5	1
4	50.2	G152	TM0044	ATG	156	159	GTA AACGACGGCCAGTGTGATGATCAGCTGTAAAG	TCCAACCTTTATGTTATTAGC	PET	1/60	5	1
6	1.3	G053	TM1613	CT	193	197	TCGAGGTCGACGGTATCACTAGGGTATTTAATGTTT	GTTAGAAGAACATGCCAC	NED	1/80	5	1
6	14.0	G005	TM0302	CT	160	186	CGCCATTTGACCATTACTCTGTTCCGAAGCTATTCC	AAACGACAGATTGGTGATG	VIC	1/20	5	1
6	66.2	G002	TM0582	CT	133	129	CGCCATTTGACCATTATCAACGGGAACAATCAG	CGGAATCGCTCTTCACTC	VIC	1/60	6	1
2	8.8	G179	TM2498	AT	144	156	GTA AACGACGGCCAGTCCCTTTGATTGAATAAGAG	CGAGTGTAGTACATATTTGGTG	PET	1/60	6	1
5	44.1	G042	TM0456	AAG	185	176	CTCGTAGACTGCGTACACACCACTGAGCCATTGTTG	GGCGATTTCTCCAAACTAC	FAM	1/80	6	1
6	46.6	G004	TM1035	AAT	144	156	TCGAGGTCGACGGTATCCATCAACCTATTACTCTTGGTC	TGACCCATATATGAAGGACTG	NED	1/60	6	1
1	16.1	G001a	TM0334	AT	130	138	GTA AACGACGGCCAGTAAAGTGCATCTAGAGGGTG	ACGCTGAGCTGAATCAATC	PET	1/10	1	2
1	35.3	G040	TM0637	AT	172	162	TCGAGGTCGACGGTATCACTAGGGTATTTAATTCG	CAATTTATCTCTTGTCTGG	NED	1/20	1	2
2	0.8	G078	TM1637	CT	167	197	CTCGTAGACTGCGTACCAAAATGTCATAGTCAAGCTGC	TGACAGGGAAAATAACAGT	FAM	1/30	1	2
3	82.4	G029	TM0127	AAG	148	136	CGCCATTTGACCATTACACATTGCGTTTGAACCTCG	GGTTCTGCTCAGCTTCGGTG	VIC	1/80	1	2
1	60.6	G031	TM0935	AT	151	139	GTA AACGACGGCCAGTGTGATAAACAACACTAAATGCTCTC	TTACATTTGCCCTAAGTTGG	PET	1/10	2	2
2	17.7	G020	TM1491	AAG	159	168	TCGAGGTCGACGGTATCTCAAAAGCTGATTTGGAGG	TTGTAAGTGAAAGCAATGG	NED	1/40	2	2
3	0.0	G048	TM0793	AT	199	185	CTCGTAGACTGCGTACCATATCGAAGGTTAGCCGCTC	TGACATCAGGATGGTACTGG	FAM	1/10	2	2
4	0.4	G045	TM1203	AT	177	197	CGCCATTTGACCATTATGAATAAGGCTCATAGATCC	CTTCAGTTGGGTTTCAAGC	VIC	1/30	2	2
2	27.4	G032	TM0377	CT	157	139	TCGAGGTCGACGGTATCAAGAGCGTTAGGAGTTGAC	TCACTCCCTGAATTTCTCTC	NED	1/30	3	2
3	44.4	G162	TM0213	AAT	178	181	CTCGTAGACTGCGTACCAACAATCCAATCGAATCAACC	TATTTATTTGTTCCAACCG	FAM	1/40	3	2
2	72.9	G143	TM0380	AT	125	123	GTA AACGACGGCCAGTCCGTGAAGAGTTATTTTGGG	TGCCATGTGGCATAGGCTTC	PET	1/80	3	2
4	59.4	G041	TM0266	CT	181	157	CGCCATTTGACCATTAGATAGCGTTCGTTAATCAGG	CCTAACATCAATCAACAC	VIC	1/60	3	2
3	21.1	G043	TM0996	AT	172	182	GTA AACGACGGCCAGTGTCCATTTACGGAACACCAG	TGCTTGGAGCTTTTGAAGG	PET	1/20	4	2
4	40.0	G147	TM0303	AAAT	172	180	TCGAGGTCGACGGTATCGGACTTTAATGTAATTTTGGCC	CCTACCTGTCCATCGAATC	NED	1/80	4	2
5	14.8	G049	TM0494	AT	185	203	CGCCATTTGACCATTACATAGCTGCAATTTCCAAGAG	TTTCGCTTGAATCAATGATG	VIC	1/40	4	2
5	31.6	G026	TM0849	GGT	129	138	CTCGTAGACTGCGTACCAACAACCTGGAGCACATCG	TTACGGGAAGCAGTGAGAGG	FAM	1/60	4	2
1	52.2	G101	TM1207	AT	161	213	TCGAGGTCGACGGTATCCACTAAAGCAATTTCTTAGGC	TTCTGACATGGACATCGGAC	NED	1/40	5	2
3	65.6	G167	TM0243	AAT	167	177	GTA AACGACGGCCAGTACCAACCCGGCCATATC	AATCAGCCTGATGGGAGTTC	PET	1/30	5	2
5	54.1	G038	TM0180	AAT	175	157	CTCGTAGACTGCGTACACAGTATTATAGGAACGGAGG	AAACAAACAGTAAAGTCTCATC	FAM	1/60	5	2
6	36.1	G034	TM0140	AT	155	145	CGCCATTTGACCATTACGAAATCAATTTGGGAGGC	TGGACAGTAATAATACATTG	VIC	1/80	5	2
6	7.7	G050	TM1597	AT	198	214	CTCGTAGACTGCGTACCATAGCGGAAGCTTCTTTATTG	ATTCAAAATCAGCATTGGC	FAM	1/40	6	2
6	57.6	G047	TM0336	GT+CT	181	197	GTA AACGACGGCCAGTTGAGCAATCAGAACCATATG	CATGTGCCTGAAATGTTACC	PET	1/40	6	2
2	49.3	G073	TM0974	AAT	175	172	CGCCATTTGACCATTAGTTTGTGCTCTGAATCTCG	ATGTGCTTGTCTCTCAAC	VIC	1/80	6	2
2	55.7	G133	TM0249	AT	148	167	TCGAGGTCGACGGTATCAATTAATAACAAAATAAACCG	CCAGAGAAAAGTCTTCTGTTAC	NED	1/40	6	2

(Table continues on next page.)

(Table continuation)

Chr. <sup>a</sup>	cM <sup>a</sup>	Name	Clone	SSR	MG-20 <sup>b</sup>	Gifu <sup>b</sup>	AF-primer (5' to 3')	R-primer (5' to 3')	Label <sup>c</sup>	Dilute
1	0.0	G063 (MS01 4433)	BM2121	AT	269	261	CTCGTAGACTGCGTACCAGAAAACCTGAAAGATGATTTTCA TCA	CCTTATGTCCTAGTTCCTACCAC TTG	FAM	1/40
1	51.4	G035	TM0356	AAT	149	157	GTA AAAACGACGGCCAGTAGGTTGAACCAATGACTCAG	AAGCATATTTCTTCCACCC	PET	1/10
2	10.8	G028	TM0153	CT	137	145	TCGAGGTCGACGGTATCATCAAGGGTTAACGATGGTC	AGTCGTCGTACAAAGTTTCCAG	NED	1/80
2	36.5	G025	TM0120	CT	119	125	CGCCATTTGACCATTCAAATTCACGCCACAATTATC	TTAAACCCGAACTCAACTATG	VIC	1/40
2	58.1	G137	TM0652	AAG	114	112	CGCCATTTGACCATTCAATTAACCGAGAATTGCTTG	CGAGGACGACATCTTCTCCG	VIC	1/40
2	60.9	G067	TM0060	AT	166	172	TCGAGGTCGACGGTATCTCAAGTGGGAGTAAGTTAGCATTCC	ATGGTTGGATAATAGACTTAGCCGA	NED	1/40
2	60.9	G069	TM0304	CT	145	133	CTCGTAGACTGCGTACCAGTCTCTGGGAATTATGAC	ATTTGTTGTGCACTCAGG	FAM	1/60
2	60.9	G072	TM0550	AC	176	156	TCGAGGTCGACGGTATCCCTGTTGGTTATCTTAGTATG	AAAACAAGTGAAGTGAAGTTAG	NED	1/20
2	60.9	G085 (ssr17)	CM0060	TC	154	156	CGCCATTTGACCATTAGTACCGGAGTAGTCCAGGATG	GCTACTGTTAAACCCCGGAAAC	VIC	1/40
2	60.9	G066	TM0060	ATG	164	166	CTCGTAGACTGCGTACCAACTTCAACCACTCTTCATC	AGCTGAAGATAATAGCGTTG	FAM	1/20
2	61.3	G071	TM0635	CT	147	167	GTA AAAACGACGGCCAGTTAATCAACCCCTGACCG	ATAACCCCTCTCAACATCG	PET	1/20
2	61.3	G070	TM0018	ATG	170	164	CGCCATTTGACCATTAGTTGAGCAAGTTAGAGGTTG	CGGATAAGAAAGGTAGAAGAG	VIC	1/60
2	68.1	G075	TM0546	AT	148	128	CTCGTAGACTGCGTACCAAGCAAAATATTTAAATACAACCTCAC	CAACCTAGAACGATAAAGCG	FAM	1/30
2	69.7	G138	TM0621	CT	136	132	CGCCATTTGACCATTGTTGCGTAACTTGAAGTTGAGCTTG	GAAACCCCTGCTGTTTCCAG	VIC	1/80
3	10.5	G009a	TM0365	AT	153	147	GTA AAAACGACGGCCAGTTGCAATGTAATGTCAGTGG	AAGGGTTCTGGAAATCAGTAG	PET	1/10
3	55.1	G006	TM0049	AT	158	176	GTA AAAACGACGGCCAGTTGGTTAGCTTACCTGTTTC	ATGTCCTGATCAAATGTTTC	PET	1/20
3	70.4	G044	TM0616	AT	167	187	TCGAGGTCGACGGTATCAAGATTCAATGCTTTCATCTC	GAACAAGTAGCAACATTTGTG	NED	1/30
4	0.4	G045	TM1203	AT	177	197	CGCCATTTGACCATTGATTAAGGTCATAGATCC	CTTCAGTTGGGTTTCAAGC	VIC	1/30
4	32.7	G146	TM0542	AAG	154	130	CGCCATTTGACCATTACCTTCAGAGAAAGAGGCGG	TGGAGACTGAGTTTCCACC	VIC	1/80
4	40.4	G039	TM1039	AT	158	174	GTA AAAACGACGGCCAGTAATATGAGCTTTCTCCGAC	GCATTGGAGATGCTTATAG	PET	1/20
4	53.8	G007	TM0046	CT	173	161	CTCGTAGACTGCGTACCAATCAACAAAACGTCCTTC	TTCTTGCCCTTCTCTGTGG	FAM	1/60
5	37.6	G014	TM0095	AT	187	177	CGCCATTTGACCATTGCTTGTGGTTTCTCCCGAC	GGGCAAAAAGAAAATAACGC	VIC	1/30
6	1.3	G021	TM0082	CT	188	212	GTA AAAACGACGGCCAGTGAAGAGAGACATAACCTAATGAAC	GGTTGGATGAAGTACAATGTC	PET	1/10
6	4.1	G054	TM0722	AT	146	160	CTCGTAGACTGCGTACCAACCACTTTTAGGAGAGG	AATTCAGTGAATCAACATGC	FAM	1/30
6	20.8	G052	TM0245	CT	156	160	CGCCATTTGACCATTATACACAACCGTCTAATCGGG	AGTCAAATGCAACATACAC	VIC	1/20
6	27.6	G030	TM0331	AAAT	148	156	CTCGTAGACTGCGTACCATTCTGTGAGATCAATTATGGC	CATCACAGTCTCAACATAG	FAM	1/80
6	49.9	G062	TM0756	AAG	145	160	TCGAGGTCGACGGTATCGCACCTACCAATAAACAGC	CTCCATTGAACGCCTTGAC	NED	1/40
6	51.1	G061	TM0228	AT	152	162	CTCGTAGACTGCGTACCATTCTTTGTTAATTCAAGTTGAC	AACTATTCATTAAATGTTTCTTC	FAM	1/40
6	55.6	G060	TM0301	AT+GT	146	142	GTA AAAACGACGGCCAGTGAACGAAAAGGGAATTTG	TTGCAACATGGATTAATCAC	PET	1/30
6	61.5	G059	TM0055	AAG	164	170	CGCCATTTGACCATTATATAACCGATGCTCACACAC	GATTAACGAACGCAAGTAG	VIC	1/40
6	63.4	G058	BM1484	AT	156	148	GTA AAAACGACGGCCAGTCACTTCTAAATCATGGAC	TTAAGTTCGGATCGATGAGC	PET	1/30
6	66.6	G057	TM1240	AT	161	157	TCGAGGTCGACGGTATCTGAATTGAATAAAATTAACAGG	CGCCATCATTTACTCTCAG	NED	1/40
6	67.0	G056	TM0508	AT	132	130	CGCCATTTGACCATTGATACATCGGAAGATACC	ATGCTTGGTGAAGATCC	VIC	1/40
6	67.4	G055	TM0885	CT	168	174	CTCGTAGACTGCGTACCATTGGATAACATGAACATAGCC	GGAAAGAGGAAGGAGAATTG	FAM	1/60

<sup>a</sup>Information refers to MG-20.

<sup>b</sup>Product size in bp.

<sup>c</sup>3'-fluorescence label of the corresponding A-primer:

FAM-LUF, 5'-CTCGTAGACTGCGTACCA-3';

VIC-BKRSV, 5'-CGCCATTTGACCATTCA-3';

NED-KS, 5'-TCGAGGTCGACGGTATC-3';

PET-M13, 5'-GTA AAAACGACGGCCAGT-3'.

<sup>d</sup>PCR products from these markers were pooled.

<sup>e</sup>Set 1 was routinely used for rough mapping; set 2 was used for further co-segregation analysis.

**Supplemental Table 4. Primers Used in this Work**

Primer Name	Use/Target	Direction	Sequence
N-166	TILLING/ <i>NENA</i>	Forward	5' -AAGTTAGAATTTATAAGGGCATCATT-3'
N-167		Reverse	5' -GGATTCCTGGCTTCCACCATTTTGTG-3'
N-156		Forward	5' -CCAGCTTGCTTTTACCTATTGGTCAT-3'
N-157		Reverse	5' -GCGCCAGCTTACTACTTACAAGTTA-3'
N-172	Transgenic complementation and sub-cellular localization/ <i>NENA</i>	Forward	5' -CAGCAAATCCACCACCACTAGTTAC-3'
N-157		Reverse	5' -GCGCCAGCTTACTACTTACAAGTTA-3'
N-171		Forward	5' -CACCGGAAAATTACACAAAAGATGGT-3'
N-168		Reverse	5' -AGAAGTGGGTTCAAATGCAGCCT-3'
N-171		Forward	5' -CACCGGAAAATTACACAAAAGATGGT-3'
N-173		Reverse	5' -CTCTCGTGAAACCTAAAATCTTG-3'
N-158		Forward	5' -CACCATGGCGAAGGAGGTGTTGAC-3'
N-168		Reverse	5' -AGAAGTGGGTTCAAATGCAGCCT-3'
S-176	Transgenic complementation/ <i>AtSeh1L</i>	Forward	5' -ATATTTTGGCCCAAGTCTTGATAAT-3'
S-175		Reverse	5' -ACTGTCAAATAGTGTGTGGGAAATG-3'
S-177		Forward	5' -ATGGCGAAATCAATGGCGACG-3'
S-178		Reverse	5' -TTAGGAGGGAAGTGGTTCAAG-3'
N-179	Transg. compl./ <i>NENA</i>	Reverse	5' -AAGGGTGGGCGCGCCGAC-3'
N-158	Y2H analysis/ <i>NENA</i>	Forward	5' -CACCATGGCGAAGGAGGTGTTGAC-3'
N-159		Reverse	5' -CTAAGAAGTGGGTTCAAATGCAG-3'
85-162	Y2H analysis and sub-cellular localization/ <i>NUP85</i>	Forward	5' -CACCATGCCCTCCGACACAGTC-3'
85-163		Reverse	5' -CTATTCATCAAGTATAGCACGACC-3'
85-183		Reverse	5' -TTCATCAAGTATAGCACGACCA-3'
133-160	Y2H analysis/ <i>NUP133</i>	Forward	5' -CACCATGTTTTTCGTGTGGAACGAAGAAG-3'
133-161		Reverse	5' -CTATTCATGGGAGAAGGCCCT-3'
13-1-191	Y2H analysis/ <i>SEC13-1</i>	Forward	5' -CACCATGCCTGCTCAGAAGGTTGAAACG-3'
13-1-194		Reverse	5' -CTACGGATCCACTGTTGTACCTGTTGCCAT-3'
13-1-195		Forward	5' -CGTTTACACTCACCGGCGACT-3'
13-1-196		Reverse	5' -TGCATTGTGAAGCACAGGTAA-3'
13-1-192	Y2H analysis/ <i>SEC13-2</i>	Forward	5' -CACCATGCCTGGTCAAAGGTTGAAACA-3'
13-1-193		Reverse	5' -CTACGGTCCACAGTCGTCACCTGTTGCCAG-3'
13-1-197		Forward	5' -CCTCACACGGTTGACACCACA-3'
13-1-198		Reverse	5' -CTCGTAAGCACAGAATGTTCAAGT-3'
120-5'	Y2H analysis/ <i>ScNup120</i>	Forward	5' -CACCATGGCATGCCTCTCAAGAATTGATG-3'
120-3'		Reverse	5' -CTATAGACCTCGTAACTCATCTCT-3'
145-5'	Y2H analysis/ <i>ScNup145</i>	Forward	5' -CACCATGTTTAATAAAAAGTGTAATAGTG-3'
145-3'		Reverse	5' -TTATATCTTATATGTACTTCATTA-3'
N-174	Expression analysis/ <i>NENA</i>	Forward	5' -AACTGGCAACTTCAGGCTGAGTTTC-3'
N-167		Reverse	5' -GGATTCCTGGCTTCCACCATTTTGTG-3'



Primer Name	Use/Target	Direction	Sequence
EF1-U23	Expression analysis/ <i>EF-1 α</i>	Forward	5' -GCAGGTCTTTGTGTCAAGTCTT-3'
EF1-L19		Reverse	5' -CGATCCAGAACCCAGTTCT-3'
NIN-201	Expression analysis/ <i>NIN</i>	Forward	5' -TGGATCAGCTAGCATGGAAT-3'
NIN-202		Reverse	5' -TCTGCTTCTGCTGTTGTCC-3'
M4-199	Expression analysis/ <i>SbtM4</i>	Forward	5' -TCTCATAGTTGCGGCACCAC-3'
M4-200		Reverse	5' -TGTCTTATTACCCAACCCTGTGC-3'
SbtS-007	Expression analysis/ <i>SbtS</i>	Forward	5' -ATTGATCACAATGCCAGAGATG-3'
SbtS-008		Reverse	5' -TGTTGGGAAGATTGTAGCAGTG-3'
40-203	Expression analysis/ <i>ENOD40-1</i>	Forward	5' -CCTCTGAACCAATCCATCAAATCCA-3'
40-204		Reverse	5' -AGGAGTGTGAGAGGTGACAGCA-3'
PT4-216	Expression analysis/ <i>PT4</i>	Forward	5' -GCTTCTTCAGTTCTGGCTGGGC-3'
PT4-217		Reverse	5' -CAGCGATGAAAGCACCTCGTGTC-3'
Ub-218	Expression analysis/ <i>Ub</i>	Forward	5' -ATGCAGATCTTCGTCAAGACCTTG-3'
Ub-219		Reverse	5' -ACCTCCCCTCAGACGAAG-3'
BM1714.2F	PCR and sequencing/ BM1714.2	Forward	5' -TGTACTTGTGCAGGAACTTCTAATAGG-3'
BM1714.2R		Reverse	5' -CCCTTATCATATAGCTGAAACACAAC-3'
BM1714.7F	PCR and sequencing/ BM1714.7	Forward	5' -TGTATTTGTGCAGAAACTTGAATCTC-3'
BM1714.7R		Reverse	5' -CCCTTATCATATATAGCTGAAACACAAC-3'
TM1643.6F	PCR/ <i>LjPT2</i>	Forward	5' -TTTCACTTTTGCAGGGAATTCA-3'
TM1643.6R		Reverse	5' -GCTTTTCCCTTGAGGTAGTGCTT-3'
TM1643.6_S1F	Sequencing/ <i>LjPT2</i>	Forward	5' -CAGGGTTTTGGAATTCTTGGAG-3'
TM1643.6_S2F		Forward	5' -CATAGACAGGATTGGAAGATTTGC-3'
TM1643.6_S3R	Reverse	5' -AGAGCCACTGTAAACCAGTAGCC-3'	
TM1643.6_S4R	Reverse	5' -GCAAAGACCGCAGCGATGAAG-3'	
MG014433F	PCR/ <i>LjPT4</i>	Forward	5' -TGGAGCAGACTTAAACCAATCC-3'
MG014433R		Reverse	5' -ACGTGTCATAACTAACCTGGGAAG-3'
MG014433_S1F	Sequencing/ <i>LjPT4</i>	Forward	5' -TGTACGGTGTACGCTTATCCTC-3'
MG014433_S2F		Forward	5' -GATGAAGGTTGAAGGTTCCAG-3'
MG014433_S3R	Reverse	5' -AGATAGTGGGTAGTCGCCTCCA-3'	
MG014433_S4R	Reverse	5' -CCATCACAGACTTGCTGAGGC-3'	
Pollux_a1fo	PCR and sequencing/ <i>POLLUX</i>	Forward	5' -AGCATTGTAGATCCCTTACTGTCC-3'
Pollux_a1re		Reverse	5' -GGCCAAAACATATCCCCATATCA-3'
Pollux_s1fo1	Sequencing/ <i>POLLUX</i>	Forward	5' -TTGCAGGATCACAACCTTACC-3'
TM0329	Map-based cloning	Forward	5' -TGGGTGAGAACTCAGAGGG-3'
		Reverse	5' -ATCCAATCCATTCTTTCTG-3'
TM0302		Forward	5' -CTCTGTTCCGAAGCTATTCC-3'
		Reverse	5' -AAACGACAGATTTGGTGATG-3'
TM0635		Forward	5' -TTAATCCACCACCCTGACCG-3'
		Reverse	5' -ATAACCCTCCTCAAACATCG-3'

## List of Figures

Figure 1. Development of AM. ....	19
Figure 2. AM, as Seen by Stereo- and Confocal Microscopy. ....	22
Figure 3. The Common SYM Signaling Network.....	27
Figure 4. Genetic Positions of ‘Power Mapping’ Markers and Symbiosis Genes.....	31
Figure 5. Pitfalls for Automated Allele Calling. ....	34
Figure 6. Relationship of Identified AM Mutants (AMPOP) to the <i>Lotus</i> TILLING Populations (GENPOP and NODPOP). ....	36
Figure 8. AM Phenotype of <i>red</i> (Kosuta, unpublished).....	41
Figure 9. Weak and Severe Arbuscule Defects in Mapping Populations of SL0181-N. ...	44
Figure 10. Co-segregation Analysis of 43 F <sub>2</sub> Mutants Originating From J5150.....	48
Figure 11. Allele Distributions in the <i>red</i> Target Region. ....	49
Figure 12. Genotype Patterns of Total Sub-populations.....	51
Figure 13. Recombinations Confining the <i>RED</i> Target Region.....	52
Figure 14. AM Colonization and Relative Expression of <i>PT4</i> in Wild Type and <i>red</i> Roots.....	53
Figure 15. M <sub>4</sub> Mutants Originating from J850 Are Impaired in Rhizobial Infection. ....	55
Figure 16. Co-segregation Analysis of SL1856-N and SL1345-N F <sub>2</sub> Mutants. ....	56
Figure 17. AM Phenotype of <i>patchy</i> . ....	58
Figure 18. Co-segregation Analysis of <i>patchy</i> . ....	59
Figure 19. Predicted G to E Substitution in the RCK Domain of POLLUX in <i>patchy</i> . ....	61
Figure 20. Crossing <i>patchy</i> with <i>pollux-2</i> Did Not Restore AM. ....	62
Figure 21. <i>patchy</i> Mutants Are Impaired in NF-induced Ca <sup>2+</sup> Spiking.....	63
Figure 22. <i>NIN</i> and <i>SbtM4</i> Expression Is Induced in <i>patchy</i> Roots at 7 DAI with <i>M. loti</i> .63	
Figure 23. Rhizobial Entrapment at Root Hairs and Rare Infection Thread Formation in <i>patchy</i> .....	65
Figure 24. Mature Nodule Are Formed at Reduced Frequency in <i>patchy</i> . ....	66
Figure 25. <i>nen</i> a Is Impaired in AM Fungal Infection. ....	68
Figure 26. AM and Nodulation Defects of <i>nen</i> a Are Temperature Dependent. ....	69
Figure 27. Map-based Cloning of <i>NENA</i> . ....	71
Figure 28. <i>NENA</i> Is a Single Copy Gene That Is Expressed in Various Tissues and Upregulated in Nodulated Roots. ....	72
Figure 30. Phylogenetic Relationships of Sec13/Seh1-like Proteins.....	76
Figure 31. <i>NENA</i> Interacts with NUP85 from <i>L. japonicus</i> and Adopts a $\beta$ -propeller Structure According to Homology Modeling.....	77
Figure 32. Perinuclear <i>in vivo</i> Localization of NUP85 and <i>NENA</i> Fusion Proteins.....	79
Figure 33. Calcium Spiking in Root Hairs of Wild Type and <i>nen</i> a-1.....	80

Figure 34. Rhizodermal Nod Factor Response Is Impaired Whereas Induction of Symbiosis Genes at Nodule Primordia Is Not Affected in <i>nenA</i> .....	81
Figure 35. Rhizobial Infection of <i>nenA</i> Does Not Occur via Root Hairs and Is Promoted by Ethylene. ....	84
Figure 36. Rhizobial Microcolonies at the Root Surface of <i>nenA-1</i> Lead to Nodule Formation and Intercellular Entry. ....	85
Figure 37. Two Models for NENA Function in RNS. ....	93
Figure 38. Segregation Model for <i>red</i> and <i>wrd</i> .....	99
Supplemental Figure 1. Genotype Patterns of <i>red</i> F <sub>2</sub> Mutants. ....	127
Supplemental Figure 2. Genotype Patterns of SL0181-N F <sub>2</sub> Individuals with Conflicting Genotypes. ....	128
Supplemental Figure 3. AM Phenotypes and Genotypes of SL0181-N Self-progeny from Selected F <sub>2</sub> Individuals.....	128
Supplemental Figure 4. <i>PT4</i> Maps to the Translocation Region at the North Tip of LG I. ....	130
Supplemental Figure 5. FUGUE Structure-based Alignment of RCK Domains from POLLUX and the Human BK Channel. ....	131
Supplemental Figure 6. Alignment of Seh1 and Sec13 Related Protein Sequences from <i>L. japonicus</i> , <i>A. thaliana</i> , <i>H. sapiens</i> and <i>S. cerevisiae</i> . ....	132
Supplemental Figure 7. Multi-Species Alignment of Seh1 and Sec13 Related Proteins.....	133
Supplemental Figure 8. 3D Projection of Typical AM Infection Sites in Wild Type and <i>nenA-1</i> .....	134
Supplemental Figure 9. The <i>NIN</i> Promoter Is Not Induced During Early Rhizodermal Response to <i>M. loti</i> but Active During Nodule Formation in <i>nenA-1</i> . ....	135
Supplemental Figure 10. Intercellular Infection of Outer Nodule Cell Layers in <i>nenA-1</i> . ....	136
Supplemental Figure 11. In Contrast to NENA, SEC13-like 1 and SEC13-like 2 Do Not Interact with NUP85 in the Gal4-Based Yeast Two-Hybrid Assay.....	136
Supplemental Figure 12. GFP-Cyclops Localizes to the Nucleus in <i>nenA-1</i> .....	137
Supplemental Figure 13. Stereomicroscopy Images of Putative and/or Confirmed Mutants.....	139
Supplemental Figure 14. Theoretical Inheritance of Mutation Load in the General TILLING Population of <i>Lotus</i> . ....	140

## List of Tables

Table 1. Multiplex PCR for Marker Combination G69/70.....	32
Table 2. Complementation Analysis between Three Mutants Impaired in Arbuscule Formation.....	39
Table 3. Segregation Ratios in Different F2 Sub-populations of <i>red</i> .....	43
Table 4. Segregation of Arbuscule Traits in <i>red</i> F3 and F4 Sub-populations.....	46
Table 5. Sequencing of <i>RED</i> -candidate Genes.....	54
Table 6. <i>nen</i> a Alleles and Symbiotic Phenotypes.....	73
Table 7. Complementation Analysis of <i>nen</i> a-1 by <i>A. rhizogenes</i> -mediated Transformation.....	74
Table 8. <i>NIN<sub>pro</sub>:GUS</i> Expression Analysis in Transgenic Roots of Wild Type and <i>nen</i> a-1 Genetic Background.....	82
Supplemental Table 1. Results of the AM Screen Performed by the Author.....	141
Supplemental Table 2. Number of Families Analyzed by the Author During the AM Screen.....	161
Supplemental Table 3. Power Mapping Marker Information.....	162
Supplemental Table 4. Primers Used in this Work.....	164

## Abbreviations, Measures and Species

A: adenine	MAMP: microbe-associated molecular pattern
AA: amino acid	MAPK: mitogen-activated protein kinases
ABA: abscisic acid	MEP: methylerythritol phosphate
Al: aluminum	min: minute(s)
AM: arbuscular mycorrhiza	mm: millimeter
AUT: autoregulation (of nodulation/mycorrhization)	N: nitrogen
AVG: aminoethoxyvinylglycine	NF: Nod factor
BF: bright field	NFR: Nod factor receptor
C: cytosine	NIN: nodule inception
Ca <sup>2+</sup> : calcium ion	NUP: nucleoporin
[Ca <sup>2+</sup> ]: calcium ion concentration	ORF: open reading frame
CCaMK: calcium and calmodulin-dependent kinase	P: phosphorus
Cd: cadmium	PAM: periarbuscular membrane
Cl: chloride	Pea: <i>Pisum sativum</i>
CLSM: confocal laser scanning microscopy	Peanut: <i>Arachis hypogaea</i>
cM: centimorgan	Petunia: <i>Petunia hybrida</i>
d: day(s)	P <sub>i</sub> : inorganic phosphate
DAI: days after inoculation	Potato: <i>Solanum tuberosum</i>
EMS: ethyl methanesulfonate	PPA: pre-penetration apparatus
ENOD: early nodulin	PT: phosphate transporter
ER: endoplasmic reticulum	RCK: domain regulating the conductivity of K <sup>+</sup>
Fe: <i>ferrum</i>	rDNA: ribosomal RNA encoding DNA
Field bean: <i>Vicia faba</i>	<i>red</i> : <i>reduced and degenerate arbuscules</i>
G: guanine	RHC: root hair curling
GFP: Green fluorescent protein	Rice: <i>Oryza sativa</i>
Glu: glutamic acid	RLK: receptor-like kinase
Gly: glycine	RNS: root nodule symbiosis
GUS: β-glucuronidase	Sbt: subtilase
h: hour(s)	sec: seconds
ha: hectare (10,000 m <sup>2</sup> )	Seh1: Sec13 homolog 1
IAA: indole-3-acetic acid	Soybean: <i>Glycine max</i>
IT: infection thread	SSR: simple sequence repeat
J: joule	SYMRK: symbiosis receptor-like kinase
JA: jasmonic acid	T: thymine
LG: linkage group	t: ton (1,000 kg)
LysM: lysine motif	TILLING: targeting induced local lesions in genomes
M: million	Tomato: <i>Lycopersicon esculentum</i>
Maize: <i>Zea mays</i>	w: week(s)
	WAI: weeks after inoculation
	y: year

## Curriculum Vitae

### PERSONAL DATA

Name: Martin Groth  
Born: 22<sup>nd</sup> February 1976, Munich, Germany  
Nationality: German

### RESEARCH INTERESTS

Based on undergraduate studies with major subjects in evolutionary biology and ecology my scientific interest has focused during the PhD on the molecular interaction between plants and microbes. Similarities in the infection processes of fungal and bacterial root symbioses involving shared mechanisms of signal transduction and the role of nucleocytoplasmic trafficking during this signal transduction have moved to the center of my research.

---

### EDUCATION

*Oct. 2004 – present:*

**Doctoral student** at the **Ludwig-Maximilians-Universität (LMU) München**.  
Topic: **Identification and characterization of genes required for arbuscular mycorrhiza**. Supervisor: Prof. Martin Parniske

*Oct. 1996 – Jul. 2003:*

**Diploma in Biology** (Grade 1,0/A) at the **LMU München**.  
Major Subject: Ecology. Minor Subjects: Molecular Evolution, Botanical Systematics, Climatology.

*Oct. 2002 – Jul. 2003:*

**Diploma thesis** about “**Sequence variation in the resistance gene *Prf* in wild tomatoes**”. Supervisors: Dr. Laura Rose and Prof. Wolfgang Stephan

*Aug. 1999 – Jun. 2000:*

**DAAD** (Deutscher Akademischer Austausch Dienst) **fellowship** at the Faculty of Natural Science and Oceanography at the **Universidad de Concepción** (Chile).  
Studies: Local flora and ecosystems, marine biology and biology of the Antarctic.

*Aug. 1986 – Mai 1995:*

Secondary school and German **university entrance qualification** (Grade 1,9) at the **Wilhelm-Hausenstein-Gymnasium München**.

### TRAININGS

*7<sup>th</sup>-11<sup>th</sup> Nov. 2005:*

INTEGRAL (Intensifying training in Europe on Genomic Research Activity in Legumes) workshop on **Transcriptomics** at the Max Planck Institute of Molecular Plant Physiology (Golm). Organizer: Prof. Michael Udvardi

7<sup>th</sup>-10<sup>th</sup> Jun. 2006:

INTEGRAL workshop on **Cell Biology** (confocal microscopy, laser capture microdissection) at the University of Torino, Department of Plant Biology. Organizer: Prof. Paola Bonfante

30<sup>th</sup>-31<sup>st</sup> Oct. 2008:

Leica course "Introduction to **FLIM**" at the LMU München, Genetics. Organizer: Dr. Arthur Schübler

---

## ACADEMIC EXPERIENCE

Oct. 2004 – present:

Research associate at the Biocenter of the **LMU München, Genetics** (Prof. Martin Parniske). In charge of **genetic screening** of an EMS-mutagenized population of *Lotus japonicus* for **arbuscular mycorrhiza mutants** and establishment of a capillary sequencer-based microsatellite analysis system for high-throughput genotyping in *Lotus japonicus*.

Feb. – Sep. 2004:

Research associate at the **Technische Universität (TU) München**, Center of Life and Food Sciences Weihenstephan, Department of Animal Breeding (Prof. Ruedi Fries). In charge of **QTL and candidate gene analysis** of energy and lipid metabolism in swine.

Nov. – Dec. 2003:

Student helper at the **LMU München, Evolutionary Biology** (Prof. Wolfgang Stephan). Analysis of **natural sequence variation** in wild tomatoes.

Mar. – June 2002:

Student helper at the **TU München, Climatology** (Prof. Peter Fabian). **Meteorological data acquisition** in the context of the SFB 607 project.

Sep. – Oct. 2001:

Student helper at the **LMU München, Ecology** (Prof. Sebastian Diehl). Participation at an **outdoor experiment near Trondheim** (Norway) in collaboration with the *Trondheim Marine Systems Research Infrastructure*.

## TEACHING

2009:

Advanced **microscopy** (4 students, 3 days)

2006 – 2008:

Annual **bioinformatics** course (10–20 students, 2 days, topics: sequence analysis, genome annotation, Vector NTI)

Supervision of one **diploma thesis** (Sebastian Wilhelm, Okt.'07-Jun.'08) and two undergraduate lab internships (Syndi Vieweg, 5<sup>th</sup> Mar.-4<sup>th</sup> May '07, Sebastian Wilhelm, 16<sup>th</sup> Okt.-8<sup>th</sup> Dec. '06)

---

## PEER-REVIEWED PUBLICATIONS

- Groth, M., Takeda, N., Perry, J., Uchida, H., Draxl, S., Brachmann, A., Sato, S., Tabata, S., Kawaguchi, M., Wang, T.L., and Parniske, M. *NENA*, a *Lotus japonicus* homolog of *Sec13*, is required for rhizodermal infection by arbuscular mycorrhiza fungi and rhizobia but dispensable for cortical endosymbiotic development. *Plant Cell* 22, 2509-2526.
- Maekawa-Yoshikawa, M., Muller, J., Takeda, N., Maekawa, T., Sato, S., Tabata, S., Perry, J., Wang, T.L., Groth, M., Brachmann, A., and Parniske, M. 2009. The temperature-sensitive *brush* mutant of the legume *Lotus japonicus* reveals a link between root development and nodule infection by rhizobia. *Plant Physiol* 149(4): 1785-1796.
- Perry, J., Brachmann, A., Welham, T., Binder, A., Charpentier, M., Groth, M., Haage, K., Markmann, K., Wang, T.L., and Parniske, M. 2009. TILLING in *Lotus japonicus* identified large allelic series for symbiosis genes and revealed a bias in functionally defective ethyl methanesulfonate alleles toward glycine replacements. *Plant Physiol* 151(3): 1281-1291.
- Takeda, N., Kistner, C., Kosuta, S., Winzer, T., Pitzschke, A., Groth, M., Sato, S., Kaneko, T., Tabata, S., and Parniske, M. 2007. Proteases in plant root symbiosis. *Phytochemistry* 68(1): 111-121.

## CONFERENCES

### Oral Presentations

- Groth, M., Takeda, N., Sato, S. and Parniske, M.: *Nena* is required for root symbiosis and shows sequence similarity to a component of the nuclear pore complex. 3ème Cycle Symposium, 16<sup>th</sup>-17<sup>th</sup> Oct. 2008, Fribourg, Switzerland
- Groth, M., Haage, K., Kosuta, S. and Parniske, M.: Identification of arbuscular mycorrhiza mutants *patchy* and *nena*. Final Colloquium of the Priority Program SPP 1084 "Mykorrhiza", 1<sup>st</sup>-3<sup>rd</sup> Oct. 2006, Tutzing, Germany
- Groth, M. and Parniske, M.: Genetics of plant-bacteria incompatibility in *Lotus*: Mapping and (Eco-)TILLING of stress tolerance genes. Project partner representative at LOTASSA kick-off meeting, 5<sup>th</sup>-8<sup>th</sup> Dec. 2005, Colonia/Montevideo, Uruguay
- Groth, M., Kosuta, S. and Parniske, M.: Genetic screening for arbuscular mycorrhiza-specific mutants in *Lotus japonicus*. 6<sup>th</sup> Colloquium of the Priority Program SPP 1084 "Mykorrhiza", 31<sup>st</sup> Oct.-1<sup>st</sup> Nov. 2005, Neustadt/Weinstraße, Germany

### Poster Presentations

- Groth, M., Takeda, N., Sato, S., Tabata, S. and Parniske, M.: *NENA* is required for root symbiosis and encodes a putative component of the nuclear pore. 19<sup>th</sup>-23<sup>rd</sup> Jul. 2009: XIV Congress of the International Society for Plant-Microbe Interactions, Quebec, Canada